



**HAL**  
open science

# Graded signal inputs to binary cell fate decisions : a quantitative approach based on ascidian neural induction

Géraldine Williaume

► **To cite this version:**

Géraldine Williaume. Graded signal inputs to binary cell fate decisions: a quantitative approach based on ascidian neural induction. *Development Biology*. Sorbonne Université, 2020. English. NNT : 2020SORUS426 . tel-03784316

**HAL Id: tel-03784316**

**<https://theses.hal.science/tel-03784316>**

Submitted on 23 Sep 2022

**HAL** is a multi-disciplinary open access archive for the deposit and dissemination of scientific research documents, whether they are published or not. The documents may come from teaching and research institutions in France or abroad, or from public or private research centers.

L'archive ouverte pluridisciplinaire **HAL**, est destinée au dépôt et à la diffusion de documents scientifiques de niveau recherche, publiés ou non, émanant des établissements d'enseignement et de recherche français ou étrangers, des laboratoires publics ou privés.



ED515 - Ecole doctorale Complexité du Vivant

**Graded signal inputs to binary cell fate  
decisions: a quantitative approach based on  
ascidian neural induction.**

Thèse de doctorat en Biologie du Développement

Par Géraldine Williaume

Sous la direction du Dr Hitoyoshi Yasuo

Présentée et soutenue publiquement le 21 Septembre 2020

Au Laboratoire de Biologie du Développement de Villefranche-sur-Mer

Devant un jury composé de:

---

Dr Vincent Bertand	Rapporteur
Dr Claire Chazaud	Rapporteuse
Dr Elise Cau	Examinatrice
Dr Sebastien Darras	Examineur
Pr Nathalie Dostatni	Examinatrice
Dr Hitoyoshi Yasuo	Directeur de thèse
Dr Clare Hudson	Membre invité

---



This work is licensed under a Creative Commons  
Attribution - Non Commercial - No Derivatives 4.0 International license

*"It seems to me that the natural world is the greatest source of excitement; the greatest source of visual beauty; the greatest source of intellectual interest. It is the greatest source of so much in life that makes life worth living."*

David Attenborough



# REMERCIEMENTS

Je tiens tout d'abord à remercier Yas, Clare et Cathy pour ces quatre années qui furent d'une richesse incroyable aussi bien scientifiquement qu'humainement. Un merci tout particulier à Yas d'avoir accepté de diriger ma thèse, j'ai un immense respect pour le scientifique que tu es et j'espère un jour arriver à ton niveau, c'est un life goal ! Un immense merci à Clare pour nos échanges scientifiques et tes conseils avisés mais aussi ta bonne humeur contagieuse. Je tiens également à remercier Cathy pour ton aide précieuse mais aussi ton écoute bienveillante particulièrement lors de la rédaction de ce manuscrit. Vous avez été tous les trois d'un soutien indéfectible et je suis consciente de la chance que j'ai d'avoir été si bien accompagnée pendant cette merveilleuse aventure qu'est le doctorat. Merci, merci, merci!

Je souhaite également remercier les membres de mon comité de thèse Carine Barreau et Nathalie Dostatni pour leurs précieux conseils au cours de ces quatre années.

Merci à mes rapporteurs, Claire Chazaud et Vincent Bertrand, ainsi qu'aux autres membres de mon jury Elise Cau et Sébastien Darras d'avoir accepté d'examiner mon travail.

Merci à Eric Queinnec qui m'a fait découvrir la richesse des organismes marins lors des cours de Biologie animale en 3<sup>e</sup> année de licence.

Merci à toutes les personnes du labo qui m'ont aidé et soutenu dans ce projet, étudiant de passage ou titulaire aguerri, un grand merci!

Merci à tout le 2<sup>e</sup> étage de Jean Maetz : Sandra, Sonia, Tsuyo, Evelyn, Jean-Michel, Stefano, Alex A, Marta, Marion L, Mandela, Gonzalo, Manon, Julie, Cat, Laurel, pour votre aide, votre présence et votre bonne humeur!

Merci à tous les autres membres du LBDV particulièrement les étudiants Anna, Julia, David, Marianne, Sophie.

Merci à nos gestionnaires Christelle et Frédéric d'avoir été des guides précieux dans les méandres administratifs de l'Université. Un grand merci également à Faisal, Philippe Dru, et Sameh pour votre aide en informatique, en hygiène et sécurité, en microscopie et surtout pour votre bonne humeur !

Merci à Martine pour tes si bons conseils et pour nous accueillir dans ta magnifique bibliothèque.

Merci à Lolo, Alex J., Axel et Régis de prendre soin chaque jour de nos jolies Ciones. Et parce qu'un bon ravitaillement est essentiel, merci à Didier, Thierry et Jocelyne de nous régaler tous les jours avec des plats tous plus savoureux les uns que les autres (Laurent se joint à moi pour vous demander la recette des fameuses lasagnes 😊).

Merci à Anne So, Alice, Laurent, Axel et François d'avoir rendu ces quatre ans plus doux. Anne-So, ma thèse n'aurait pas été la même sans toi, merci d'avoir été là!

Merci à ma famille sur qui j'ai pu compter pendant ces quatre années. Un merci particulier à Josefa pour nos (trop) long facetimes.

Et enfin, parce que le doctorat ne s'arrête pas une fois les portes du labo refermées, je veux remercier Théophile. Merci pour ton soutien, tes conseils et ta confiance. Merci d'être toujours là, dans les bons comme les moins bons moments.

*Enfin, je souhaite dédicacer ce manuscrit au Dr R. Williaume, mon grand-père, homme de sciences qui m'a inspirée pendant ces quatre années de doctorat et qui m'étonne chaque jour par l'étendue de ses connaissances, de la chirurgie à la Cione en passant par l'histoire de France, rien ne t'échappe.*





# Table des matières

<b>INTRODUCTION</b> .....	- 1 -
<b>I. Morphogen gradients in development</b> .....	- 3 -
1) Shh in vertebrate neural tube .....	- 8 -
2) Interpretation of Bicoid gradient.....	- 19 -
<b>II. ERK signalling dynamics</b> .....	- 29 -
1) Background .....	- 29 -
2) Temporal dynamics of ERK signalling .....	- 32 -
3) Dose response kinetics of ERK signalling .....	- 36 -
4) ERK signalling in multicellular contexts .....	- 42 -
<b>III. Ascidian embryos: a model in developmental biology</b> .....	- 59 -
1) Background .....	- 59 -
2) Nomenclature system of ascidian embryonic cells .....	- 61 -
3) Polarisation of the ascidian egg.....	- 62 -
4) Regionalization of the ascidian embryo along the A-P axis.....	- 63 -
<b>IV. State of the art for neural induction in <i>Ciona intestinalis</i> embryos</b> .....	- 69 -
1) Ascidian larval central nervous system and its cell lineages .....	- 69 -
2) Neural induction in <i>Ciona</i> embryos.....	- 75 -
3) Antagonistic inputs during neural induction .....	- 80 -
<b>V. Objectives</b> .....	- 85 -
<b>RESULTS</b> .....	- 87 -
<b>I. ephrin-mediated “dampening” of FGF signalling underlies the spatial precision of ascidian neural induction</b> .....	- 89 -
<i>Manuscript in preparation</i> .....	- 89 -

II. Toward the mechanism underlying the switch-like transcriptional response of the <i>Otx</i> gene during neural induction .....	- 175 -
1) Introduction .....	- 175 -
2) Results and discussion.....	- 176 -
3) Materials and Methods .....	- 186 -
<b>DISCUSSION &amp; PERSPECTIVES</b> .....	- 191 -
I. Correlation between the level of signals and the contact surface between inducing and responding cells.....	- 195 -
1) ephrin/Eph signalling .....	- 195 -
2) FGF signalling .....	- 196 -
3) Distribution at the cell surface .....	- 198 -
4) Perspectives.....	- 200 -
II. Mechanisms involved in the convergence of FGF and ephrin signalling ..	- 203 -
III. Potential mechanisms behind the ON/OFF response at the level of the <i>Otx</i> gene .....	- 209 -
<b>CONCLUSION</b> .....	- 215 -
<b>APPENDICES</b> .....	- 217 -
APPENDIX 1: FGF and ephrin signalling.....	- 217 -
<b>REFERENCES</b> .....	- 225 -





# INTRODUCTION

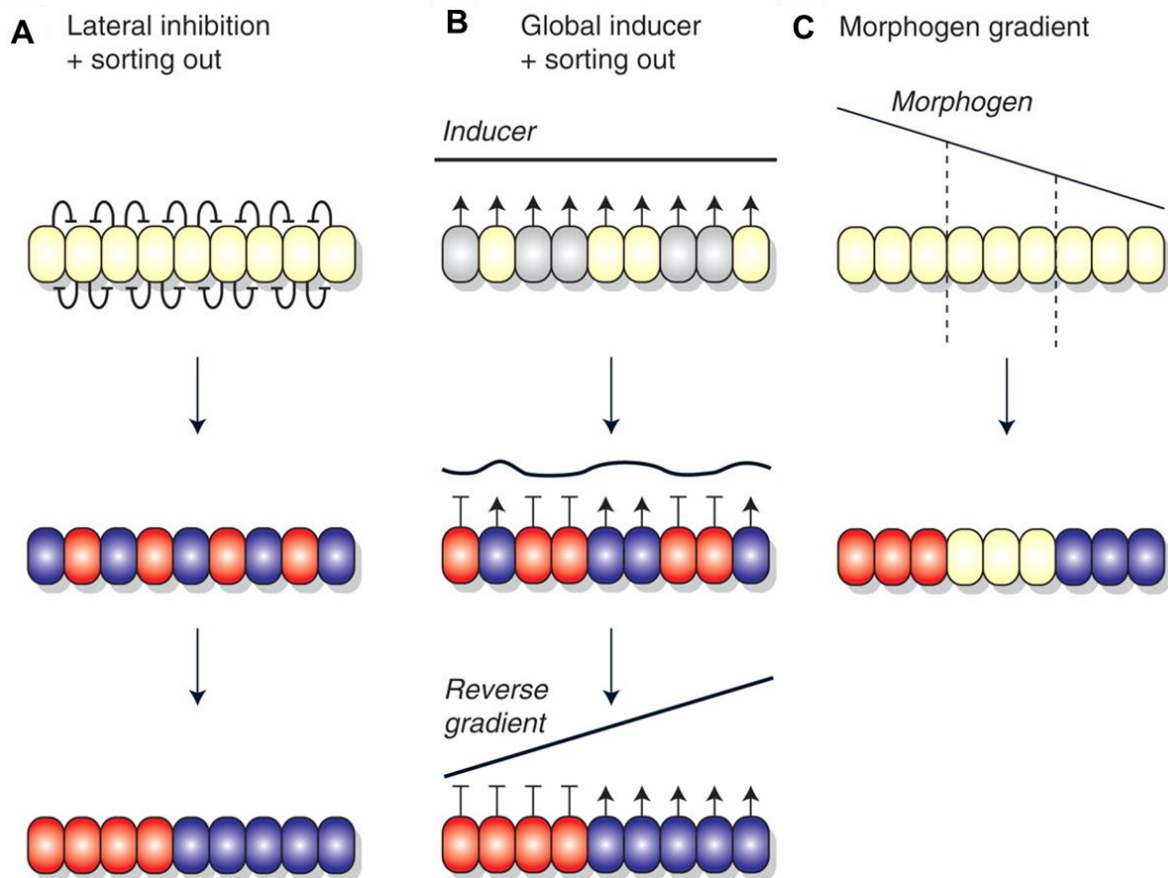


**Figure 1:** Alternative ways of patterning cells during development. (A, B) Patterning without positional information: This is a two-step process in which different cell types first differentiate mixed up with each other, and then sort out. The initial differentiation can be controlled by strictly local interactions between the cells, as in lateral inhibition (A), or by a global signal to which cells respond with different sensitivities and whose concentration they regulate by negative feedback (B). Once sorting has occurred, the global inducer forms a reverse gradient, which could then convey positional information for further patterning events. (C) Patterning by “positional information”: A group of undifferentiated cells is patterned by a morphogen diffusing from a pre-established source, producing a concentration gradient. Cells respond according to the local morphogen concentration, becoming red, white, or blue. (Adapted from Kay and Thompson 2009)

## I. Morphogen gradients in development

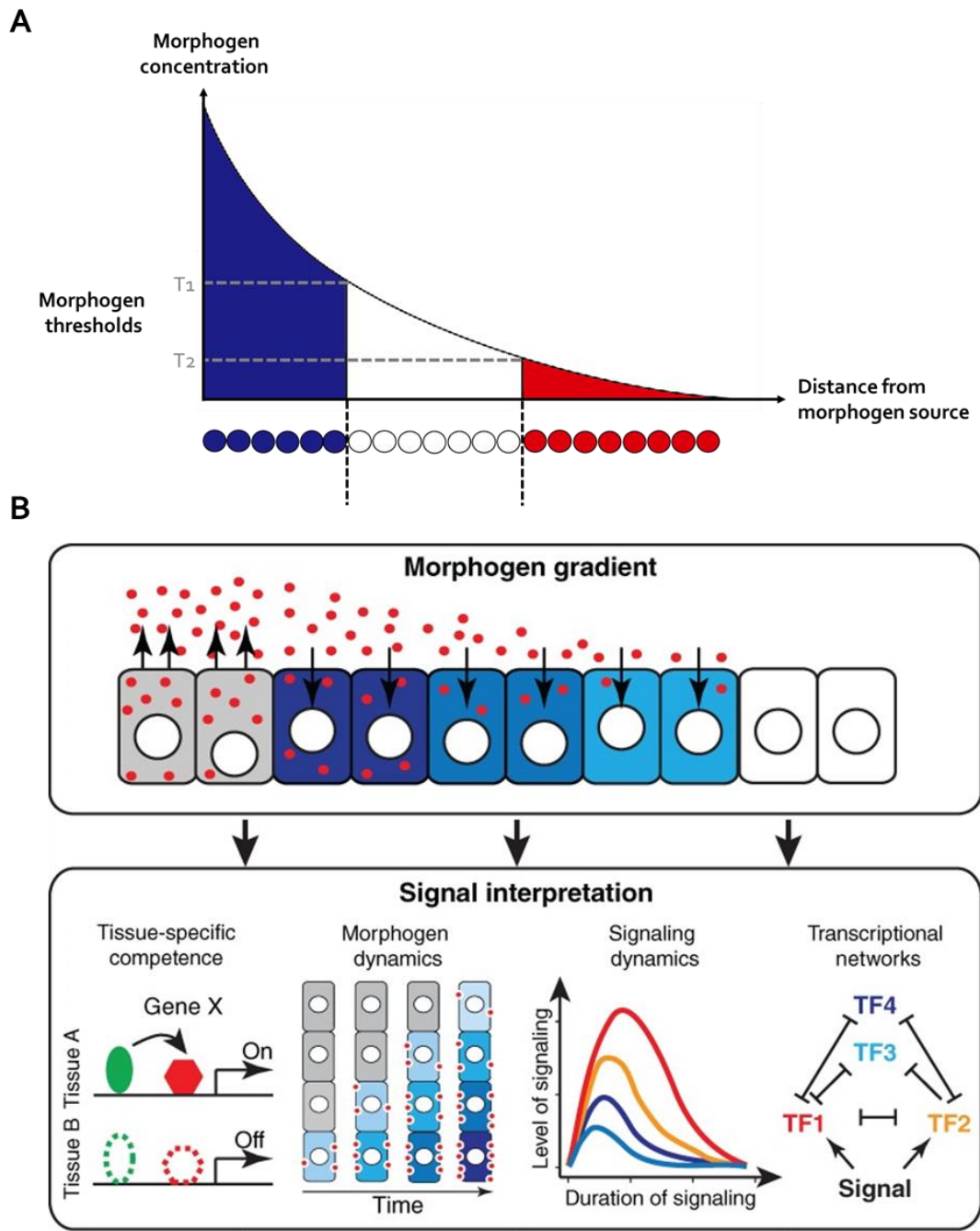
---

Two central questions in developmental biology are how cell type diversity is generated and how these types are organized into patterns of structural and functional significance. Different mechanisms can orchestrate this spatial patterning. For instance, different cell types are generated in a salt and pepper mixture in a field of cells via lateral inhibitions or heterogeneous signals and cell sorting then rearranges them into sharply bordered domains (Figure 1A-B ; Xiong et al. 2013; Kay and Thompson 2009). However, despite the existence of such mechanisms controlling spatial patterning, the most prominent one is morphogen patterning that mechanistically couples specification and spatial arrangement. This mechanism involves a gradient of a diffusible signal across a field of naive cells that defines spatial domains of cell types between concentration thresholds (Figure 1C).

The concept of “gradient” has long been recognised in order to account for pattern formation in developing embryos and regenerating tissues. Using earthworms and marine hydroids, Thomas Morgan found that regeneration occurs at different rates when animals were cut at different levels along the body axis. In order to explain these results, he suggested that there are graded “substances” along the animal and that this gradient determines both the polarity of the system and the rate of regeneration (Morgan, 1901). The term “morphogen” appears later when Alan Turing first used it to stand for any biochemical substances that diffuse between cells and generate specific responses at particular concentrations (Turing, 1952).

Lewis Wolpert then discussed, in his seminal paper of 1969, the ways that gradients might generate patterns of cell fates in a developmental field and introduced the conceptual framework of 'positional information' (Wolpert, 1969). He famously used the tricolour of the French flag to define the problem of pattern formation. In the framework of positional information, each cell in a developing or regenerating tissue acquires a unique positional value by measuring the concentration of "morphogen" that displays a spatial gradient across the field and the cell differentiates according to this positional value (Figure 2A). One of the critical requirements for this gradient model to work is the assumption that cells in a field exhibit a threshold response to specific morphogen concentrations. Finally, Francis Crick provided a mathematical theory for how a gradient might form through diffusion of the morphogen from a source at one end of the developmental field to a "sink" that destroys the chemical at the other (Crick, 1970).

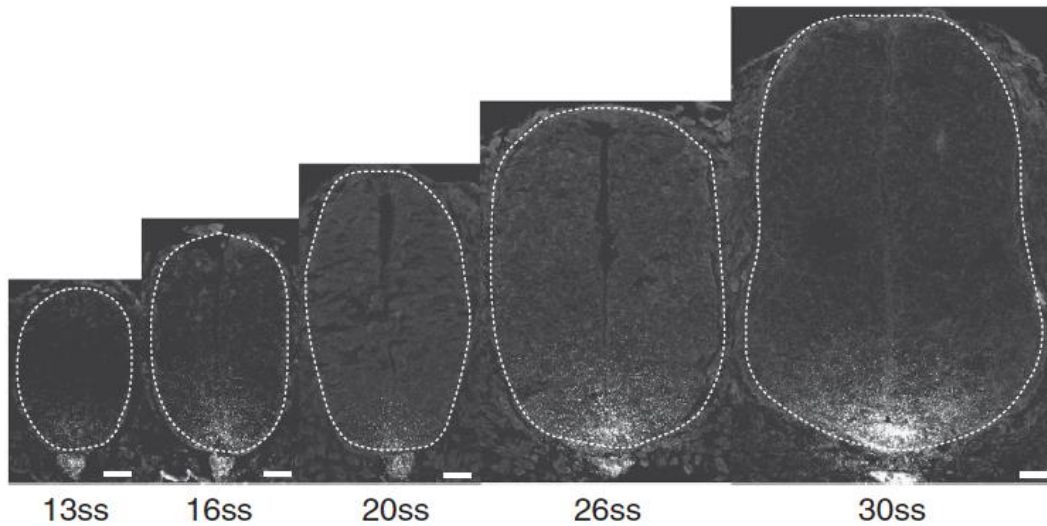
All these concepts have had a profound influence in the developmental biology community and paved the way for more detailed studies on morphogen gradients. During the 1980s and 1990s, several molecules were identified as graded patterning signals. Among these molecules, Bicoid in *Drosophila* and Sonic Hedgehog in vertebrates stand out as bona-fide morphogens based on their graded distributions and their abilities to induce distinct cellular outputs in a concentration-dependent manner. Identification of these molecules has been followed by extensive studies focusing mainly on two questions: how does a gradient form? And how do cells respond to graded signals to control differential gene expression? Over the last



**Figure 2:** (A) Schematic drawing of the Wolpert French Flag model. Cells sense if they are exposed to morphogen concentrations below or above given thresholds ( $T_1$  and  $T_2$ ) and adopt blue, white or red fate. (B) Tissue patterning during embryonic development relies on the differential induction of target genes by morphogen gradients. Induction of target genes depends not only on the level of the morphogen, but also the specific competence of receiving cells, the ability of cells to decode dynamics of morphogen signaling, and the regulatory logic of downstream transcriptional networks. (WIREs Authors, 2017)

decades, improvement of experimental techniques has made it possible to address these questions quantitatively. It has turned out that a morphogen gradient does not necessarily form via simple diffusion across its target tissue (reviewed in Zhu and Scott, 2004) and that gradient interpretations involve activation of transcriptional networks consisting of both positive and negative feedback loops (Briscoe and Small, 2015) (Figure 2B).

In the following chapter, I will describe the current understanding of how cells respond to graded signals to control differential gene expression with sharp boundaries by focusing on the above-mentioned two morphogens, Bicoid in *Drosophila* blastoderm embryos and Sonic Hedgehog in vertebrate neural tubes.

**A****B**

Neural tube time (hph: hours post headfold stage)	Embryonic stage	Number of somites
0 hph	E7.5	0
8 hph	E8.0	3-4
18 hph	E8.4	8-9
20 hph	E8.5	10-11
40 hph	E8.75	20-22
50 hph	E9.0	25-27
60 hph	E9.5	30-32
70 hph	E10.0	35-37
80 hph	E10.5	40
90 hph	E11.0	NA
100 hph	E11.5	NA

**Figure 3:** (A) SHH immunostaining in embryos of the indicate somite stages (ss) from E8.5 (around 10ss) to E10.5 (around 40ss). Scale bar 20 $\mu$ m. (B) Standardized nomenclature for mouse embryo staging. (Adapted from Cohen et al. 2015; Balaskas et al. 2012)

## 1) Shh in vertebrate neural tube

During the patterning of the neural tube along the dorsal-ventral (D-V) axis in vertebrate embryos, Sonic Hedgehog (Shh) acts as a morphogen. Shh is secreted by the ventral notochord and the floor plate and spreads to form a gradient along the dorso-ventral axis of the embryo neural tube (Figure 3). This gradient is responsible of the subdivision of the ventral half of neural tube into five neural progenitor domains; p3, pMN, p2, p1 and p0. Each of them will generate a different types of neurons: pMN generates motor neurons while p0, p1, p2 and p3 generate V0, V1, V2 and V3 interneurons, respectively (Jessell, 2000). The identity of each of these neuron types is dictated by different combinations of transcription factors (TFs) expressed in the neuronal progenitors (Guillemot, 2007).

p3 progenitors express Nkx2.2 while pMN progenitors express Olig2 and a low level of Pax6. Finally, p2 and p1 progenitors express a high level of Pax6 but not Olig2 (Figure 4A). The order of appearance of these TFs during neural tube patterning correlates with the concentration and duration of Shh required for their activation.

Experiments performed on chick neural explants showed that the increase of two or three folds of Shh concentrations promotes the switch of progenitor identities towards more ventral fates (Briscoe et al. 2000; Dessaud et al. 2007; Ericson et al. 1997; Roelink et al. 1995). Importantly, the same identity switch from dorsal to ventral fates can be obtained when the duration of exposure time to Shh is increased, suggesting that not only the strength of the Shh signal but also the duration to which cells are exposed are crucial in the neural tube patterning (Dessaud et al., 2007;

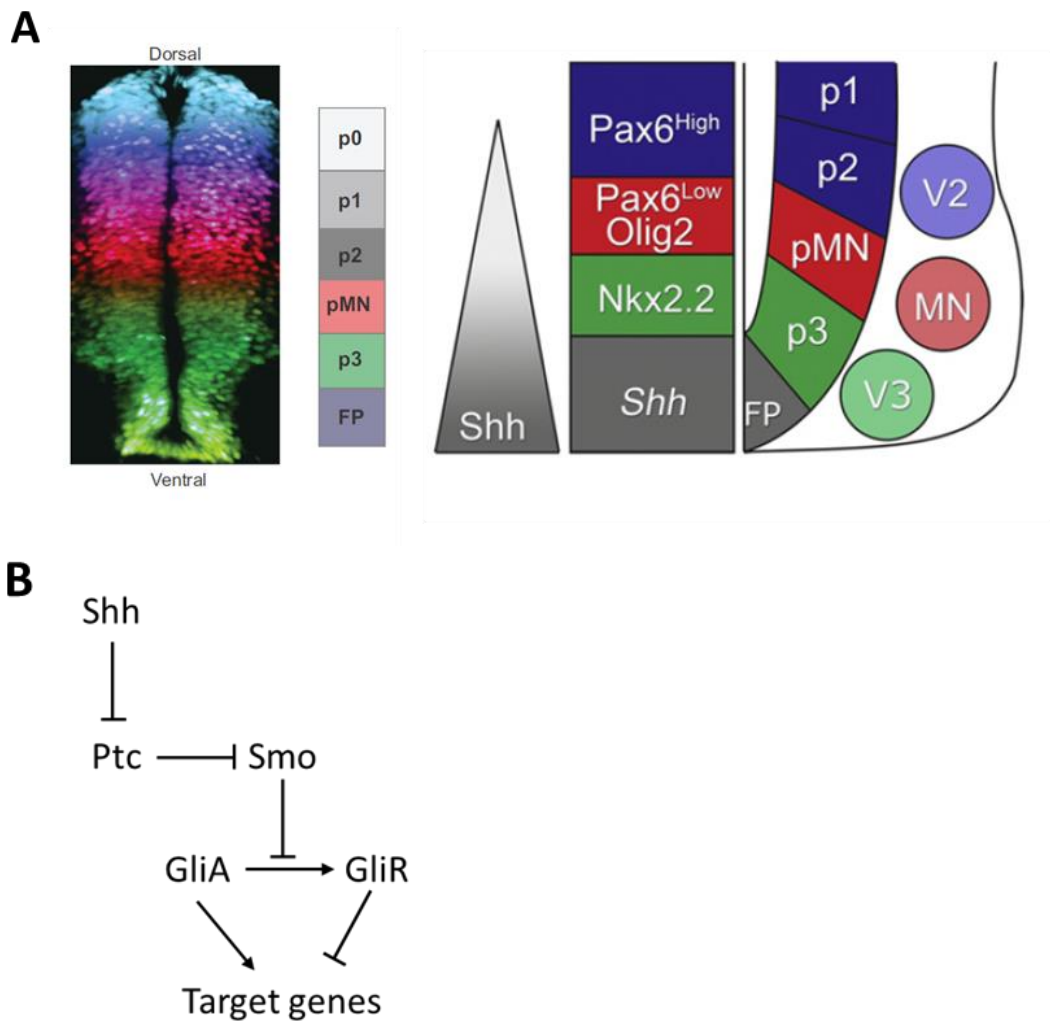


**Figure 4:** Neural progenitors establishment by Shh signalling. (A) Shh, secreted from the notochord and floor plate (FP), forms a gradient in the neural tube that divides ventral neural progenitors into molecularly distinct domains. V3 interneurons are generated from Nkx2.2+ p3 progenitors; motor neurons (MN) from Olig2+ pMN progenitors; and V2 neurons are derived from p2 progenitors, expressing Pax6, but not Olig2. (B) Shh binds to the transmembrane receptor Ptc, and this relieves repression on a second transmembrane protein, Smo. Smo activation initiates intracellular signal transduction, culminating in the regulation of Gli family TFs (Briscoe and Thérond, 2013), which are bifunctional transcriptional repressors and activators. In the absence of signal, Gli proteins are either completely degraded or processed to form transcriptional repressors (GliR), whereas Shh signalling inhibits GliR formation and instead activating forms of Gli proteins (GliA) are generated. (Adapted from Balaskas et al. 2012; Briscoe and Small 2015)

Ericson et al, 1996). Shh gradient provides cells with quantitative information which is interpreted via transcriptional regulations. The Gli family of transcription factors plays a central role in this process (Matise and Joyner, 1999). There are three members, Gli1–3, which are all expressed in vertebrate neural tubes (Lee et al., 1997; Sasaki et al., 1997). Gli2 and Gli3 are bifunctional, which work as transcriptional activators in their full-length forms (GliA) and repressors in their truncated forms (GliR) (Ruiz i Altaba, 1999; Sasaki et al., 1999). Gli1 lacks the N-terminal repressor domain and functions exclusively as an activator (Park et al., 2000). Regulation of Gli2 and 3 by Shh requires two transmembrane proteins Patched (Ptc) and Smoothed (Smo) (reviewed in Briscoe and Thérond, 2013). In the absence of Shh, Ptc inhibits Smo, leading to ubiquitination of Gli proteins. This ubiquitination results in a truncated form of Gli, GliR, which translocates into the nucleus and represses target genes. While Gli3 mainly functions as a transcriptional repressor (Litingtung and Chiang, 2000), a majority of truncated Gli2 is degraded. In presence of Shh, Shh binds to Ptc, releasing Smo from Ptc-mediated inhibition. Activated Smo blocks GliR formation and promote the formation of full-length of Gli, GliA. GliA then go to the nucleus activate Shh target genes (Figure 4B). During the neural tube patterning, Gli1 and Gli2 mainly represent GliA activity (Matise et al., 1998; Park et al., 2000). Thus, the outcome of this tightly regulated signalling cascade results in the patterning of the progenitor domains in the ventral neural tube. This cascade functions by feeding into a transcriptional network involving cross-repressive circuits (see below).

As described above, the duration of Shh signalling is an important parameter in the neural tube patterning (Dessaud et al, 2007; Ericson et al, 1996). Importantly, the amplitude of Shh gradient also increases during the neural tube patterning (Chamberlain et al, 2008). Then, at initial stages of neural tube patterning, Shh-GFP ligands localise at the apical region of ventral-most cells and then spread dorsally over time, which is accompanied by progressively-increasing levels of Shh-GFP ligands (Chamberlain et al, 2008). Since Shh gradient progresses dorsally over time, the ventral-most cells are exposed to Shh at higher concentrations and during a longer period than dorsally-located cells. These dynamic changes match with the induction of ventral genes requiring increasing level or duration of Shh signals (Dessaud et al, 2007). During initial stages of neural tube patterning, ventral-most cells exposed to a low concentration of Shh for a short period express Olig2, a pMN fate specifier (Chamberlain et al, 2008). The expression domain of Olig2 spreads rapidly to more dorsal position when Shh gradient progresses dorsally. At the same time, the level of Shh in the ventral cells increases and these cells stop expressing Olig2 and express Nkx2.2 a progenitor marker more ventral than Olig2 requiring higher level of Shh for its activation.

However, dynamics of intracellular Shh signalling does not follow that of Shh protein gradient described above. The reporter transgene, *Tg(GBS-GFP)*, in which eight concatemerized binding sites for Gli transcription factors regulate GFP expression, appears to faithfully monitor dynamics of intracellular Shh signalling (Balaskas et al, 2012). This reporter activity thus represents net activity of GliA and

GliR. Measures of Gli activity show an increase of intracellular Shh signalling during early developmental times to reach a peak between 20 and 50 hours post headfold (hph) (Figure 5B). Then, intracellular Shh signalling decreases to become low at 80hph (Balaskas et al, 2012). Contrary to Shh protein gradient which spreads dorsally over times, the intracellular level of Shh signalling is highly dynamics: it reaches a peak and then drops drastically, almost disappearing. This difference supports the idea that ventral progenitor cells exhibit the adaptation to Shh signals over time, which is consistent with the observation that chick neural explants become gradually desensitised to Shh signals (Dessaud et al, 2007). The underlying mechanism of this adaptation includes downregulation of Gli2 protein expression during neural tube patterning (Cohen et al. 2015).

The dynamics of Gli activity during neural tube patterning was directly compared to expression of Shh-downstream genes, namely Pax6, Olig2 and Nkx2.2 to address how the dynamic Gli activities are translated to generate and maintain the precise neural tube patterning (Balaskas et al., 2012). At each stage, Nkx2.2 expression domain was correlated with domain reporting the highest levels of Gli activity (Figures 5Ai-5Aiv). At 18hph, cells with low levels of Gli activity express Olig2 and low levels of Pax6 (Figures 5Aii and 5Av). At 50 hph, cells expressing Olig2 and Pax6 show a clear decrease in *Tg(GBS-GFP)* activity (Figures 5Aiii and 5Avi). Finally, high levels of Pax6 were only observed in cells without any Gli activity. However, cells positioned at the boundary p3/pMN show the same level of Gli activity but they express either Olig2 or Nkx2.2. Thus, the induction of Nkx2.2 and Olig2 does not appear to be determined

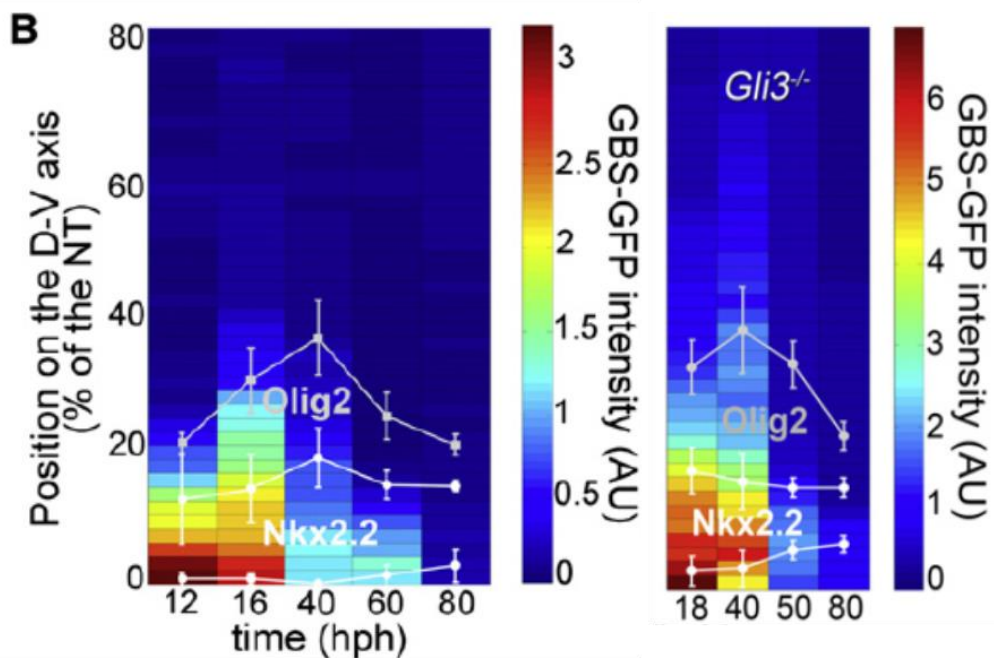
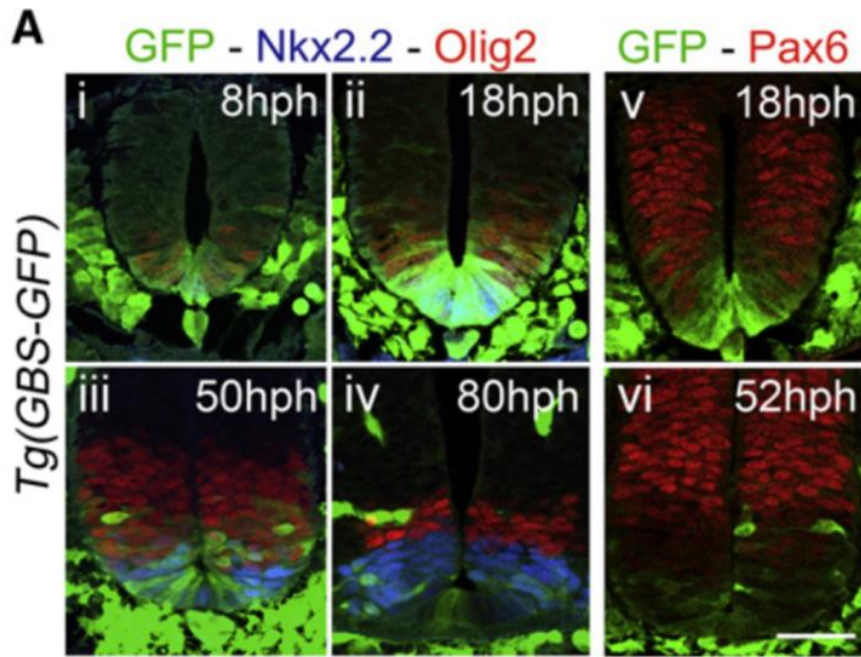


**Figure 5:** (A) GFP (green), Olig2 (red), Nkx2.2 (blue), and Pax6 (red) at brachial level in *Tg(GBS-GFP)* embryos at the indicated stages. (B) Heat map of GFP intensity in *Tg(GBS-GFP)* embryos and *Tg(GBS-GFP) Gli3<sup>-/-</sup>* embryos at relative positions measured from the basal side of floor plate cells (percentage [%] of the neural tube) at the indicated stages. The position of the dorsal boundary of Olig2<sup>+</sup> and the dorsal and ventral boundaries of Nkx2.2<sup>+</sup> domains (mean  $\pm$ SD) are indicated. Scale bars, 50  $\mu$ m. (Adapted from Balaskas et al. 2012)

simply by a fixed threshold of Gli activity. Analysis of mice mutant lacking *Gli3* (*Gli3*<sup>-/-</sup>) further supports this absence of a clear correlation between Gli activity and gene expression (Balaskas et al, 2012). Since Gli3 has a repressor function in the Shh signalling, *Gli3*<sup>-/-</sup> mutants show an increase of *Tg(GBS-GFP)* activity. However, despite this increase, no difference in the expression profile of Olig2 and Nkx2.2 were observed (Figure 5B). Taken together, these results demonstrate that thresholds at the level of Gli are not sufficient to pattern correctly the neural identities.

Within the neural tube, boundaries position of p3 and pMN is partly regulated by cross-repressive interactions between Pax6, Olig2 and Nkx2.2 (Briscoe et al., 1999; Briscoe et al., 2000; Ericson et al., 1997; Novitsch et al., 2001) (Figure 6). Accordingly, Pax6 represses Nkx2.2, whereas Olig2 inhibits Pax6 expression. Conversely, Nkx2.2 represses Pax6 and Olig2. This cross-repressive transcription circuit plays a crucial role, in association with the Gli activity gradient, in establishing the Shh morphogen response in neural progenitors. Mathematical modelling of the Pax6-Olig2-Nkx2.2 network permits to link the temporal dynamics with the graded response established in neural progenitors (Figure 6) (Balaskas et al, 2012). At  $t_0$ , low levels of Shh produced by the notochord are translated in a low level of intracellular GliA, which is not sufficient to induce Olig2 or Nkx2.2 or to repress Pax6. Shh production subsequently increases, leading to formation of GliA gradient at  $t_1$ . The GliA gradient activates *Olig2* in the ventral-most cells, in which Olig2 represses *Pax6*. When GliA gradient reaches its peak at  $t_2$ , *Nkx2.2* is induced in cells that have been exposed to the highest levels of Shh and Nkx2.2 in turn represses *Olig2* and *Pax6*. When the GliA gradient retracts at  $t_3$ ,

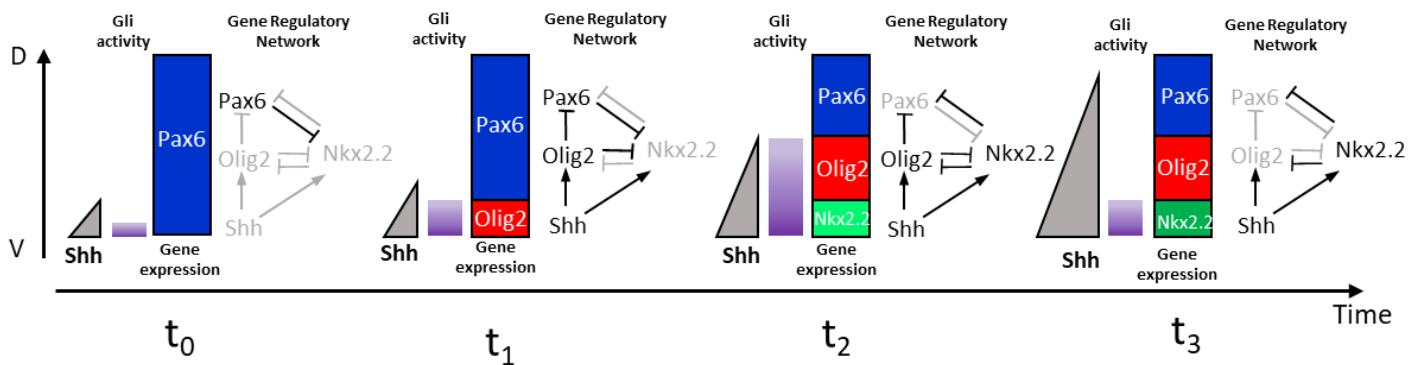


**Figure 6:** Schematic of Shh signalling-mediated patterning of the ventral neural tube. At  $t_0$ , low levels of Shh protein, emanating from the notochord, are translated into low levels of intracellular Gli activity, which are not sufficient to induce Olig2 and Nkx2.2 or to repress Pax6. As development progresses, increasing production of Shh ligand generates a gradient of Gli activity that increases in amplitude ( $t_1$ ), then reaches a peak ( $t_2$ ) before retracting ( $t_3$ ). Gli activity is interpreted by ventral progenitors by the GRN: Olig2 is initially induced ( $t_1$ ) and represses Pax6. Subsequently, Nkx2.2 is induced ( $t_2$ ) and represses Pax6 and Olig2. Hysteresis maintains these domains of expression as the amplitude of the Gli activity decreases ( $t_3$ ). (Adapted from Balaskas et al. 2012)

the expression domains of Nkx2.2, Olig2 and Pax6 are maintained. This is due to hysteresis (i.e. memory of the signal) conferred by the gene regulatory network: the level of Shh/Gli required to maintain the expression of Nkx2.2 is lower than the one needed to initially induce Nkx2.2 (Balaskas et al, 2012). Thus, even when the level of Shh/Gli is low at t3, it is sufficient to maintain the expression of Nkx2.2 and therefore the expression of Olig2 and Pax6 in the right order to pattern the neural tube.

Shh morphogen in the developing vertebrate neural tube is a complex and fascinating system to study how a morphogen signal is integrated and interpreted by cells. Shh gradient along the D-V axis of the neural tube is translated at the intracellular level into a gradient of net-transcriptional activity of Gli. This gradient of Gli activity will then feed into a transcriptional network involving cross-repressive circuits between Pax6, Olig2 and Nkx2.2. Importantly, this transcriptional network integrates dynamic inputs in both spatial and temporal dimensions so that neural progenitors adopt and maintain the right neuronal identities. For example, the differential responses of Nkx2.2 and Olig2 to the spatio-temporal gradient of Shh are determined by the regulatory architecture of the transcriptional network and not by differences in the intrinsic responsiveness of these two genes to Shh signals (Balaskas et al, 2012). I should highlight that this conclusion is consistent with the role of the transcriptional network downstream of Bcd gradient operating during nuclear cycle 14 in the *Drosophila* cellular blastoderm embryo but is in a stark contrast to the switch-like transcriptional response of *hb* gene to Bcd gradient in syncytium blastoderm embryos.



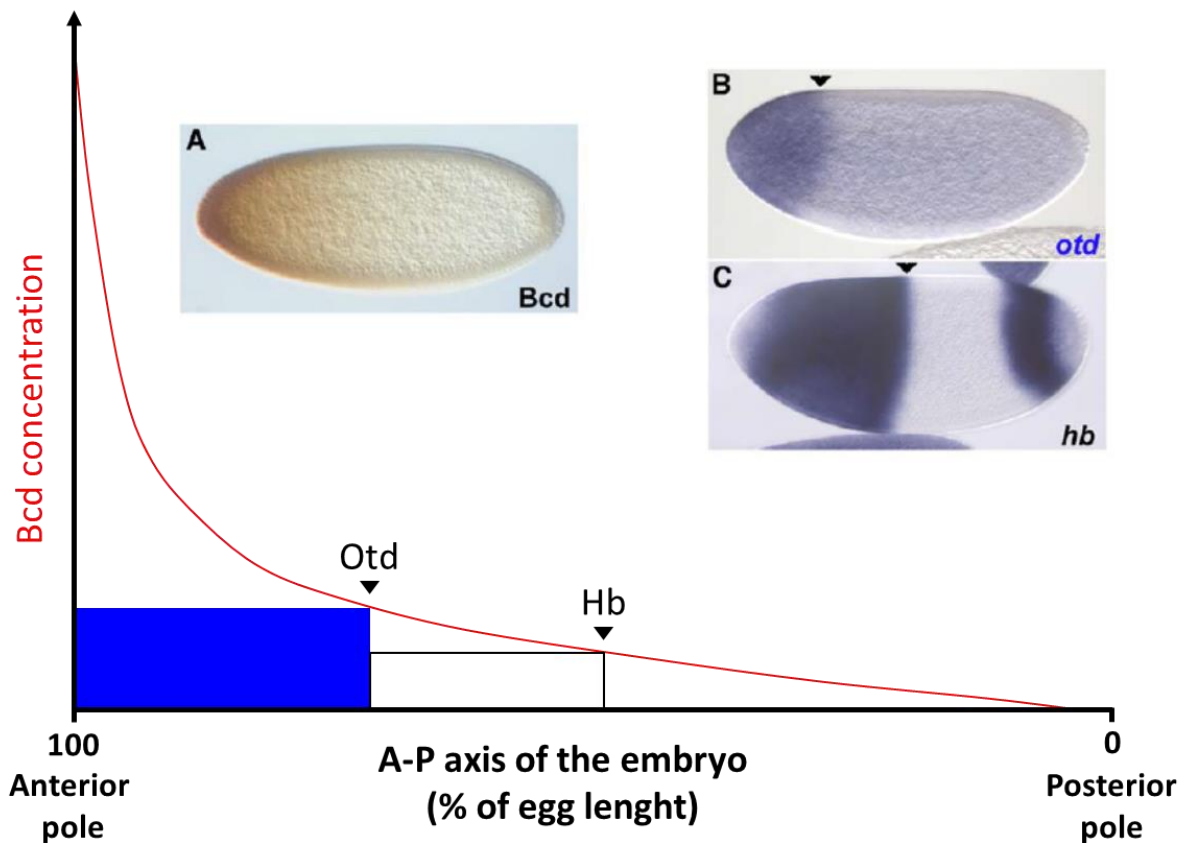


**Figure 7:** The Bcd Morphogen in the blastoderm embryo and the French Flag Model. The Bcd gradient with its highest point at the anterior pole revealed by antibody staining (A) and expression of the two Bcd target genes, *otd* (B) and *hb* (C), revealed by in situ hybridization performed with antisense probes. The position of the posterior border of expression is indicated with arrowheads. The concentration gradient of the Bcd protein (arbitrary units) is indicated on the graph by a dotted line as a function of the percentage of EL. According to the French flag model, the two target genes, *otd* (blue) and *hb* (white), are expressed at concentrations of Bcd above a specific threshold indicated by the arrowheads. Note that the posterior expression of *hb* is not dependent on Bcd. Anterior is at the left. (Adapted from Crauk and Dostatni 2005)

## 2) Interpretation of Bicoid gradient

### a. Background

Early embryogenesis of *Drosophila* is unique with cell cycles proceeding without cytokinesis, forming a syncytium blastoderm. At the nuclear cycle (nc) 14, cellularisation takes place enveloping the nucleus with plasma membranes. In this atypical system, the maternal gene, *bicoid* (*bcd*), is involved in the anterior patterning of *Drosophila* embryo: *bcd* mutant embryos lack head and thoracic segments and duplicates posterior structures at the anterior pole (Frohnhofer and Nüsslein-Volhard, 1986). Bcd is a homeodomain transcription factor that directly activates expression of its target genes in distinct anterior domains embryo (Driever and Nüsslein-Volhard, 1988a; Driever and Nüsslein-Volhard, 1988b). *bcd* mRNA is present in the unfertilized egg anchored to the cortex of the anterior pole in an inactive configuration. Fertilization triggers activation of mRNA translation and the Bcd proteins diffuse and form a gradient along the anterior-posterior (A-P) axis. Bcd proteins are distributed in an exponential concentration gradient with a maximum at the anterior tip (Figure 7) and that increases or decreases in Bcd gradient levels in the embryo cause a corresponding posterior or anterior shift of anterior anlagen in the embryo (Driever and Nüsslein-Volhard, 1988a; Driever and Nüsslein-Volhard, 1988b). These shifts of anlagen correlate with corresponding shifts of posterior boundaries of Bcd-dependent genes (Struhl and Macdonald 1989). These studies have thus placed *Bcd* as the first bona-fide morphogen.

The Bcd gradient was thought to form following the “Synthesis/Diffusion/Degradation (SDD)” model proposed by Crick (Crick 1970). In this model, it is assumed that Bcd proteins are synthesized at a constant rate at the anterior pole and then diffuse freely along the A-P axis of the embryo. Importantly, the model assumes that Bcd proteins are degraded homogeneously in the embryo. Bcd gradient is established in 90 minutes in embryos following fertilization, indicating that Bcd molecules move rapidly (Gregor et al., 2007a). While fluorescence recovery after photo-bleaching (FRAP) experiments have shown that they diffuse too slowly to be compatible with the first establishment (90 mins) of the gradient via a simple diffusion model (Gregor et al., 2007a), a subsequent study based on fluorescence correlation spectroscopy (FCS) has revealed instead a higher diffusion coefficient of Bicoid molecules that is consistent with the idea that the Bcd gradient formation operates under the regime of the SDD model (Abu-Arish et al., 2010).

Bcd-target genes are expressed with sharp-posterior borders that are precisely placed along the A-P length of blastoderm embryos. Then, to what extent is the Bcd gradient precise and reproducible? Immunofluorescence analyses showed that the Bcd gradient exhibits some variability among embryos, indicating that the variability of Bcd gradient is somehow filtered to establish the precise borders of target gene expression (Houchmandzadeh et al., 2002). This study was followed by quantitative live imaging to establish the temporal and spatial dynamics of Bcd gradient in blastoderm embryos (Gregor et al., 2007b). A series of direct measurements demonstrated that the Bcd gradient is indeed reproducible from embryo to embryo.

Similarly, within single embryos, the Bcd gradient is precisely converted to expression of its target *Hunchback* (*Hb*) (Gregor et al., 2007b). It should be noted that the latter finding is based on Hb protein levels at nc14. It should also be highlighted that the posterior boundary separating Hb-high and Hb-low nuclei is very steep despite the subtle difference in the Bcd concentration (approximately 10%) on either side of the boundary (Gregor et al., 2007b). How such precision is achieved will be the subject that I aim to synthesize in the following section.

#### **b. Switch-like transcriptional activation of Bcd target genes**

The gap gene *hb* represents the best studied Bcd target gene. *hb* is expressed in a broad domain in the anterior half of the syncytium blastoderm embryo (Tautz, 1988; Tautz et al., 1987). Early studies have revealed that the extent to which a Bicoid target gene is expressed along the A-P axis appears to depend on the affinity of Bcd binding sites in its enhancer: the higher the affinity of Bcd binding sites is, the more posteriorly the expression domain of target gene expands (Driever et al., 1989; Struhl et al., 1989). Importantly, it was also observed that when the number of Bcd-binding sites, whether they were low- or high-affinity sites, was increased in reporter constructs, the posterior boundary of reporter expression becomes sharper. Accordingly, it was proposed that cooperative binding effects might contribute to the sharpening of the border of expression (Driever et al., 1989). Consistent with this proposal, it has been shown that a recombinant Bicoid protein binds cooperatively to its sites within a *hunchback* enhancer element, resulting in a sigmoidal binding curve (Ma et al., 1996). Specifically,

a Bcd monomer which binds a high-affinity site facilitates the binding of a second Bcd monomer to an adjacent low-affinity site (Burz, 1998). Later, this cooperative DNA binding has been proved to be a key mechanism for transcriptional regulation of the Bcd target genes. Using a genetic screen in yeast, *Bcd* mutants with no cooperative DNA binding were isolated. When these mutant forms of *Bcd* were introduced to *Drosophila*, they were unable to control the level of target genes including *hb* and were unable to generate a sharp posterior border in the *hb* expression domain (Lebrecht et al., 2005). Despite these accumulating evidences supporting that the affinity and cooperativity of Bcd binding underlie the transcriptional interpretation of Bcd gradient, it has been shown that the boundary positions of a large set of Bcd target genes do not correlate with the affinity or number of Bcd binding sites in their associated regulatory sequences (Ochoa-Espinosa et al., 2005).

It is now clear that other elements in target gene promoters and the integration of positive and negative transcriptional inputs from proteins bound to these elements are major determinants for the interpretation of positional information along the A-P axis. Among these regulators are Bcd-targets themselves, highlighting that the gradient interpretation operates at the level of transcriptional network involving cross-regulations. Bcd first activates *sloppy-paired 1 (slp1)* and *giant (gt)*, both of which encode repressors and set the anterior boundaries of *runt (run)* and *krüppel (kr)*. Run and Kr are themselves transcriptional repressors. Together with the maternal repressor Capicua (Cic) which is excluded from the terminal regions of the embryo, Run and Kr act to set the posterior boundaries of Bcd-target genes including *slp1* and *gt*. Therefore,

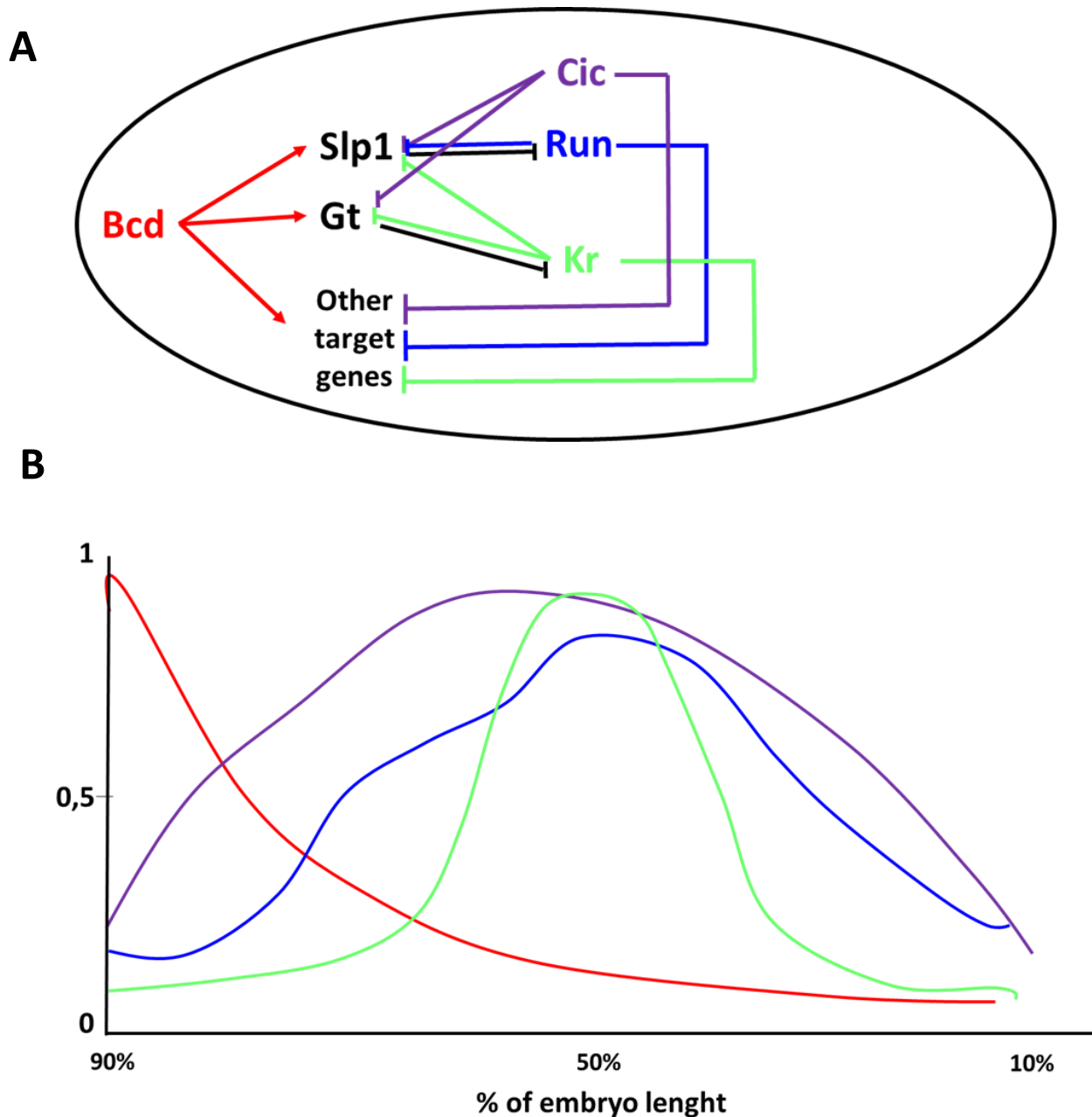


**Figure 8:** A Network of Repressors Registers Bcd-Dependent Posterior Expression Boundaries. (A) Model of gene expression boundary registration in the anterior half of the embryo. The Cic repression gradient is established via Tor downregulation of Cic at the anterior tip. Bcd activates *slp1* and *gt*, which encode repressors that set the anterior boundaries of run and Kr transcription. The Cic, Run, and Kr gradients repress Bcd-dependent activation of target genes, including *slp1* and *gt* themselves. (B) Average expression profiles of Bcd (n = 8), Kr (n = 6), Run (n = 8), and Cic (n = 8). (Adapted from Chen et al. 2012)

Run, Cic and Kr are the principal components of a repression system that correctly orders posterior boundaries of Bcd-target genes across the anterior half of the embryo (Figure 8) (Chen et al., 2012). Finally, in embryos in which the Bcd gradient has been flattened by genetic manipulation, several target genes continue to form well-defined boundaries that are shifted in position but nonetheless correctly ordered along the patterning axis, challenging a simple relationship between Bcd gradient and threshold responses (Chen et al., 2012; Löhr et al., 2009; Ochoa-Espinosa et al., 2009). However, many of these studies was conducted during nc14. The Bcd gradient is already established at nc8, more than two hours before these analyses were conducted. Furthermore, it has been shown that a synthetic reporter containing only Bcd binding sites could establish a sharp expression border (Crauk and Dostatni, 2005). In order to address how the Bcd gradient is interpreted to activate target genes with sharp borders, it is necessary to focus on those activated during early stages. I will discuss below a series of studies focusing on transcriptional interpretation of the Bcd gradient to activate one of such genes, *hb*.

RNA-FISH has allowed to detect nascent *hb* transcripts as bright dots, each of which represents an active *hb* locus, enabling to quantify the probability for an *hb* locus to be in an active or inactive (Porcher and Dostatni, 2010). *hb* loci become active in anterior nuclei as early as at nc9 with a clear posterior border. However, the posterior border remains somehow variable from embryo to embryo during nc9 and nc10 (SD 4.6% and 5.5% relative to embryo length (EL), respectively). At nc11, thirty minutes after nc8, *hb* expression becomes reproducible with the precision of 2.3% EL among

embryos. The minimal distance between *hb*-ON and *hb*-OFF nuclei in the posterior border region is estimated at around 2% EL at nc11, indicating that a relative difference in Bcd concentration of 10% can be converted into an ON or OFF state of the *hb* locus in the border region (Porcher and Dostatni, 2010).

Expression of endogenous *hb* is initiated at two different promoters, the distal promoter P1 and the proximal promoter P2, with P2 mediating the early Bcd-dependent expression (Schröder et al., 1988). The MS2-MCP system was applied to shed light on dynamics of the *hb* expression boundary formation during early nuclear cycles by generating *Drosophila* embryos carrying a transgene driving a reporter gene with MS2 repeats under control of the P2 promoter (Lucas et al., 2018). At each nuclear interphase (from nc11 to nc13), *hb* expression first occurs in the anterior then proceeds to the boundary region, which is likely reflecting dose-dependent activation by Bicoid. Furthermore, transcription of the *hb-MS2* reporter is bursty both in the anterior and boundary regions (Desponds et al., 2016) with *hb* transcription output (see Lucas et al., 2018 for the definition) being more variable around the boundary than in the anterior region. The *hb-MS2* reporter has also revealed that the *hb* boundary is established within 3 minutes at each nc with a very high steepness (Hill coefficient of around 7) (Lucas et al., 2018). This indicates that the system is able to measure extremely rapidly subtle differences of Bcd concentration and produce a sharp border. To understand how embryos can interpret the Bcd gradual information into a switch-like response in only 3 minutes, theoretical modelling has been conducted. The model is based on the cooperativity between six Bcd binding sites of the *hb* promoter. This model is able to

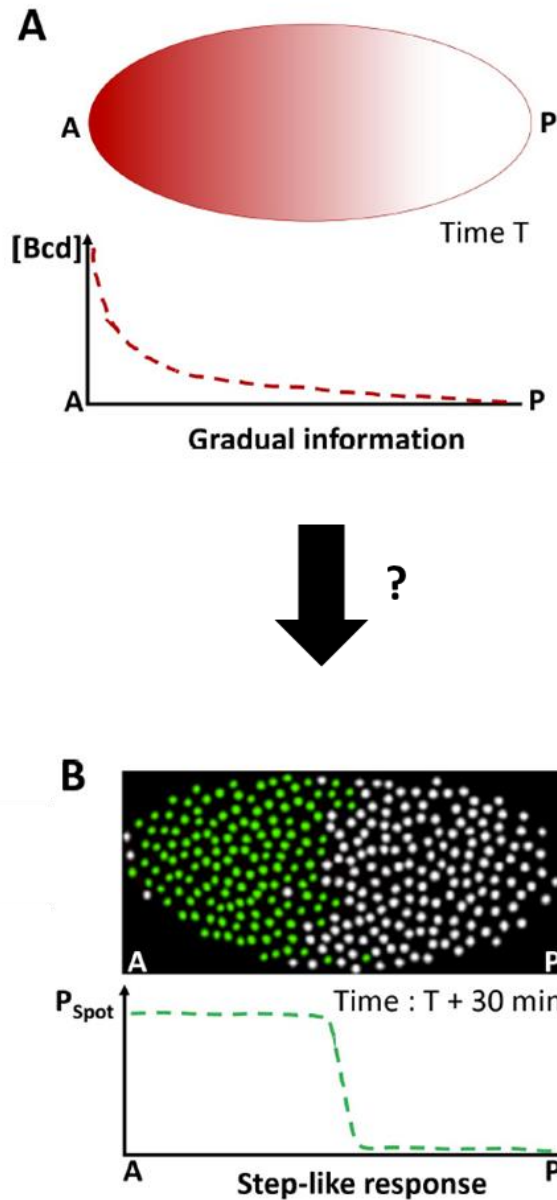


**Figure 9:** The Bicoid system transforms the gradual information contained in the Bicoid concentration gradient into a step-like response in 30 min. (A) At nc 8 ( $T = 1$  hr), the Bicoid exponential gradient (red) is steadily established with its highest concentration at the anterior pole (A) and its lowest concentration at the posterior pole (P). The first hints of zygotic transcription are detected by RNA FISH marking the onset of zygotic transcription. (B) At nc 11 ( $T = 1$  hr 30 min), the main Bicoid target gene, hunchback (hb), is expressed within a large anterior expression domain. hb expression is schematized here from RNA FISH data: nuclei where ongoing transcription at the hb loci is detected are shown in green and nuclei silent for hb are shown in white. (Adapted from Lucas et al. 2018)

reproduce the speed of the process but is not sufficient to explain the steepness of the boundary of *hb* expression domain (Lucas et al., 2018). This result indicates that repressors of maternal origin expressed as gradients in the posterior region could contribute to the steepness of the *hb* boundary similarly to the role played by zygotic repressors (Run and Kr) at nc14. Potential candidates include Caudal, which forms a posterior-to-anterior gradient but so far has been described as a transcriptional activator (Juven-Gershon et al., 2008), or Capicua, a transcriptional repressor present in the center of the A-P axis (Löhr et al., 2009).

In summary, despite its central role in setting gene expressions along the A-P axis of the *Drosophila* blastoderm, it is yet to fully understand how the smooth Bcd gradient is converted to switch-like transcription activation of target genes (Figure 9). The affinity of the binding sites and the cooperativity play a crucial role in the interpretation of the gradient. It has also been shown in late blastoderm embryos that Bcd takes part in a more complex regulatory network involving mutual repressions to order gene expression along the A-P axis. However, the fact that synthetic reporters with only Bcd binding sites "can" establish remarkably steep posterior boundaries suggests that Bcd and Bcd binding sites are sufficient to generate a switch-like transcriptional response (Crauk and Dostatni, 2005). It would be interesting to study dynamics of the synthetic reporter by applying the MS2-MCP system.



## II. ERK signalling dynamics

---

My PhD project involves quantitative descriptions of FGF-induced ERK activation and immediate early transcriptional responses during an embryonic induction. In this section, I will describe our current understandings of ERK signalling dynamics.

### 1) Background

The Extracellular-signal-Regulated Kinase (ERK) signalling pathway is used repeatedly during embryonic development in metazoans for patterning, cell fate determination, cell proliferation and cell migration (Brewer et al, 2016). In studies on animal models of development, loss or reduction of ERK activation results in severe developmental defects. Excessive ERK signalling, well known for its link to cancers (Hanahan and Weinberg, 2011), has also recently been linked to a large class of human developmental syndromes called RASopathies (Rauen, 2013). Affected individuals display congenital malformations, including craniofacial malformations and cardiac abnormalities, along with neurocognitive delay and an increased risk of cancer. Thus, precise control of ERK activity is critical in both embryonic and adult life. Since both reduced and excessive activation of the ERK signalling pathway can derail normal development, its developmental control must be understood quantitatively. However, quantitative analyses of ERK signalling in *in vivo* multicellular contexts are recent and still limited (Boxtel et al., 2018; de la Cova et al., 2017; Hiratsuka et al., 2015; Johnson

and Toettcher, 2019; Johnson et al., 2017; Lim et al., 2015; Moreno et al., 2019; Ogura et al., 2018).

The basic biochemistry of the ERK signalling pathway is well elucidated (Kolch, 2000). The ERK signalling cascade is frequently employed to transduce ligand-activated receptor tyrosine kinases (RTKs). Downstream of receptor activation, the core components, including the small GTPase Ras (most notably H-Ras or K-Ras), the serine/threonine kinase Raf and the threonine/tyrosine kinase MEK, culminate in the activation of the serine/threonine kinase ERK (Figure 10). Ras is membrane-anchored and exhibits two regulatory states; a GDP-bound inactive state and GTP-bound active state. The regulatory status of Ras is controlled by the opposing activities of guanine nucleotide-exchange factors (GEFs), typically SOS, which catalyses the exchange of GDP for GTP, and GTPase-activating proteins (GAPs), which increase the rate of GTP hydrolysis to GDP. GTP-bound active Ras recruits Raf to the cell membrane for activation. Raf phosphorylates and activates MEK, which in turn phosphorylates and activates ERK. The covalent modification of ERK takes place at two sites, generally in a non-processive (=distributive) manner, that is, one modification per substrate-enzyme collision (Burack and Sturgill, 1997; Ferrell and Bhatt, 1997). Activated ERK then phosphorylates a number of protein targets, including transcription factors, to modulate their activity. For example, the transcriptional activity of Ets1 and Ets2, transcription factors belonging to the E-twenty-six (ETS) family, are stimulated by ERK-dependent phosphorylation (reviewed in McCarthy et al., 1997; Sharrocks, 2001; Yang et al., 1996).

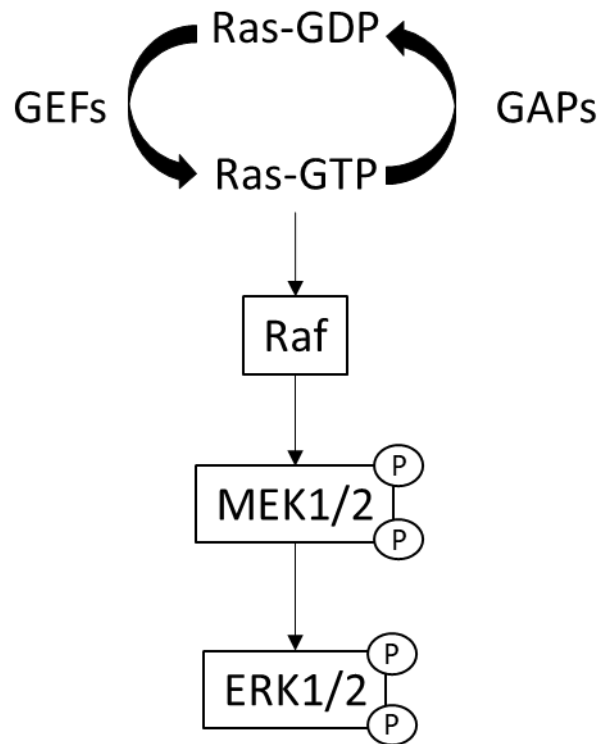


**Figure 10:** ERK signalling cascade. Ras is membrane-anchored and exhibits two regulatory states; a GDP-bound inactive state and GTP-bound active state. The regulatory status of Ras is controlled by the opposing activities of guanine nucleotide-exchange factors (GEFs), typically SOS, which catalyses the exchange of GDP for GTP, and GTPase-activating proteins (GAPs), which increase the rate of GTP hydrolysis to GDP. GTP-bound active Ras recruits Raf to the cell membrane for activation. Raf phosphorylates and activates MEK, which in turn phosphorylates and activates ERK.

In the genome of the ascidian *Ciona robusta*, ERK signalling pathway components are present as single representative orthologues (e.g. *Ciona* MEK1/2 represents both vertebrate MEK1 and MEK2) (Satou et al., 2003). Curiously, the *Ciona* genome lacks genes encoding classical Ras, including H-Ras, K-Ras, and N-Ras (Keduka et al., 2009; Satou et al., 2003). The lack of classical Ras is compensated by M-Ras, which mediates the ERK signalling pathway in *Ciona* embryos as it also can in mammalian cells (Keduka et al., 2009; Kimmelman et al., 2002; Sun et al., 2006).

## 2) Temporal dynamics of ERK signalling

A growing number of studies are revealing that the temporal dynamics of intracellular signalling cascades encode fundamental information that controls cell fate decisions (Purvis and Lahav, 2013). The recent development of genetically encoded reporters of ERK activity have allowed its real-time, quantitative measurement at single-cell resolution. The techniques include Förster Resonance Energy Transfer (FRET) (Komatsu et al., 2011), nuclear translocation (Regot et al., 2014) and intracellular aggregation (Zhang et al., 2018) of fluorescent proteins induced by phosphorylation of ERK substrate peptides, and ERK tagged with fluorescent proteins showing activity-dependent nuclear–cytoplasmic shuttling (Ando et al., 2004). These studies have revealed that ERK signalling can be transduced in cells as a single transient pulse, oscillatory pulses (Albeck et al., 2013; Aoki et al., 2013; Hiratsuka et al., 2015) or sustained activation (Yamamoto et al., 2006) and they have led to the hypothesis that

information encoded as temporal dynamics instructs cells to express a variety of outcomes (reviewed in Purvis and Lahav 2013).

A rat adrenal pheochromocytoma cell line, PC12, is a classic biological system whereby distinct modes of temporal dynamics of ERK activation induce different cell fate decisions. Treatment of PC12 cells with nerve growth factor (NGF) induces sustained ERK activation and promotes neuronal differentiation whereas stimulation with epidermal growth factor (EGF) induces transient ERK activation, leading to cell proliferation (Marshall, 1995). When PC12 cells overexpressing exogenous EGF receptors are treated with EGF, they exhibit a sustained ERK activation and differentiate into neurons, indicating that the duration (=cumulative dosage) of ERK activation controls the cell fate decision (Traverse et al., 1994). Network configuration in which the ERK signalling cascade is embedded appears to determine its temporal dynamics. Modular Response Analysis (MDA) (Kholodenko, 2007) has revealed that, upon EGF stimulation, the network exhibits a negative feedback whereas a positive feedback is deployed following NGF stimulation (Santos et al., 2007).

Oscillatory pulses of ERK activation is also linked to a specific cellular response (Aoki et al., 2013). Normal rat kidney epithelial (NRK-52E) cells exhibit stochastic ERK activity pulses when they are at intermediate cell density. In contrast, when they are cultured at low cell density, NRK-52E cells exhibit sustained basal ERK activation. Importantly, the two modes of ERK signalling dynamics correlate with cell proliferation rates in the two culture conditions with cells at sparse densities replicating more slowly than those at intermediate densities. In order to address this correlation directly, Aoki

et al (2013) have successfully developed a light-inducible ERK activation system based on the CRY2-CIB1 interaction. The system involves blue light-dependent membrane recruitment of CRY2-fused C-Raf via membrane-bound CIB1 (CIB1-KRasCT) (Figure 11A). Synthetic ERK activity pulses generated by this optogenetic system accelerated cell proliferation while synthetic sustained activation didn't affect proliferation rates.

As described above, one of the prominent outputs of ERK activation is transcriptional activation. Activated (double-phosphorylated form) ERK translocates to the nucleus and controls transcription of immediate early genes (IEGs). Whether the temporal dynamics of ERK activation influences transcription of immediate early genes was addressed by combining optogenetic control of the ERK signalling cascade and direct observation of transcriptional activities using the MS2/MCP system in NIH 3T3 cells (Wilson et al., 2017). In this study, the Phy-PIF system was used to generate the catalytic domain of SOS fused to PIF and a membrane-tethered photo-switchable Phy-CAAX so that the membrane localisation of PIF-SOScat can be triggered on and off by exposure to 650 and 750nm light (Opt-SOS system) (Figure 11B). Synthetic sustained ERK activation was applied, all five tested IEGs exhibits similar dynamics with a transient peak of activation followed by "adaptation" to the basal level. This adaptation is mediated in part by a negative feedback consisting of dephosphorylation of the nuclear ERK by DUSPs (dual specificity phosphatases), which are themselves IEGs of ERK signalling. When cells are challenged with synthetic oscillatory ERK activation with 20 mins ONs interspaced with variable lengths of OFF, the five genes tested are

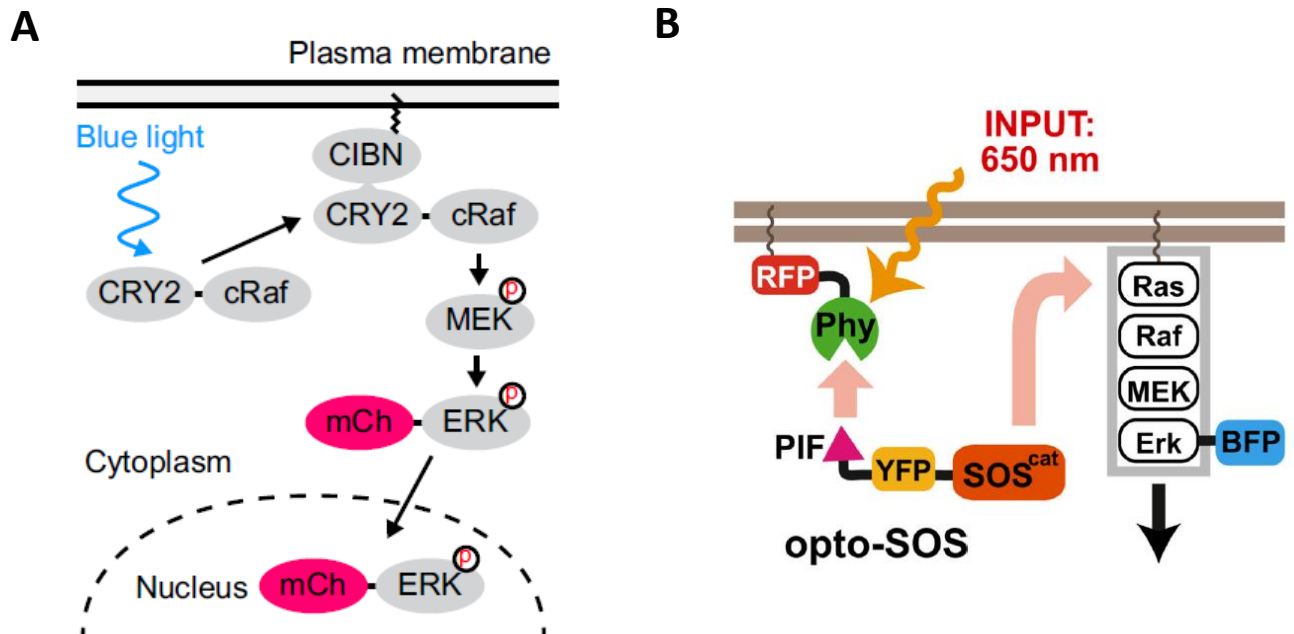


**Figure 11:** (A) Scheme of light-switchable ERK activation system. This system was based on *Arabidopsis thaliana* cryptochrome 2 (CRY2)-fused cRaf protein which is recruited to the plasma membrane through CRY2 binding to the N-terminal domain of CIB1 (CIBN) in a blue light-dependent manner (Adapted from Aoki et al. 2013). (B) Opto-SOS is an optogenetic tool for engineering a light-gated switch to drive Ras activation. Opto-SOS refers to the cytoplasmic PIF-SOScat fusion (tagged with YFP on its Nterminus) construction and the membrane-localized PhyB (PhyB-mCherry-CAAX) construction. Light drives the heterodimerization of membrane-localized Phy with a cytoplasmic PIF-tagged SOScat construct, leading to Ras activation and nuclear translocation of BFP-Erk2. (Adapted from Toettcher, Weiner, and Lim 2013)

activated to the maximum level in response to different OFF lengths, indicating that IEG activation operates through a mechanism similar to bandpass filter in response to ERK activation pulses (Wilson et al., 2017).

Finally, ERK activity is also controlled at the level of subcellular localisation of this kinase. In quiescent cells, ERK remains in the cytoplasm via its binding to MEK (Fukuda et al., 1997). In response to stimulation, MEK-mediated phosphorylation of ERK induces its dissociation from the MEK-ERK complex (Adachi et al., 1999). Dissociated and activated ERK then translocates from the cytoplasm to the nucleus (Khokhlatchev et al., 1998). In fibroblasts, stimulation with EGF induces ERK activation while activated ERK remains predominantly in the cytoplasm and promotes cellular senescence. In contrast, ERK activation by phorbol myristate acetate (PMA) triggers the nuclear translocation of active ERK and promotes cell proliferation (Whitehurst et al., 2004). This study thus highlights that differences in the subcellular compartmentalisation of active ERK contributes to generation of discrete phenotypic responses to distinct environmental stimuli that activate a common core signal transduction module.

### **3) Dose response kinetics of ERK signalling**

In addition to the difference in temporal dynamics, ERK activation exhibits distinct dose response kinetics in response to increasing doses of stimuli, ranging from switch-like, gradual to linear responses. In particular, a switch-like property of ERK activation kinetics seems to be appropriate for mediating cellular processes where the state

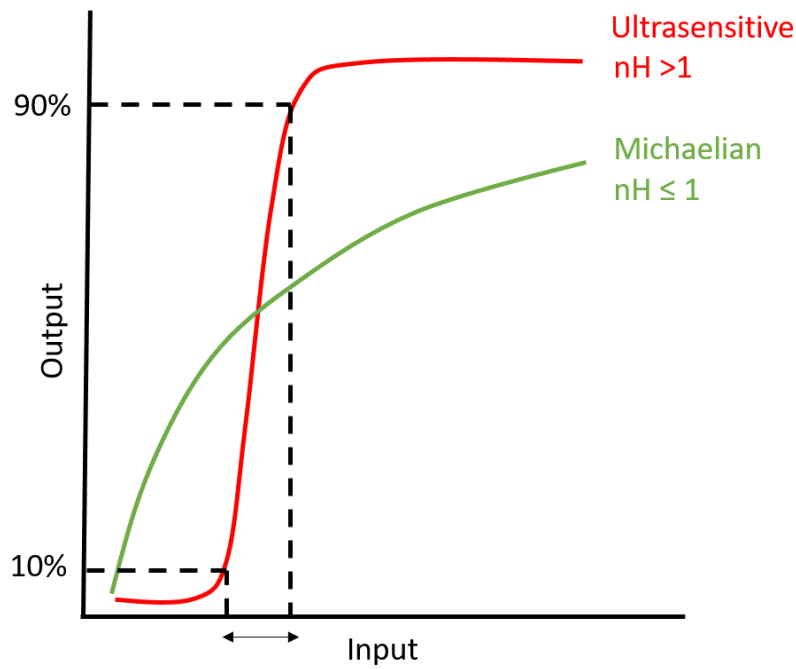


**Figure 12:** Relationship between input and output for Michaelian and ultrasensitive systems. In the Michaelian response, the level of output increases gradually with the input signal, in a hyperbolic manner. In this case the Hill number is equal or lower than 1. In contrast, in the ultrasensitive response, the output signal increases in a sigmoidal way with the input signal. For an ultrasensitive response, the Hill number is more than 1. (Adapted from Shah and Sarkar 2011)

transition emerges. In biochemistry, a switch-like response is described as an 'ultrasensitive' response (Goldbeter and Koshland, 1981). When the output of a switch-like response is plotted against the input (e.g. ligand concentration), a sigmoidal curve is obtained (Figure 12). In contrast, a non-ultrasensitive response is typically represented by a hyperbolic (or graded) curve and called a 'Michaelian' response (Figure 12). The steepness of dose-response curves can be quantified as Hill coefficient ( $n_H$ ). Michaelian response has Hill coefficient of 1 while ultrasensitive responses have Hill coefficient of  $>1$ ; the higher the  $n_H$  is, the more switch-like a response is (Figure 12).

At least four classes of broad and conceptually distinct theoretical mechanisms have been described to underlie ultrasensitivity in biochemical reactions. These are zero-order kinetics, multistep modification, stoichiometric inhibition and positive feedback (reviewed in James E. Ferrell and Ha 2014a; 2014b; 2014c). Zero-order ultrasensitivity operates in a reversible reaction in which the levels of opposing enzymes (e.g. phosphatase and kinase) are limiting and the substrate is in excess, such that the rates of the opposing reactions become essentially independent of the substrate concentration (Goldbeter and Koshland, 1981). In the zero-order regime, over the threshold level, small changes in the ratio of the opposing enzyme levels result in large changes in the substrate output. Multistep modification (e.g. multiple phosphorylations required for activation of a protein) is another mechanism that can generate ultrasensitivity. With this mechanism, non-processivity (also called distributivity), whereby one modification event occurs per enzyme-substrate

interaction, and cooperativity, such that modification of one site increases the chance of a subsequent modification, generate ultrasensitivity. Stoichiometric inhibition also generates ultrasensitivity via a buffering effect in which an inhibitor competes with the substrate for enzyme interaction. Finally, positive feedback (or double negative feedback) loops can generate ultrasensitivity. Importantly, in signalling cascades involving several layers of reactions, combinations of these mechanisms can increase the level of ultrasensitivity.

Theoretical studies indicate that the ERK signalling pathway itself is inherently capable of generating ultrasensitive switch-like responses (Ferrell and Bhatt, 1997; Ferrell and Machleder, 1998; Huang and Ferrell, 1996; Markevich et al., 2004; Qiao et al., 2007). This inherent ultrasensitive response of the ERK signalling pathway is thought to depend upon the distributive dual phosphorylation of ERK and can be enhanced by positive feedback loops. Consistently, ultrasensitive ERK responses have been documented in mammalian cell culture systems and have been shown in some cases to depend upon feedback loops (Altan-Bonnet and Germain, 2005; Das et al., 2009; Santos et al., 2007). Despite these clear examples of ultrasensitive ERK responses, it is equally the case that, in many mammalian cell culture systems, the kinetics of ERK activation in response to extracellular stimuli is hyperbolic (gradual) (MacKeigan et al., 2005; Perrett et al., 2013; Santos et al., 2007; Sturm et al., 2010; Whitehurst et al., 2004) and even linear (Nunns and Goentoro, 2018). Molecular crowding in the physiological condition could account in part for the gradual response with ERK being dually-phosphorylated in a processive, but not distributive, manner

(Aoki et al., 2011). The signal network configuration in which the ERK pathway is embedded also likely accounts for these different output responses. For example, in PC12 cells, EGF stimulation, which leads to a transient ERK activation by triggering a negative feedback loop, exhibits a gradual response while NGF stimulation, deploying a positive feedback to activate ERK sustainably, exhibits a switch-like response (Santos et al., 2007).

How a gradual ERK activation does is translated to control cell fate decisions? It has been shown that, in Swiss 3T3 cells treated with PDGF, a gradual ERK activation is converted to a switch-like activation of its immediate early genes (MacKeigan et al, 2005). How is this “digitalisation” of graded ERK signals to a switch-like transcriptional activation controlled? One potential mechanism includes a control at the level of nuclear translocation of ERK. As described above, PC12 cells treated with EGF exhibit gradual activation of ERK. However, it has been shown that the nuclear translocation of ERK operates in a switch-like manner in response to increasing doses of EGF (Figure 13A-C) (Shindo et al., 2016). It remains unknown whether specific transcriptional logics underlie the switch-like activation of immediate early genes downstream of ERK activation.

Finally, an ultrasensitive ERK activation response has also been evaluated in an in vivo system, during *Xenopus* oocyte maturation. In this system, the ERK signalling cascade consists of Mos-MEK-ERK and exhibits a switch-like response to progesterone stimulation. Distributive phosphorylation of ERK and a positive feedback

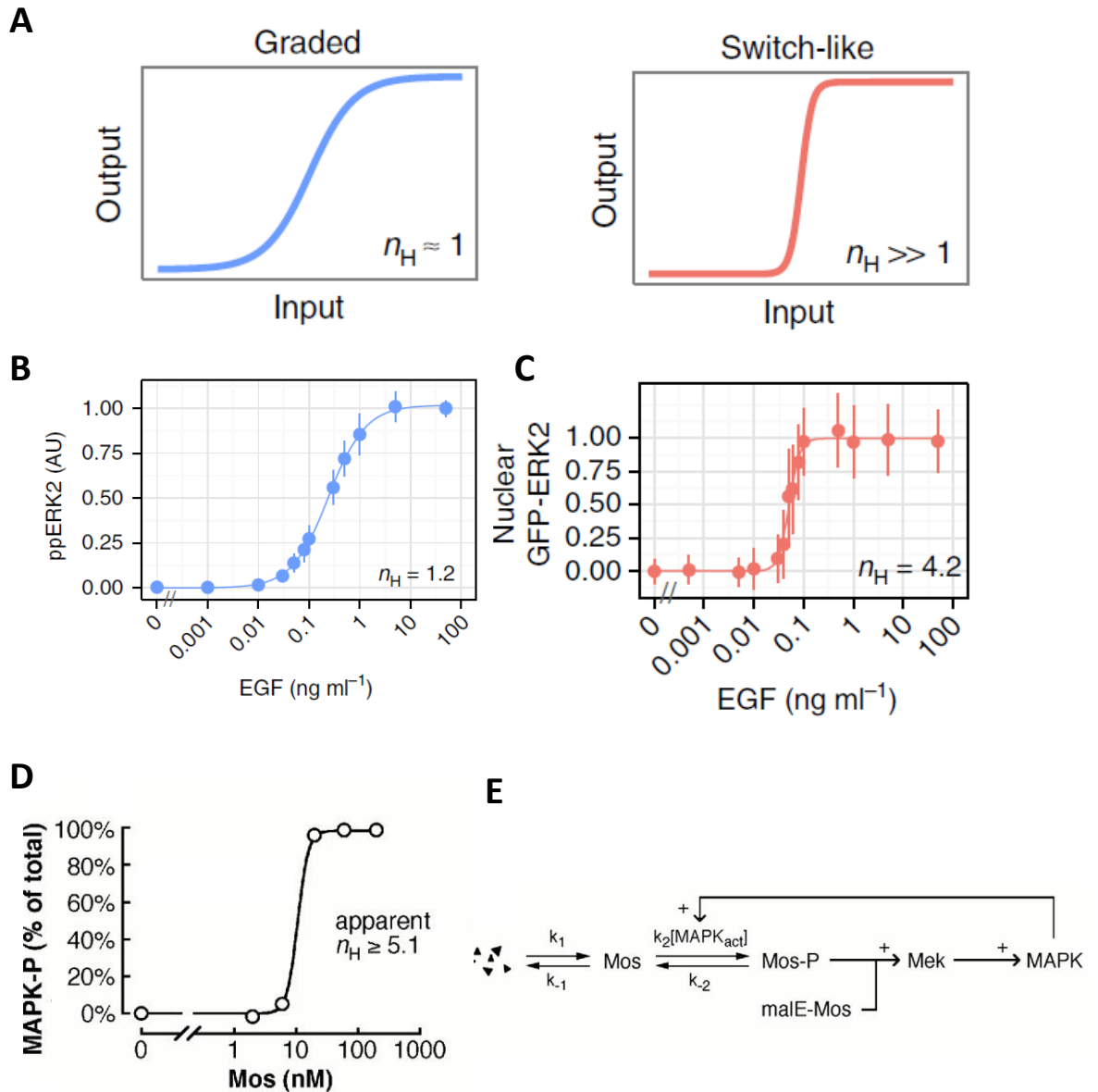


**Figure 13:** (A) Schematic representation of the graded and switch like response (B) Curve of the means of phosphorylated ERK2 (a.u.) plotted as a function of EFG concentration for three different experiments. Hill coefficient were calculated thanks to curve fitting with Hill function (C) Levels of nuclear GFP-ERK2 at 8min after stimulation plotted as a function of EGF concentration with s.d. A minimal number of 180cells was observed for each condition. Hill coefficient was obtained by curve fitting with Hill function. (Adapted from Shindo et al. 2016). (D) Ultrasensitivity as a means of providing a positive feedback system with both a stable off state and a stable on state. Responses of pools of 10 to 20 oocytes to microinjected malE-Mos. The response is ultrasensitive with  $n_H > 5$ . (E) Mos synthesis, destruction, and stabilization reactions. The feedback from MAPK to Mos could be direct, as shown here, or indirect.(Adapted from Ferrell and Machleder 1998)

loop are thought to underlie the ultrasensitivity of the response (Ferrell and Bhatt, 1997; Ferrell and Machleder, 1998; Huang and Ferrell, 1996). These pioneering studies have also highlighted the importance to study at the single cell level when addressing kinetics of signalling response (Figure 13D-E).

#### **4) ERK signalling in multicellular contexts**

The ERK signalling pathway is evolutionary conserved and repeatedly used during embryonic development in metazoans for patterning, cell fate determination, cell proliferation and cell migration (Brewer et al., 2016). Despite the profound developmental defects associated with both reduced and excessive levels of ERK signalling, its quantitative analyses in *in vivo* multicellular contexts are rare, in particular, in relation to a threshold response. I will describe in the following sections some of the best described developmental processes depending on ERK signalling.

##### **a. ERK-mediated patterning of terminal regions and neuroectoderm of the *Drosophila* blastoderm**

*Drosophila* early embryos are syncytium as a result of the first 13 cell cycles taking place without cytokinesis. Cellularisation encompasses the nucleus with the plasma membrane, leading to approximately 5000 cells of uniform cells surrounding the internal yolk. The cellular blastoderm is subdivided into three germ layers and segments arranged in anterior-posterior order. At this stage, ERK signalling plays a

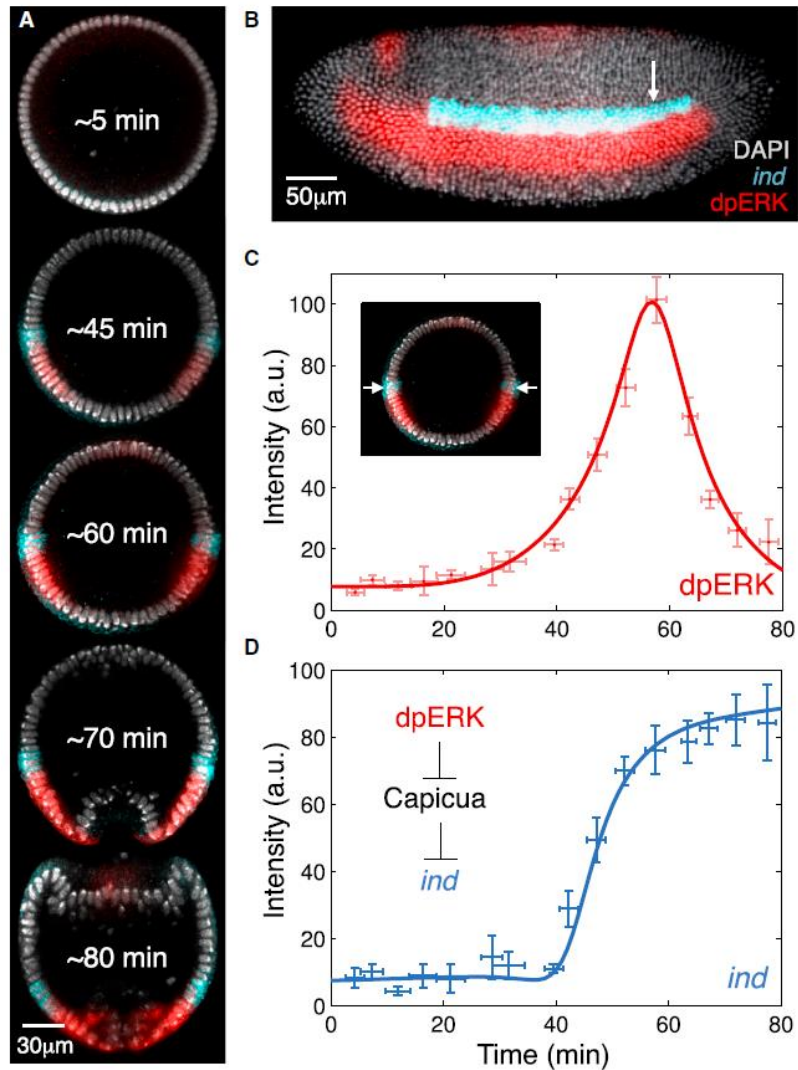


**Figure 14:** Kinetics of ERK Activation and Expression of Its Target Gene (A and B) ERK activation and expression of *ind* during the third and fourth hours of development. Optical cross-sections of embryos are shown in (A). Time indicates an estimated developmental age of a given snapshot. 0 min corresponds to the onset of nuclear cycle 14. The embryo in (B) is positioned with its anterior side to the left and the dorsal side on top. The arrow indicates the position where optical cross-sections were imaged. (C) ERK activation within the *ind* expression domain is transient. (D) *ind* mRNA is induced shortly after ERK is activated and persists after ERK activation decays. ERK activates *ind* by antagonizing its repression by the uniformly distributed transcriptional repressor Capicua. The time courses of dpERK and *ind* are plotted at the center of the *ind* expression domain, indicated by the arrow in (C). Analysis is based on a dataset from 140 embryos, co-stained with dpERK antibody and *ind* probe, and imaged together in the same microfluidic device. Error bars correspond to the SEM. (From Lim et al. 2015)

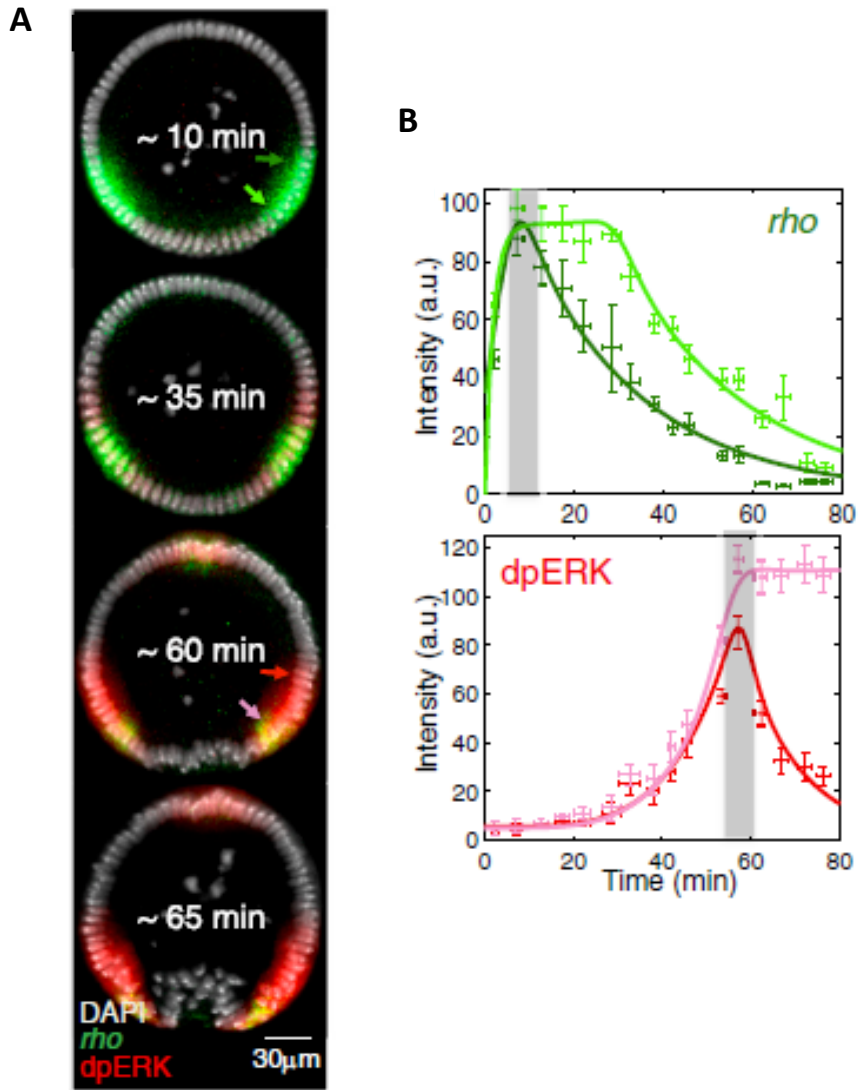


**Figure 15:** Spatiotemporal Control of ERK Activation (A) Joint dynamics of rho and dpERK: ERK activation is delayed with respect to rho expression. Arrows indicate the positions where the signal was analyzed. (B) rho and dpERK at two positions along the DV axis, corresponding to the ventral (light green and light red) and dorsal (dark green and red) borders of the rho pattern. The duration of rho expression decreases from ventral to dorsal boundaries of the domain. Accordingly, ERK activation kinetics changes from a sustained pattern to a transient one. 137 embryos co-stained with rho probe and dpERK antibody were analyzed. Gray shading indicates 5-min time windows where rho and dpERK are at their peak levels. (Adapted from Lim et al. 2015)

major role in specifying two territories, namely the neuroectoderm and the terminal regions. The trunk region of the blastoderm at the pregastrulation stage is subdivided into mesoderm, neuroectoderm, dorsal ectoderm, and amnioserosa in a ventral-to-dorsal order. The neuroectoderm is further subdivided into three longitudinal stripes of ventral, intermediate, and lateral rows. The intermediate row of cells is marked by expression of *intermediate neuroblasts defective (ind)* gene, which is controlled by EGF Receptor (EGFR)-stimulated ERK signalling. In order to determine the spatio-temporal pattern of ERK activation in relation to *ind* expression, Lim et al. imaged a large number of fixed embryos stained with anti-dpERK antibody and a probe for *ind* mRNA, and reconstructed the time course of expression (Figure 14)(Lim et al., 2015). At the *ind* expression site along the dorsal-ventral axis, dpERK level shows a single pulse of activation that peaks at 60 min after the initiation of cellularisation (Figure 14). *ind* expression begins at 40 min when the dpERK level reaches 20% of its peak level (Figure 14). When the ERK activation pulse is delayed by almost 1 h and dampened to a quarter of its value in the wild-type embryo by a genetic manipulation, *ind* expression is also accordingly delayed without altering its position or level (Lim et al., 2015). This result supports the model that *ind* transcription is triggered as a threshold response to a cumulative dose of ERK activity. Capicua (Cic), an HMG-box repressor, acts as a sensor of ERK signalling in this case. In the absence of ERK signalling, Cic is localised predominantly to the nucleus, where it represses *ind*. ERK signalling promotes nuclear export and subsequent degradation of Cic, which appears to be controlled by direct phosphorylation (Grimm et al., 2012). As a consequence, the ERK-

independent transcriptional activators can initiate the expression of *ind* as long as the strength of the provided ERK signals exceeds a threshold value.

The ligand for EGFR activation in the neuroectoderm is Spitz (TGF $\beta$ -like protein), which is ubiquitously expressed as an inactive membrane-bound form. Cleavage by the Rhomboid (*rho*) protease converts Spitz into its active secreted form (Shilo, 2005). Lim et al. demonstrated that *rho* expression prefigures that of dpERK 40 min prior (Figure 15). The quantitative analysis is consistent with a simple model that dpERK expression is near direct readout of *rho* transcription (Lim et al., 2015). This result argues against the diffusion model of EGF ligands, because ERK activation pattern would be broader if they diffuse in a long distance.

ERK signalling is also deployed during earlier stages of *Drosophila* development to pattern head structures at the anterior pole and gut endoderm at the posterior pole of the larva. In this developmental context, ERK signalling is induced by a uniformly expressed receptor tyrosine kinase Torso (Tor), which is activated by its ligand produced locally at the embryonic poles (Mineo et al., 2018). Quantitative measurements of ERK activation have revealed graded distributions of dpERK peaking at the termini, indicating that active ERK diffuses within syncytium from localised activation sites at the poles (Coppey et al., 2008). This shows a sharp contrast to the localised ERK activation described above in the cellularising blastoderm. dpERK gradient at the terminal regions becomes steeper progressively with embryonic stages from nuclear cycle 10 to 14. This gradient sharpening is attributed to the increasing number of syncytium nuclei that are proposed to act as traps diffusing dpERK (Coppey

et al., 2008). Surprisingly, the graded activity of ERK at the terminal region does not seem to be important. The activation of Opt-Sos converts the dpERK gradient to a plateau of uniformly high dpERK level (Johnson et al., 2017). However, a localised activation of Opt-Sos at the termini rescues complete loss of Tor activity (Johnson et al., 2019). These results demonstrated that normal terminal patterning is possible under conditions of excessive dosage or disruption of graded spatial distribution activated ERK.

Another interesting feature of the ERK activation in the terminal region includes asymmetry in ERK activation levels between the anterior and posterior ends: the anterior levels of dpERK are significantly higher than the posterior levels (Kim et al., 2010). This asymmetry is due to ERK substrate competition whereby anteriorly-localised substrates of ERK such as Bcd and Hb compete with MAPK phosphatases, negative regulators of ERK (Kim et al., 2010). Importantly, this substrate competition leads to an asymmetric degradation of Cic between the anterior and posterior terminal regions with this transcriptional repressor degraded less at the anterior end. Finally, it should be noted that a similar substrate competition mechanism was also observed in a mammalian cell culture system (Bardwell et al., 2003).

In the anterior and posterior termini, activated Tor promotes the expression of *tailless (tll)* and *huckebein (hkb)*, required for terminal cell fates, and *folded gastrulation (fog)* and *mist*, required for invagination of posterior midgut, a posterior terminus derived structure. Based on a blue light-responsive hetero-dimerisation pair, the iLID/SSPB (Guntas et al., 2015; Johnson et al., 2017) has successfully implemented

an optogenetic control of Ras activation (Opt-Sos) in the *Drosophila* system. The uniform light illumination of Opt-Sos embryos has a dominant effect in the trunk region. With 30 min illumination, the stripe of *ind* expression in the neuroectoderm widened by about 2-fold, indicating augmentation of Rho-dependent ERK activity. An illumination of more than 60 mins results in loss of *ind* expression and wide-spread expression of *tll*, *hkb*, *fog* and *mist*, target genes of Tor-dependent ERK activity. The extended expression of the terminal genes is accompanied with widespread contractile activity of myosin mimicking posterior midgut invagination (Johnson and Toettcher, 2019). Through a series of experiments testing different light illumination protocols changing duration, pulse frequency, and signal amplitude during 90 mins of the pre-gastrulation stage, it was concluded that a cumulative dosage of ERK activity provided either as a single long pulse or multiple short pulses, triggers the all-or-none cell fate switch (Johnson and Toettcher, 2019). This conclusion is in accordance with the duration-dependent cell fate switch observed in PC12 cells (see above). Consistent with the switch-like operation of dosage-dependent cell fate decision, induction kinetics of *hkb* and *mist* in response to increasing durations of synthetic ERK activation exhibit threshold responses while that of *tll* a linear response. It remains to be addressed how the threshold response of ERK-target genes is controlled, while it constitutes a very interesting research topic.

## **b. Graded ERK signalling in patterning of the *Drosophila* embryonic ventral ectoderm**

The *Drosophila* embryonic ventral ectoderm is patterned by a graded activation of the EGFR during stage 10 (note that the cellular blastoderm stage described above correspond to st 5, about 80 mins before the onset of st 10). The principal ligand in this system is Spitz, which is secreted by a single row of midline cells in the ventral ectoderm due to Rho expressed specifically in these midline cells (Golembo et al., 1996). The binding of Spitz to EGFR activates ERK signalling, which regulates a battery of target genes by inducing the expression of the ETS-domain transcriptional activator PointedP1 (PntP1) and promoting the degradation of the antagonizing ETS-domain transcriptional repressor Yan (Gabay et al., 1996). The degradation of Yan is triggered by ERK-mediated phosphorylation (Rebay and Rubin, 1995).

In this developmental context, Spitz appears to diffuse and activate ERK in a graded manner across approximately three rows of cells. In contrast, the degradation of Yan exhibits a switch-like response: Yan proteins are absent from the first two rows, whereas the adjacent distal rows display Yan at high levels (Figure 16A-D) (Melen et al., 2005). A number of mechanisms may account for the generation of this sharp threshold. A threshold could be generated, for example, by a cooperative effect, if multiple ERK-dependent reactions, par exemple via several phosphorylation sites on Yan, are required for Yan degradation (Ferrell and Ha, 2014a). Alternatively, a putative positive feedback that facilitates either MAP kinase activation or Yan degradation could also lead to such a threshold response (Ferrell and Ha, 2014b). A third mechanism,

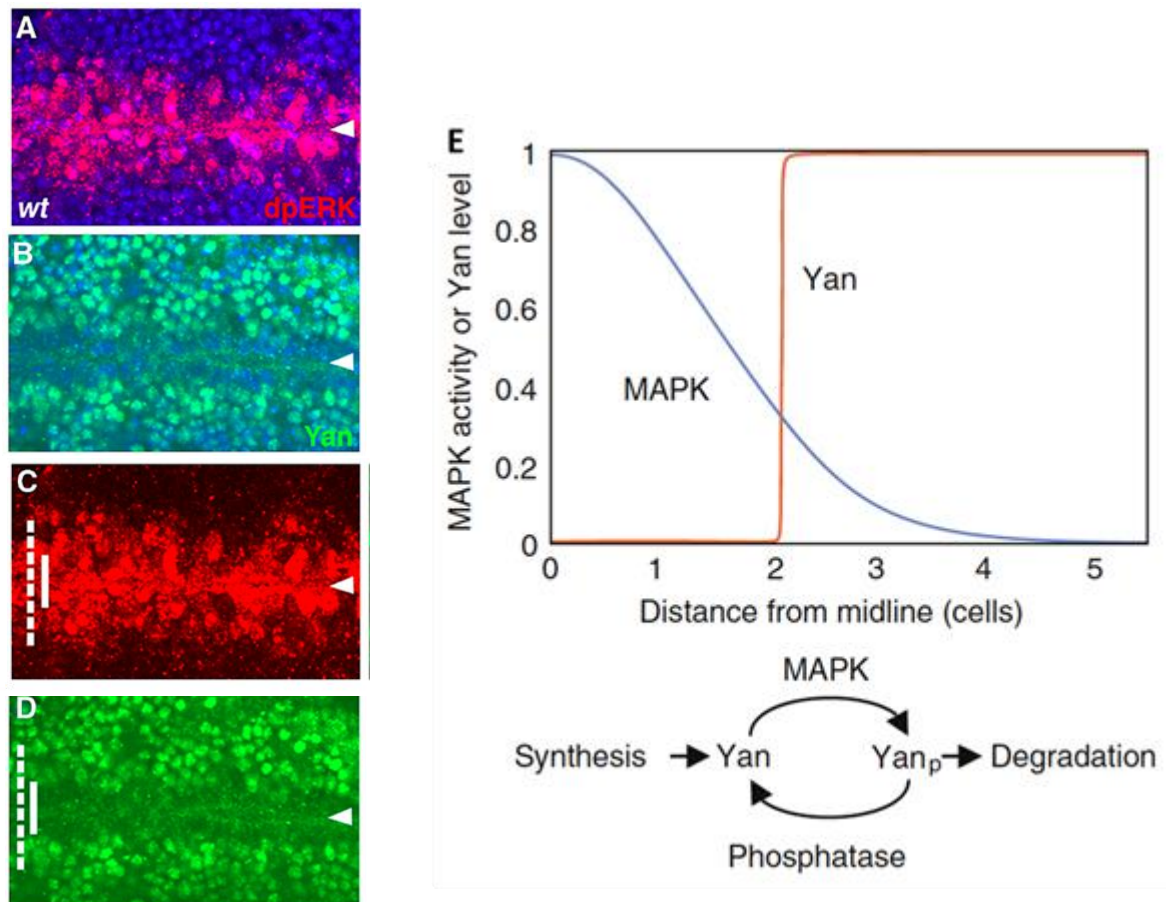


**Figure 16:** Graded MAPK activation in the ventral ectoderm and Yan degradation. **(A, C)** Wild-type embryo at stage 10 shows graded activation of MAPK that is detected with dpERK antibodies (red). DAPI staining is in blue. The activating ligand, Spitz, emanates from the midline glial cells (arrowhead) to trigger EGFR in the adjacent cells. In a given row, not all the cells display the same level of activated MAPK, whereas the expression of target genes is uniform. **(B, D)** Within the domain of MAPK activation, the degradation pattern of Yan (green) at the same stage shows a much more restricted and sharp response. The dashed line denotes dpERK borders, the nested solid line represents Yan degradation boundaries. **(E)** (Top) Schematic representation of MAPK activity and total Yan level as a function of distance from midline of ventral ectoderm in the *Drosophila* embryo (adapted from Melen et al, 2005). The smooth gradient in MAPK translates into an all-or-none transition in the level of Yan protein. (Bottom) The Yan phosphorylation–dephosphorylation network involves the kinase MAPK, a yet unidentified phosphatase, as well as synthesis of Yan and degradation of the phosphorylated form of the protein, Yan<sub>p</sub>. (Adapted from Melen et al. 2005; Goldbeter 2005)

'zero-order ultrasensitivity' implies opposing modification reactions, both of which function at the zero-order regime (i.e. enzymes are saturated with their reactants) (Ferrell and Ha, 2014a; Goldbeter and Koshland, 1981).

In order to distinguish these qualitatively different mechanisms, Melen et al (2005) applied a combination of theoretical and experimental analyses, which provided evidence that a zero-order ultrasensitivity-like mechanism underlies the all-or-none degradation switch of Yan in response to graded ERK signals. The model consists of a regulatory cycle of phosphorylation by ERK and dephosphorylation by unknown phosphatase with Yan produced continuously at a fixed rate while phosphorylated Yan degraded (Figure 16E). Similar to the classical model proposed by Goldbeter and Koshland (1981), a switch-like behaviour is generated when the substrate, Yan, is in excess with respect to the dissociation constants for the two opposing enzymes (Melen et al., 2005). To my knowledge, the Yan degradation in the ventral ectoderm of *Drosophila* embryos represents the first example of a developmental threshold response associated with zero-order ultrasensitivity.

### **c. ERK signalling in *C.elegans* vulval patterning**

The *Caenorhabditis elegans* hermaphrodite vulva represents one of the best studied models for signal transduction and cell fate determination during organogenesis. The vulval precursor cells (VPCs) are a developmental equivalent group of six ventral epithelial cells (Pn.p cells, numbered from P3.p to P8.p) (Sternberg, 2005) (Figure 17A). The anchor cell (AC) in the overlying gonad induces VPCs to assume a highly

reproducible 3°-3°-2°-1°-2°-3° pattern of cell fates. The relative position of the AC to VPCs determines this specific pattern with P6.p in closest proximity to the inducer cell. The AC secretes a diffusible EGF-like ligand, LIN-3 (Hill and Sternberg, 1992). LIN-3/EGF is thought to form a short-range gradient across P5.p, P6.p and P7.p peaking at P6.p, which assumes 1° fate while the adjacent VPCs take on 2° fate. LET-23/EGF receptor mediates this paracrine induction activating the canonical Ras/ERK pathway. This constitutes a “morphogen gradient model”, positing that strong EGF signal induces 1° fate while diminished EGF signal directly promotes 2° fate (Figure 17A-B) (Katz et al., 1995; Katz et al., 1996). Consistently, an ERK-responsive reporter (*egl-17-CFP-LacZ*) is initially expressed in P5.p, P6.p and P7.p with higher expression in P6.p, thereby indicating a graded signal (Yoo et al., 2004).

In contrast, a “sequential induction model” proposes that EGF induces only the most proximal VPC, which adopts 1° fate. Subsequently, this presumptive 1° cell expresses DSL (Delta/Serrate/Lag2) ligands that, via the LIN-12/Notch receptor, laterally induce neighbouring VPCs to assume 2° fate (Chen and Greenwald, 2004). Accordingly, the LET-23/EGF receptor (EGFR) is necessary for 1° but not 2° fate induction (Koga and Ohshima, 1995; Simske and Kirn, 1995). This key result is consistent with the observations that activation of LIN-12/Notch can specify a 2° fate in the absence of an anchor cell (Greenwald et al., 1983) or of LET-23/EGFR signalling (Sternberg and Horvitz, 1989), and strongly supports that the direct induction of 2° fate by LIN-3/EGF is not necessary. During the course of the vulval patterning, presumptive 2° cells (P5.p and P7.p) progressively acquire mechanisms to quench LET-23/EGFR

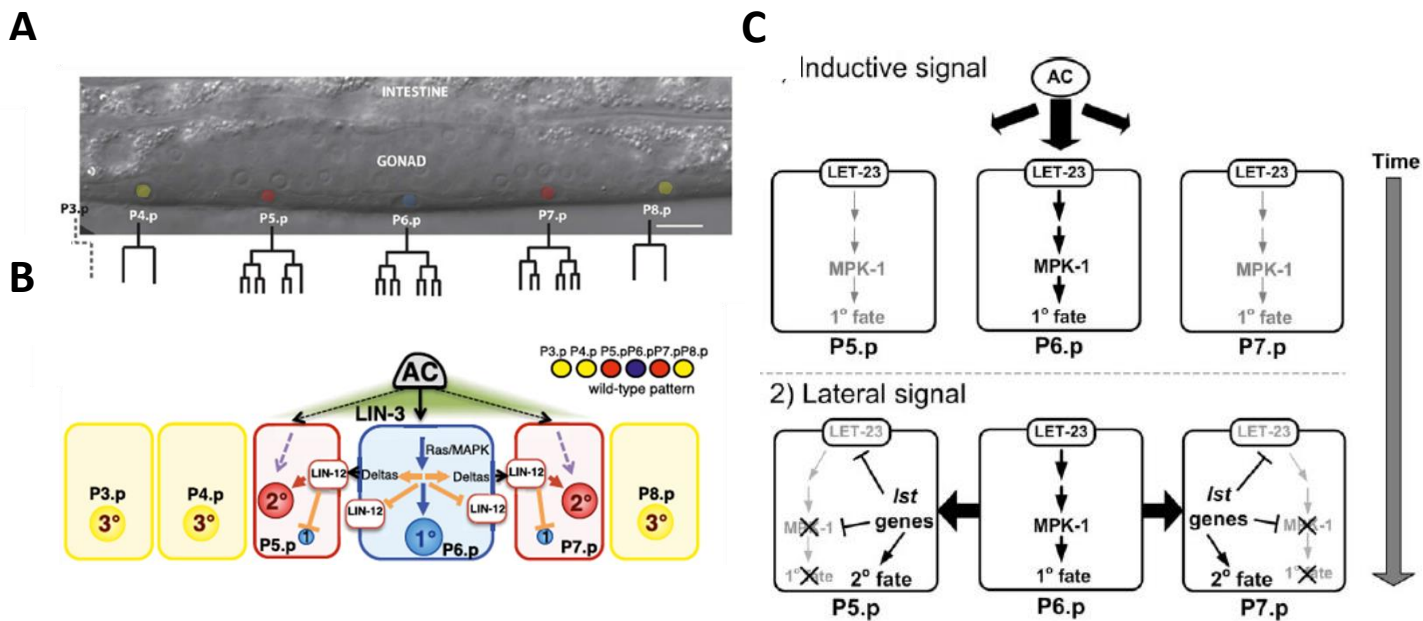


**Figure 17:** (A) Differential Interference Contrast (DIC) microscopy image showing five of the six VPCs, with cell lineages shown below. The 3 VPCs which are the closest to the AC (P5.p, P6.p and P7.p) are induced to undergo three rounds of division to produce the 22 cells of the vulva. The others uninduced cells divide once. (B) Scheme of the vulval network. Ras-MAPK pathway is in blue, Notch pathway in red and interactions between the two pathways in orange. LIN-3 secreted by AC is in green. (Adapted from Gauthier and Rocheleau 2017; Barkoulas et al. 2013). (C) Revised model for the signaling events underlying VPC specification. The inductive signal activates the EGFR-MAPK pathway maximally in P6.p, and detectably in P5.p and P7.p. However, lateral signaling leads to activation of *Ist* gene expression in P5.p and P7.p, and those *Ist* genes that encode negative regulators of the EGFR-MAPK pathway counteract the effect of the inductive signal on P5.p and P7.p. Other *Ist* genes are presumably required for correct execution of the 2° fate. (From Yoo 2004)

signalling. One of such quenching mechanisms includes a LIN-12/Notch-mediated induction of LIP-1/ERK protein phosphatase that attenuates ERK (Berset et al., 2001). An additional mechanism to quench EGF signals in the presumptive 2° cells operates via preferential degradation of LET-23/EGFR. In mid-L2 larvae, around when the vulval induction is thought to begin, LET-23/EGFR is weakly but uniformly expressed in all VPCs (Kaech et al., 1998). In early L3 larvae, LET-23/EGFR expression is strongly upregulated in the 1° VPC P6.p, where it accumulates on the basolateral membrane, maximising its availability to LIN-3/EGF ligands (Figure 17C). At the same time, LET-23/EGFR becomes undetectable in the P5.p and P7.p cells. This differential regulation of LET-23/EGFR is controlled by EPS-8, whose expression is upregulated in P6.p. EPS-8 associates with the localisation complex (LIN-2/LIN-7/LIN-10) to retain the EGFR on the basolateral membrane (Figure 18A-B). Low levels of EPS-8 in the neighbouring VPCs result in the rapid degradation of the EGFR (Stetak et al., 2006). Together with the LIP-1/ERK protein phosphatase, this mechanism contributes to reduce the EGF/ERK signalling in the presumptive 2° cells.

Finally, another layer of control ensuring specification of exactly one cell with 1° cell could be provided by the rapid sequestration of the diffusible LIN-3/EGF ligand by P6.p. Indeed, ectopic induction of distal VPCs with 1° fate occurs only when cells closest to the AC are ablated, supporting the idea that VPCs sensing EGF at its highest concentration are capturing ligand before it can diffuse away (Sternberg and Horvitz, 1986). When LET-23/EGFR expression is partially reduced, less EGF sequestration by P6.p could lead to increased ligand diffusion to more distal VPCs, accounting for

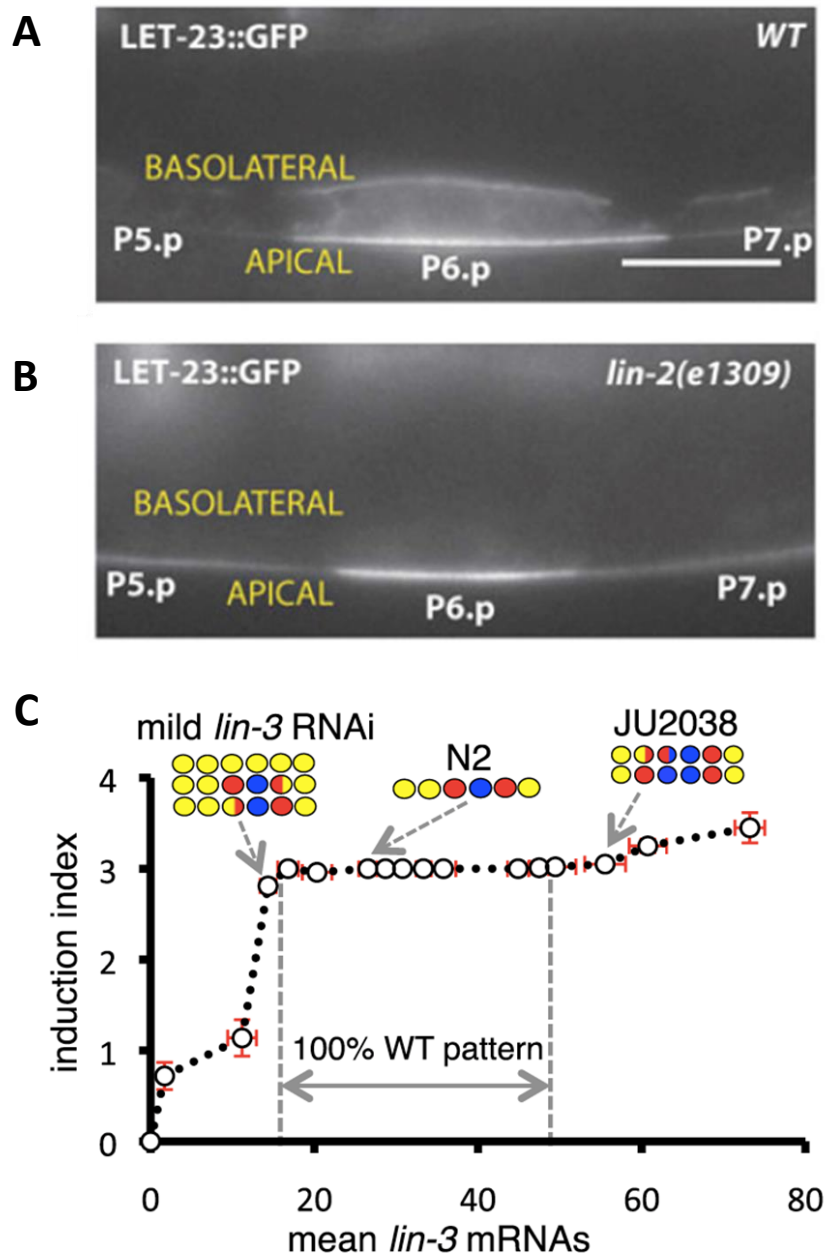


**Figure 18:** (A) In the WT larva, LET-23::GFP (EGFR) is strongly expressed in P6.p to both apical and basolateral membranes. (B) Inhibition of the LIN-2/7/10 complex in a *lin-2(e1309)* mutant gives an exclusive apical localization of LET-23::GFP and a vulvaless phenotype. Scale bars 10  $\mu$ m. (Adapted from Gauthier and Rocheleau 2017). (C) Graph showing the induction index (average number of induced cells), for each perturbation line as a function of the mean of detected *lin-3* mRNAs. VPCs exposed approximately to threefold increase of the LIN-3/EGF signal are still patterned into the WT pattern. (Adapted from Barkoulas et al. 2013)

the apparent hypersensitivity in these mutants (Hajnal et al., 1997). These quenching mechanisms altogether provide a highly efficient system to attenuate the EGF/ERK signalling in the presumptive 2° cells. It has been demonstrated that VPCs exposed to approximately threefold increased levels of the AC-derived LIN-3/EGF are still patterned into the wild-type 3°-3°-2°-1°-2°-3° pattern (Barkoulas et al., 2013) (Figure 18C). Therefore, the mechanisms ensure that the EGF/ERK signalling is actively transduced only in P6.p to induce the 1° fate. In other words, they ensure that diffusible ligands impact only one cell in the closest proximity to the signalling source.

Temporal dynamics of ERK activation in VPCs has been recently documented by implementing the kinase translocation reporter (KTR) system to *C. elegans* (de la Cova et al., 2017; Regot et al., 2014). High temporal resolution imaging of the ERK-KTR biosensor in VPCs during the late L2 stage has revealed that ERK temporal dynamics is pulsatile. Importantly, the graded signal of LIN-3/EGF appears to be converted to frequency-modulated, rather than amplitude-modulated, ERK activation pulses with P6.p exhibiting highest frequencies (average 3 pulses per hr compared to average 0.5 pulses per hr in P7.p). Optogenetic approaches will be required to address how the observed ERK activation dynamics is translated to control the cell fate decision during vulval patterning. The developmental equivalence of the six VPCs would provide an ideal biological system for such studies.

During VPC patterning, ERK-mediated phosphorylation induces structural changes in at least two transcription factors, LIN-31 forkhead transcription factor and LIN-1 ETS transcription factor. These transcription factors form a complex and act as

repressors in the absence of ERK activation. ERK phosphorylate the C-terminal domain of LIN-1, disrupting the repressor complex and potentially converting LIN-1 into an activator. Furthermore, dissociation of the repressor complex exposes a phosphorylation site in the transactivation domain of LIN-31 so that it also becomes an activator when phosphorylated by ERK (Tan et al., 1998).

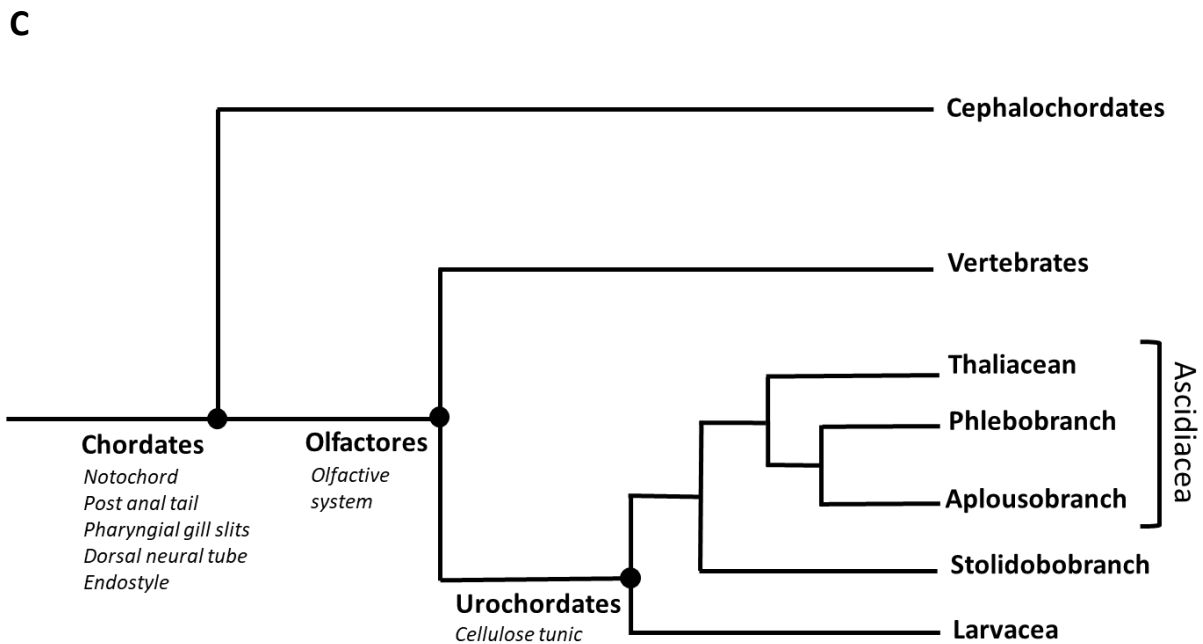
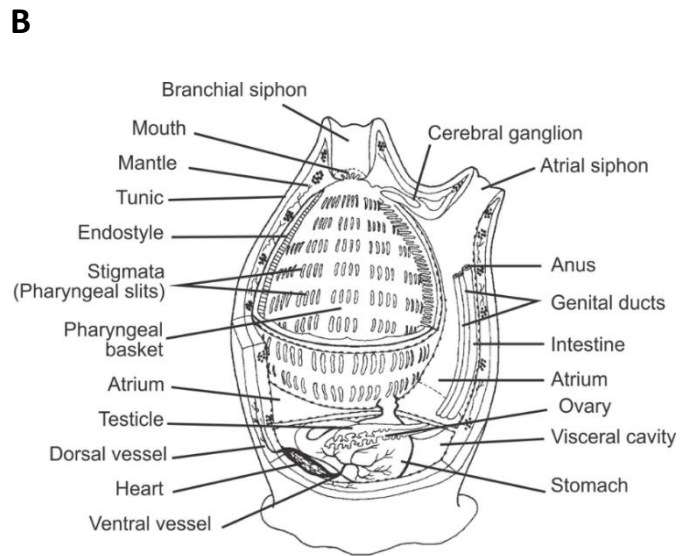


**Figure 19:** (A-B) Photo and schematic drawing of an adult *Ciona intestinalis* (C) Phylogenetic tree with main chordates group and detailed Urochordate groups. Main synapomorphies for each group are in italic. (Adapted from Delsuc et al. 2018)

### III. **Ascidian embryos: a model in developmental biology**

---

#### 1) Background

Tunicates, also called Urochordates, are the sister-group of vertebrates, with which they form a monophyletic group, Olfactores (Delsuc et al., 2006). The tunicates are classified into three groups: Ascidiacea, sea squirts, which are sessile and either solitary or colonial ; Thaliacea, which are pelagic with complex life cycles with both solitary and colonial forms ; and Larvacea, which are solitary pelagic animals (Figure 19C). Recent molecular analysis put Thaliacea as a sister group of Phlebobranch and Aplousobranch but the position of this group remains unclear (Alié et al., 2020). Ascidian larvae exhibit a tadpole form with typical chordate-body plan with an axial notochord and dorsal neural tube (Kovalevsky, 1859). Tadpoles then settle and undergo metamorphosis to adopt a benthic adult form (Figure 19A-B). Ascidiaceans are hermaphrodite and fertilization takes place externally following a release of a large number of gametes into the water. Embryos of solitary ascidians have been studied in developmental biology for decades. In 1887, Laurent Chabry first described the mosaic development of ascidian embryos based on blastomere ablation experiments (Chabry, 1887). Then, in 1905, Conklin described cell lineages of embryos and how invariant they are (Conklin, 1905). Ascidian embryos present several characteristics that make them a unique chordate model for studying developmental events. They develop into a swimming larva approximately in 24 hours. Their embryogenesis proceeds with a small number of cells that exhibit quasi-invariant cell division cycle and orientation (e.g.

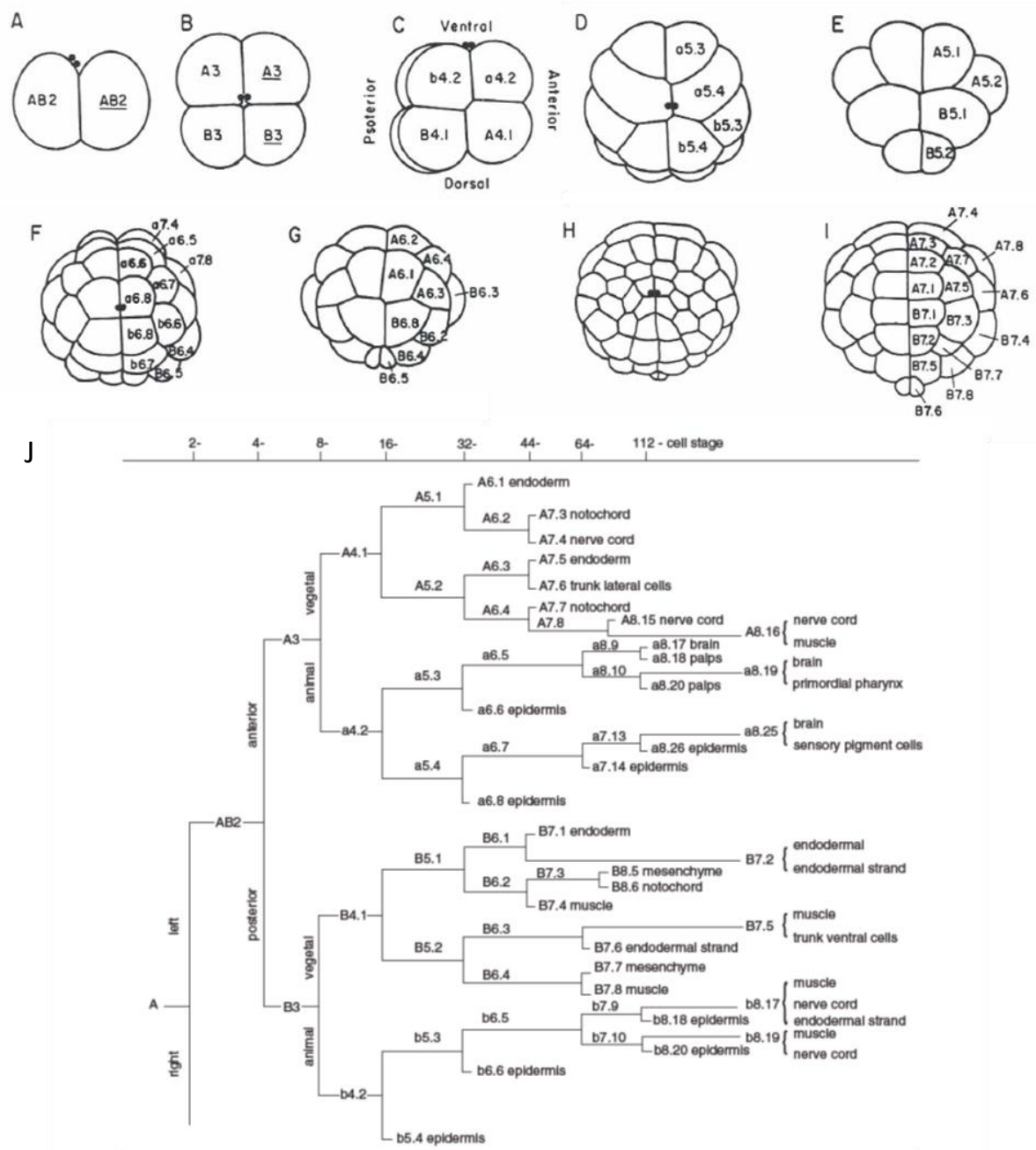


**Figure 20:** Early development and cell lineages of ascidian embryo (A) 2-cell (2c) stage, posterior pole view (B) 4c stage, animal pole view (C) 8c stage, right side view (D-E) 16c stage, animal (D) and vegetal (E) views (F-G) 32-cell stage, animal (F) and vegetal (G) views (H-I) 64c stage, animal (H) and vegetal (I) views. Cells from the right side are underlined only for the 2c stage and the 4c stage. (J) Developmental fate segregation. Since the lineage is bilaterally symmetrical, only the left half is shown. (Adapted from Venuti and Jeffery 1989; Satoh 2014).

gastrulation starts at 112-cell stage). Finally, cell lineages are well documented up to gastrulae stage with the exception of neural lineages in which complete cell lineages are revealed for certain neuronal cell types (Nishida, 1987; Nishida and Satoh, 1983; Stolfi et al., 2011). Five ascidian species including *Halocynthia roretzi*, *Ciona savignyi*, *Ciona intestinalis*, *Ciona robusta*, and *Phallusia mammillata* represent main ascidian models for developmental biology studies. *Ciona intestinalis* and *Ciona robusta* had been studied as same species under the name of *Ciona intestinalis*. In early 2000s, molecular studies concluded that *C. intestinalis* was indeed composed of four distinct lineages named type A, B, C and D. *C. intestinalis* type A and type B were later reclassified as *C. robusta* and *C. intestinalis*, respectively (Brunetti et al., 2015). In our group, we have mainly been working with *Ciona intestinalis* (type B).

## **2) Nomenclature system of ascidian embryonic cells**

The naming system for cells composing the ascidian embryo has been established by Conklin in 1905 (Conklin, 1905). Each cell is named by a letter followed by 2 numbers. All cells are classified into four groups based on their embryonic origins at the 8-cell stage, which are represented by the first letter: “A” for anterior-vegetal origin, “B” for posterior-vegetal origin, “a” for anterior-animal origin and “b” for posterior-animal origin. The first number corresponds to the number of cell cycles counting the first cell cycle of the zygote as 1 and the second number represents the filiation of a cell meaning

that a cell with the second number  $n$  divides into two daughter cells with the second numbers  $2n-1$  and  $2n$  (Venuti and Jeffery, 1989) (Figure 20 A-I).

### 3) Polarisation of the ascidian egg

Ascidian eggs become polarized along the animal-vegetal (A-V) axis during oocyte maturation. The germinal vesicle is located close to the future animal pole of the mature oocyte where the polar bodies will be released (Prodon et al., 2008). Following the Germinal Vesicle Break Down (GVBD), the meiotic spindle translocates to the animal pole. Concomitantly, a specific group of maternal transcripts associated with cortical endoplasmic reticulum (this group of transcripts is called postplasmic/PEM RNAs), and mitochondria enriched in the subcortical region, become cleared from the animal pole. Matured eggs are arrested in metaphase I of meiosis. Fertilization occurs in the environment. Several mechanisms are existing to avoid polyspermy (Lambert et al., 1997). The sperm entry point defines the future posterior pole of the embryo. Following fertilization, two phases of cytoplasmic reorganization take place. The sperm entry first induces a calcium wave that propagates the entire egg. This results in a cortical contraction, driven by cortical actomyosin networks, leading to the concentration of the postplasmic/PEM RNAs and subcortical mitochondria to the vegetal pole. The second phase of reorganization occurs, between the end of the meiosis and the first cleavage, mediated by an astral microtubule-driven migration of male pronucleus. During this phase, postplasmic/PEM RNAs and subcortical mitochondria translocate to the future

posterior pole called PVC (Posterior Vegetal Cytoplasm). At the end of the cytoplasmic reorganization, the ascidian zygote shows a clear polarity with the animal-vegetal axis determined during the oocyte maturation and the anterior-posterior axis defined by the localization of postplasmic RNAs and mitochondria. The first cytokinesis divides the zygote along the anterior-posterior axis, producing a bilaterally symmetrical embryo.

The postplasmic/PEM RNAs located at the posterior pole are equally divided between the two blastomeres. The second cell division takes place along the animal-vegetal axis producing two anterior cells and two posterior cells. The third cell division, leading to the 8-cell stage, results in generation of the animal and vegetal hemispheres of the embryo. At this stage, the four founder lineages are established: the a-line (anterior-animal), the b-line (posterior-animal), the A-line (anterior-vegetal) and the B-line (posterior-vegetal) (Figure 20J). The animal and vegetal hemispheres largely correspond to ectoderm and mesendoderm lineages, respectively.

#### 4) Regionalization of the ascidian embryo along the A-P axis

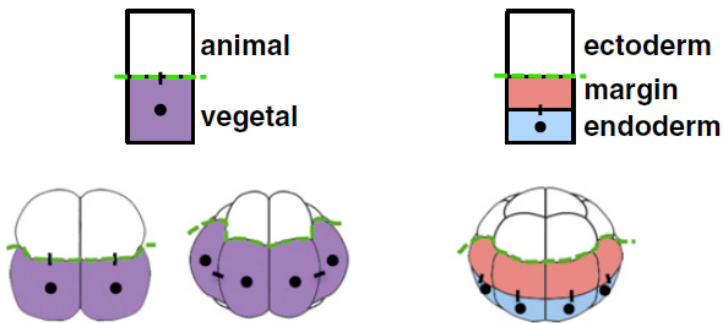
The establishment of the three germ layers in ascidian embryos involves differential nuclear  $\beta$ -catenin levels associated with the first two animal-vegetal orientated divisions. As described above, the first animal-vegetal orientated division, leading to the 8-cell stage, segregate the embryo into mesendoderm and ectoderm lineages (Conklin 1905; Nishida 1987). This lineage segregation operates as a binary fate choice controlled by differential nuclear  $\beta$ -catenin activity: high nuclear  $\beta$ -catenin

activity promotes mesendoderm fates while low nuclear  $\beta$ -catenin activity results in a default ectoderm fates (Hudson et al., 2013; Imai et al., 2000; Rothbacher et al., 2007). Nuclear  $\beta$ -catenin, activated only in the vegetal hemisphere via unknown mechanisms, represses the maternal factor GATA4/5/6 (formerly GATAa), leading to differential transcriptional activity of GATA4/5/6 between animal and vegetal hemispheres (Rothbacher et al., 2007). This repression is mediated by formation of a ternary complex between  $\beta$ -catenin, TCF and GATA4/5/6, resulting in titration of free GATA4/5/6 (Oda-Ishii et al., 2016). At the 16-cell stage, GATA4/5/6 activates the ectoderm gene program in the animal hemisphere (Horikawa et al., 2013; Rothbacher et al., 2007), while the  $\beta$ -catenin/TCF complex promotes the mesendoderm gene program in the vegetal hemisphere (Hudson et al., 2016; Imai et al., 2000). The mesendoderm gene program downstream of nuclear  $\beta$ -catenin includes *Foxa.a*, *Foxd* and *FGF9/16/20*. Each of these three factors are required for specification of both mesoderm and endoderm lineages and their combinatorial activity is sufficient to reprogram ectoderm lineages to adopt mesendoderm fates (Hudson et al., 2016).

Cell divisions leading to the 16-cell stage take place in the medio-lateral axis in the vegetal hemisphere. As described above, cells in the vegetal hemisphere start to express the mesendoderm gene program, *Foxa.a*, *Foxd* and *FGF9/16/20* (Hudson et al., 2016). The following cell divisions leading to the 32-cell stage take place along the A-V axis in the mesendoderm lineage, segregating it into neuromesoderm lineage (at the margin side) and endoderm lineage (at the vegetal pole side). The neuromesoderm lineage will generate mesoderm (notochord) and posterior parts of the central nervous

step 1: 8-16 cell stage  
“animal-vegetal choice”

step 2: 32-cell stage  
“margin-endoderm choice”



$\beta$ -catenin activity		region
8 to 16	32	
OFF	OFF	Ecto
ON	OFF	Margin
ON	ON	Endo

**Figure 21:** Between 16c stage and 32-cell stage,  $\beta$ -catenin activation sequence of ON-to-ON specifies endoderm, OFF-to-OFF ectoderm, and ON-to-OFF neuromesoderm. (From Hudson et al. 2013)

system and might represent an equivalent of bi-potent neuromesodermal progenitors in vertebrate embryos (Attardi et al., 2018). The segregation of the mesendoderm lineage is also controlled a differential activation of nuclear  $\beta$ -catenin, which exhibit a higher activity in the endoderm lineage (Hudson et al., 2013). In the endoderm lineage, nuclear  $\beta$ -catenin, together with the mesendoderm specifiers, *Foxa.a*, *Foxd* and *FGF9/16/20*, activates the endoderm gene program. Since the mesendoderm specifiers themselves are targets of nuclear  $\beta$ -catenin in the previous cell cycle, the endoderm transcriptional network is initiated via a coherent feed-forward loop (Hudson et al., 2016). In the neuromesoderm lineage, the mesendoderm specifiers activate expression of the *Zic-r.b* gene (formerly *ZicL*), which is required for both mesoderm and neural fates (Imai et al., 2002). Importantly, *GATA4/5/6*, now released from the repressive association with  $\beta$ -catenin/TCF complex in the neuromesoderm lineage, is directly involved in the transcriptional activation of *Zic-r.b* (Imai et al., 2016), while *FoxD* keeps *GATA*-mediated ectoderm gene expression repressed in this lineage (Tokuhiro et al., 2017).

Altogether, the segregation of the major embryonic lineages (ectoderm, mesoderm and endoderm) in ascidian embryos operates following a surprisingly simple Boolean-like function: a  $\beta$ -catenin activation sequence of ON-to-ON specifies endoderm, OFF-to-OFF ectoderm, and ON-to-OFF neuromesoderm (Hudson et al., 2013) (Figure 21). These ON/OFF sequences of nuclear  $\beta$ -catenin activity have a direct consequence on transcriptional activity of *GATA4/5/6*, segregating the embryos into *GATA*-ON and  $\beta$ -catenin-ON domains.

In the following section, I will discuss how neural lineages are segregated from both ectoderm and neuromesoderm lineages.

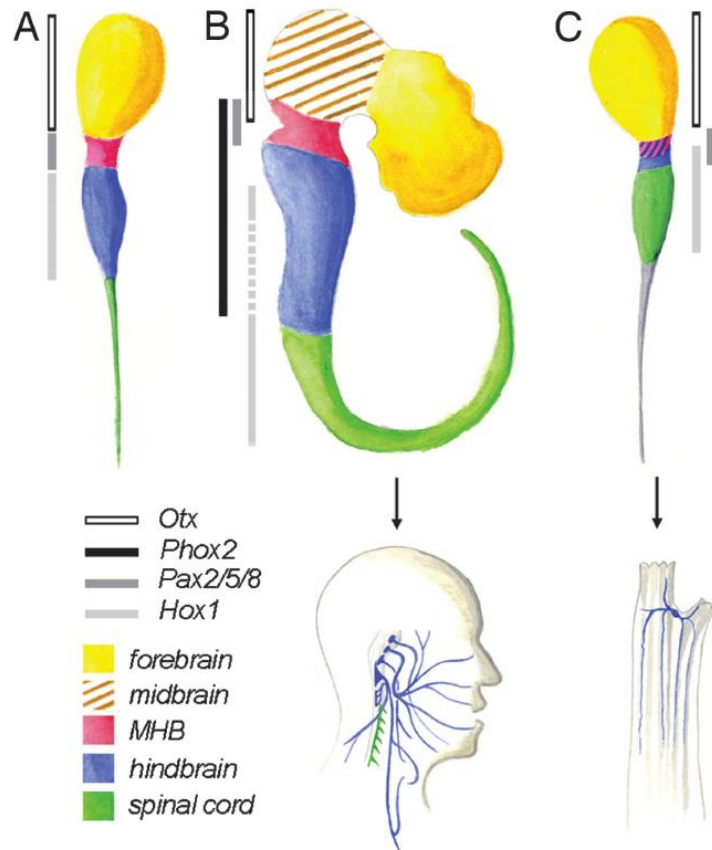


**Figure 22:** Homologies between rostrocaudal regions of the ascidian larva and the vertebrate CNS and between their motoneuronal derivatives. (A) Previous model proposed for the ascidian tripartite brain based on gene expression in *H. roretzi* (B) Up: Rostrocaudal partition of the vertebrate CNS (C) up: New version of the ascidian larval brain. B lower and C lower Schematic of vertebrate (B lower) and adult ascidian (C lower) motoneurons color-coded according to their origin and nature. Blue indicates branchiovisceral motoneurons born in the hindbrain; green indicates somatic motoneurons born in the spinal cord. From (Dufour et al., 2006)

#### IV. State of the art for neural induction in *Ciona intestinalis* embryos

---

##### 1) Ascidian larval central nervous system and its cell lineages

The central nervous system (CNS) of ascidian larvae is composed of three morphological domains, the anterior-most sensory vesicle, followed by a narrow 'neck' region, a trunk ganglion and tail nerve cord (Dufour et al., 2006). This tubular structure forms through rolling up of the neural plate (Hashimoto et al., 2015). The developing ascidian CNS can be directly compared to its vertebrate counterpart, with many conserved molecular features such as expression of the *Otx* gene anteriorly and *Hox* genes posteriorly (Figure 22). However, homologies between the vertebrate and the ascidian CNS are not entirely resolved (Dufour et al., 2006; Ikuta and Saiga, 2007; Imai et al., 2002; Wada et al., 1998). The ascidian CNS consists of approximately 330 cells, of which 177 are identified as neurons. A comprehensive connectome of all its neurons and synapses has been recently compiled using serial-section electron microscopy (Ryan et al., 2016). The ascidian central nervous system derives from the a-, b- and A-lineages (Nishida and Satoh, 1983). The a-line neural lineages contribute to sensory vesicle. The A-line lineages generate the lateral and ventral cells of the posterior sensory vesicle, trunk ganglion and tail nerve cord, while the b-line lineages give rise to the dorsal most row of cells of the neural tube, from the posterior part of the sensory vesicle to the tail nerve cord (Cole and Meinertzhagen, 2004; Nishida, 1987) (Figure 23). Both a- and b-line neural lineages originate from ectoderm lineages while the A-line neural lineage is segregated from mesendoderm lineages by way of a

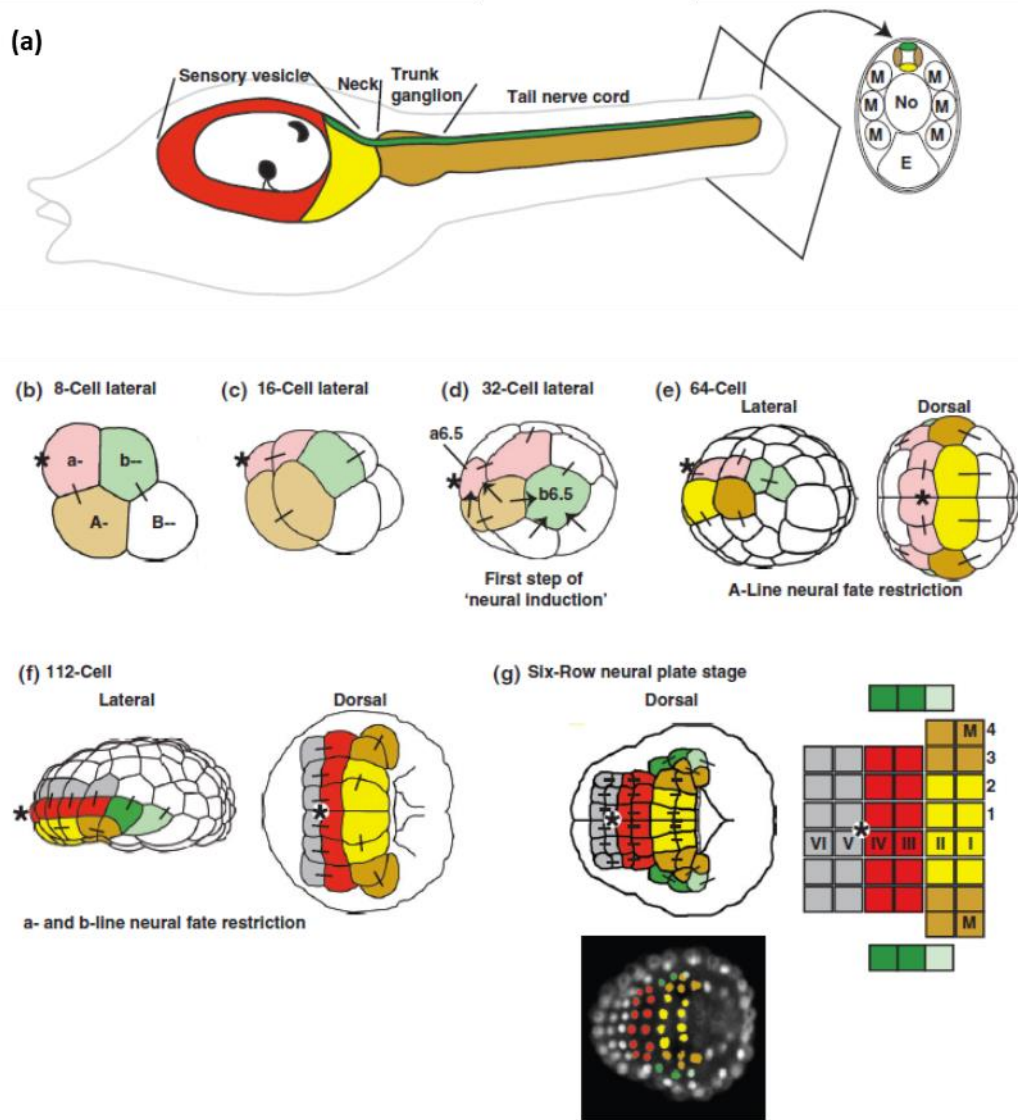


**Figure 23:** Lineages of the central nervous system. (a) Drawing in lateral view of an ascidian larval central nervous system (CNS) showing the sensory vesicle, neck, trunk ganglion, and tail nerve cord. For illustration, the CNS has been greatly enlarged within the larvae. To the right of the larva is shown a transverse section of the tail showing the organization of the nerve cord (colored), muscles (M), notochord (No), and endoderm (E). (a–g) The embryos drawings are all shown with anterior to the left. Lineages are identical on each side of the bilaterally symmetrical embryo. The side from which the embryo is viewed is indicated. Sister cell relationships are indicated by bars connecting the cells. The color code is as follows: red: a-line lineage CNS-fate restricted; pink: a-line CNS lineages before fate restriction; gray: anterior non-CNS a-line neural plate; yellow: medial A-line neural plate derivatives; tan: lateral A-line neural plate derivatives; pale tan: A-line neural lineages before neural fate restriction; green: b-line CNS; pale green: b-line neural lineages before fate restriction. Note: posterior–lateral A-

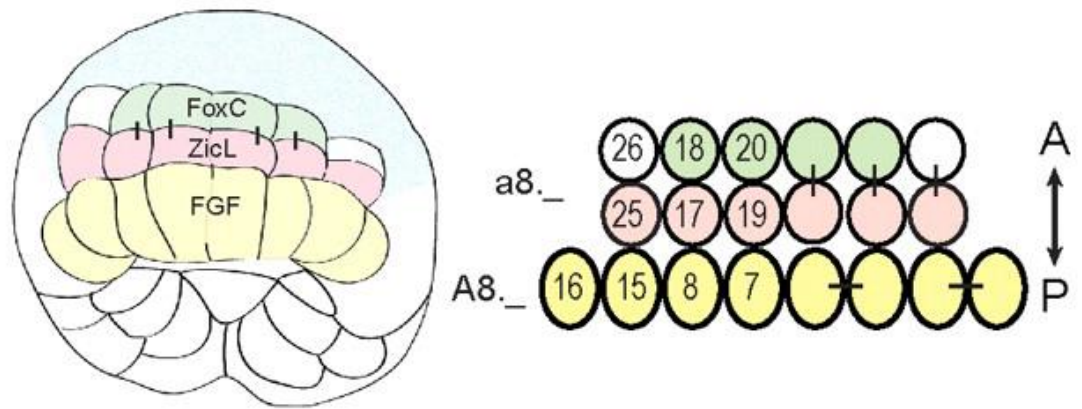
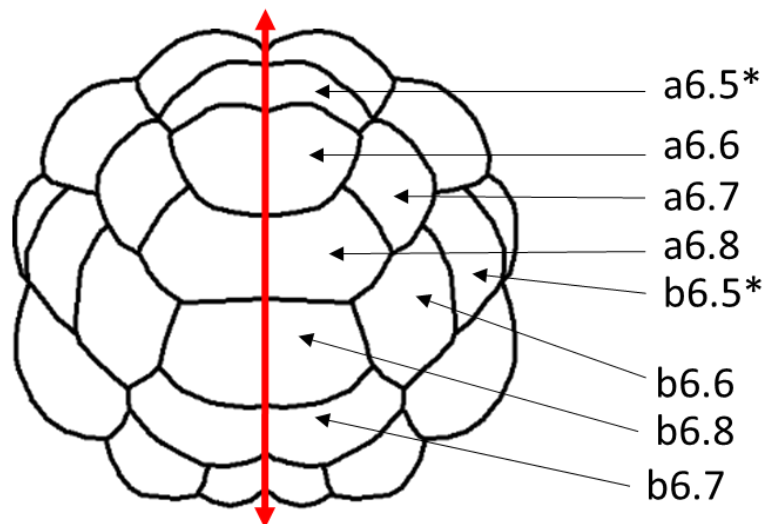
transient neuromesoderm state.

The molecular mechanisms controlling initial steps of neural fate specification are well characterised. The a- and b-lines are specified as neural lineages within ectodermal cells at the 32-cell stage by a process equivalent to induction of the vertebrate anterior neural plate (Bertrand et al., 2003; Hudson et al., 2013). The ectodermal cells adopt either neural or epidermal fates depending on their response to the neural inducer, FGF9/16/20. This inductive process results in activation of a MAP kinase, ERK1/2, in four ectodermal cells [two a-line (a6.5) and two b-line (b6.5) cells], which acquire neural fates (Figure 24B). This inductive process represents the subject of my PhD study and will be described more in detail later. During subsequent two cell cycles, until early gastrula stage (112-cell stage), ERK1/2 remains active in the a-line neural lineages (unpublished data). At the 64-cell stage, the lateral a-line neural plate precursors are segregated from epidermal fate to give rise to one row of six cells (Figure 23). When these six cells divide along the anterior-posterior (A-P) axis during

---

line 'CNS lineages' also contribute to muscle. For simplicity, this lineage is considered as 'neural fate restricted' here. The contribution of the posterior-most b-line (pale green in f-g) is not resolved. An asterisk marks the anterior-most border of the CNS. Major events in CNS development are indicated below the drawings. The arrows on (d) indicate the FGF neural inducing signals. (g) On the right of the neural plate stage embryo drawing is a schematic representation of the neural plate. The neural plate is a grid-like organization of cells aligned in four columns whereby column 1 is the medial-most column and column 4 the lateral-most. The six rows are named rows I to VI with row I the posterior most. 'M' is the muscle cell that derives from the A-line neural lineages. Below the drawings is a six-row stage embryo with nuclear staining. Nuclei are colored according to the lineages shown in the figure. (Adapted from Hudson, 2016)

the generation of the 112-cell stage embryo, an important cell fate segregation takes place: the separation of CNS neural plate precursors (row III/IV) from the non-CNS anterior neural plate precursors (row V/VI) (Figure 24). This fate segregation also involves FGF signals, with FGF-ERK signalling promoting CNS over non-CNS fate and resulting in *Zic-related.b* (*Zic-r.b*, formally *ZicL*) expression in CNS precursors and *Foxc* in non-CNS precursors (Wagner and Levine, 2012) (Figure 24A). Thus, FGF signals govern the first two neural segregation steps, 'neural induction' and CNS specification. During the first step of neural induction, the neural precursors are prevented from precociously adopting the CNS neural fate (*Zic-r.b*-positive) by a neural lineage takes place in parallel to a-line and involves similar mechanisms. *Otx* and *Nodal* are induced in the b6.5 neural precursors by FGF signals at the 32-cell stage (Figure 24B). The differential activation of *Nodal* by FGF in b-but not a-line cells, is governed by *Foxa.a* (formally *FoxAa*) (Imai, 2006; Lamy, 2006; Ohta and Satou, 2013). *Foxa.a* is expressed in all a-line cells where it blocks transcriptional activation of *Nodal*. How *Foxa.a* is differentially activated between a-and b-lineages is not yet clear, though the ooplasmic segregation in the zygote that establish the anterior-posterior axis is likely to be involved. *Nodal* and *Otx* are required for the specification of b-line neural lineage (Roure et al., 2014). By the early gastrula stage, two cell divisions of the b6.5 lineage have resulted in the segregation of the CNS lineages from the lateral non-CNS border lineages (Figure 23). At the 6-row neural plate stage, the b-lineages divide along the anterior-posterior axis. The mechanisms leading to b-line neural fate segregation have not yet been addressed.

**A****B**

**Figure 24:** (A) Neural plate in *Ciona* embryo. LEFT: Schematic drawing of the 112c stage embryo with cells expressing FoxC (green) and their sister cells expressing ZicL (pink). Vegetal A-line neural precursors in yellow express FGF9/16/20. In blue, non neural ectoderm. RIGHT: Nascent neural plate (three rows of cells). Bars indicate sister cells. The a-line refers to cells from the anterior ectoderm, a8.\_ indicates cells in the eight generation. A-line indicates the anterior vegetal lineage (Adapted from Wagner and Levine, 2012). (B) Animal pole view of the late 32 cell stage ascidian embryo. Red line indicates the medial axis, asterisks indicate neural precursor cells.

In contrast to the a- and b-line neural lineages that originate from ectoderm of the animal hemisphere, the A-line neural lineage derives from the vegetal hemisphere and is closely associated with mesendoderm lineages (Figure 23). Three rounds of asymmetric cell divisions sequentially segregate the A-line neural lineage. The first two rounds of the asymmetric cell divisions are driven by differential activation of the  $\beta$ -catenin/TCF complex and are described in the previous section. They are leading to segregation of endoderm and neuromesoderm lineages (Hudson et al., 2013). In the last and third round of asymmetric cell division, the neuromesodermal lineage segregates into mesoderm and neural lineages at the 44-cell stage. Differential activation of ERK1/2 controls this lineage segregation with the MAP kinase activated in mesoderm precursors but repressed in A-line neural precursors by directional ephrin/Eph signals originating from overlying ectoderm cells (Picco et al., 2007). I will describe later in detail about ephrin/Eph-mediated attenuation of ERK activation, which is deployed recurrently during ascidian embryogenesis. During the next cell cycle leading to the 112-cell early gastrula stage, ERK1/2 activation remains attenuated in the A-line neural lineage (Yasuo and Hudson, 2007). By this stage, the A-line neural lineage is composed of a single row of eight cells, which subsequently divide along the anterior-posterior axis to form rows I and II of the 6-row stage neural plate. I would like to highlight the dichotomy in terms of requirement for FGF-ERK signals between the a- and the A-line neural lineages; for the a-line, the signals are required to induce neural fates, while, for the A-line, they have to be attenuated to promote neural fates.

## 2) Neural induction in *Ciona* embryos

As described above, in ascidian embryos, neural induction starts at the 32-cell stage, segregating a- and b-line neural lineages. At this stage, the embryo consists of 16 ectoderm cells in the animal hemisphere and 16 mesendoderm cells in the vegetal hemisphere. Among the 16 ectoderm cells, two pairs of cells, a6.5 and b6.5, are induced as neural progenitors. FGF signals were identified as a potential neural inducing signal since a treatment of isolated a4.2 cells (anterior animal cell of the 8-cell stage embryo) with basic FGF (=FGF2) resulted in induction of neural and neuronal characteristics (Hudson and Lemaire, 2001; Inazawa et al., 1998). Subsequently, it was shown that the Ras-MEK-ERK cascade mediates the neural induction (Hudson et al., 2003). These studies also characterised activation of ERK and transcriptional activation of *Otx* gene in the four neural precursors as the first molecular readouts of the neural induction (Hudson and Lemaire, 2001; Hudson et al., 2003). Finally, when the neural induction is inhibited, all ectodermal cells adopt epidermal fates. In contrast, when they are treated with basic FGF (bFGF), they become neural (Hudson and Lemaire, 2001; Hudson et al., 2003). These results thus revealed that 1) all ectoderm cells are competent to respond to FGF signals and adopt neural fates and 2) ascidian neural induction operates as a binary fate choice between epidermal and neural fates.

FGF9/16/20 has been identified as the endogenous FGF ligand acting as the neural inducer (Bertrand et al., 2003) (see appendix 1 for more details about FGF biology). *FGF9/16/20* starts to be expressed in mesendoderm lineages at the 16-cell

stage and the expression is maintained in the following 32-cell stage with a stronger expression level observed in A-lineages compared to B-lineages. When *FGF9/16/20* is knocked-down, the *Otx* expression in the four neural precursors is lost and they express instead epidermis-specific genes. Conversely, overexpression of *FGF9/16/20* mRNA in ectoderm explants leads to an ectopic expression of *Otx* in a majority of ectoderm cells (Bertrand et al., 2003).

FGF-mediated neural inducing signals has been directly linked to the transcriptional activation of *Otx* gene (Bertrand et al., 2003). Detailed dissections of the promoter region of the *Otx* gene resulted in identification of an enhancer element of 54-bp long, named a-element, which is sufficient to drive a reporter gene expression in both a- and b-neural lineages and is required for the promoter activity in neural lineages (Bertrand et al., 2003). This short enhancer element contains two ETS and three GATA binding sites and *Ets1/2* and *Gata4/5/6* are identified as the candidate transcription factors mediating its enhancer activity (Bertrand et al., 2003). Vertebrate *Ets1* and *Ets2* and *Drosophila* orthologue, *Pnt-P2*, are known targets of ERK and mediators of its transcriptional response (Brunner et al., 1994; O'Neill and Rubin, 1994; Yang et al., 1996). In contrast, in ascidians, *Gata4/5/6* plays a key role in transcriptional activation of ectoderm-specific genes during early cleavage stages (Horikawa et al., 2013; Rothbacher et al., 2007). The neural-specific activity of the a-element depends on asynergy between the ETS and GATA binding sites since both sites are required for the neural specificity and, in the absence of the ETS binding sites, the enhancer becomes active broadly in ectoderm, indicating that ETS binding sites mediate active

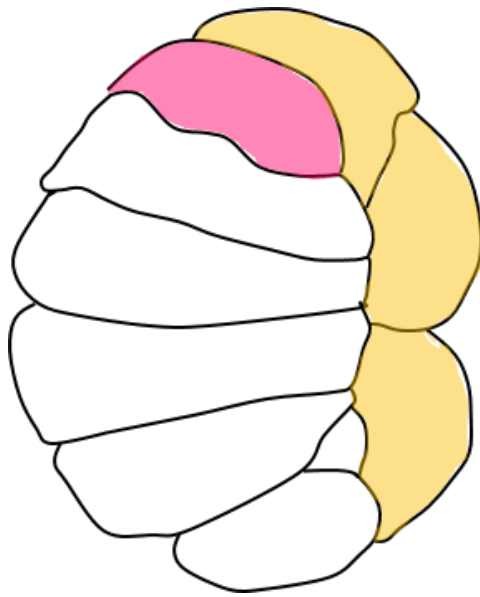
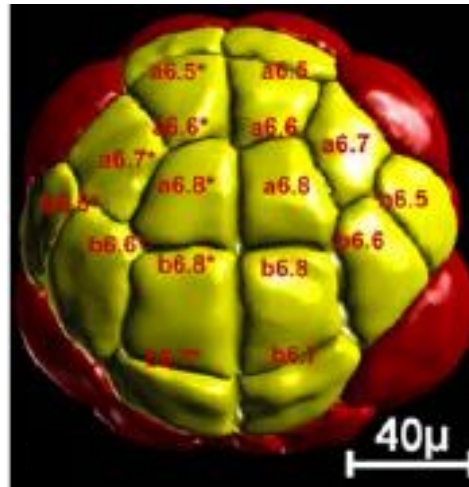


**Figure 25:** Sagittal view of the late 32-cell stage ascidian embryo. Anterior is up, animal pole on the left. Mesendoderm cells expressing FGF9/16/20 are in yellow and a6.5 cell in pink. Note that all ectoderm cells are in direct contact with mesendoderm cells.

repression of the enhancer activity in ectoderm (Rothbacher et al., 2007). In the result section Part 2, I will describe our characterisation of such a repressor and its potential involvement in generating a bimodal response of *Otx* transcriptional activation. Finally, it should be noted that both endogenous *Otx* expression and a-element activity can be induced in ectoderm explants by FGF signals in the absence of protein synthesis, indicating that the transcriptional activation of *Otx* gene is a direct response to FGF signals (Bertrand et al., 2003).

While all ectoderm cells are competent to respond to FGF signals and are in direct contact with FGF9/16/20-expressing mesendoderm cells, only four out of total 16 ectoderm cells are induced as neural precursors (Figure 25). The invariant nature of ascidian embryogenesis has enabled to address this intriguing question *via* quantification of cell surface contacts between the FGF-expressing mesendoderm cells and ectoderm cells during neural induction. This revealed that each ectoderm cell has a different area of cell surface contact with FGF-expressing mesendoderm cells, such that the neural precursors have the largest area of cell contact (Figure 26, Tassy et al. 2006). Assuming that the level of FGF signalling that a cell receives is proportional to the area of cell contact with FGF-expressing mesendoderm cells, a threshold mechanism was proposed in which a larger area of cell contact results in above-threshold levels of FGF signal reception and hence ERK activation and *Otx* expression (Tassy et al., 2006). This hypothesis requires an additional assumption that FGF9/16/20 is not diffusible and acts as a short-range signal. Indeed, this seems to be the case. When *FGF9/16/29* was knocked-down in single mesendoderm cells, its effect

A



B

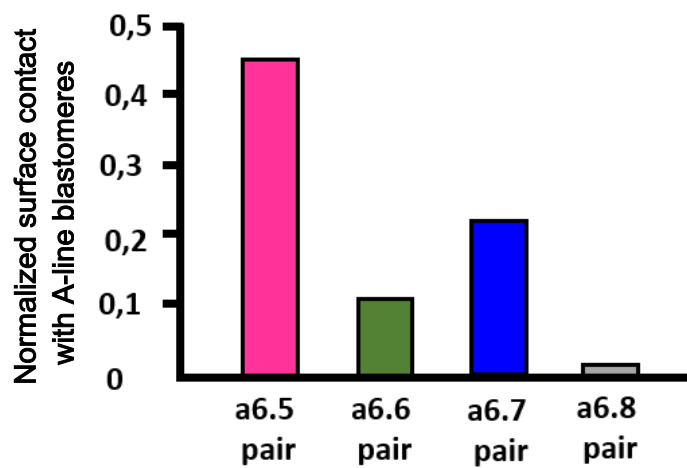


**Figure 26:** (A) Animal view of a reconstruction of a whole embryo at the 32-cell stage. Anterior is up. Animal and vegetal cells are shown in yellow and red, respectively. (B) Surface of contact between a-line cells and the A-line blastomeres. Surfaces were normalized by dividing each value by the total surface of the animal blastomere. Areas were averaged for each cell pair. For each cell, the analysis of a single embryo at the late 32-cell stage is presented. (Adapted from Tassy et al., 2006).

was observed only in directly overlying neural precursors (Miyazaki et al., 2007).

### 3) Antagonistic inputs during neural induction

The emerging model of ascidian neural induction described above has been further elaborated with discoveries of negative regulators of the process. *Efna.d* (formerly *ephrin-Ad*) is one of such regulators. *Efna.d* is expressed in the ectoderm cells themselves (Figure 27) (Ohta and Satou, 2013; Ohta et al., 2015; Picco et al., 2007). Our previous work has shown that forward ephrin/Eph signals, mediated intracellularly via p120RasGAP, act antagonistically to FGF signals, negatively regulating the ERK pathway during early ascidian development (Haupaix et al., 2013; Haupaix et al., 2014; Picco et al., 2007). When *Efna.d* was knocked down, additional ectoderm cells responded to neural inducing FGF signals, exhibited ERK activation and express *Otx* (Ohta and Satou, 2013 ; our unpublished data). Thus, intact ephrin signals are critical for ascidian ectoderm cells to correctly exhibit a threshold response to FGF signals. Since ephrin ligands are membrane-anchored ligands, they are assumed to be proportional to the level of ephrin signal that the cell receives. Consistently, neural precursors have the smallest area of cell contact with other ectoderm cells. Based on this assumption, Ohta et al developed a Boolean function to account for *Otx* expression under control of diverse signalling inputs, including FGF and ephrin signals. This parameter-free approach has concluded that differential expression of *Otx* in the neural lineages is primarily determined by differential inputs of expected to act as short-range

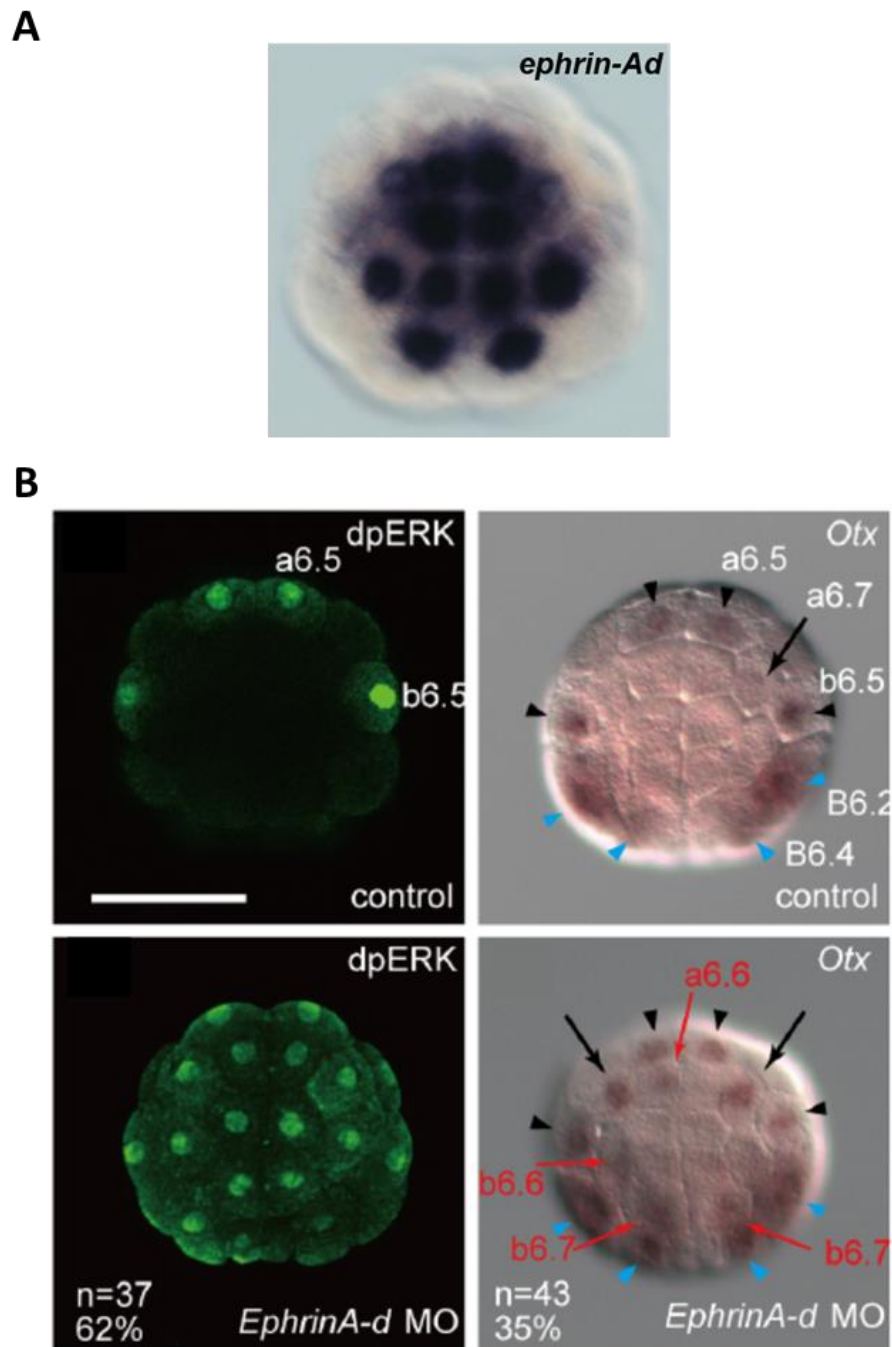


**Figure 27:** (A) Expression of *EfnA.d* in the late 32-cell stage embryo (animal pole view). (B) Effects of knockdown of *EfnA.d* on ERK activation (anti-dpERK IF) and *Otx* expression (in situ hybridisation) in 32-cell stage embryos (Adapted from Ohta and Satou, 2013).

signals (see appendix 1 for more details). In a similar manner to FGF9/16/20, the area of cell surface contact between ectoderm cells could be mediated by *Efna.d* signals, but not by those of FGF9/16/20 signals (Ohta et al., 2015). As I will describe in the result section Part 1, our experimental data argue against this conclusion.

In addition to *Efna.d*, two TGF- $\beta$  superfamily members, *Admp* and *Gdf1/3-r*, are implicated in regulation of *Otx* expression during neural induction (Ohta and Satou, 2013). When these two ligands are simultaneously knocked-down, *Otx* expresses ectopically in ectoderm cells without affecting the spatial pattern of ERK activation. Contrary to this observation, the ectopic activation of *Otx* is dependent on FGF9/16/20 signalling including MEK and Ets1/2, leading the authors to propose that ERK signals are active even in non-neural ectoderm cells while the activation levels are too low to detect experimentally and that these sub-detection levels of ERK activation are sufficient to activate *Otx* expression in the absence of *Admp/Gdf1/2-r* signals. In other words, *Admp/Gdf1/2-r* signals repress *Otx* expression in response to the sub-detection levels of ERK activation. Consistently, two putative Smad-binding sites and one Smad4-binding site were identified within 100 bp upstream of the  $\alpha$ -element and, when the 100-bp region was placed upstream of the  $\alpha$ -element driving a reporter gene, the number of embryos expressing the reporter was reduced while increasing the ratio of embryos exhibiting neural-specific expression of the reporter (Ohta and Satou, 2013). In addition to the *Admp/Gdf1/2-r*-mediated repression, the spatial precision of *Otx* expression mediated via the  $\alpha$ -element appears to be achieved by submaximal recognition motifs of the ETS and GATA binding sites (Farley et al., 2015). It has been

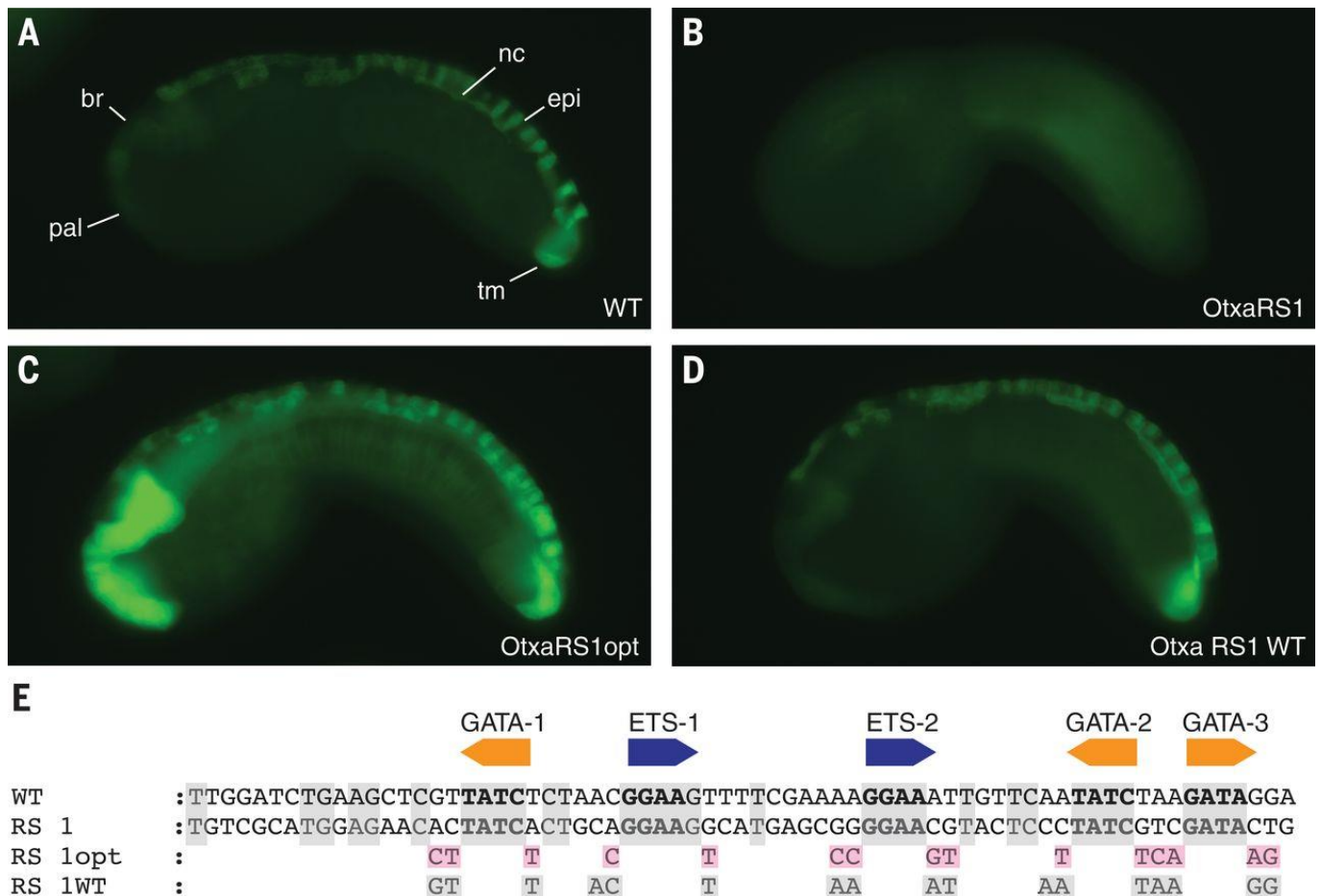


**Figure 28:** Suboptimal binding sites are sufficient for tissue-specific expression. (A) Embryo electroporated with WT *Otx-a* enhancer; GFP can be seen in the anterior brain (br), palps (pal), dorsal nerve cord (nc), dorsal midline epidermis (epi), and two tail muscle cells (tm). (B) Embryo electroporated with *Otx-a* RS1, a synthetic enhancer variant identified in our screen that shows no GFP expression. (C) Embryo electroporated with *Otx-a* Random-Synthesized (RS) 1opt, with all five core sites changed to have optimized flanking sequence; expression can be seen in endogenous location and in notochord, mesenchyme, endoderm, and posterior brain. (D) Embryo electroporated with *Otx-a* RS1 WT with all five core sites mutated to have WT flanking sequences; expression can be seen in endogenous *Otx-a* location only. (E) Sequence of WT, *Otx-a* RS1, *Otx-a* RS1 opt, and *Otx-a* RS1 WT enhancer variants. Gray boxes highlight bases conserved in WT *Ciona intestinalis* *Otx-a* sequence; pink boxes highlight bases that were changed to match identified “optimal” flanking motifs. All images were taken at the same exposure time, 500 ms. (Adapted from Farley et al. 2015)

shown that the GATA and ETS binding sites in the  $\alpha$ -element contain imperfect matches to consensus motifs, rendering their binding affinities reduced. When these sites are optimised to match the consensus motifs, the enhancer activity becomes robust but also loses its spatial precision (Figure 28).

Altogether, these results highlight that enhancer activity of the *Otx*  $\alpha$ -element is “weaken” via multiple mechanisms to achieve its spatial specificity.

## V. Objectives

---

During my PhD project, I aimed to unravel the mechanisms that permit cells to interpret a gradual signal into an ON/OFF response. As shown in this introduction, interpretation of gradual signal by cell is a key process to succeed embryogenesis. A lot of studies exist but very few take place in a multicellular context of a developing embryo. Thus, I used the neural induction model of *Ciona intestinalis* embryos during which gradual signals lead to the binary choice of ectodermal cells between neural and epidermal fate. At the 32-cell stage, *Ciona* embryos are composed of 16 ectodermal cells and 16 mesendodermal cells. During the neural induction process, four cells among the 16 ectodermal cells will adopt a neural fate in response to two antagonistic signals, FGF expressed by the mesendodermal cells and ephrin by the neighbouring ectodermal cells. The 16 ectodermal cells are competent to adopt a neural fate but only the two pairs of neural precursors will do so. The four neural precursors will show an activation of the kinase ERK followed by the expression of the *Otx* gene. Then, we wondered how cells interpret these two antagonistic signals to make a binary choice between neural fate and epidermis fate. In order to understand the mechanisms involved during the neural induction process, we studied in a quantitative manner ERK activation but also the activation of the *Otx* gene expression.

I would like to highlight that my PhD project was fully part of the team research project. It is then complicated to isolate specifically my personal contribution. My main contributions to the part I of the results (paper manuscript) are found in figures 1, 2, 3,

7, 8 and Supplementary figures 1, 3, 4, 8, 11,12. On the part II of the results part, my main contributions are on the figure 31 and table 1 (ERF results).

# RESULTS



# I. ephrin-mediated “dampening” of FGF signalling underlies the spatial precision of ascidian neural induction

---

*Manuscript in preparation*

**Signal dampening and a bimodal transcriptional response underlie spatial precision of an embryonic induction**

**Géraldine Williaume<sup>1\*</sup>, Cathy Sirour<sup>1\*</sup>, Nicolas Haupaix<sup>1,4</sup>, Sophie Du Buyl<sup>2</sup>, Geneviève Dupont<sup>3</sup>, Clare Hudson<sup>1\*§</sup> and Hitoyoshi Yasuo<sup>1\*§</sup>**

\* equal contribution

§ corresponding authors: hudson@obs-vlfr.fr; yasuo@obs-vlfr.fr

1- Sorbonne Université, CNRS, Laboratoire de Biologie du Développement de Villefranche-sur-mer (LBDV), 06230 Villefranche-sur-mer, France.

2- Applied Physics Research Group, Vrije Universiteit Brussel, Brussels, Belgium.

3- Unité de Chronobiologie Théorique, Faculté des Sciences, CP231, Université Libre de Bruxelles, Boulevard du Triomphe, B-1050 Brussels, Belgium. 4- Nicolas current address: Center for Interdisciplinary Research in Biology, Collège de France, 11 Place Marcelin Berthelot, 75005 Paris, France

## SUMMARY

Precise regulation of FGF-Ras-ERK signalling is critical for development, homeostasis and disease, highlighting the importance of a quantitative understanding of this signalling pathway. We describe in a semi-quantitative manner the FGF-dependent activation of an immediate early gene, *Otx*, during ascidian neural induction, whereby precisely four out of a total of 16 ectoderm cells adopt neural fate. The entire induction process takes less than 30 minutes, encompassing a single cell cycle of the responding cells. The levels of ERK activation in ectoderm cells correlates with their area of cell surface contact with the FGF-expressing mesendoderm cells. Mathematical analysis predicts greater sensitivity to changes in surface contact compared to changes in ligand concentration, consistent with our experimental observations. Antagonistic ephrin signals dampen ERK activation levels, so that only neural precursors exhibit high enough levels of ERK activation for the threshold response of *Otx* transcription. Together, these findings provide a comprehensive view of how the spatial precision of a lineage segregation is achieved in a contact-dependent embryonic induction.

## INTRODUCTION

FGF signalling is implicated in a variety of cellular and developmental processes, controlling decisions of differentiation, survival, proliferation, morphology, patterning and migration, as well as playing an important role in homeostasis and pathology in adults. Mutations affecting FGFs or the downstream signalling cascades can have disastrous consequences for development and health. The Ras-MEK-ERK signal transduction cascade is one of the principle mediators of FGF-signalling in vivo. In the context of developmental fate decisions, ERK alters the gene expression profile of a responding cell by modifying the activity of transcriptional factors, which leads to a change in the developmental trajectory of the cell.

Activation of the ERK pathway can be stimulated via various growth factors. The temporal dynamics and sensitivity/kinetics of the ERK activation response to growth factor stimulation varies depending on the signalling context (cell type, growth factor). ERK activation dynamics can be sustained, transient or oscillatory/pulsatile. Different sensitivities to the concentration of growth factor result in ERK responses that are switch-like (ultrasensitivity, bistability), gradual, linear, or with different oscillatory frequencies. Thus, the intracellular Ras/MEK/ERK cascade can be intrinsically gradual or switch-like, depending on the cellular and signalling context. In turn, differences in the dynamics (duration of activity, frequency of pulses), amplitude, or cumulative load of the ERK cascade output can promote distinct cellular responses

Despite the importance of the Ras-MEK-ERK signalling cascade in driving developmental processes, there are few quantitative studies on the control of ERK in an in vivo multicellular context (Aoki et al., 2017; Coppey et al., 2008b; de la Cova et al., 2017b; Hiratsuka et al., 2015b; Johnson and Toettcher, 2019a; Lim et al., 2015b; Melen et al., 2005b; Ogura et al., 2011; van Bortel et al., 2018; Wong et al., 2018). Here we present neural induction in *Ciona intestinalis* as a unique model to study quantitatively FGF-ERK signalling in single cells within a multicellular context. This signal transduction event takes place in the period of a single cell cycle of approximately 30 minutes and results in the direct induction of an immediate-early gene.

Ascidians are marine invertebrate chordates that develop with a fixed cell lineage and small number of cells, which makes them an ideal system for studying individual cell behaviour in a multi-cellular context. Four founder lineages are established at the 8-cell stage, the a- and

b-lineages (ectoderm) in the animal half of the embryo and the A- and B-lineages (mesendoderm and some neural) of the vegetal half (Conklin, 1905b; Nishida and Satoh, 1983b). Cells are named throughout development with the letter (a-, b-, A-, B-) denoting this embryonic origin. Embryos are bilaterally symmetrical, forming a left and a right half, so each cell name refers to a pair of cells. In ascidian embryos, FGF/MEK/ERK signals play a multitude of roles during fate diversification. One well-studied role of FGF signalling is initiating the segregation of neural from ectoderm lineages at the 32-cell stage of development, which represents the initial step of neural induction in ascidian embryos. 32-cell stage embryos consist of 16 animal (ectoderm) and 16 vegetal (mesendoderm) cells (Figure 1A). Among the eight pairs of ectoderm cells, two pairs, a6.5 and b6.5, adopt lineages contributing to the larval central nervous system (CNS), specifically, the anterior-most part of the sensory vesicle (a6.5) and the dorsal neural tube (b6.5) (Nicol and Meinertzhagen, 1988; Nishida, 1987b). At the 32-cell stage of development, the a6.5 and b6.5 cells exhibit ERK activation and express the *Otx* gene in response to FGF9/16/20 emitted from underlying mesendoderm cells (Bertrand et al., 2003b; Hudson et al., 2003a; Nishida, 2003; Ohta and Satou, 2013a). *Otx* is a direct target of FGF9/16/20 pathway, being induced in the absence of protein synthesis, via ETS and GATA transcription factors (Bertrand et al., 2003b; Miya and Nishida, 2003). When neural induction is inhibited, all ectoderm cells adopt epidermal fate. Thus, ascidian neural induction operates as a binary fate decision, neural versus epidermis. All ectoderm cells are competent to respond to FGF9/16/20 and activate *Otx* (Hudson and Lemaire, 2001b; Miyazaki et al., 2007b; Ohta and Satou, 2013a). FGF9/16/20 appears to have a short range effect, acting only between cells that are in direct contact (Miyazaki et al., 2007b). Reconstruction of 32-cell stage embryos shows that all ectoderm cells are in direct contact with vegetal FGF9/16/29-expressing mesendoderm cells and that the neural precursors a6.5 and b6.5 have the largest area of cell surface contact with the FGF9/16/20-expressing cells (Tassy et al., 2006b). A threshold model was proposed whereby a6.5 and b6.5 are the only two cells with high enough exposure to FGF-ligands for neural induction to take place (Tassy et al., 2006b). a6.7 cells has the next highest area of cell surface contact with vegetal cells and these cells occasionally also express *Otx* (Ohta and Satou, 2013a; Tassy et al., 2006b). a6.7 can perhaps be considered at an intermediate position, close to the threshold for *Otx* induction. At the next cell division, a6.7 will divide into one neural precursor and one epidermal precursor at the 64-cell stage of

development, so this intermediate exposure may be required to prime this cell for the correct specification of neural fates that subsequently takes place in this lineage.

In addition to FGF9/16/20, which induces neural fate, an ephrin ligand, *Efna.d*, is expressed in the ectoderm cells themselves and acts via Eph3/p120RasGAP to attenuate the Ras-MEK-ERK cascade and prevent ectopic *Otx* activation in non-neural precursors (Haupaix et al., 2013; Ohta and Satou, 2013; Ohta et al., 2015; Picco et al., 2007; this study). Ectoderm cells with the highest cell surface contact with FGF-expressing vegetal cells (a6.5 and b6.5) have the lowest cell surface contact with ephrin-expressing ectoderm cells and visa-versa (Figure 1) (Ohta and Satou, 2013a; Tassy et al., 2006b). A theoretical analysis based on Boolean function suggests that the differential exposure to *Efna.d* alone should be sufficient to account for the observed pattern of *Otx* expression (Ohta et al., 2015a).

In previous studies, non-quantitative means of measuring ERK activity and *Otx* gene expression were used. Therefore, it was not possible to test the exact nature of the response of individual cells to FGF signals. For example, it is not clear if 'non-responding cells' receive below threshold levels of FGF9/16/20 and therefore do not exhibit ERK activation or whether their response is simply below the level of detection for standard immunofluorescence. We also do not know the exact role that ephrin/Eph signals play in establishing this pattern of ERK activation. Similarly, while much progress has been made on understanding the transcriptional regulation of *Otx* induction (Bertrand et al., 2003b; Farley et al., 2015b; Ohta et al., 2015a; Rothbacher et al., 2007b), the exact nature of transcriptional response of the *Otx* gene is not yet clear. In this study, we attempt to address these issues, measuring, in a semi-quantitative manner, the activation of both ERK and *Otx* expression in both normal, and ephrin/Eph-signal perturbed embryos.

## RESULTS

### Each ectoderm cell exhibits a specific configuration with respect to its neighbouring cells

Of the eight pairs of ectoderm cells in 32-cell stage embryos, we focused on the four pairs of a-line cells, namely a6.5, a6.6, a6.7 and a6.8. The a-line ectoderm cells are in contact with A-line mesendoderm, but not B-line cells, which express lower levels of *FGF9/16/20* compared to A-line cells (e.g. Bertrand et al., 2003; Imai et al., 2002; Tassy et al., 2006, our unpublished). We first confirmed that each a-line ectoderm cell exhibits a distinct area of cell surface contact with A-line mesendoderm cells (Figure 1). In order to address how variable these cell configurations might be in *Ciona* embryos, we reconstructed a total of 21 embryos, selected precisely at the late 32-cell stage from four independent fertilisations. In order to obtain robust membrane staining, critical for automated segmentation, we expressed in embryos GFP-fused with a pleckstrin homology domain (PH-GFP) (Carroll et al., 2003) and processed embryos for anti-GFP immunofluorescence (IF) (Figure 1A). Confocal scanned embryos were reconstructed using Amira software (Figure 1A). The areas of cell surface contacts of a-line ectoderm cells were measured and normalised for cell size (area of surface contact/total cell surface) to give relative area of cell surface contact. a6.5 consistently has the largest relative area of surface contact with A-line vegetal cells, with strong statistical support for differences between each cell type such that a6.7 has the second largest area of contact, followed by a6.6 and a6.8 (Figure 1B). The graph (Figure 1B) reveals some overlap between the relative surface contacts between the different cells, particularly a6.6, a6.8 and a6.7. In order to address whether the variation in our measurements was between or within embryos, we calculated the percentage of embryos in which the relationships  $a6.5 > a6.7$ ,  $a6.7 > a6.6$  and  $a6.6 > a6.8$  were observed, considering each embryo half independently. In the vast majority of embryo halves, the relationships  $a6.5 > a6.7 > a6.6 > a6.8$  were observed (Table 1). Thus, there is a distinct order among a-line ectoderm cells in terms of their relative areas of cell surface contact with neural inducing A-line mesendoderm cells. As shown in previous studies (Ohta and Satou, 2013a; Tassy et al., 2006b), the area of cell surface contact of individual ectoderm cells to FGF-expressing mesendoderm cells correlates strongly and inversely to the area of cell surface contact with neighbouring ectoderm cells that express ephrin ligands (Figure 1C). Thus, cells that experience higher levels of contact with FGF-expressing mesendoderm cells

experience at the same time lower levels of contact with ephrin-expressing cells, and visa-versa.

### **a-line ectoderm cells exhibit distinct levels of ERK activation**

ERK activation levels in individual a-line ectoderm cells appears to correlate with the area of cell surface contact with A-line mesendoderm cells. We quantified active ERK levels in individual a-line ectoderm cells based on immunofluorescence (IF) staining for dually phosphorylated ERK (dpERK). To this end, we removed the signal amplification process from our original protocol of anti-dpERK IF (Haupaix et al., 2013a; Stolfi et al., 2011b) (see materials and methods for details). Anti-Histone 3 (H3) IF was conducted in parallel to segment nuclei for quantification of nuclear dpERK IF signals (Figure 2A,B). We first analysed large batches of embryos from a single fertilisation. Approximately 50 embryos at the late 32-cell stage were processed for anti-dpERK and anti-H3 IF in a single tube, aligned on a single cover slip and rendered transparent. Mean pixel intensity of nuclear dpERK IF signal revealed that each cell exhibited a distinct level of ERK activation (Figure 2B, S1A, C). a6.5 consistently exhibited the highest levels, followed by a6.7, a6.6 and a6.8, a pattern that appeared remarkably similar to the area of cell surface contact measured between inducing and responding cells (Figures 1B, 2B, S1A, C). In the vast majority of embryos, the relationship  $a6.5 > a6.7 > a6.6 > a6.8$  was observed when analysed at the level of individual embryo halves (Table 1).

During neural induction, activation of ERK depends upon the FGF/MEK/ERK signalling pathway (Hudson et al., 2003a). Comparing groups of untreated and U0126-treated embryos, processed for dpERK IF under identical conditions (same tube), we found that the nuclear dpERK signal was strongly reduced in a6.5 and a6.7 (Figure S1E). Inhibition of FGF signalling in only one half of the embryo allowed us to compare ERK activation levels between control and FGF-inhibited halves within the same embryo. mRNA for *Ciona dnFGFRc* or *PH-GFP* was injected into one cell of the two-cell stage embryo together with fluorescent dextran as tracer and processed for anti-dpERK IF at the late 32-cell stage (Figure 3B). While the ratio of injected/control side for nuclear dpERK signals was around 1 for *PH-GFP* injected embryos (no statistically significant difference from 1, following one sample t-test against 1), *dnFGFRc* injected embryos showed a significant reduction in nuclear dpERK IF signals in a6.5, a6.7 and

a6.6 (Figure 3B). Thus, the differential activation of ERK between the different a-line cells is FGF-signal dependent.

### **Quantitative measurement of ERK activity in ectoderm cells using a biosensor**

Similar results to that obtained with anti-dpERK IF were obtained with ERK-kinase translocation reporter (ERK-KTR), a biosensor of ERK activity (Figure 4). ERK-KTR is comprised of an ERK docking site, bipartite nuclear localization signal (bNLS), and nuclear export signal (NES), with ERK phosphorylation sites located within the bNLS and NES. This biosensor resides in the nucleus and, upon phosphorylation, is exported into the cytoplasm. Thus, ERK-KTR is excluded from nuclei following ERK activation (de la Cova et al., 2017b; Regot et al., 2014b). We applied this assay to *Phallusia mammillata*, an ascidian species belonging to the same order, Enterogonia, as *Ciona* (Delsuc et al., 2018a). *Phallusia* eggs and embryos translate injected mRNA efficiently and are highly transparent, permitting live imaging of fluorescent proteins (Prodon et al., 2010). *ERK-KTR-mClover* mRNA (de la Cova et al., 2017b; Regot et al., 2014b) was injected in *Phallusia* eggs together with *NLS-tdTomato* mRNA for nuclear identification. The measured cytoplasmic/nuclear (C/N) ratio of ERK-KTR signals for each a-line ectoderm cell at the late 32-cell stage revealed a similar profile to the data we obtained with anti-dpERK IF, although we were unable to detect significant differences between a6.6 and a6.8 (Figure 4B, Table 1). The ERK-KTR biosensor also allowed visualisation of the temporal profile of ERK activity. The time of each acquisition was aligned by fixing Time 0 to the time point of A6.4 nuclear membrane breakdown (NEBD). Figure 4C shows the ERK-KTR signal during the 32-cell stage from -4 minutes prior to A6.4 NEBD for embryos injected at the 2-cell stage on one side with *dnFGFR* mRNA. We observed a gradual increase in ERK-KTR during this time period in all cells in both control and *dnFGFR*-injected halves. A similar result was seen in embryos treated with U0126 (Figure S2A). This gradual increase over time is therefore not due to FGF/MEK signals, but most likely due to continuous translation of the biosensor over time. In our analysis with anti-dpERK IF, we showed that levels of ERK activity in a6.8 were close to unstimulated levels (Figure 3B, Figure S1E). ERK-KTR C/N ratios of a6.8 in the control sides also appeared similar to those observed in all cells in the *dnFGFR*-injected side (Figure 4C, black line). We therefore normalised all C/N ratios obtained in our temporal sequence with that of a6.8 from the same embryo half. By analysing the C/N ratios of ERK-KTR normalised to a6.8

levels, we found that during the time period of analysis, ERK activity in a6.5 is significantly higher than a6.6 and a6.7 ( $P \leq 0.0006$ , in paired t-tests). Normalised ERK activity levels appear to remain stable to the end of the 32-cell stage in all cells (Figure 4D, Figure S2B).

So far, we have shown that ERK activation is dependent on the FGF/MEK signalling pathway (Figures 3-4, Figures S1E), with highest levels of ERK activation in a6.5 cells (Figures 2, 4, Figure S1).

### **Nuclear ERK activation levels correlate with cell surface contacts**

In the experiments presented so far, the profile of nuclear ERK activation levels measured in the a-line ectoderm cells appears remarkably similar to the profile obtained from measuring their relative areas of cell surface contact with the FGF-expressing mesendoderm cells (compare Figure 1B to Figure 2B, S1A,C). Consistently, when both relative area of cell surface contact with A-line mesendoderm cells and ERK activation level are measured for each ectoderm cell, these two measurements exhibit a high degree of correlation (Spearman correlations of 0.69- 0.89,  $P < 0.0001$ ) (Figure 2D, S3 Controls). This is consistent with the idea that area of cell surface contact is correlated with the level of the FGF-signal that each cell receives. However, because there is an inverse relationship between the level of cell surface contact with inducing FGF-expressing mesendoderm cells and that of ephrin-expressing ectoderm cells (Figure 1C), we could not at this point rule out whether the differential levels of ERK activation in each a-line cell was causally correlated to its area of mesendoderm (FGF) cell contact or that of ectoderm (ephrin) cell contact, or both. We therefore next addressed the role of ephrin/Eph signals in this process.

### **ephrin/Eph signals lower the amplitude of ERK activation**

In embryos in which Eph signals were inhibited, we found that levels of ERK activity increased in all cells, but the relative differential pattern of ERK activation levels between the different a-line cells was maintained. We made use of several tools, dominant negative forms of Eph3 and p120RasGAP and a small molecule inhibitor of EphB4, NVP-BHG712 (henceforth NVP). *dnEph3* (*Eph $\Delta$ C*) and *dnp120RasGAP* (*RG $\Delta$ GAP*) have previously been shown to block ephrin/Eph signals in *Ciona* embryos (Haupaix et al., 2013a; Picco et al., 2007b). NVP-

treatment of *Ciona* embryos generates similar results (Fiuza et al., 2020). In the first instance, since cell surface contacts correlate with ERK activation levels in the 32-cell *Ciona* embryo (Figure 2D) and ephrin/Eph signals are a known mediator controlling cell adhesion and cell shape in many developmental contexts (Klein, 2012), we wanted to address whether inhibition of ephrin/Eph signals alters cell surface contacts between the a-line ectoderm cells and the A-line mesendoderm cells. 8-cell stage embryos were injected in a4.2, the founder cell of the a-line ectoderm lineages, on one side, with fluorescent dextran and *dnEph3* mRNA. We could detect no difference in the cell surface contacts measured between control and injected halves of resultant 32-cell stage embryos, despite ectopic ERK activation detected in all a6.7 cells on the injected side (Figure 3A). Similarly, the cell surface contacts were quantified in control and NVP-treated embryos, with no significant difference detected between the two conditions (Figure S4). We conclude therefore that inhibition of ephrin/Eph signals does not measurably alter cell surface contacts in 32-cell stage *Ciona* embryos.

Analysing a large data set of NVP-treated embryos, we found that the profile of ERK activation detected between the different a-line ectoderm cells appeared very similar to control embryos (Figure 2C, Figure S1B,D) (Table 1). In order to directly compare ERK activation levels between control and NVP-treated embryos, we injected embryos with fluorescent dextran and placed them in the same tube as NVP-treated embryos from the same fertilisation. Immunofluorescence and confocal acquisition were then conducted under identical conditions. Higher levels of ERK activity were observed in NVP-treated embryos with consistent statistical support for a6.5 and a6.7 cells (Figure S5).

We confirmed this result by injecting either *dnEph3* or *dnp120RasGAP* together with fluorescent dextran (for identification) into one cell of the two-cell stage embryo (Figure 3B). At the late 32-cell stage, we compared the levels of nuclear dpERK IF signal in injected 'v' control cells from each half of the same embryo. As described above, injections of *PH-GFP* gave a ratio of injected/control that was not significantly different from 1 (Figure 3B, *PH-GFP*). However, injection of *dnEph3* or *dnp120RasGAP* resulted in an increase in signal on the injected side, with statistical support for all cells (Figure 3B). We conclude that a-line cells exhibit higher levels of nuclear dpERK IF signal when ephrin/Eph signals are compromised.

These results suggest that the differential contact with FGF-expressing cells is sufficient to create the a6.5>a6.7>a6.6>a6.8 pattern of ERK activation, independently of intact ephrin/Eph signals (Table 1). Consistent with this idea, when both the relative area of cell

surface contact with A-line mesendoderm cells and ERK activation level are measured for each ectoderm cell in NVP-treated embryos, these two measurements exhibit a high degree of correlation (Spearman correlations of 0.7881 and 0.8356,  $P < 0.0001$ ) (Figure 2E, Figure S3). This is consistent with the possibility that ERK activation levels in ectoderm cells are determined by the area of their cell surface contact with FGF-expressing mesendoderm cells. Eph signals contribute to this process by lowering the level of response to FGF signals.

### **Dose response of ectoderm cells to FGF**

Adopting an ex vivo approach, we found that ephrin/Eph signals impact the amplitude but not the kinetics of ERK activation response to increasing concentrations of FGF in ectoderm cells. We dissected embryos to isolate ectodermal explants (Figure 5A). Isolated ectodermal explants develop into epidermis (Bertrand et al., 2003b). Treating explants with bFGF mimics neural induction so that they adopt neural fates (Bertrand et al., 2003b; Hudson and Lemaire, 2001b; Inazawa et al., 1998b). Since neural induction occurs during the 32-cell stage of development, we decided to start our FGF-treatment soon after the ectoderm cells have divided at the very early 32-cell stage. Sibling embryos exited the 32-cell stage approximately 25 minutes later with cytokinesis of the vegetal cells to give rise to the 44-cell embryo.

Addressing the temporal dynamics of the response of cells to exogenous FGF, we found that the levels of dpERK first peaked before stabilising at around 15-24 minutes (Figure 5B, Figure S6A-B). The entire temporal response was sensitive to Eph inhibition, with higher dpERK levels in NVP-treated embryos at the peak as well as at steady state (Figure S6C). The response of cells in isolated ectodermal explants appears different to the dynamics of ERK activation measured with ERK-KTR in whole embryo, in which no peak of activation was observed during our period of analysis (Figure 4, Figures S2). This is most likely due to the sudden exposure of the cells to FGF resulting in an excitation peak before achieving steady state. A peak of ERK activation followed by a steady state response to exogenous application of growth factors is frequently reported in in vitro cell culture systems (Ahmed et al., 2014; Blum et al., 2019; Francavilla et al., 2013; Regot et al., 2014b; Ryu et al., 2015).

We conducted our dose response analysis by collecting FGF-treated ectodermal explants at 18 minutes after addition of bFGF, when dpERK levels are relatively stable. 12 experimental replicates of control versus NVP-treated explants, treated with increasing doses

of bFGF, were analysed by western blot (Figure 5C). It should be noted that we made sure that all detected signals were within the linear range of antibody detection (see materials and methods for details). Similar to the IF results, NVP-treatment resulted in a greater amplitude in the ERK activation response (Figure 5C, Figure S6D). Non-linear regression of the average dose response of ectoderm cells to increasing concentrations of FGF gave a best-fit Hill coefficient of 0.77 (confidence interval 0.5050 to 1.146;  $r^2=0.8032$ ,  $n=115$ ) for control explants and 0.59 (confidence interval 0.2939 to 1.109;  $r^2=0.6627$ ,  $n=115$ ) for NVP-treated explants (Figure 5C). Thus, Eph signals appear to lower the amplitude but not impact the overall kinetics of ERK activation response, giving a slightly lower best-fit Hill coefficient for NVP-treated explants compared to controls.

The western blot analysis did not allow us to address the response of individual cells to FGF treatment. Using anti-dpERK IF, we therefore addressed the possibility that ectoderm cells responded in a variable but binary manner, such that, at a given concentration of FGF, different proportions of cells respond in an ON-OFF manner (Figure 5D, Figure S7A). However, this analysis showed no evidence for bimodal responses. Rather, individual ectoderm cells responded with wide variation to each dose of FGF, but the average response increased with the concentration of FGF. The western blot analysis indicated that cells responded first with a large peak in ERK activity before stabilising. Analysis of dpERK IF signals in single ectoderm cells during the peak of activation also showed a wide variation, with no evidence of bimodality (Figure S7B). This suggests that, under ex vivo conditions, cells respond variably and gradually to increasing concentrations of FGF and we found no evidence for a binary ERK activation response either during the peak or stable phase of activation. Indeed, Hartigan's diptest for unimodality (Hartigan, 1985)

( <https://cran.r-project.org/web/packages/diptest/index.html>) found no evidence for diversion from a unimodal distribution in the nuclear dpERK IF levels in ectoderm cells under either the in vivo or ex vivo conditions we tested (Figure S8 A,B,D).

So far, we have shown in vivo that, the differential area of cell surface contact with neural inducing mesendoderm cells is sufficient to explain the differential ERK activation pattern between the a-line cells ( $a_{6.5} > a_{6.7} > a_{6.6} > a_{6.8}$ ). ephrin/Eph signals reduce the amplitude of the ex vivo and in vivo responses, but does not appear to fundamentally alter

the pattern of the response. We found no evidence for bimodality at the level of ERK activation in response to either contact with FGF-expressing cells (endogenous FGF) or exogenous FGF.

### **Mathematical analysis of graded signal inputs based on the area of cell surface contacts**

Based on our results described so far, we propose that the area of the cell surface contacts with the mesendoderm cells, in other words, the number of FGF receptors that are exposed to a uniform concentration of FGF ligands, is the determining factor for the level of the ERK activation response (Figure 6A). This is conceptually different to a classical morphogen gradient with a signalling source, whereby cells are exposed to different concentrations of ligands (Figure 6B). We wanted to address how these two different signalling scenarios might impact the cellular response. In the following mathematical analysis of the neural induction system, we assume that the density of the FGFR is the same for all cells, FGF acts as a short-range ligand, and the concentration of FGF in the extracellular space, between the mesendoderm cells and the ectoderm cells, is constant. Thus, [Fgf] is the same for all cells, but the number of active FGFR is different from one cell to another, because the area of surface (i.e number of FGFR) exposed to the ligands is different.

The effective input into the ERK cascade would therefore be the number of receptors bound to FGF ( $R_A$ , for active receptors). The number of active receptors ( $R_A$ ) can be expressed as:

$$R_A = R \cdot \frac{[Fgf]}{[Fgf] + K_D} \quad (1)$$

where R is the number of receptors in contact with FGF, [Fgf] the concentration of FGF and  $K_D$  the binding constant of FGF to its receptor. A non-cooperative relation ( $n_H=1$ ) is taken, because one FGF binds to one FGF receptor. The ERK signalling cascade is assumed to be non-linear, so the relationship between ERK activity and active receptors ( $R_A$ ) is non-linear:

$$Erk^A = Erk_{max} \frac{R_A^n}{R_A^n + K_{DR}^n}$$

where  $Erk_{max}$  is the maximal cellular ERK activity, and  $K_{DR}$  is the number of FGF-bound receptors leading to half maximal activity. This can be re-written as

$$Erk^* = \frac{Erk^A}{Erk_{max}} = \frac{R_A^n}{R_A^n + K_{DR}^n} \quad (2)$$

Inserting (1) into (2), one can get

$$Erk^* = \frac{R^n \left( \frac{[Fgf]}{[Fgf] + K_D} \right)^n}{R^n \left( \frac{[Fgf]}{[Fgf] + K_D} \right)^n + K_{DR}^n} \quad (3)$$

When measuring ERK activity ( $Erk^A$ ) as a function of cell surface contact, what is in fact measured is the ERK activity as a function of R. In the experiments shown in Figure 2D,E, and Figure S3, we revealed a strong correlation in this relationship (relative R against relative ERK activity). For simplicity, here we focused on the relationship between cell surface contact and ERK activity in Eph-signal inhibited embryos (NVP-treated embryos, Figure 2E and Figure S3 ‘NVP2’). Fitting Hill functions to these two datasets gave us a best-fit Hill coefficient ( $n_H$ ) of 2.6 (experiment ‘NVP1’) and 1.6 (experiment ‘NVP2’) (Supplementary Table 1). We took our first NVP Hill coefficient of 2.6 and placed it in equation (3) (Figure 6C).

From equation (3), we can see that the relation between ERK activity ( $Erk^*$ ) and the number of receptors in contact with FGF (R) is not the same as the relation between ERK activity ( $Erk^*$ ) and [Fgf]. From (3), we expect that if we keep R constant but vary [Fgf], the Hill coefficient between  $Erk^*$  and [Fgf] never reaches 2.6 but remains smaller (Figure 6D). This graph (Figures 6D) shows the effective Hill coefficient for the relation between  $Erk^*$  and [Fgf]. The exact value of this Hill coefficient depends on the value of R, but never reaches as high as 2.6 (Figure 6D, Supplementary File 1). This is in qualitative agreement with the ex vivo western blot experiments where the number of receptors is kept constant (sum of the exposed receptors on all cells) but [Fgf] is varied, and which is thus a way of measuring Erk activity ( $Erk^*$ ) as a function of [Fgf] at constant R. We can mathematically express the relationship between the Hill function of “ERK versus R” ( $n$ ) and the Hill function of “ERK versus [FGF]” ( $n_H$ ) (Supplementary File 1). This shows that, for a given  $n$ ,  $n_H$  is equal to or smaller than  $n$ , with the exact  $n_H$  depending on ratio of the  $K_{DR}/R$  (the concentration of activated receptor when ERK is at half maximum/the number of receptors exposed).

Therefore, the mathematical analysis shows that, based on our initial assumptions, cells in the embryo should be more sensitive to changes in area of cell surface contacts with inducer cells than they would be to changes in FGF ligand concentrations, which is consistent with our experimental observations.

## Mathematical modelling of differential FGF and ephrin signalling inputs.

It has previously been proposed that differential inputs of ephrin is sufficient to generate the differential pattern of *Otx* activation (and thus an inferred differential pattern of ERK activity, with higher activity in a6.5 cells) (Ohta et al., 2015a). Our experimental data and mathematical analysis show that each a-line cells experiences a differential area of cell surface contact with FGF-expressing mesendoderm cells and that this correlates with the level of ERK activation exhibited by each cell whether or not the ephrin signalling pathway is intact (Figure 2D-E, Figure S3, Figure 6). Thus, it is unlikely that differential ephrin inputs alone are sufficient to explain the differential pattern of ERK activity among a-line cells.

In order to try to understand more about the relationship between ephrin and FGF inputs in terms of ERK activation, we modelled the activation status of ERK by both SOS (downstream of FGF/FGFR signals) and p120RasGAP (downstream of ephrin/Eph signals) (Figure 6E and Figure S9). In our model (Figure 6E), Ras-GDP is transformed into Ras-GTP at a rate  $V_1$ , mediated by SOS following Michaelian kinetics. Ras-GTP is converted back into Ras-GDP by two different processes: one mediated by p120RasGAP following Michaelian kinetics with a rate  $V_2$  and the other mediated by ephrin- and cell surface contact-independent GAP activity with a linear rate  $k_b$ . We evoked the presence of basal GAP activity in addition to ephrin-controlled p120RasGAP since available transcriptome datasets (Brozovic et al., 2018) indicate the presence of transcripts for at least three further RasGAPs in the early ascidian embryo (*IQGAP1/2/3*, *Neurofibromin*, *RASA2/3*). Furthermore, modelling in the presence of ephrin-independent RasGAP activity made predictions that were more consistent with our experimental data (Figure S9). We assume that Ras-GTP activates ERK with a Hill relationship and that the total amount of Ras-GDP and Ras-GTP is conserved. So, we only consider the fraction of Ras-GTP

$$\text{(i.e. } \frac{[Ras-GTP]}{[Ras-GDP]+[Ras-GTP]}, \text{ called T).}$$

The fraction of Ras-GDP = 1-T. Similarly, we consider the fraction of ERK activity, called Erk\*, which represents the Erk activity divided by the maximal possible ERK activity.

The evolution equation for T is given by:

$$\frac{dT}{dt} = V_1 \frac{(1-T)}{K_1+(1-T)} - V_2 \frac{T}{K_2+T} - k_b T \quad (1)$$

This equation is solved at equilibrium to get the value of T for different values of  $V_1$  (SOS activity),  $V_2$  (p120RasGAP activity) and  $k_b$  (ephrin-independent rate of transformation of Ras-GTP into Ras-GDP). The fraction of active ERK is also assumed to be at equilibrium and is given by:

$$Erk^* = \frac{T^2}{K_{erk}^2 + T^2} \quad (2)$$

The aim of the calculations is to evaluate qualitatively the impact of SOS, p120RasGAP and ephrin-independent transformation of Ras-GTP into Ras-GDP ( $k_b$ ) on ERK activity. Thus, standard values of parameters are taken:  $K_1 = K_2 = K_{erk} = 0.5$ . The concentration of FGF, ephrin and number of receptors are not explicitly considered. A Hill coefficient of 2 was chosen to consider a non-linear activation of the ERK pathway. We varied  $V_1$ ,  $V_2$  and  $k_b$  (Figure 6E, Figure S9). Taking for example the activation of ERK with  $k_b=0.2$  (Figure 6E) (for other  $k_b$  conditions, see Figure S9) we can see that, at a fixed (medium to high) SOS activity, differential p120RasGAP can generate a wide range of ERK values. This is compatible with the theory and experiments reported previously (Ohta et al., 2015a). Any activation of ERK depends on active SOS, consistent with the strong down regulation of ERK when FGF signals are inhibited (Figure 3, Figure 4C, Figure S1E) (Hudson et al., 2003a; Kim and Nishida, 2001; Nishida, 2003; Picco et al., 2007b). Similarly, at a fixed, medium to low p120RasGAP activity, differential SOS can generate a wide range of ERK activity. Differential SOS is sufficient to generate a wide range of ERK activity even in the absence of p120RasGAP activity. This is consistent with our observations that differential levels of ERK activity between the a-line ectoderm cells are maintained even if Eph signals are compromised (Figure 2B-E; Figure S1; Figure S3). At high p120RasGAP activity levels, ERK is strongly suppressed, consistent with the repression of ERK and ERK-dependent cell fates when ephrin ligands are overexpressed (Haupaix et al., 2013a; Ohta and Satou, 2013a; Picco et al., 2007b). We conclude that the model, which depends on the presence of an ephrin-independent RasGAP activity, fits well with experimental observations. This model allows us to make the following conclusions. Both differential SOS (at fixed zero to intermediate level of RasGAP) or differential p120RasGAP (at fixed intermediate to high level of SOS) are predicted to be capable of creating a pattern of ERK activation across a field of cells. However, the optimum spread of the range of possible ERK activation levels takes place when both FGF and ephrin signals are differential (i.e. a diagonal

rather than horizontal or vertical line across the graph). We conclude that it is likely, under the physiological conditions of the embryo, that both FGF- and ephrin- signalling contribute to the pattern of ERK activation.

### **Semi-quantitative measurements of *Otx* transcription**

The *Otx* gene is activated directly by FGF/MEK/ERK signals in *Ciona* embryos at the late 32-cell stage (Bertrand et al., 2003b; Hudson et al., 2003a; Miyazaki et al., 2007b). *Otx* is expressed in a6.5 and b6.5, with occasional expression also in a6.7 (Ohta and Satou, 2013a; Tassy et al., 2006b). To quantify the transcriptional activation of *Otx* under various conditions, we chose a semi-quantitative approach using single molecule fluorescence in situ hybridisation (smFISH) (Figure 7A). In ascidian embryos at early cleavage stages, newly transcribed transcripts are detected in the nucleus. This is also the case for *Otx* expression in ectoderm cells at the 32-cell stage. Taking advantage of this feature, we quantified smFISH signals as the number of spots in each nucleus (see materials and methods for details). We first analysed control whole embryos collected at the late 32-cell stage from different batches and processed separately (Figure 7B). This revealed that a6.5 has the strongest levels of *Otx* gene activity, with a6.7 showing low or intermediate levels of activation. a6.6 and a6.8 showed low numbers of spots. Between the four independent experiments, similar profiles were obtained, enabling us to pool data onto one graph (Figure 7B). Looking at the temporal profile of *Otx* gene activation in a6.5, in which embryos were timed by comparing to a reference time-lapse video (see material and methods for details), we observed that *Otx* transcription reached maximum activation approximately 15 minutes after the onset of the cell cycle, corresponding to the moment when vegetal cells decompact and embryos adopt a flattened shape (Figure S10). Levels of *Otx* nuclear spot counts remained stable to the end of the cell cycle. For the remaining experiments, we analysed *Otx* expression at the 'late' 32-cell stage (around 18 minutes into the 32-cell stage).

*Otx* expression levels were reduced by inhibition of FGF signalling and enhanced by inhibition of Eph signalling (Figure 7C-D), consistent with previous studies using non quantitative methods (Bertrand et al., 2003b; Ohta and Satou, 2013a). While embryos injected with *PH-GFP* mRNA into one cell at the two-cell stage showed no difference in *Otx* activity between control and injected halves, injection of *dnFGFR* resulted in strong down regulation

of *Otx* transcriptional activation in a6.5 and a6.7. Cells with low numbers of spots, a6.6 and a6.8, showed no difference between control and *dnFGFR* injected halves. Next, we inhibited ephrin/Eph signals by injection of *dnEph3* or *dnp120RasGAP* mRNA. This resulted in a significant increase in *Otx* transcription in a6.7. In these experiments, a6.7 expressed *Otx* at levels similar to a6.5. Treating embryos with 8 $\mu$ M NVP had an even stronger effect on the pattern of *Otx* expression, with ectopic activation seen not only in a6.7, but also in a6.6 cells in 4 out of 6 experiments (in total 32/77 a6.6 cells had more than 100 spots) (Figure 8A, 8D, S11A, S12). We observed ectopic *Otx* activation in a6.8 in 1 experiment (Figure S11A). When NVP-treated embryos were treated in parallel with high doses of the MEK inhibitor U0126, all expression of *Otx* was suppressed, suggesting that inhibition of Eph signals results in ectopic activation of *Otx* via activation of the ERK pathway (Figure 8A, Figure S11A).

### **The *Otx* transcriptional response is bimodal**

The data suggests that, in control embryos, the ERK activation levels observed in a6.5 correspond to the above-threshold level for maximum *Otx* transcriptional activation. Intermediate levels of ERK activation in a6.7 partially activate *Otx* in some cases, while levels in a6.6 and a6.8 are not sufficient for any *Otx* activation. Following Eph inhibition, ERK activation levels increase in all cells, sufficient to evoke a full *Otx* response in a6.7 and sometimes also *Otx* activation in a6.6. Under all of these conditions, cells appear to fall into two groups, with low *Otx* spot counts, or high spot counts. This strongly suggests a bimodal response of *Otx* to different levels of ERK activation. This idea was supported by an ex vivo assay in which ectodermal explants were treated with increasing doses of exogenous FGF (Figure 8B, Figure S11B-D). Earlier, we showed that treating ectoderm cells with increasing doses of FGF resulted in a gradual increase in average ERK activation levels (Figure 5, Figure S7). Under similar conditions, the response of *Otx* was strikingly different (Figure 8B, Figure S11B-D). The *Otx* output appeared binary in nature with either high or low numbers of spots. Carrying out Hartigan's diptest on the spot counts for *Otx*, the null hypothesis of a unimodal distribution was strongly rejected (i.e supporting at least bimodality) both in the control embryos and in the ex vivo dose response experiments (Figure S8C, E). ephrin/Eph-inhibited embryos also maintained a bimodal *Otx* response despite ectopic activation of *Otx* (Figure S8F-

G). We conclude that ectodermal cells respond to FGF with a gradual ERK activation response, which is then converted to a bimodal *Otx* transcriptional output.

We found further evidence for a sigmoidal relationship between the activation levels of ERK and the levels of *Otx* transcription by making use of half-embryo injections. This experiment assumes that ephrin/Eph signals affects *Otx* expression only via its effect on ERK activation levels (for evidence of this, see Figures 8A, S11A and later). We injected *dnEph3* mRNA and fluorescent dextran into one cell of the two-cell embryo. At the late 32-cell stage, one group of the embryos was processed for *Otx* smFISH and the other group were processed for anti-dpERK IF. We therefore collected datasets of both ERK activation and *Otx* transcription levels in eight different cell types (a6.5 control, a6.6 control, a6.7 control, a6.8 control, a6.5 dnEph3, a6.6 dnEph3, a6.7 dnEph3, a6.8 dnEph3). For each of these eight cell types, we plotted the average level of nuclear dpERK IF signals, normalised to the dpERK signal level of control side a6.8 (a6.8=0), against the average number of *Otx* spots. This revealed a sigmoidal curve. Non-linear regression gave best-fit Hill coefficients of 3.374, 6.65 and 10.68 for three independent experiments (Figure 8C and Figure S11E-F). This suggests that *Otx* responds to different levels of ERK activation in a sigmoidal manner, consistent with a threshold response and a bimodal output.

### **Recovery of wild-type *Otx* expression pattern in Eph-inhibited embryos by reduced MEK signalling**

Taking all our data together, we conclude that ascidian neural induction exhibits a threshold response at the level of the *Otx* transcription. In this system, the threshold for full *Otx* activation is set such that a6.5 cells and some a6.7 cells respond, whereas a6.6 and a6.8 cells do not respond. Our data suggest that ephrin/Eph signals reduce the levels of ERK activation in all a-line cells, which is required to maintain a6.7 and a6.6 below the threshold for full *Otx* induction. Thus, it should be possible to recover control *Otx* expression in Eph-inhibited embryos by some other means of ERK inhibition. This was indeed the case. We treated embryos with NVP and suboptimal doses of the MEK inhibitor U0126 (Figure 8D, Figure S12). NVP-treatment resulted in an 'ON' state of *Otx* activation in a6.7 and sometimes a6.6. Treatment of sibling NVP-treated embryos with low doses of U0126 resulted in a recovery of the wild type pattern of *Otx* gene expression, restricted predominantly to a6.5. Thus, broadly

lowering MEK activation levels in NVP-treated embryos is sufficient to re-establish the wild type pattern of *Otx* activation. Our data suggests that this critical function is achieved during normal embryogenesis by ephrin/Eph signals.

## **DISCUSSION**

In this manuscript, we describe in a semi-quantitative manner, an FGF-dependent embryonic induction leading to the activation of an immediate early gene. The entire induction process takes less than 30 minutes, encompassing a single cell cycle of the responding cells. Two processes account for the spatial precision of this embryonic induction, antagonism between FGF and ephrin signalling pathways, which dampens the inductive FGF signal, and the bimodal transcriptional response of the immediate early gene. Specific characteristics (invariant cell division patterns, small cell numbers) of ascidian embryos enable single cell analyses in a multicellular context. Our experimental data and mathematical analyses are consistent with the following model of the FGF-induced transcriptional response of the *Otx* gene during neural induction in *Ciona* embryos. In embryos, the levels of ERK activation in ectoderm cells closely correlates with their area of cell surface contact with the FGF-expressing mesendoderm cells (Figure 2D-E, Figure S2). The ERK activation is dampened by differential ephrin/Eph signalling inputs (Figure 6). *Otx* transcription is activated by above-threshold levels of ERK activation, generating a bimodal output. The reduction in ERK activation levels by ephrin/Eph signals, together with the bimodal transcriptional response of *Otx*, are critical to achieve the spatial precision of neural induction in the ectoderm of the 32-cell ascidian embryo.

### **Cell surface contact relative to ERK**

Our data support the idea that the area of the cell surface exposed to FGF ligands, in other words, the number of FGF receptors that are exposed to a constant concentration of FGF ligands, is a determining factor for the amplitude of the ERK activation response (Figure 6A) (Guignard et al., 2017; Tassy et al., 2006b). We show a strong correlation between the area of cell surface contact with mesendoderm cells and the level of ERK activity in a-line ectoderm cells (Figure 2D,E, Figure S3). Mathematical analysis of ERK activation levels as a function of either the activated receptor (cell surface contact) or FGF ligand concentration predict that ERK levels should respond with a higher sensitivity to changes in cell surface contact than it

should to changes in FGF ligand concentration, which is qualitatively consistent with our in vivo versus in vitro data (Figures 2, 5C, Figure S3). Greater sensitivities to changes in cell geometry relative to ligand concentration may have contributed to the highly conserved geometry of ascidian embryos over vast evolutionary times (Delsuc et al., 2018a). A recent study modelling the area of cell surface contact as signal strength for a variety of signals reached a similar conclusion on the importance of embryo geometry (Guignard et al., 2017).

If, as we propose, cell surface contact determines the number of activated FGF receptors, then FGF9/16/20 must be acting at very short range from its site of expression in this system. Consistent with a limited diffusion of FGF9/16/20, evidence from *Halocynthia roretzi*, a species of ascidian that belong to a different order of tunicates compared to *Ciona* and *Phallusia*, suggests that FGF signalling takes place between only juxtaposed cells (Miyazaki et al., 2007b). Limited diffusion of FGF9/16/20 is also consistent with ours and others data and models (Guignard et al., 2017; Tassy et al., 2006b). FGF ligands bind to heparan sulphate (HS), which have dual effects. HS binding increases the affinity of FGF to the FGFR and reduces FGF ligand diffusion in the extracellular space, effectively increasing the local concentration of ligand (Ornitz and Itoh, 2015a). The distribution of HS in ascidian embryos and how it might contribute to cell signalling has not been addressed. A spontaneous mouse mutant, affecting the affinity of FGF9 for HS-proteoglycans is caused by mutation of an asparagine residue, highly conserved among different FGF ligands including *Ciona* FGF9/16/20 (amino acid position 236 of Aniseed transcript model sequence KH.C2.125.v1.A.nonSL4-1) (Harada et al., 2009; Tassy et al., 2010). The potential role for HS in limiting FGF9/16/20 diffusion in ascidian embryos requires investigation.

### **Kinetics of ERK activation**

The levels of ERK activation detected in individual ectoderm cells gave no evidence for a bimodal response. Tassy et al showed that the cell surface contacts between a-line and mesendoderm during the 32-cell stage (early- mid- late-) are stable (Tassy et al., 2006b). Here we show that levels of ERK activity also appear stable during the 32-cell stage (Figure 4). This suggests that the system is at equilibrium. In the ex vivo ectoderm explant system (Figure 5), a sharp increase in FGF concentration, due to addition of FGF to the medium, results in an excitable peak of ERK activity, which then stabilises to steady state within approximately 15 minutes (Figure 5B, Figure S6A-C). We found no evidence for an excitable peak, oscillatory or

pulsing behaviour in ERK activity in ectoderm cells in the in vivo context (Figure 4, Figure S2). Based on the precise control of activation level and dynamics by optogenetics, it has been shown that cumulative load of ERK activity controls a cell fate decision in *Drosophila* blastoderm embryos (Johnson and Toettcher, 2019a). It will be interesting to address whether this is also the case in ascidian neural induction.

### **Role of ephrin in ERK response**

In addition to FGF signals, the a-line ectoderm cells are also exposed to ephrin ligands via cell surface contact with neighbouring ectoderm cells. While the differential contact with FGF expressing cells is sufficient to create a differential pattern of ERK activation among a-line ectoderm cells, we have shown that ephrin/Eph signals reduce the amplitude of the response of ERK in both the in vivo context, whereby cells are exposed to different areas of contact with FGF-expressing cells, as well as the in vitro context, in which cells were exposed to increasing FGF ligand concentrations (Figure 3, Figures S5, Figure 5C). An increase in ERK activation levels when ephrin/Eph signals are compromised, which we show here quantitatively, is consistent with ectopic ERK activation (shown or inferred) following ephrin/Eph inhibition in other studies in ascidian embryos (Haupaix et al., 2013a; Haupaix et al., 2014b; Ohta and Satou, 2013a; Picco et al., 2007b; Shi and Levine, 2008; Stolfi et al., 2011b) as well as the ability of forward ephrin signalling to inhibit ERK activation in mammalian cell lines (Miao et al., 2001). Our mathematical modelling indicates that the combination of differential FGF and differential ephrin inputs allows the optimum range of possible ERK activities across a field of cells (Figure 6E; Figure S9). During neural induction, the Eph-mediated reduction of ERK activation levels is critical for the correct spatial pattern of the immediate-early transcriptional target of ERK, the *Otx* gene (this study) (Ohta and Satou, 2013a).

We have some tentative evidence that ephrin/Eph signals may also increase the overall sensitivity of the system. Despite large or unpredictable confidence intervals, we found that when comparing best-fit Hill coefficients between control and NVP-treated embryo datasets, the Hill coefficient was consistently lower when ephrin/Eph signals were compromised (Supplementary Table 1). This will require further investigation.

In summary, our experimental data and theoretical predictions are consistent with the idea that FGF and ephrin signalling both contribute to the differential pattern of ERK activation between a-line ectoderm cells and subsequently, for the correct spatial pattern of *Otx*.

### **Cellular integration of the two signalling pathways**

In our model, we propose that antagonism between FGF and forward ephrin signals occurs at the level of regulation of Ras activity via SOS and p120RasGAP, respectively. However, activation of FGF receptors should take place at the 'basal' membrane of ectoderm cells, the membrane domain in contact with FGF-expressing mesendoderm cells. In contrast, activation of Eph receptors should take place laterally where cells contact their neighbouring ectoderm cells. Identifying precisely where and how these activated signalling components converge is essential to fully understand this system. It is possible that endocytosis of activated receptors is playing a role in the convergence of these signalling pathways. Endocytosis was originally thought to be an effective means to attenuate signal transduction by internalising receptors or ligand-receptor complexes. However, an increasing number of studies show that active signalling could continue after receptor internalisation (Irannejad et al., 2015; Murphy et al., 2009b). Furthermore, early endosomes might be acting as a platform for crosstalk between signalling pathways (Pálffy et al., 2012a). The role of receptor endocytosis during FGF signal transduction is starting to be addressed. It has been shown, during mesoderm induction in *Xenopus* embryos, that FGF-dependent ERK activation requires clathrin-mediated endocytosis of activated FGF receptors (Jean et al., 2010a). In contrast, in *Ciona intestinalis*, caveolin-mediated endocytosis is implicated in FGF signal transduction during the asymmetric cell division of cardiac progenitors (Cota and Davidson, 2015). Both clathrin- and caveolin-mediated endocytosis are also implicated for internalisation of activated Eph receptors (Bouvier et al., 2010a; Irie et al., 2005; Vihanto, 2006a). Moreover, signalling from the internalised Eph receptors persists after endocytosis (Boissier et al., 2013; Marston et al., 2003). Ascidian neural induction involves crosstalk between FGF and ephrin signalling pathways originating from basal and lateral plasma membranes, respectively, and this may therefore constitute an ideal *in vivo* system to address the potential role of endocytosis-mediated signal integration.

### **ERK to *Otx***

Our data show that, while the response of ERK to different areas of cell surface contact are relatively gradual, the transcriptional activation of *Otx* shows a switch-like response. The *Otx* output for individual cells in response to different levels of cell surface contact *in vivo* or different concentrations of FGF *ex vivo* is either high or low, with very few intermediate levels

(Figure 7-8, Figures S8, S10-12). Hartigan's diptest for unimodality strongly supports at least a bimodal distribution (Figure S8). The upstream regulatory sequences for *Otx* are well studied. A minimal enhancer of 55 bp, the  $\alpha$ -element, has been shown to be sufficient to drive specific expression of a reporter gene in only  $\alpha 6.5$  and  $\beta 6.5$  neural precursors (Bertrand et al., 2003b). This element contains 3 GATA sites and 2 ETS sites that act together to activate the *Otx* gene (Bertrand et al., 2003b). The GATA sites are responsible for general ectoderm activity while the ETS sites mediate FGF responses. Controlled levels of ERK are critical for the correct *Otx* output (Figures 7, 8, Figure S12) with ectopic activation of *Otx* in non-neural ectoderm cells when Eph signals are compromised (Figures 7, 8, Figure S11A, S12). This can be rescued by a general dampening of ERK activity using low doses of the MEK inhibitor U0126 (Figure 8D, Figures S12). This data suggests that *Otx* is activated at a specific threshold of ERK activity. As well as the dampening of ERK response to FGF by ephrin, there are several additional repressive inputs that act directly on *Otx* gene regulation itself. Firstly, the ETS and GATA sites are suboptimal, both in terms of their recognition motifs having reduced binding affinities as well as the suboptimal spacing of the binding sites (Farley et al., 2015b). This suboptimisation weakens the transcriptional activity of the  $\alpha$ -element and is essential to maintain spatial specificity (Farley et al., 2015b). Secondly, the ETS sites themselves appear to repress enhancer activity in non-neural ectoderm suggesting the presence of negative regulatory factors that compete with positive regulation by Ets1/2 at the ETS binding sites (Rothbächer et al., 2007). Finally, *Otx* transcription is also weakened by Smad signalling via a Smad-response element found upstream of the  $\alpha$ -element (Ohta and Satou, 2013a). It has been proposed that two TGF $\beta$  ligands, Admp and Gdf1/3-like, act to repress *Otx* activation in response to low levels of ERK activation in non-neural ectoderm cells (Ohta and Satou, 2013a). All of these negative regulatory mechanisms appear to sharpen the *Otx* transcriptional response during neural induction and it will be very interesting to address how these different inputs contribute to the mechanism generating the switch-like kinetics of the *Otx* transcriptional output.

### **Other systems**

A quantitative analysis of ERK has been conducted in several other multicellular developmental contexts, in response to EGF or Torso receptor signalling in *Drosophila* embryos (Coppey et al., 2008; Johnson and Toettcher, 2019; Lim et al., 2015), in response to

FGF in zebrafish (van Boxtel et al., 2018) and in response to EGF during *C. elegans* vulval development (de la Cova et al., 2017b) as well as the EGFR ligand-dependent relay propagation of ERK activation in mouse epidermis (Hiratsuka et al., 2015b) and *Drosophila* tracheal placode (Ogura et al., 2018a).

In zebrafish, during mesoderm formation, the ERK activation response to FGF signals appears rather gradual and involves the diffusion of FGF ligands (van Boxtel et al., 2018; Yu et al., 2009). In *C. elegans* vulva, the ERK activation in response to EGF is frequency modulated and initially graded between cells, but subsequently becomes sharply restricted to just a single cell (P6.p) by layers of regulatory mechanisms (de la Cova et al., 2017b; Hajnal et al., 1997b; Schmid and Hajnal, 2015; Stetak et al., 2006b; Yoo, 2004b). In the *Drosophila* syncytium embryo, a gradient of sustained ERK activity in response to localised Torso receptor activation at the termini of the embryo is required for anterior and posterior development (Coppey et al., 2008b; Furriols, 2003; Mineo et al., 2018b). The gradient of dpERK is established and refined by nuclear trapping (Coppey et al., 2008b). During cellularisation of early *Drosophila* embryos, a pulse of ERK activity in the ventral ectoderm in response to Spitz, an EGFR ligand, regulates expression of the neurogenic gene, *ind* (Lim et al., 2015b). In this system, the ERK cascade appears to act as a sensor of receptor activation since halving the number of EGFRs results in reduction of ERK activation levels by approximately half (Lim et al., 2015b). Thus, reducing the number of receptors that are 'exposed' to ligand would result in a corresponding reduction in the number of active receptors and reduced ERK output. This bears some similarity to the cell surface contact model for ascidian embryos in which changes in the cell surface contact would change the number of active receptors and correspondingly the ERK output response. In this system, EGFR ligands are predicted to act at very short range (Hayashi and Ogura, 2020; Lim et al., 2015b). Interestingly, transcriptional activation of *ind* appears to take place as a threshold response to ERK levels, as we propose here for *Otx* induction (Lim et al., 2015b). Later, in the stage 10 ventral ectoderm, graded activation of ERK by localised active Spitz ligands in the ventral midline is converted to a sharp degradation of Yan, an ETS-domain transcriptional repressor by a zero-order ultrasensitivity-like mechanism (Melen et al., 2005b).

In mouse skin epithelia, spontaneous ERK activity is propagated in an EGFR- and EGFR-ligand- dependent manner to control cell division during tissue homeostasis and wound healing (Hiratsuka 2015). In the case of the *Drosophila* tracheal placode invagination, an EGFR-dependent relay mechanism propagates activation of switch-like ERK throughout the placode

to control myosin cable formation at the boundary between cells exhibiting inactive and active ERK to drive placode invagination (Ogura et al., 2018a). Interestingly, modelling this process incorporates cell-contact dependent Spitz (ligand) stimulation, suggesting no or very little diffusion of the ligand.

We have shown in this study that ERK activation levels correlate with the areas of cell contact surfaces with inducing cells in a rather gradual way, that ERK signalling is dampened by ephrin signalling and that the transcriptional response of an immediate-early gene of ERK is switch-like, consistent with a threshold response. In conclusion, ascidian neural induction represents an important and simple multicellular system that should shed light on the mechanisms of action of the FGF signalling pathway, a pathway critical for development, homeostasis and health.

## MATERIALS AND METHODS

### Ascidians

Adult *Ciona intestinalis* were purchased from the Station Biologique de Roscoff (France). Ascidian embryo culture (Hudson, 2020; Sardet et al., 2011a) and microinjection (Sardet et al., 2011a; Yasuo and McDougall, 2018a) have been described. Blastomere names, lineage and fate maps were described previously (Conklin, 1905b; Nishida, 1987b). The late 32-cell stage was defined visually under binocular microscope, as when vegetal cells decompact and embryos become flattened in shape, corresponding to approximately 5-7 minutes before vegetal cells exhibit the first sign of cytokinesis.

### Injection constructs and inhibitor treatment

*pRN3-PH-GFP* is a gift from Dr Alex McDougall (Prodon et al., 2010) and mRNA was injected at concentration of 1.5µg/µl. *pRN3-dnFGFR (FGFRΔC)* was reported previously (Hudson et al., 2007) and mRNA was injected at a concentration of 1 µg/µl. *pRN3-dnp120RasGAP (RasΔGAP)* is described previously (Haupaix et al., 2013a) and mRNA was injected at a concentration of 1.5µg/µl. *pRN3-dnEph3 (Eph3ΔC)* was described previously (Picco et al., 2007b) and was injected at a concentration of 1.25µg/µl. *pSPE3-ERK-KTR-mClover* was generated by a Gateway reaction of *pSPE3-RfA* (Roure et al., 2007) and *pENTR-ERKKTRClover* (Regot et al., 2014) and mRNA was injected at a concentration of 1.5µg/µl together with *NLS-tdTomato* mRNA at 3µg/µl. *NLS-tdTomato* mRNA was synthesised from *pRN3-NLS-tdTomato* consisting of a single N-terminal NLS (5'-ATGACTGCTCCAAAGAAGAAGCGTAAGGTA-3') fused to the *tdTomato* ORF. All mRNAs were synthesised using mMACHINE T3 kit (Invitrogen/ Thermo Fisher Scientific, Massachusetts, USA). U0126 (Calbiochem/Merck, Darmstadt, Germany) was diluted into artificial sea water to the required concentration. 'High dose' was 2µM. NVPBHG712 was purchased from Tocris Bioscience (Bristol, UK) or Sigma-Aldrich (Missouri, USA) and used at a concentration of 4 or 8µM, determined empirically. For concentrations tests, we analysed *Otx* expression at the 44-cell stage (Fiuza et al., 2020) and ERK activation levels by western blot and anti-dpERK IF (Figure S5 and data not shown). Dextran-tetramethylrhodamine (ref: D1868, Invitrogen/Thermo Fisher Scientific, Massachusetts, USA) was made to 50mg/ml in water, and injected at 1/4 dilution.

### **Immunofluorescence (IF)**

Embryos were fixed at the late 32-cell stage in PIPES-sucrose-FA fix with 0.05% Triton-X (Stolfi et al., 2011b) for 25 minutes, then fixative was gradually replaced with PBS/Triton0.1% followed by washes (3 times 10 minutes). Blocking was carried out for 30 minutes in PBS-Triton0.1%-Blocking reagent 0.5% (ref: 11096176001, Roche/Sigma-Aldrich, Missouri, USA). Embryos were then placed in blocking reagent plus antibody overnight at 4°C. For anti-dpERK IF, we used at 1/100, either anti-phospho ERK1/2 (Thr202/Tyr204) monoclonal antibody (4B11B69) (ref: 675502, lot: B196626, Biolegend, California, USA) or anti-phospho-ERK1/2 (Thr202, Tyr204) monoclonal antibody (MILAN8R) (ref: 14-9109-80, lot: 2350233, eBioscience/ThermoFisher, Massachusetts, USA). For anti-H3 IF, we used anti-Histone H3 XP Rabbit monoclonal antibody(D1H2) (ref: 4499T, Cell Signaling Technology, Massachusetts, USA) at 1/100. Goat-anti-GFP (ref: ab5450, abcam, Cambridge, UK) was used at 1/250 (for embryo segmentation only). Following, the overnight incubation in primary antibodies, embryos were washed in PBS-Tween (0.1%) (3 times 30 minutes) and then placed in PBS-0.1%Tween-0.5% blocking reagent (Roche) containing corresponding secondary antibodies: Alexa Fluor 555 Donkey anti-Goat IgG (H+L) Cross-Adsorbed Secondary Antibody (ref: A-21432, Invitrogen/Thermo Fisher Scientific, Massachusetts, USA) (for embryo segmentation only); Alexa Fluor 488 Donkey anti-rabbit IgG (H+L) (ref: 711-545-152, Jackson ImmunoResearch, Pennsylvania, USA); Alexa Fluor 647 Donkey anti-mouse IgG (H+L) (ref: 715-605-150, Jackson ImmunoResearch, Pennsylvania, USA) at 1/250 for 2 hours at room temperature (in the dark), followed by washes in PBS-0.1%Tween, 3 times 1 hour at room temperature and 1 overnight at 4°C. In one experiment, shown in Figure 3A, non-quantitative anti-dpERK IF based on tyramide signal amplification was used as described (Haupaix et al., 2013a; Stolfi et al., 2011b).

### **Image acquisition of IF-labelled embryos**

Embryos in PBS-0.1%Tween were aligned into lines, with animal pole side down, on poly-L-lysine coated coverslips. Aligning embryos was carried out in a small volume of methylcellulose (1% in PBS) placed on the coverslip to prevent embryos falling onto the coverslip by gravity. For membrane-stained PH-GFP embryos, we first cleared embryos aligned

on a coverslip with progressive concentrations of SeeDB (20%, 40%, 60%, final 80%) (Ke et al., 2013). The coverslip was then mounted with spacers (strips of coverslip n°0) on a slide in 80% SeeDB followed by acquisition with a HCX PL APO 63x/1.4-0.6 oil immersion objective on a Leica SP5 confocal microscope (Leica, Wetzlar, Germany) with a z-step of 0.3µm at 512 x 512 pixels, 8 bits per pixel. For subsequent acquisition of anti-dpERK and H3 IF images, the slide was placed in a petri dish filled with PBS and the coverslip was gently recovered from the slide. For acquisition of anti-dpERK and anti-H3 IF images, the coverslip was incubated twice for 5 minutes in 100% methanol, before mounted in a drop of benzyl alcohol:benzyl benzoate (BABB) 2:1 (Dent et al., 1989) on a slide with spacers (strips of coverslip n°0). The anti-dpERK and anti-H3 signals were then acquired using an HCX PL APO 63x/1.4-0.6 oil immersion objective on a Leica SP5 confocal microscope with a z-step of 1µm, at 512 x512 pixels, 12 bits per pixel. Confocal lasers were adjusted between control and NVP-treated embryos in order to obtain maximum range around the different intensities unless stated that samples were processed under identical (same tube) conditions. In experiments that included injection of lineage tracer (dextran-TRITC), a snap shot was taken to identify the injected cells.

Imaris software (Oxford instruments, Abingdon, UK) was used for quantification of dpERK. H3 channels were used to segment nuclei, enabling automated measurements of the mean pixel intensity of each nucleus in dpERK channels.

### **Embryo reconstruction with Amira software**

Embryo reconstruction and surface area calculations were carried out with Amira software (Thermo Fisher Scientific, Massachusetts, USA). Briefly, the stack was opened with the software and a “Membrane Enhancement Filter” was applied to enhance the membrane signal and suppress any cytoplasmic background. From this cleaned stack, outer surface of the embryo was segmented with the “magic wand” tool and assigned to an “Exterior” object. Then a semi-automatic process was carried out in order to obtain a precise segmentation. Each cell was tagged manually with the “brush” tool in each dimension (XY, XZ and YZ) and assigned to an object with the name of the corresponding cell. A watershed segmentation was applied which generated automatically 32 objects corresponding to the total 32 cells of the embryo. At this step and only if necessary, some cells were corrected by hand with the “brush” tool. A smoothing pipeline (smooth labels and remove island) was then applied in order to remove

any isolated pixels. Finally, the 3D surface was generated by the software and surface data were computed and extracted as an Excel file.

In one set of experiments, from Figure 3A, embryos were stained with Alexa Fluor 488-phalloidin and non-quantitative anti-dpERK staining was used as described above. For membrane staining, embryos were incubated in Alexa Fluor 488 phalloidin/PBS/0.1% Triton (2 units/100 $\mu$ L, Life Technologies, A12379) overnight at 4°C (Robin et al., 2011a). After washing in PBS/0.1% Triton (3 times, 5 min), embryos were attached to poly-L-lysine-coated coverslips. Coverslips were then immersed in isopropanol series (5 min in 20%, 40%, 60%, 80%, 2x100%) and finally embryos were cleared in BABB. Coverslips were mounted on a slide with spacers and embryos were imaged with a HCX PL APO 63x/1.4-0.6 oil immersion objective on a Leica SP5 confocal microscope (Leica, Wetzlar, Germany). Optical sections were set at 2 $\mu$ m. The processes of embryo reconstruction and surface data calculation were described previously (Robin et al., 2011b) and conducted with slight modifications. We used 3 different software packages: Amira software (Thermo Scientific), 3DStudioMax (3dsMax, Autodesk) and 3D Virtual Embryo (3DVE, ANISEED (Tassy et al., 2010)). Briefly, the stack was opened with Amira software. The outer surface of the embryo was segmented with the “magic wand” tool and assigned to an “Exterior” object. Then a manual segmentation of each cell was carried out with a graphic tablet, by delimiting cells manually one by one (Wacom, Kazo, Japan). At the beginning of a cell, the contour was drawn with the “brush” tool in the xy dimension and then the contour was filled. 2 or 3 slices after, the same process was done until reaching the end of the cell. Intermediate slices were then interpolated and included in the selection. The selection corresponding to the cell was assigned to an object with the corresponding name. This procedure was repeated for the total 32 cells of the embryo. A smoothing pipeline (smooth labels and remove island) was applied in order to remove any isolated pixels. The 3D surfaces were generated by Amira software and exported in a format compatible with 3dsMax software (VRML). With this software, on each cell, a process of normalisation of the vertex was done in order to unify all the surfaces and another pipeline of smoothing was applied. Then, the virtual embryo with smoothed cell surfaces was exported in a format compatible with 3DVE software (Wavefront) (Robin et al., 2011b). Finally, surfaces and the cell-cell contact surfaces were calculated with 3DVE.

The semi-automated reconstruction using Amaris and PH-GFP labelled embryos described first was far superior in ease and rapidity and was used for all other reconstructions.

## **ERK-KTR**

*ERK-KTR-mClover* mRNA was injected in *Phallusia mammillata* eggs together with *NLS-tdTomato* mRNA. Injected eggs were incubated at least for one hour before fertilisation. After fertilisation, embryos were left to develop until the 16-cell stage, then placed in a glass bottom dish covered with multi-microwells made with MY-134 polymer (My Polymers Ltd, Nes-Ziona, Israel) (Engl et al., 2014) and coated with 0.1% gelatin. Embryos were placed in wells so that a-line ectoderm cells were facing directly to the coverglass. Multi-position live-imaging was carried out with a HC PL APO 40x/1.10 water immersion objective on a Leica SP5 confocal microscope. Optical sections were set at 2µm and stacks were acquired every 2 minutes at 256 x 256 pixels, 8 bits per pixel. Image quantification was carried out with ImageJ software (Rueden et al., 2017). First, the background was subtracted from the ERK-KTR hyperstack using a custom-made Java plugin. A ROI was set on the largest disc corresponding to each nucleus of the a-line ectoderm cells, in each time point using the NLS-Tomato hyperstack. Then, these ROIs were applied on the ERK-KTR hyperstack and a mean intensity measurement was obtained for each nucleus. On the z-slice with the nucleus largest disc, a mean intensity measurement of the ROI defined manually by tracing the contour of the corresponding cell was also obtained for each a-line ectoderm cell at each time point. The nuclear ERK-KTR mean intensity measured in the nucleus was normalized by the "cytoplasmic" ERK-KTR mean intensity. Finally, where indicated in the text, the nuclear/cytoplasmic ratios for each side of an embryo was normalized by the nuclear/cytoplasmic ratio of the corresponding a6.8 cell for each time point.

## **Ex vivo FGF dose response treatment**

For the in vitro experiments, embryos were bisected at the 8-cell stage into ectoderm (animal) and mesendoderm (vegetal) halves and cultured in BSA-ASW in petri dishes as described (Hudson and Lemaire, 2001b). For NVP-treatment, explants were placed in 4µM NVPBHG712 when sibling embryos reached the late 16-cell stage. Explants and embryos from the same fertilisation were observed under dissection microscope until cells started dividing towards the 32-cell stage, then placed in various concentrations of basic-FGF (FGF-2) (ref: F-0291, Sigma-Aldrich, Missouri, USA).

For precise fixation times, the final minutes of incubation were carried out directly in the preparation tubes. For anti-dpERK IF, samples were fixed and processed as described above. For western blots, explants were collected at various time points for temporal response or precisely at 18 minutes. In each dose response experiment, explants from the same batch of embryos were treated with or without NVPBHG712, in addition to bFGF, collected for western blot and processed in parallel. To be within the linear range, between 6 and 10 explants were collected per tube. Seawater was removed to 5 $\mu$ l and 5 $\mu$ l 2x Laemmli buffer (1.25mM Tris.HCl pH6.8, 20% glycerol, 4% SDS, 0.1% Bromophenol blue, 200mM DTT) was added, vortexed and boiled for 2 minutes. On every gel, a standard whole 32-cell stage embryo sample dilution series was loaded (for example: 1, 4, 8 and 12 whole embryos) to ensure that all samples were within the linear range for the two antibodies used.

Samples were loaded, with standard molecular weight markers onto 12% precast polyacrylamide gels (Mini-Protean TGX™ gels, ref: 4561046, Biorad, California, USA) and migrated under standard conditions. Transfer was carried out onto PVDF membrane (Hybond™ P0.45, ref: 10600023, Amersham/Sigma-Aldrich, Missouri, USA) under standard conditions with a Biorad wet electroblotting system for 2 hours at 60 volts, with ice pack and stirrer. For antibody economy, the membrane was cut between the 28 and 130 kDa markers. Membrane was rinsed in TBS-0.1%Tween, then the same solution with 5% milk powder for 1 hour at room temperature. Membranes were placed in the milk solution with 1/1000 rabbit anti-dpERK (D13.14.4E) (ref: 4370, lot: 15 and 17, Cell Signalling Technology) and 1/1000 rabbit anti-protein kinase C zeta type (PKC $\zeta$ ) (C-20) (ref: sc-216, Lot: B0810, Santa Cruz Biotechnology, Texas, USA), sealed in plastic bags and gently rocked overnight at 4°C. After washes in TBS-0.1%Tween, membrane was placed in 5% powdered milk solution with 1/10000 goat anti-rabbit-HRP (ref: 111-035-144, Jackson Immunoresearch) for two hours at room temperature followed by TBS-0.1%Tween washes. Western blots were revealed with SuperSignal West Femto Maximum Sensitivity Substrate (ref: 34095, Thermo Fisher Scientific) according to manufacturer's instructions, using the Fusion FX ECL machine (Vilber Lourmat, Collegien, France) and Fusion Software. For both dpERK and PKC $\zeta$ , a linear range of between one and 12 whole embryos could be obtained under these conditions. In the 16-bit images obtained for each western blot for each signal (dpERK and PKC $\zeta$ ) some saturation was tolerated at high embryo load in the linear range to get the best possible signal range around the samples (in which no saturation was tolerated). Images were quantified with Fuji software

after background subtraction (rolling ball 50 pixels) (Schindelin et al., 2012). Each dpERK value was normalised by the loading control PKC $\zeta$  value and data between blots was normalised by dividing each dpERK/PKC $\zeta$  ratio with the ratio of the 4 whole embryo standard loaded onto every gel in the linear range test. Quantified points outside of the linear range (either dpERK or PKC $\zeta$ ), signal considerably higher than other points or obscured by particles or bubbles during antibody incubation) were removed from the analysis (See Supplementary data file-all westerns for details). In total, 10 out of 240 points were removed.

### **Single molecule fluorescent *in situ* hybridization (smFISH)**

For smFISH, a commercially available kit (RNAscope<sup>®</sup> Fluorescent Multiplex Assay, Advanced Cell Diagnostics/Bio-Techne, Minnesota, USA) with RNAscope Probe- *Ci-Otx* (#421381-C1) was used. Briefly, embryos were fixed at late 32-cell stage in 4% PFA, 0.5M NaCl, 0.1M MOPS, overnight at 4°C and then dehydrated in ethanol for storage. After rehydration, embryos were permeabilized in Pretreat4 (provided by the kit) for 30 min and post-fixed in PFA 4%/PBS-Tween 0.1%. Probe hybridization was carried out overnight at 40°C in a water bath. Then, post-hybridization steps were conducted according to manufacturer's instructions. The last amplification step was carried out with the fluorescent label Atto 550. Nuclei were counter-stained for 2 min with the DAPI solution provided by the kit. Finally, embryos were mounted and oriented one by one in Citifluor AF-1 (ref: AF1-100, Biovalley France, Illkirch-Graffenstaden, France) and imaged thereafter with a HC PL CS2 63x/1.4 oil immersion objective on a Leica SP8 confocal microscope. Images were obtained with high pixel resolution (90-150nm) and smFISH spots were counted in segmented nucleus of each a-line cell with Imaris software (Oxford Instruments). For all *Otx* smFISH spot counts, values of 0 were changed to 0.1 so graphs could be presented with a logarithmic scale. In order to test whether this method allows us to detect *Otx* transcripts in a semi-quantitative manner, we injected synthetic *Otx* mRNA (0.1, 0.2, 0.4ng/ $\mu$ l) into single a4.2 cells of 8-cell stage embryos and analysed them with *Otx* smFISH at 16-cell stage before endogenous *Otx* expression started. We found that this method allows us to detect incremental two-fold increases of transcript levels in *Ciona* embryos (not shown). Furthermore, histograms of spot intensity showed a single peak, which is consistent with one spot representing one transcript.

In the experiment showing recovery of control *Otx* expression pattern in NVPBHG712-treated embryos by simultaneous treatment with a low dose of U0126, the following

procedure was adopted. Embryos were treated with 8 $\mu$ M NVPBHG712 from late 16-cell stage and various concentrations of U0126, empirically chosen, around 0.2 $\mu$ M. Following *Otx* smFISH, a few embryos from each experimental condition were verified, firstly, for the efficiency of NVPBHG712-treatment (ectopic *Otx*) and, secondly, for the best 'recovery' dose of U0126. Once the best 'recovery' dose was chosen, all embryos in the three conditions, control, NVPBHG712 alone, and NVPBHG712 plus the chosen dose of U0126, were mounted and scanned by confocal microscopy using the above procedure.

### **Temporal dynamics of *Otx* transcriptional activation**

Even though embryos were collected from synchronised batches, hand screened to ensure that all embryos were morphologically at the same stage, we noticed some slight asynchronies when embryos were fixed at 3 minute intervals. Therefore, we decided that after processing for *Otx* smFISH, every embryo would be verified for its exact developmental stage and rescaled by comparison to a time-lapse movie of mesendoderm cells. During the 32-cell stage, the cell cycle of mesendoderm cells is advanced compared to that of ectoderm cells. Consistently, during this developmental stage, the mesendoderm nuclei display dynamic changes in terms of their relative positions and their morphology. Embryos were fixed every 3 minutes from the early 32-cell stage, processed for *Otx* smFISH and DAPI counter-stained. After confocal acquisition of *Otx* smFISH signals, embryos were re-photographed from the vegetal side using a wide-field fluorescence microscope. The stage of each embryo was then verified by comparing the DAPI-stained nuclei of the medial A-line and B-line endoderm precursors to the time-lapse movie of the corresponding cells. After every embryo was verified in this way, embryos from one fixation time point were occasionally re-grouped with those in a different fixation time point to match the time-lapse movie based developmental stage. Figure S10A shows images acquired by confocal microscopy of embryos stained with DAPI, and matched to the time-lapse movie to illustrate the position of the endoderm nuclei relative to the nuclei of a6.5 neural precursors at various time points.

### **Graphs and statistical tests**

All data graphical representations and statistical tests were conducted with Prism 8-GraphPad software (California, USA).

## **Modelling**

All modelling was carried out with Matlab software (Mathworks, Massachusetts, USA). For the data fitting in Figure 6C we used the best fit Hill coefficient obtained from data presented in Figure 1E. The best-fit Hill coefficients we obtained by plotting ERK activity against relative cell surface contact had very wide or unpredictable confidence intervals (Supplementary Table 1), probably due to the few cellular configurations available in the embryo and the variability in the measured ERK activity. Hill coefficients were, however, none-the-less reasonably consistent between experiments (For NVP-treated embryos 2.6 and 1.6 and for control embryos 3.9 (control 1), 3.4 (control 2), 5.3 (control 3) and 3.6 (control 3 technical replicate). We therefore tentatively took our first NVP Hill coefficient of 2.6 and placed it in equation (3) (Figure 6C).

## ***Ciona robusta* Unique Gene Identifiers for ascidian genes relevant to this study.**

For more components of the FGF signalling pathway refer to: (Brozovic et al., 2018; Satou et al., 2003; Satou et al., 2005).

FGF9/16/20: Cirobu.g00004295

M-Ras: Cirobu.g00011870

ERK1/2: Cirobu.g00011469

MEK1/2: Cirobu.g00011301

FGFRc: Cirobu.g00014992

Efna.d: Cirobu.g00005918

Eph3 (now called Eph.c): Cirobu.g00008427

Otx: Cirobu.g00006940

p120RasGAP (also known as RASA1): Cirobu.g00011424

IQGAP: Cirobu.g00013174

Neurofibromin: Cirobu.g00010667

RASA2/3: Cirobu.g00000569

## **Acknowledgements**

We would like to thank Benoit Godard for the micro-wells, Christian Rouvière for the custom-made java plugin for background subtraction in Image J, Remi Dumollard for the NLS

sequence; Delphine Dauga for advice on manual 3D embryo reconstruction; Konner Winkley and Michael Veeman for advice on semi-automated segmentation; Axel Duchene, Laurent Gilletta and Régis Lasbleiz for animal husbandry; the Alex McDougall team for sharing *Phallusia* eggs/sperms. The team of H. Y. is supported by the Centre National de la Recherche Scientifique (CNRS), the Université Pierre et Marie Curie, the Fondation ARC pour la Recherche sur le Cancer (PJA 20131200223) and the Agence Nationale de la Recherche (ANR-17-CE13-0003-01). Work of Geneviève Dupont is funded by..... and work of Sophie du Buyl is funded by.....

## REFERENCES

- Abu-Arish, A., Porcher, A., Czerwonka, A., Dostatni, N. and Fradin, C.** (2010). High Mobility of Bicoid Captured by Fluorescence Correlation Spectroscopy: Implication for the Rapid Establishment of Its Gradient. *Biophys. J.* **99**, L33–L35.
- Adachi, M., Fukuda, M. and Nishida, E.** (1999). Two co-existing mechanisms for nuclear import of MAP kinase: passive diffusion of a monomer and active transport of a dimer. *EMBO J.* **18**, 5347–5358.
- Ahmed, S., Grant, K. G., Edwards, L. E., Rahman, A., Cirit, M., Goshe, M. B. and Haugh, J. M.** (2014). Data-driven modeling reconciles kinetics of ERK phosphorylation, localization, and activity states. *Mol. Syst. Biol.* **10**, 718.
- Albeck, J. G., Mills, G. B. and Brugge, J. S.** (2013a). Frequency-Modulated Pulses of ERK Activity Transmit Quantitative Proliferation Signals. *Mol. Cell* **49**, 249–261.
- Albeck, J. G., Mills, G. B. and Brugge, J. S.** (2013b). Frequency-modulated pulses of ERK activity transmit quantitative proliferation signals. *Mol. Cell* **49**, 249–261.
- Alié, A., Hiebert, L. S., Scelzo, M. and Tiozzo, S.** (2020). The eventful history of nonembryonic development in tunicates. *J. Exp. Zoolog. B Mol. Dev. Evol.*
- Altan-Bonnet, G. and Germain, R. N.** (2005). Modeling T cell antigen discrimination based on feedback control of digital ERK responses. *PLoS Biol.* **3**, e356.
- Ando, R., Mizuno, H. and Miyawaki, A.** (2004). Regulated Fast Nucleocytoplasmic Shuttling Observed by Reversible Protein Highlighting. *Science* **306**, 1370–1373.
- Aoki, K., Yamada, M., Kunida, K., Yasuda, S. and Matsuda, M.** (2011a). Processive phosphorylation of ERK MAP kinase in mammalian cells. *Proc. Natl. Acad. Sci.* **108**, 12675–12680.
- Aoki, K., Yamada, M., Kunida, K., Yasuda, S. and Matsuda, M.** (2011b). Processive phosphorylation of ERK MAP kinase in mammalian cells. *Proc. Natl. Acad. Sci.* **108**, 12675–12680.
- Aoki, K., Kumagai, Y., Sakurai, A., Komatsu, N., Fujita, Y., Shionyu, C. and Matsuda, M.** (2013a). Stochastic ERK Activation Induced by Noise and Cell-to-Cell Propagation Regulates Cell Density-Dependent Proliferation. *Mol. Cell* **52**, 529–540.
- Aoki, K., Kumagai, Y., Sakurai, A., Komatsu, N., Fujita, Y., Shionyu, C. and Matsuda, M.** (2013b). Stochastic ERK Activation Induced by Noise and Cell-to-Cell Propagation Regulates Cell Density-Dependent Proliferation. *Mol. Cell* **52**, 529–540.
- Aoki, K., Kondo, Y., Naoki, H., Hiratsuka, T., Itoh, R. E. and Matsuda, M.** (2017). Propagating Wave of ERK Activation Orients Collective Cell Migration. *Dev. Cell* **43**, 305–317.e5.
- Attardi, A., Fulton, T., Florescu, M., Shah, G., Muresan, L., Lenz, M. O., Lancaster, C., Huisken, J., van Oudenaarden, A. van and Steventon, B.** (2018). Neuromesodermal progenitors are a conserved source of spinal cord with divergent growth dynamics. *Development* **145**,

- Auciello, G., Cunningham, D. L., Tatar, T., Heath, J. K. and Rappoport, J. Z.** (2013). Regulation of fibroblast growth factor receptor signalling and trafficking by Src and Eps8. *J. Cell Sci.* **126**, 613–624.
- Azaripour, A., Lagerweij, T., Scharfbillig, C., Jadcak, A. E., Willershausen, B. and Van Noorden, C. J. F.** (2016). A survey of clearing techniques for 3D imaging of tissues with special reference to connective tissue. *Prog. Histochem. Cytochem.* **51**, 9–23.
- Balaskas, N., Ribeiro, A., Panovska, J., Dessaud, E., Sasai, N., Page, K. M., Briscoe, J. and Ribes, V.** (2012). Gene Regulatory Logic for Reading the Sonic Hedgehog Signaling Gradient in the Vertebrate Neural Tube. *Cell* **148**, 273–284.
- Bardwell, A. J., Abdollahi, M. and Bardwell, L.** (2003). Docking sites on mitogen-activated protein kinase (MAPK) kinases, MAPK phosphatases and the Elk-1 transcription factor compete for MAPK binding and are crucial for enzymic activity. *Biochem. J.* **370**, 1077–1085.
- Barkoulas, M., van Zon, J. S., Milloz, J., van Oudenaarden, A. and Félix, M.-A.** (2013). Robustness and Epistasis in the *C. elegans* Vulval Signaling Network Revealed by Pathway Dosage Modulation. *Dev. Cell* **24**, 64–75.
- Berset, T., Hoier, E. F., Battu, G., Canevascini, S. and Hajnal, A.** (2001). Notch Inhibition of RAS Signaling Through MAP Kinase Phosphatase LIP-1 During *C. elegans* Vulval Development. *Science*.
- Bertrand, V., Hudson, C., Caillol, D., Popovici, C. and Lemaire, P.** (2003a). Neural tissue in ascidian embryos is induced by FGF9/16/20, acting via a combination of maternal GATA and Ets transcription factors. *Cell* **115**, 615–627.
- Bertrand, V., Hudson, C., Caillol, D., Popovici, C. and Lemaire, P.** (2003b). Neural tissue in ascidian embryos is induced by FGF9/16/20, acting via a combination of maternal GATA and Ets transcription factors. *Cell* **115**, 615–627.
- Blum, Y., Mikelson, J., Dobrzyński, M., Ryu, H., Jacques, M., Jeon, N. L., Khammash, M. and Pertz, O.** (2019). Temporal perturbation of ERK dynamics reveals network architecture of FGF2/MAPK signaling. *Mol. Syst. Biol.* **15**,.
- Bohr, C.** (1904). Die Saurestoffe des genuinen Blutfarbstoffes und des aus dem Blute darstellten Hämoglobins. *Cent. Für Physiol* **23**,.
- Boissier, P., Chen, J. and Huynh-Do, U.** (2013). EphA2 Signaling Following Endocytosis: Role of Tiam1: EphA2 Endocytosis and Tiam1. *Traffic* **14**, 1255–1271.
- Böttcher, R. T. and Niehrs, C.** (2005). Fibroblast Growth Factor Signaling during Early Vertebrate Development. *Endocr. Rev.* **26**, 63–77.
- Bouvier, D., Tremblay, M.-È., Riad, M., Corera, A. T., Gingras, D., Horn, K. E., Fotouhi, M., Girard, M., Murai, K. K., Kennedy, T. E., et al.** (2010a). EphA4 is localized in clathrin-coated and synaptic vesicles in adult mouse brain. *J. Neurochem.* **113**, 153–165.
- Bouvier, D., Tremblay, M.-È., Riad, M., Corera, A. T., Gingras, D., Horn, K. E., Fotouhi, M., Girard, M., Murai, K. K., Kennedy, T. E., et al.** (2010b). EphA4 is localized in clathrin-coated and synaptic vesicles in adult mouse brain. *J. Neurochem.* **113**, 153–165.

- Boxtel, A. L. van, Economou, A. D., Heliot, C. and Hill, C. S.** (2018). Long-Range Signaling Activation and Local Inhibition Separate the Mesoderm and Endoderm Lineages. *Dev. Cell* **44**, 179-191.e5.
- Brewer, J. R., Mazot, P. and Soriano, P.** (2016a). Genetic insights into the mechanisms of Fgf signaling. *Genes Dev.* **30**, 751–771.
- Brewer, J. R., Mazot, P. and Soriano, P.** (2016b). Genetic insights into the mechanisms of Fgf signaling. *Genes Dev.* **30**, 751–771.
- Briscoe, J. and Small, S.** (2015). Morphogen rules: design principles of gradient-mediated embryo patterning. *Development* **142**, 3996–4009.
- Briscoe, J. and Théron, P. P.** (2013). The mechanisms of Hedgehog signalling and its roles in development and disease. *Nat. Rev. Mol. Cell Biol.* **14**, 416–429.
- Briscoe, J., Sussel, L., Serup, P., Hartigan-O'Connor, D., Jessell, T. M., Rubenstein, J. L. R. and Ericson, J.** (1999). Homeobox gene Nkx2.2 and specification of neuronal identity by graded Sonic hedgehog signalling. *Nature* **398**, 622–627.
- Briscoe, J., Pierani, A., Jessell, T. M. and Ericson, J.** (2000). A Homeodomain Protein Code Specifies Progenitor Cell Identity and Neuronal Fate in the Ventral Neural Tube. *Cell* **101**, 435–445.
- Brozovic, M., Dantec, C., Dardaillon, J., Dauga, D., Faure, E., Gineste, M., Louis, A., Naville, M., Nitta, K. R., Piette, J., et al.** (2018). ANISEED 2017: extending the integrated ascidian database to the exploration and evolutionary comparison of genome-scale datasets. *Nucleic Acids Res.* **46**, D718–D725.
- Brunetti, R., Gissi, C., Pennati, R., Caicci, F., Gasparini, F. and Manni, L.** (2015). Morphological evidence that the molecularly determined *Ciona intestinalis* type A and type B are different species: *Ciona robusta* and *Ciona intestinalis*. *J. Zool. Syst. Evol. Res.* **53**, 186–193.
- Brunner, D., Dicker, K., Hafen, E. and Klimbtt, C.** (1994). The ETS domain protein Pointed-P2 Is a target of MAP kinase in the Sevenless signal transduction pathway. *4*.
- Burack, W. R. and Sturgill, T. W.** (1997). The activating dual phosphorylation of MAPK by MEK is nonprocessive. *Biochemistry* **36**, 5929–5933.
- Burz, D. S.** (1998). Cooperative DNA-binding by Bicoid provides a mechanism for threshold-dependent gene activation in the Drosophila embryo. *EMBO J.* **17**, 5998–6009.
- Butti, R., Das, S., Gunasekaran, V. P., Yadav, A. S., Kumar, D. and Kundu, G. C.** (2018). Receptor tyrosine kinases (RTKs) in breast cancer: signaling, therapeutic implications and challenges. *Mol. Cancer* **17**,.
- Carroll, M., Levasseur, M., Wood, C., Whitaker, M., Jones, K. and McDougall, A.** (2003). Exploring the mechanism of action of the sperm-triggered calcium-wave pacemaker in ascidian zygotes. *J. Cell Sci.* **116**, 4997–5004.
- Casaletto, J. B. and McClatchey, A. I.** (2012). Spatial regulation of receptor tyrosine kinases in development and cancer. *Nat. Rev. Cancer* **12**, 387–400.
- Chabry, L.** (1887). *Embryologie normale et tératologique des Ascidie*. Paris: Felix Alcan Editeur.

- Chamberlain, C. E., Jeong, J., Guo, C., Allen, B. L. and McMahon, A. P.** (2008). Notochord-derived Shh concentrates in close association with the apically positioned basal body in neural target cells and forms a dynamic gradient during neural patterning. *Development* **135**, 1097–1106.
- Chen, N. and Greenwald, I.** (2004). The lateral signal for LIN-12/Notch in *C. elegans* vulval development comprises redundant secreted and transmembrane DSL proteins. *Dev. Cell* **6**, 183–192.
- Chen, H., Xu, Z., Mei, C., Yu, D. and Small, S.** (2012). A System of Repressor Gradients Spatially Organizes the Boundaries of Bicoid-Dependent Target Genes. *Cell* **149**, 618–629.
- Cohen, M., Kicheva, A., Ribeiro, A., Blassberg, R., Page, K. M., Barnes, C. P. and Briscoe, J.** (2015). Ptch1 and Gli regulate Shh signalling dynamics via multiple mechanisms. *Nat. Commun.* **6**, 6709.
- Cole, A. G. and Meinertzhagen, I. A.** (2004). The central nervous system of the ascidian larva: mitotic history of cells forming the neural tube in late embryonic *Ciona intestinalis*. *Dev. Biol.* **271**, 239–262.
- Conklin, E.** (1905a). Mosaic development in ascidian eggs. *J. Exp. Zool.*
- Conklin, E. G.** (1905b). The organisation and cell lineage of the ascidian egg. *J Acad Natl Sci Phila.* 1–119.
- Coppey, M., Boettiger, A. N., Berezhkovskii, A. M. and Shvartsman, S. Y.** (2008a). Nuclear Trapping Shapes the Terminal Gradient in the *Drosophila* Embryo. *Curr. Biol.* **18**, 915–919.
- Coppey, M., Boettiger, A. N., Berezhkovskii, A. M. and Shvartsman, S. Y.** (2008b). Nuclear trapping shapes the terminal gradient in the *Drosophila* embryo. *Curr. Biol. CB* **18**, 915–919.
- Cota, C. D. and Davidson, B.** (2015). Mitotic Membrane Turnover Coordinates Differential Induction of the Heart Progenitor Lineage. *Dev. Cell* **34**, 505–519.
- Crauk, O. and Dostatni, N.** (2005). Bicoid Determines Sharp and Precise Target Gene Expression in the *Drosophila* Embryo. *Curr. Biol.* **15**, 1888–1898.
- Crick, F.** (1970). Diffusion in Embryogenesis. 3.
- Crocker, J., Abe, N., Rinaldi, L., McGregor, A. P., Frankel, N., Wang, S., Alsaadi, A., Valenti, P., Plaza, S., Payre, F., et al.** (2015). Low affinity binding site clusters confer hox specificity and regulatory robustness. *Cell* **160**, 191–203.
- Das, A., Salloum, F. N., Xi, L., Rao, Y. J. and Kukreja, R. C.** (2009). ERK phosphorylation mediates sildenafil-induced myocardial protection against ischemia-reperfusion injury in mice. *Am. J. Physiol. Heart Circ. Physiol.* **296**, H1236-1243.
- Davis, S., Gale, N. W., Aldrich, T. H., Maisonpierre, P. C., Lhotak, V., Pawson, T., Goldfarb, M. and Yancopoulos, G. D.** (1994). Ligands for EPH-related receptor tyrosine kinases that require membrane attachment or clustering for activity. *Science* **266**, 816–819.
- de la Cova, C., Townley, R., Regot, S. and Greenwald, I.** (2017a). A Real-Time Biosensor for ERK Activity Reveals Signaling Dynamics during *C. elegans* Cell Fate Specification. *Dev. Cell* **42**, 542-553.e4.

- de la Cova, C., Townley, R., Regot, S. and Greenwald, I.** (2017b). A Real-Time Biosensor for ERK Activity Reveals Signaling Dynamics during *C. elegans* Cell Fate Specification. *Dev. Cell* **42**, 542-553.e4.
- Delsuc, F., Brinkmann, H., Chourrout, D. and Philippe, H.** (2006). Tunicates and not cephalochordates are the closest living relatives of vertebrates. *Nature* **439**, 965–968.
- Delsuc, F., Philippe, H., Tsagkogeorga, G., Simion, P., Tilak, M.-K., Turon, X., López-Legentil, S., Piette, J., Lemaire, P. and Douzery, E. J. P.** (2018a). A phylogenomic framework and timescale for comparative studies of tunicates. *BMC Biol.* **16**, 39.
- Delsuc, F., Philippe, H., Tsagkogeorga, G., Simion, P., Tilak, M.-K., Turon, X., López-Legentil, S., Piette, J., Lemaire, P. and Douzery, E. J. P.** (2018b). A phylogenomic framework and timescale for comparative studies of tunicates. *BMC Biol.* **16**,.
- Dent, J. A., Polson, A. G. and Klymkowsky, M. W.** (1989). A whole-mount immunocytochemical analysis of the expression of the intermediate filament protein vimentin in *Xenopus*. *Development* **105**, 61.
- Desponds, J., Tran, H., Ferraro, T., Lucas, T., Romero, C. P., Guillou, A., Fradin, C., Coppey, M., Dostatni, N. and Walczak, A. M.** (2016). Precision of Readout at the hunchback Gene: Analyzing Short Transcription Time Traces in Living Fly Embryos. *PLoS Comput. Biol.* **12**, e1005256.
- Dessaud, E., Yang, L. L., Hill, K., Cox, B., Ulloa, F., Ribeiro, A., Mynett, A., Novitsch, B. G. and Briscoe, J.** (2007). Interpretation of the sonic hedgehog morphogen gradient by a temporal adaptation mechanism. *Nature* **450**, 717–720.
- Di Fiore, P. P. and De Camilli, P.** (2001). Endocytosis and Signaling: An Inseparable Partnership. *Cell* Vol. **106**, 1–4,.
- Dorey, K. and Amaya, E.** (2010). FGF signalling: diverse roles during early vertebrate embryogenesis. *Development* **137**, 3731–3742.
- Driever, W. and Nüsslein-Volhard, C.** (1988a). A gradient of bicoid protein in *Drosophila* embryos. *Cell* **54**, 83–93.
- Driever, W. and Nüsslein-Volhard, C.** (1988b). The bicoid protein determines position in the *Drosophila* embryo in a concentration-dependent manner. *Cell* **54**, 95–104.
- Driever, W., Thoma, G. and Nüsslein-Volhard, C.** (1989). Determination of spatial domains of zygotic gene expression in the *Drosophila* embryo by the affinity of binding sites for the bicoid morphogen. *Nature* **340**, 363–367.
- Du, Z. and Lovly, C. M.** (2018). Mechanisms of receptor tyrosine kinase activation in cancer. *Mol. Cancer* **17**, 58.
- Dufour, H. D., Chettouh, Z., Deyts, C., de Rosa, R., Goridis, C., Joly, J.-S. and Brunet, J.-F.** (2006). Precranial origin of cranial motoneurons. *Proc. Natl. Acad. Sci.* **103**, 8727–8732.
- Ebisuya, M.** (2005). The duration, magnitude and compartmentalization of ERK MAP kinase activity: mechanisms for providing signaling specificity. *J. Cell Sci.* **118**, 2997–3002.

- Engl, W., Arasi, B., Yap, L. L., Thiery, J. P. and Viasnoff, V.** (2014). Actin dynamics modulate mechanosensitive immobilization of E-cadherin at adherens junctions. *Nat. Cell Biol.* **16**, 584–591.
- Ericson, J., Morton, S., Kawakami, A., Roelink, H. and Jessell, T. M.** (1996). Two Critical Periods of Sonic Hedgehog Signaling Required for the Specification of Motor Neuron Identity. *Cell* **87**, 661–673.
- Ericson, J., Rashbass, P., Schedl, A., Brenner-Morton, S., Kawakami, A., van Heyningen, V., Jessell, T. M. and Briscoe, J.** (1997). Pax6 Controls Progenitor Cell Identity and Neuronal Fate in Response to Graded Shh Signaling. *Cell* **90**, 169–180.
- Farley, E. K., Olson, K. M., Zhang, W., Brandt, A. J., Rokhsar, D. S. and Levine, M. S.** (2015a). Suboptimization of developmental enhancers. *Science* **350**, 325–328.
- Farley, E. K., Olson, K. M., Zhang, W., Brandt, A. J., Rokhsar, D. S. and Levine, M. S.** (2015b). Suboptimization of developmental enhancers. *Science* **350**, 325–328.
- Fehrenbacher, N., Bar-Sagi, D. and Philips, M.** (2009). Ras/MAPK signaling from endomembranes. *Mol. Oncol.* **3**, 297–307.
- Ferrell, J. E. and Bhatt, R. R.** (1997). Mechanistic studies of the dual phosphorylation of mitogen-activated protein kinase. *J. Biol. Chem.* **272**, 19008–19016.
- Ferrell, J. E. and Ha, S. H.** (2014a). Ultrasensitivity part I: Michaelian responses and zero-order ultrasensitivity. *Trends Biochem. Sci.* **39**, 496–503.
- Ferrell, J. E. and Ha, S. H.** (2014b). Ultrasensitivity part II: multisite phosphorylation, stoichiometric inhibitors, and positive feedback. *Trends Biochem. Sci.* **39**, 556–569.
- Ferrell, J. E. and Ha, S. H.** (2014c). Ultrasensitivity part III: cascades, bistable switches, and oscillators. *Trends Biochem. Sci.* **39**, 612–618.
- Ferrell, J. E. and Machleder** (1998). The Biochemical Basis of an All-or-None Cell Fate Switch in *Xenopus* Oocytes. *Science* **280**, 895–898.
- Ferrell Jr., J. E.** (1998). The Biochemical Basis of an All-or-None Cell Fate Switch in *Xenopus* Oocytes. *Science* **280**, 895–898.
- Fiuza, U.-M., Negishi, T., Rouan, A., Yasuo, H. and Lemaire, P.** (2020). A *Nodal/Eph* signalling relay drives the transition from apical constriction to apico-basal shortening in ascidian endoderm invagination. *Developmental Biology*.
- Francavilla, C., Rigbolt, K. T. G., Emdal, K. B., Carraro, G., Vernet, E., Bekker-Jensen, D. B., Streicher, W., Wikström, M., Sundström, M., Bellusci, S., et al.** (2013). Functional Proteomics Defines the Molecular Switch Underlying FGF Receptor Trafficking and Cellular Outputs. *Mol. Cell* **51**, 707–722.
- Freeman, J. B. and Dale, R.** (2013). Assessing bimodality to detect the presence of a dual cognitive process. *Behav. Res. Methods* **45**, 83–97.
- Frohnhofer, H. G. and Nüsslein-Volhard, C.** (1986). Organization of anterior pattern in the *Drosophila* embryo by the maternal gene bicoid. *Nature* **324**, 120–125.

- Fukuda, M., Gotoh, Y. and Nishida, E.** (1997). Interaction of MAP kinase with MAP kinase kinase: its possible role in the control of nucleocytoplasmic transport of MAP kinase. *EMBO J.* **16**, 1901–1908.
- Furriols, M.** (2003). NEW EMBO MEMBER'S REVIEW: In and out of Torso RTK signalling. *EMBO J.* **22**, 1947–1952.
- Gabay, L., Scholz, H., Golembo, M., Klaes, A., Shilo, B. Z. and Klämbt, C.** (1996). EGF receptor signaling induces pointed P1 transcription and inactivates Yan protein in the Drosophila embryonic ventral ectoderm. *Dev. Camb. Engl.* **122**, 3355–3362.
- Gauthier, K. and Rocheleau, C.** (2017). C. elegans Vulva Induction: An In Vivo Model to Study Epidermal Growth Factor Receptor Signaling and Trafficking. *Methods Mol. Biol. Clifton NJ* **1652**, 43–61.
- Giorgetti, L., Siggers, T., Tiana, G., Caprara, G., Notarbartolo, S., Corona, T., Pasparakis, M., Milani, P., Bulyk, M. L. and Natoli, G.** (2010). Noncooperative Interactions between Transcription Factors and Clustered DNA Binding Sites Enable Graded Transcriptional Responses to Environmental Inputs. *Mol. Cell* **37**, 418–428.
- Goldbeter, A.** (2005). Zero-order switches and developmental thresholds. *Mol. Syst. Biol.* **1**, 2005.0031.
- Goldbeter, A. and Koshland, D. E.** (1981). An amplified sensitivity arising from covalent modification in biological systems. *Proc. Natl. Acad. Sci.* **78**, 6840–6844.
- Golembo, M., Raz, E. and Shilo, B. Z.** (1996). The Drosophila embryonic midline is the site of Spitz processing, and induces activation of the EGF receptor in the ventral ectoderm. *Dev. Camb. Engl.* **122**, 3363–3370.
- Greenwald, I. S., Sternberg, P. W. and Horvitz, H. R.** (1983). The lin-12 locus specifies cell fates in caenorhabditis elegans. *Cell* **34**, 435–444.
- Gregor, T., Wieschaus, E. F., McGregor, A. P., Bialek, W. and Tank, D. W.** (2007a). Stability and Nuclear Dynamics of the Bicoid Morphogen Gradient. *Cell* **130**, 141–152.
- Gregor, T., Tank, D. W., Wieschaus, E. F. and Bialek, W.** (2007b). Probing the Limits to Positional Information. *Cell* **130**, 153–164.
- Grimm, O., Zini, V. S., Kim, Y., Casanova, J., Shvartsman, S. Y. and Wieschaus, E.** (2012). Torso RTK controls Capicua degradation by changing its subcellular localization. *Development* **139**, 3962–3968.
- Guignard, L., Fiuza, U.-M., Leggio, B., Faure, E., Laussu, J., Hufnagel, L., Malandain, G., Godin, C. and Lemaire, P.** (2017). Contact-dependent cell communications drive morphological invariance during ascidian embryogenesis. *bioRxiv* 238741.
- Guillemot, F.** (2007). Spatial and temporal specification of neural fates by transcription factor codes. *Development* **134**, 3771–3780.
- Guntas, G., Hallett, R. A., Zimmerman, S. P., Williams, T., Yumerefendi, H., Bear, J. E. and Kuhlman, B.** (2015). Engineering an improved light-induced dimer (iLID) for controlling the localization and activity of signaling proteins. *Proc. Natl. Acad. Sci.* **112**, 112–117.

- Hajnal, A., Whitfield, C. W. and Kim, S. K.** (1997a). Inhibition of *Caenorhabditis elegans* vulval induction by gap-1 and by let-23 receptor tyrosine kinase. *Genes Dev.* **11**, 2715–2728.
- Hajnal, A., Whitfield, C. W. and Kim, S. K.** (1997b). Inhibition of *Caenorhabditis elegans* vulval induction by gap-1 and by let-23 receptor tyrosine kinase. *Genes Dev.* **11**, 2715–2728.
- Hanafusa, H., Torii, S., Yasunaga, T. and Nishida, E.** (2002). Sprouty1 and Sprouty2 provide a control mechanism for the Ras/MAPK signalling pathway. *Nat. Cell Biol.* **4**, 850–858.
- Hanahan, D. and Weinberg, R. A.** (2011). Hallmarks of Cancer: The Next Generation. *Cell* **144**, 646–674.
- Hansen, M. J., Dallal, G. E. and Flanagan, J. G.** (2004). Retinal Axon Response to Ephrin-As Shows a Graded, Concentration-Dependent Transition from Growth Promotion to Inhibition. *Neuron* **42**, 717–730.
- Harada, M., Murakami, H., Okawa, A., Okimoto, N., Hiraoka, S., Nakahara, T., Akasaka, R., Shiraishi, Y., Futatsugi, N., Mizutani-Koseki, Y., et al.** (2009). FGF9 monomer–dimer equilibrium regulates extracellular matrix affinity and tissue diffusion. *Nat. Genet.* **41**, 289–298.
- Hartigan, P. M.** (1985). Algorithm AS 217: Computation of the Dip Statistic to Test for Unimodality. *Appl. Stat.* **34**, 320.
- Hartigan, J. A. and Hartigan, P. M.** (1985). The Dip Test of Unimodality. *Ann. Stat.* **13**,
- Hashimoto, H., Robin, F. B., Sherrard, K. M. and Munro, E. M.** (2015). Sequential Contraction and Exchange of Apical Junctions Drives Zippering and Neural Tube Closure in a Simple Chordate. *Dev. Cell* **32**, 241–255.
- Haugsten, E. M., Sørensen, V., Kunova Bosakova, M., de Souza, G. A., Krejci, P., Wiedlocha, A. and Wesche, J.** (2016). Proximity Labeling Reveals Molecular Determinants of FGFR4 Endosomal Transport. *J. Proteome Res.* **15**, 3841–3855.
- Haupaix, N., Stolfi, A., Sirour, C., Picco, V., Levine, M., Christiaen, L. and Yasuo, H.** (2013a). p120RasGAP mediates ephrin/Eph-dependent attenuation of FGF/ERK signals during cell fate specification in ascidian embryos. *Dev. Camb. Engl.* **140**, 4347–4352.
- Haupaix, N., Stolfi, A., Sirour, C., Picco, V., Levine, M., Christiaen, L. and Yasuo, H.** (2013b). p120RasGAP mediates ephrin/Eph-dependent attenuation of FGF/ERK signals during cell fate specification in ascidian embryos. *Development* **140**, 4347–4352.
- Haupaix, N., Abitua, P. B., Sirour, C., Yasuo, H., Levine, M. and Hudson, C.** (2014a). Ephrin-mediated restriction of ERK1/2 activity delimits the number of pigment cells in the *Ciona* CNS. *Dev. Biol.* **394**, 170–180.
- Haupaix, N., Abitua, P. B., Sirour, C., Yasuo, H., Levine, M. and Hudson, C.** (2014b). Ephrin-mediated restriction of ERK1/2 activity delimits the number of pigment cells in the *Ciona* CNS. *Dev. Biol.* **394**, 170–180.
- Hayashi, S. and Ogura, Y.** (2020). ERK signaling dynamics in the morphogenesis and homeostasis of *Drosophila*. *Curr. Opin. Genet. Dev.* **63**, 9–15.

- Hill, R. J. and Sternberg, P. W.** (1992). The gene *lin-3* encodes an inductive signal for vulval development in *C. elegans*. *Nature* **358**, 470–476.
- Himanen, J. P., Yermekbayeva, L., Janes, P. W., Walker, J. R., Xu, K., Atapattu, L., Rajashankar, K. R., Mensinga, A., Lackmann, M., Nikolov, D. B., et al.** (2010). Architecture of Eph receptor clusters. *Proc. Natl. Acad. Sci.* **107**, 10860–10865.
- Hirai, H., Maru, Y., Hagiwara, K., Nishida, J. and Takaku, F.** (1987). A novel putative tyrosine kinase receptor encoded by the *eph* gene. *Science* **238**, 1717–1720.
- Hiratsuka, T., Fujita, Y., Naoki, H., Aoki, K., Kamioka, Y. and Matsuda, M.** (2015a). Intercellular propagation of extracellular signal-regulated kinase activation revealed by in vivo imaging of mouse skin. *Elife* **4**, e05178.
- Hiratsuka, T., Fujita, Y., Naoki, H., Aoki, K., Kamioka, Y. and Matsuda, M.** (2015b). Intercellular propagation of extracellular signal-regulated kinase activation revealed by in vivo imaging of mouse skin. *eLife* **4**, e05178.
- Horikawa, Y., Matsumoto, H., Yamaguchi, F., Ishida, S. and Fujiwara, S.** (2013). Transcriptional regulation in the early ectodermal lineage of ascidian embryos. *Dev. Growth Differ.* **55**, 776–785.
- Houchmandzadeh, B., Wieschaus, E. and Leibler, S.** (2002). Establishment of developmental precision and proportions in the early *Drosophila* embryo. *Nature* **415**, 798–802.
- Huang, C. Y. and Ferrell, J. E.** (1996a). Ultrasensitivity in the mitogen-activated protein kinase cascade. *Proc. Natl. Acad. Sci.* **93**, 10078–10083.
- Huang, C. Y. and Ferrell, J. E.** (1996b). Ultrasensitivity in the mitogen-activated protein kinase cascade. *Proc. Natl. Acad. Sci. U. S. A.* **93**, 10078–10083.
- Hubbard, S. R. and Miller, W. T.** (2007). Receptor tyrosine kinases: mechanisms of activation and signaling. *Curr. Opin. Cell Biol.* **19**, 117–123.
- Hudson, C.** (2016). The central nervous system of ascidian larvae: Nervous system development in ascidians. *Wiley Interdiscip. Rev. Dev. Biol.* **5**, 538–561.
- Hudson, C.** (2020). A Simple Method to Identify Ascidian Brain Lineage Cells at Neural Plate Stages Following In Situ Hybridization. In *Brain Development* (ed. Sprecher, S. G.), pp. 325–345. New York, NY: Springer New York.
- Hudson, C. and Lemaire, P.** (2001a). Induction of anterior neural fates in the ascidian *Ciona intestinalis*. *Mech. Dev.* **100**, 189–203.
- Hudson, C. and Lemaire, P.** (2001b). Induction of anterior neural fates in the ascidian *Ciona intestinalis*. *Mech. Dev.* **100**, 189–203.
- Hudson, C., Darras, S., Caillol, D., Yasuo, H. and Lemaire, P.** (2003a). A conserved role for the MEK signalling pathway in neural tissue specification and posteriorisation in the invertebrate chordate, the ascidian *Ciona intestinalis*. *Dev. Camb. Engl.* **130**, 147–159.

- Hudson, C., Darras, S., Caillol, D., Yasuo, H. and Lemaire, P.** (2003b). A conserved role for the MEK signalling pathway in neural tissue specification and posteriorisation in the invertebrate chordate, the ascidian *Ciona intestinalis*. *Development* **130**, 147–159.
- Hudson, C., Lotito, S. and Yasuo, H.** (2007). Sequential and combinatorial inputs from Nodal, Delta2/Notch and FGF/MEK/ERK signalling pathways establish a grid-like organisation of distinct cell identities in the ascidian neural plate. *Dev. Camb. Engl.* **134**, 3527–3537.
- Hudson, C., Kawai, N., Negishi, T. and Yasuo, H.** (2013).  $\beta$ -Catenin-Driven Binary Fate Specification Segregates Germ Layers in Ascidian Embryos. *Curr. Biol.* **23**, 491–495.
- Hudson, C., Sirour, C. and Yasuo, H.** (2016). Co-expression of Foxa.a, Foxd and Fgf9/16/20 defines a transient mesendoderm regulatory state in ascidian embryos. *eLife* **5**,.
- Iguchi, K., Matsunaga, S., Nakano, T., Usui, S. and Hirano, K.** (2006). Inhibition of caveolin-1 expression by incadronate in PC-3 prostate cells. *Anticancer Res.* **26**, 2977–2981.
- Ikuta, T. and Saiga, H.** (2007). Dynamic change in the expression of developmental genes in the ascidian central nervous system: Revisit to the tripartite model and the origin of the midbrain–hindbrain boundary region. *Dev. Biol.* **312**, 631–643.
- Imai, K. S.** (2004). Gene expression profiles of transcription factors and signaling molecules in the ascidian embryo: towards a comprehensive understanding of gene networks. *Development* **131**, 4047–4058.
- Imai, K. S.** (2006). Regulatory Blueprint for a Chordate Embryo. *Science* **312**, 1183–1187.
- Imai, K., Takada, N., Satoh, N. and Satou, Y.** (2000).  $\beta$ -catenin mediates the specification of endoderm cells in ascidian embryos. *12*.
- Imai, K. S., Satoh, N. and Satou, Y.** (2002a). Early embryonic expression of FGF4/6/9 gene and its role in the induction of mesenchyme and notochord in *Ciona savignyi* embryos. *Dev. Camb. Engl.* **129**, 1729–1738.
- Imai, K. S., Satoh, N. and Satou, Y.** (2002b). Region specific gene expressions in the central nervous system of the ascidian embryo. *Mech. Dev.* **119**, S275–S277.
- Imai, K. S., Hudson, C., Oda-Ishii, I., Yasuo, H. and Satou, Y.** (2016). Antagonism between  $\beta$ -catenin and Gata.a sequentially segregates the germ layers of ascidian embryos. *Development* **143**, 4167–4172.
- Inazawa, T., Okamura, Y. and Takahashi, K.** (1998a). Basic fibroblast growth factor induction of neuronal ion channel expression in ascidian ectodermal blastomeres. *J. Physiol.* **511**, 347–359.
- Inazawa, T., Okamura, Y. and Takahashi, K.** (1998b). Basic fibroblast growth factor induction of neuronal ion channel expression in ascidian ectodermal blastomeres. *J. Physiol.* **511**, 347–359.
- Irannejad, R., Tsvetanova, N. G., Lobingier, B. T. and von Zastrow, M.** (2015). Effects of endocytosis on receptor-mediated signaling. *Curr. Opin. Cell Biol.* **35**, 137–143.

- Irie, F., Okuno, M., Pasquale, E. B. and Yamaguchi, Y.** (2005). EphrinB–EphB signalling regulates clathrin-mediated endocytosis through tyrosine phosphorylation of synaptojanin 1. *Nat. Cell Biol.* **7**, 501–509.
- Jean, S., Mikryukov, A., Tremblay, M. G., Baril, J., Guillou, F., Bellenfant, S. and Moss, T.** (2010a). Extended-Synaptotagmin-2 Mediates FGF Receptor Endocytosis and ERK Activation In Vivo. *Dev. Cell* **19**, 426–439.
- Jean, S., Mikryukov, A., Tremblay, M. G., Baril, J., Guillou, F., Bellenfant, S. and Moss, T.** (2010b). Extended-Synaptotagmin-2 Mediates FGF Receptor Endocytosis and ERK Activation In Vivo. *Dev. Cell* **19**, 426–439.
- Jessell, T. M.** (2000). Neuronal specification in the spinal cord: inductive signals and transcriptional codes. *Nat. Rev. Genet.* **1**, 20–29.
- Johnson, H. E. and Toettcher, J. E.** (2019a). Signaling Dynamics Control Cell Fate in the Early Drosophila Embryo. *Dev. Cell* **48**, 361-370.e3.
- Johnson, H. E. and Toettcher, J. E.** (2019b). Signaling Dynamics Control Cell Fate in the Early Drosophila Embryo. *Dev. Cell* **48**, 361-370.e3.
- Johnson, H. E., Goyal, Y., Pannucci, N. L., Schüpbach, T., Shvartsman, S. Y. and Toettcher, J. E.** (2017). The Spatiotemporal Limits of Developmental Erk Signaling. *Dev. Cell* **40**, 185–192.
- Johnson, H. E., Shvartsman, S. Y. and Toettcher, J. E.** (2019). Optogenetic rescue of a developmental patterning mutant. *bioRxiv* 776120.
- Juven-Gershon, T., Hsu, J.-Y. and Kadonaga, J. T.** (2008). Caudal, a key developmental regulator, is a DPE-specific transcriptional factor. *Genes Dev.* **22**, 2823–2830.
- Kaech, S. M., Whitfield, C. W. and Kim, S. K.** (1998). The LIN-2/LIN-7/LIN-10 complex mediates basolateral membrane localization of the C. elegans EGF receptor LET-23 in vulval epithelial cells. *Cell* **94**, 761–771.
- Katz, W. S., Hill, R. J., Clandinin, T. R. and Sternberg, P. W.** (1995). Different Levels of the C, elegans Growth Factor LIN-3 Promote Distinct Vulval Precursor Fates. **11**.
- Katz, W. S., Lesa, G. M., Yannoukakos, D., Clandinin, T. R., Schlessinger, J. and Sternberg, P. W.** (1996). A point mutation in the extracellular domain activates LET-23, the Caenorhabditis elegans epidermal growth factor receptor homolog. *Mol. Cell. Biol.* **16**, 529–537.
- Kay, R. R. and Thompson, C. R. L.** (2009). Forming Patterns in Development without Morphogen Gradients: Scattered Differentiation and Sorting Out. *Cold Spring Harb. Perspect. Biol.* **1**, a001503–a001503.
- Ke, M.-T., Fujimoto, S. and Imai, T.** (2013). SeeDB: a simple and morphology-preserving optical clearing agent for neuronal circuit reconstruction. *Nat. Neurosci.* **16**, 1154–1161.
- Keduka, E., Kaiho, A., Hamada, M., Watanabe-Takano, H., Takano, K., Ogasawara, M., Satou, Y., Satoh, N. and Endo, T.** (2009). M-Ras evolved independently of R-Ras and its neural function is conserved between mammalian and ascidian, which lacks classical Ras. *Gene* **429**, 49–58.

- Khokhlatchev, A. V., Canagarajah, B., Wilsbacher, J., Robinson, M., Atkinson, M., Goldsmith, E. and Cobb, M. H.** (1998). Phosphorylation of the MAP Kinase ERK2 Promotes Its Homodimerization and Nuclear Translocation. *Cell* **93**, 605–615.
- Kholodenko, B. N.** (2007). Untangling the signalling wires. *Nat. Cell Biol.* **9**, 247–249.
- Kim, G. J. and Nishida, H.** (2001). Role of the FGF and MEK signaling pathway in the ascidian embryo. *Dev. Growth Differ.* **43**, 521–533.
- Kim, Y., Coppey, M., Grossman, R., Ajuria, L., Jiménez, G., Paroush, Z. and Shvartsman, S. Y.** (2010). MAPK substrate competition integrates patterning signals in the Drosophila embryo. *Curr. Biol. CB* **20**, 446–451.
- Kimmelman, A. C., Nuñez Rodriguez, N. and Chan, A. M.-L.** (2002). R-Ras3/M-Ras induces neuronal differentiation of PC12 cells through cell-type-specific activation of the mitogen-activated protein kinase cascade. *Mol. Cell. Biol.* **22**, 5946–5961.
- Klein, R.** (2012). Eph/ephrin signalling during development. *Development* **139**, 4105–4109.
- Koga, M. and Ohshima, Y.** (1995). Mosaic analysis of the let-23 gene function in vulval induction of *Caenorhabditis elegans*. *Development* **121**, 2655–2666.
- Kolch, W.** (2000). Meaningful relationships: the regulation of the Ras/Raf/MEK/ERK pathway by protein interactions. *Biochem. J.* **351**, 289–305.
- Komatsu, N., Aoki, K., Yamada, M., Yukinaga, H., Fujita, Y., Kamioka, Y. and Matsuda, M.** (2011). Development of an optimized backbone of FRET biosensors for kinases and GTPases. *Mol. Biol. Cell* **22**, 4647–4656.
- Kovalevsky, A.** (1859). *Mémoires de l'Académie impériale des sciences de St.-Petersbourg*. St.-Petersburg : L'Académie.
- Lambert, C., Goudeau, H., Franchet, C., Lambert, G. and Goudeau, M.** (1997). Ascidian eggs block polyspermy by two independent mechanisms: One at the egg plasma membrane, the other involving the follicle cells. *Mol. Reprod. Dev.* **48**, 137–143.
- Lamy, C.** (2006). Ci-FoxA-a is the earliest zygotic determinant of the ascidian anterior ectoderm and directly activates Ci-sFRP1/5. *Development* **133**, 2835–2844.
- Le Borgne, R.** (2005). The roles of receptor and ligand endocytosis in regulating Notch signaling. *Development* **132**, 1751–1762.
- le Gallic, L., Sgouras, D., Beal, G. and Mavrothalassitis, G.** (1999). Transcriptional Repressor ERF Is a Ras/Mitogen-Activated Protein Kinase Target That Regulates Cellular Proliferation. *Mol. Cell. Biol.* **19**, 4121–4133.
- Le Roy, C. and Wrana, J. L.** (2005). Clathrin- and non-clathrin-mediated endocytic regulation of cell signalling. *Nat. Rev. Mol. Cell Biol.* **6**, 112–126.
- Lebrecht, D., Foehr, M., Smith, E., Lopes, F. J. P., Vanario-Alonso, C. E., Reinitz, J., Burz, D. S. and Hanes, S. D.** (2005). Bicoid cooperative DNA binding is critical for embryonic patterning in *Drosophila*. *Proc. Natl. Acad. Sci.* **102**, 13176–13181.

- Lee, J., Platt, K. A., Censullo, P. and Ruiz i Altaba, A.** (1997). Gli1 is a target of Sonic hedgehog that induces ventral neural tube development. *Dev. Camb. Engl.* **124**, 2537–2552.
- Lemmon, M. A. and Schlessinger, J.** (2010). Cell Signaling by Receptor Tyrosine Kinases. *Cell* **141**, 1117–1134.
- Lifanov, A. P.** (2003). Homotypic Regulatory Clusters in Drosophila. *Genome Res.* **13**, 579–588.
- Lim, B., Dsilva, C. J., Levario, T. J., Lu, H., Schüpbach, T., Kevrekidis, I. G. and Shvartsman, S. Y.** (2015a). Dynamics of Inductive ERK Signaling in the Drosophila Embryo. *Curr. Biol.* **25**, 1784–1790.
- Lim, B., Dsilva, C. J., Levario, T. J., Lu, H., Schüpbach, T., Kevrekidis, I. G. and Shvartsman, S. Y.** (2015b). Dynamics of Inductive ERK Signaling in the Drosophila Embryo. *Curr. Biol. CB* **25**, 1784–1790.
- Lisabeth, E. M., Falivelli, G. and Pasquale, E. B.** (2013). Eph Receptor Signaling and Ephrins. *Cold Spring Harb. Perspect. Biol.* **5**, a009159–a009159.
- Litingtung, Y. and Chiang, C.** (2000). Specification of ventral neuron types is mediated by an antagonistic interaction between Shh and Gli3. *Nat. Neurosci.* **3**, 979–985.
- Löhr, U., Chung, H.-R., Beller, M. and Jäckle, H.** (2009). Antagonistic action of Bicoid and the repressor Capicua determines the spatial limits of Drosophila head gene expression domains. *Proc. Natl. Acad. Sci.* **106**, 21695–21700.
- Lucas, T., Tran, H., Perez Romero, C. A., Guillou, A., Fradin, C., Coppey, M., Walczak, A. M. and Dostatni, N.** (2018). 3 minutes to precisely measure morphogen concentration. *PLOS Genet.* **14**, e1007676.
- Ma, X., Yuan, D., Diepold, K., Scarborough, T. and Ma, J.** (1996). The Drosophila morphogenetic protein Bicoid binds DNA cooperatively. *Development* 1195–1206.
- Macia, E., Ehrlich, M., Massol, R., Boucrot, E., Brunner, C. and Kirchhausen, T.** (2006). Dynasore, a Cell-Permeable Inhibitor of Dynamin. *Dev. Cell* **10**, 839–850.
- MacKeigan, J. P., Murphy, L. O., Dimitri, C. A. and Blenis, J.** (2005a). Graded Mitogen-Activated Protein Kinase Activity Precedes Switch-Like c-Fos Induction in Mammalian Cells. *Mol. Cell. Biol.* **25**, 4676–4682.
- MacKeigan, J. P., Murphy, L. O., Dimitri, C. A. and Blenis, J.** (2005b). Graded Mitogen-Activated Protein Kinase Activity Precedes Switch-Like c-Fos Induction in Mammalian Cells. *Mol. Cell. Biol.* **25**, 4676–4682.
- Markevich, N. I., Hoek, J. B. and Kholodenko, B. N.** (2004a). Signaling switches and bistability arising from multisite phosphorylation in protein kinase cascades. *J. Cell Biol.* **164**, 353–359.
- Markevich, N. I., Hoek, J. B. and Kholodenko, B. N.** (2004b). Signaling switches and bistability arising from multisite phosphorylation in protein kinase cascades. *J. Cell Biol.* **164**, 353–359.
- Marshall, C. J.** (1995). Signaling: Transient versus Sustained Extracellular Signal-Regulated Kinase Activation. *Cell* **80**, 178–185.

- Marston, D. J., Dickinson, S. and Nobes, C. D.** (2003). Rac-dependent trans-endocytosis of ephrinBs regulates Eph–ephrin contact repulsion. *Nat. Cell Biol.* **5**, 879–888.
- Matise, M. P. and Joyner, A. L.** (1999). Gli genes in development and cancer. *Oncogene* **18**, 7852–7859.
- Matise, M. P., Epstein, D. J., Park, H. L., Platt, K. A. and Joyner, A. L.** (1998). Gli2 is required for induction of floor plate and adjacent cells, but not most ventral neurons in the mouse central nervous system. *Dev. Camb. Engl.* **125**, 2759–2770.
- Matsuo, I. and Kimura-Yoshida, C.** (2014). Extracellular distribution of diffusible growth factors controlled by heparan sulfate proteoglycans during mammalian embryogenesis. *Philos. Trans. R. Soc. B Biol. Sci.* **369**, 20130545.
- Mayor, S., Parton, R. G. and Donaldson, J. G.** (2014). Clathrin-Independent Pathways of Endocytosis. *Cold Spring Harb. Perspect. Biol.* **6**, a016758–a016758.
- McCarthy, S. A., Chen, D., Yang, B. S., Garcia Ramirez, J. J., Cherwinski, H., Chen, X. R., Klagsbrun, M., Hauser, C. A., Ostrowski, M. C. and McMahon, M.** (1997). Rapid phosphorylation of Ets-2 accompanies mitogen-activated protein kinase activation and the induction of heparin-binding epidermal growth factor gene expression by oncogenic Raf-1. *Mol. Cell. Biol.* **17**, 2401–2412.
- Melen, G. J., Levy, S., Barkai, N. and Shilo, B.** (2005a). Threshold responses to morphogen gradients by zero-order ultrasensitivity. *Mol. Syst. Biol.* **1**,.
- Melen, G. J., Levy, S., Barkai, N. and Shilo, B.** (2005b). Threshold responses to morphogen gradients by zero-order ultrasensitivity. *Mol. Syst. Biol.* **1**,.
- Meyers, J., Craig, J. and Odde, D. J.** (2006). Potential for Control of Signaling Pathways via Cell Size and Shape. *Curr. Biol.* **16**, 1685–1693.
- Miaczynska, M.** (2013). Effects of Membrane Trafficking on Signaling by Receptor Tyrosine Kinases. *Cold Spring Harb. Perspect. Biol.* **5**, a009035–a009035.
- Miao, H., Wei, B.-R., Peehl, D. M., Li, Q., Alexandrou, T., Schelling, J. R., Rhim, J. S., Sedor, J. R., Burnett, E. and Wang, B.** (2001). Activation of EphA receptor tyrosine kinase inhibits the Ras/MAPK pathway. *Nat. Cell Biol.* **3**, 527–530.
- Mineo, A., Furriols, M. and Casanova, J.** (2018a). The trigger (and the restriction) of Torso RTK activation. *Open Biol.* **8**, 180180.
- Mineo, A., Furriols, M. and Casanova, J.** (2018b). The trigger (and the restriction) of Torso RTK activation. *Open Biol.* **8**, 180180.
- Miya, T. and Nishida, H.** (2003). An Ets transcription factor, HrEts, is target of FGF signaling and involved in induction of notochord, mesenchyme, and brain in ascidian embryos. *Dev. Biol.* **261**, 25–38.
- Miyazaki, Y., Nishida, H. and Kumano, G.** (2007a). Brain induction in ascidian embryos is dependent on juxtaposition of FGF9/16/20-producing and -receiving cells. *Dev. Genes Evol.* **217**, 177–188.

- Miyazaki, Y., Nishida, H. and Kumano, G.** (2007b). Brain induction in ascidian embryos is dependent on juxtaposition of FGF9/16/20-producing and -receiving cells. *Dev. Genes Evol.* **217**, 177–188.
- Moreno, E., Valon, L., Levillayer, F. and Levayer, R.** (2019). Competition for Space Induces Cell Elimination through Compaction-Driven ERK Downregulation. *Curr. Biol.* **29**, 23-34.e8.
- Morgan, T. H.** (1901). *Regeneration*. Macmillan.
- Murphy, J. E., Padilla, B. E., Hasdemir, B., Cottrell, G. S. and Bunnett, N. W.** (2009a). Endosomes: a legitimate platform for the signaling train. *Proc. Natl. Acad. Sci.* **106**, 17615–17622.
- Murphy, J. E., Padilla, B. E., Hasdemir, B., Cottrell, G. S. and Bunnett, N. W.** (2009b). Endosomes: A legitimate platform for the signaling train. *Proc. Natl. Acad. Sci.* **106**, 17615–17622.
- Nicol, D. and Meinertzhagen, I. A.** (1988). Development of the central nervous system of the larva of the ascidian, *Ciona intestinalis* L. I. The early lineages of the neural plate. *Dev. Biol.* **130**, 721–736.
- Nikolov, D. B., Xu, K. and Himanen, J. P.** (2013). Eph/ephrin recognition and the role of Eph/ephrin clusters in signaling initiation. *Biochim. Biophys. Acta BBA - Proteins Proteomics* **1834**, 2160–2165.
- Nishida, H.** (1987a). Cell Lineage Analysis in Ascidian Embryos by Intracellular Injection of a Tracer Enzyme. 16.
- Nishida, H.** (1987b). Cell lineage analysis in ascidian embryos by intracellular injection of a tracer enzyme. III. Up to the tissue restricted stage. *Dev. Biol.* **121**, 526–541.
- Nishida, H.** (2003). Spatio-temporal pattern of MAP kinase activation in embryos of the ascidian *Halocynthia roretzi*. *Dev. Growth Differ.* **45**, 27–37.
- Nishida, H. and Satoh, N.** (1983a). Cell Lineage Analysis in Ascidian Embryos by Intracellular Injection of a Tracer Enzyme. 13.
- Nishida, H. and Satoh, N.** (1983b). Cell lineage analysis in ascidian embryos by intracellular injection of a tracer enzyme. I. Up to the eight-cell stage. *Dev. Biol.* **99**, 382–394.
- Novitsch, B. G., Chen, A. I. and Jessell, T. M.** (2001). Coordinate Regulation of Motor Neuron Subtype Identity and Pan-Neuronal Properties by the bHLH Repressor Olig2. *Neuron* **31**, 773–789.
- Nunns, H. and Goentoro, L.** (2018). Signaling pathways as linear transmitters. *eLife* **7**,.
- Ochoa-Espinosa, A., Yucel, G., Kaplan, L., Pare, A., Pura, N., Oberstein, A., Papatsenko, D. and Small, S.** (2005). The role of binding site cluster strength in Bicoid-dependent patterning in *Drosophila*. *Proc. Natl. Acad. Sci.* **102**, 4960–4965.
- Ochoa-Espinosa, A., Yu, D., Tsirigos, A., Struffi, P. and Small, S.** (2009). Anterior-posterior positional information in the absence of a strong Bicoid gradient. *Proc. Natl. Acad. Sci.* **106**, 3823–3828.
- Oda-Ishii, I., Kubo, A., Kari, W., Suzuki, N., Rothbacher, U. and Satou, Y.** (2016). A Maternal System Initiating the Zygotic Developmental Program through Combinatorial Repression in the Ascidian Embryo. *PLOS Genet.* **12**, e1006045.

- Ogura, Y., Sakaue-Sawano, A., Nakagawa, M., Satoh, N., Miyawaki, A. and Sasakura, Y.** (2011). Coordination of mitosis and morphogenesis: role of a prolonged G2 phase during chordate neurulation. *Dev. Camb. Engl.* **138**, 577–587.
- Ogura, Y., Wen, F.-L., Sami, M. M., Shibata, T. and Hayashi, S.** (2018a). A Switch-like Activation Relay of EGFR-ERK Signaling Regulates a Wave of Cellular Contractility for Epithelial Invagination. *Dev. Cell* **46**, 162-172.e5.
- Ogura, Y., Wen, F.-L., Sami, M. M., Shibata, T. and Hayashi, S.** (2018b). A Switch-like Activation Relay of EGFR-ERK Signaling Regulates a Wave of Cellular Contractility for Epithelial Invagination. *Dev. Cell* **46**, 162-172.e5.
- Ohta, N. and Satou, Y.** (2013a). Multiple signaling pathways coordinate to induce a threshold response in a chordate embryo. *PLoS Genet.* **9**, e1003818.
- Ohta, N. and Satou, Y.** (2013b). Multiple Signaling Pathways Coordinate to Induce a Threshold Response in a Chordate Embryo. *PLoS Genet.* **9**, e1003818.
- Ohta, N., Waki, K., Mochizuki, A. and Satou, Y.** (2015a). A Boolean Function for Neural Induction Reveals a Critical Role of Direct Intercellular Interactions in Patterning the Ectoderm of the Ascidian Embryo. *PLoS Comput. Biol.* **11**, e1004687.
- Ohta, N., Waki, K., Mochizuki, A. and Satou, Y.** (2015b). A Boolean Function for Neural Induction Reveals a Critical Role of Direct Intercellular Interactions in Patterning the Ectoderm of the Ascidian Embryo. *PLoS Comput. Biol.* **11**, e1004687.
- O'Neill, M. and Rubin, G. M.** (1994). The Activities of Two Ets-Related Transcription Factors Required for Drosophila Eye Development Are Modulated by the Ras/MAPK Pathway. **11**.
- Ong, S. H., Guy, G. R., Hadari, Y. R., Laks, S., Gotoh, N., Schlessinger, J. and Lax, I.** (2000). FRS2 Proteins Recruit Intracellular Signaling Pathways by Binding to Diverse Targets on Fibroblast Growth Factor and Nerve Growth Factor Receptors. *Mol. Cell. Biol.* **20**, 979–989.
- Ornitz, D. M. and Itoh, N.** (2015a). The Fibroblast Growth Factor signaling pathway. *Wiley Interdiscip. Rev. Dev. Biol.* **4**, 215–266.
- Ornitz, D. M. and Itoh, N.** (2015b). The Fibroblast Growth Factor signaling pathway. *Wiley Interdiscip. Rev. Dev. Biol.* **4**, 215–266.
- Pálffy, M., Reményi, A. and Korcsmáros, T.** (2012a). Endosomal crosstalk: meeting points for signaling pathways. *Trends Cell Biol.* **22**, 447–456.
- Pálffy, M., Reményi, A. and Korcsmáros, T.** (2012b). Endosomal crosstalk: meeting points for signaling pathways. *Trends Cell Biol.* **22**, 447–456.
- Park, H. L., Bai, C., Platt, K. A., Matise, M. P., Beeghly, A., Hui, C. C., Nakashima, M. and Joyner, A. L.** (2000). Mouse Gli1 mutants are viable but have defects in SHH signaling in combination with a Gli2 mutation. *Dev. Camb. Engl.* **127**, 1593–1605.
- Pasquale, E. B.** (2005). Eph receptor signalling casts a wide net on cell behaviour. *Nat. Rev. Mol. Cell Biol.* **6**, 462–475.

- Patel, A. L. and Shvartsman, S. Y.** (2018). Outstanding questions in developmental ERK signaling. *Development* **145**, dev143818.
- Perrett, R. M., Fowkes, R. C., Caunt, C. J., Tsaneva-Atanasova, K., Bowsher, C. G. and McArdle, C. A.** (2013a). Signaling to Extracellular Signal-regulated Kinase from ErbB1 Kinase and Protein Kinase C: FEEDBACK, HETEROGENEITY, AND GATING. *J. Biol. Chem.* **288**, 21001–21014.
- Perrett, R. M., Fowkes, R. C., Caunt, C. J., Tsaneva-Atanasova, K., Bowsher, C. G. and McArdle, C. A.** (2013b). Signaling to Extracellular Signal-regulated Kinase from ErbB1 Kinase and Protein Kinase C: FEEDBACK, HETEROGENEITY, AND GATING. *J. Biol. Chem.* **288**, 21001–21014.
- Picco, V., Hudson, C. and Yasuo, H.** (2007a). Ephrin-Eph signalling drives the asymmetric division of notochord/neural precursors in *Ciona* embryos. *Dev. Camb. Engl.* **134**, 1491–1497.
- Picco, V., Hudson, C. and Yasuo, H.** (2007b). Ephrin-Eph signalling drives the asymmetric division of notochord/neural precursors in *Ciona* embryos. *Dev. Camb. Engl.* **134**, 1491–1497.
- Poliakov, A., Cotrina, M. and Wilkinson, D. G.** (2004). Diverse Roles of Eph Receptors and Ephrins in the Regulation of Cell Migration and Tissue Assembly. *Dev. Cell* **7**, 465–480.
- Porcher, A. and Dostatni, N.** (2010). The Bicoid Morphogen System. *Curr. Biol.* **20**, R249–R254.
- Porcher, A., Abu-Arish, A., Huart, S., Roelens, B., Fradin, C. and Dostatni, N.** (2010). The time to measure positional information: maternal Hunchback is required for the synchrony of the Bicoid transcriptional response at the onset of zygotic transcription. *Development* **137**, 2795–2804.
- Prodon, F., Sardet, C. and Nishida, H.** (2008). Cortical and cytoplasmic flows driven by actin microfilaments polarize the cortical ER-mRNA domain along the a–v axis in ascidian oocytes. *Dev. Biol.* **313**, 682–699.
- Prodon, F., Chenevert, J., Hébras, C., Dumollard, R., Faure, E., Gonzalez-Garcia, J., Nishida, H., Sardet, C. and McDougall, A.** (2010). Dual mechanism controls asymmetric spindle position in ascidian germ cell precursors. *Dev. Camb. Engl.* **137**, 2011–2021.
- Purvis, J. E. and Lahav, G.** (2013). Encoding and Decoding Cellular Information through Signaling Dynamics. *Cell* **152**, 945–956.
- Qiao, L., Nachbar, R. B., Kevrekidis, I. G. and Shvartsman, S. Y.** (2007). Bistability and Oscillations in the Huang-Ferrell Model of MAPK Signaling. *PLoS Comput. Biol.* **3**, 8.
- Rapraeger, A. C., Krufka, A. and Olwin, B. B.** (1991). Requirement of Heparan Sulfate for bFGF-Mediated Fibroblast Growth and Myoblast Differentiation. *Sci. New Ser.* **252**, 1705–1708.
- Rauen, K. A.** (2013a). The RASopathies. *Annu. Rev. Genomics Hum. Genet.* **14**, 355–369.
- Rauen, K. A.** (2013b). The RASopathies. *Annu. Rev. Genomics Hum. Genet.* **14**, 355–369.
- Rebay, I. and Rubin, G. M.** (1995). Yan functions as a general inhibitor of differentiation and is negatively regulated by activation of the Ras1/MAPK pathway. *Cell* **81**, 857–866.
- Regot, S., Hughey, J. J., Bajar, B. T., Carrasco, S. and Covert, M. W.** (2014a). High-Sensitivity Measurements of Multiple Kinase Activities in Live Single Cells. *Cell* **157**, 1724–1734.

- Regot, S., Hughey, J. J., Bajar, B. T., Carrasco, S. and Covert, M. W.** (2014b). High-Sensitivity Measurements of Multiple Kinase Activities in Live Single Cells. *Cell* **157**, 1724–1734.
- Robin, F. B., Dauga, D., Tassy, O., Sobral, D., Daian, F. and Lemaire, P.** (2011a). Imaging of Fixed Ciona Embryos for Creating 3D Digital Replicas. *Cold Spring Harb. Protoc.* **2011**, pdb.prot065854-pdb.prot065854.
- Robin, F. B., Dauga, D., Tassy, O., Sobral, D., Daian, F. and Lemaire, P.** (2011b). Creating 3D Digital Replicas of Ascidian Embryos from Stacks of Confocal Images. *Cold Spring Harb. Protoc.* **2011**, pdb.prot065862-pdb.prot065862.
- Roelink, H., Porter, J. A., Chiang, C., Tanabe, Y., Chang, D. T., Beachy, P. A. and Jessell, T. M.** (1995). Floor plate and motor neuron induction by different concentrations of the amino-terminal cleavage product of sonic hedgehog autoproteolysis. *Cell* **81**, 445–455.
- Rossi, F. M. V., Guicherit, O. M., Spicher, A., Kringstein, A. M., Fatyol, K., Blakely, B. T. and Blau, H. M.** (1998). Tetracycline-regulatable factors with distinct dimerization domains allow reversible growth inhibition by p16. *Nat. Genet.* **20**, 389–393.
- Rossi, F. M. V., Kringstein, A. M., Spicher, A., Guicherit, O. M. and Blau, H. M.** (2000). Transcriptional Control: Rheostat Converted to On/Off Switch. *Mol. Cell* **6**.
- Rothbacher, U., Bertrand, V., Lamy, C. and Lemaire, P.** (2007a). A combinatorial code of maternal GATA, Ets and -catenin-TCF transcription factors specifies and patterns the early ascidian ectoderm. *Development* **134**, 4023–4032.
- Rothbacher, U., Bertrand, V., Lamy, C. and Lemaire, P.** (2007b). A combinatorial code of maternal GATA, Ets and -catenin-TCF transcription factors specifies and patterns the early ascidian ectoderm. *Development* **134**, 4023–4032.
- Rothbacher, U., Bertrand, V., Lamy, C. and Lemaire, P.** (2007). A combinatorial code of maternal GATA, Ets and beta-catenin-TCF transcription factors specifies and patterns the early ascidian ectoderm. *Dev. Camb. Engl.* **134**, 4023–4032.
- Roure, A. and Darras, S.** (2016). Msxb is a core component of the genetic circuitry specifying the dorsal and ventral neurogenic midlines in the ascidian embryo. *Dev. Biol.* **409**, 277–287.
- Roure, A., Rothbacher, U., Robin, F., Kalmar, E., Ferone, G., Lamy, C., Missero, C., Mueller, F. and Lemaire, P.** (2007). A Multicassette Gateway Vector Set for High Throughput and Comparative Analyses in Ciona and Vertebrate Embryos. *PLOS ONE* **2**, e916.
- Roure, A., Lemaire, P. and Darras, S.** (2014). An *Otx/Nodal* Regulatory Signature for Posterior Neural Development in Ascidians. *PLoS Genet.* **10**, e1004548.
- Rueden, C. T., Schindelin, J., Hiner, M. C., DeZonia, B. E., Walter, A. E., Arena, E. T. and Eliceiri, K. W.** (2017). ImageJ2: ImageJ for the next generation of scientific image data. *BMC Bioinformatics* **18**, 529.
- Ruiz i Altaba, A.** (1999). Gli proteins encode context-dependent positive and negative functions: implications for development and disease. *Dev. Camb. Engl.* **126**, 3205–3216.
- Ryan, K., Lu, Z. and Meinertzhagen, I. A.** (2016). The CNS connectome of a tadpole larva of *Ciona intestinalis* (L.) highlights sidedness in the brain of a chordate sibling. *eLife* **5**.

- Ryu, H., Chung, M., Dobrzyński, M., Fey, D., Blum, Y., Lee, S. S., Peter, M., Kholodenko, B. N., Jeon, N. L. and Pertz, O.** (2015). Frequency modulation of ERK activation dynamics rewires cell fate. *Mol. Syst. Biol.* **11**, 838.
- Santos, S. D. M., Verveer, P. J. and Bastiaens, P. I. H.** (2007a). Growth factor-induced MAPK network topology shapes Erk response determining PC-12 cell fate. *Nat. Cell Biol.* **9**, 324–330.
- Santos, S. D. M., Verveer, P. J. and Bastiaens, P. I. H.** (2007b). Growth factor-induced MAPK network topology shapes Erk response determining PC-12 cell fate. *Nat. Cell Biol.* **9**, 324–330.
- Sardet, C., McDougall, A., Yasuo, H., Chenevert, J., Pruliere, G., Dumollard, R., Hudson, C., Hebras, C., Le Nguyen, N. and Paix, A.** (2011a). Embryological methods in ascidians: the Villefranche-sur-Mer protocols. *Methods Mol. Biol. Clifton NJ* **770**, 365–400.
- Sardet, C., McDougall, A., Yasuo, H., Chenevert, J., Pruliere, G., Dumollard, R., Hudson, C., Hebras, C., Le Nguyen, N. and Paix, A.** (2011b). Embryological methods in ascidians: the Villefranche-sur-Mer protocols. *Methods Mol. Biol. Clifton NJ* **770**, 365–400.
- Sasaki, H., Hui, C., Nakafuku, M. and Kondoh, H.** (1997). A binding site for Gli proteins is essential for HNF-3beta floor plate enhancer activity in transgenics and can respond to Shh in vitro. *Dev. Camb. Engl.* **124**, 1313–1322.
- Sasaki, H., Nishizaki, Y., Hui, C., Nakafuku, M. and Kondoh, H.** (1999). Regulation of Gli2 and Gli3 activities by an amino-terminal repression domain: implication of Gli2 and Gli3 as primary mediators of Shh signaling. *Development* **126**, 3915–3924.
- Satoh, N.** (2014). *Developmental Genomics of Ascidians*.
- Satou, Y., Imai, K. and Satoh, N.** (2002). Fgf genes in the basal chordate *Ciona intestinalis*. *Dev. Genes Evol.* **212**, 432–438.
- Satou, Y., Sasakura, Y., Yamada, L., Imai, K. S., Satoh, N. and Degnan, B.** (2003a). A genomewide survey of developmentally relevant genes in *Ciona intestinalis*: V. Genes for receptor tyrosine kinase pathway and Notch signaling pathway. *Dev. Genes Evol.* **213**, 254–263.
- Satou, Y., Sasakura, Y., Yamada, L., Imai, K. S., Satoh, N. and Degnan, B.** (2003b). A genomewide survey of developmentally relevant genes in *Ciona intestinalis*: V. Genes for receptor tyrosine kinase pathway and Notch signaling pathway. *Dev. Genes Evol.* **213**, 254–263.
- Satou, Y., Kawashima, T., Shoguchi, E., Nakayama, A. and Satoh, N.** (2005). An integrated database of the ascidian, *Ciona intestinalis*: towards functional genomics. *Zoolog. Sci.* **22**, 837–843.
- Schindelin, J., Arganda-Carreras, I., Frise, E., Kaynig, V., Longair, M., Pietzsch, T., Preibisch, S., Rueden, C., Saalfeld, S., Schmid, B., et al.** (2012). Fiji: an open-source platform for biological-image analysis. *Nat. Methods* **9**, 676–682.
- Schlessinger, J.** (2014). Receptor Tyrosine Kinases: Legacy of the First Two Decades. *Cold Spring Harb. Perspect. Biol.* **6**, a008912–a008912.
- Schmid, T. and Hajnal, A.** (2015). Signal transduction during *C. elegans* vulval development: a NeverEnding story. *Curr. Opin. Genet. Dev.* **32**, 1–9.

- Schröder, C., Tautz, D., Seifert, E. and Jäckle, H.** (1988). Differential regulation of the two transcripts from the *Drosophila* gap segmentation gene *hunchback*. *EMBO J.* **7**, 2881–2887.
- Seiradake, E., Harlos, K., Sutton, G., Aricescu, A. R. and Jones, E. Y.** (2010). An extracellular steric seeding mechanism for Eph-ephrin signaling platform assembly. *Nat. Struct. Mol. Biol.* **17**, 398–402.
- Sgouras, D. N., Athanasiou, M. A., Beal, G. J., Fisher, R. J., Blair, D. G. and Mavrothalassitis, G. J.** (1995). ERF: an ETS domain protein with strong transcriptional repressor activity, can suppress ets-associated tumorigenesis and is regulated by phosphorylation during cell cycle and mitogenic stimulation. *EMBO J.* **14**, 4781–4793.
- Shah, N. A. and Sarkar, C. A.** (2011). Robust Network Topologies for Generating Switch-Like Cellular Responses. *PLoS Comput. Biol.* **7**, e1002085.
- Shankaran, H., Ippolito, D. L., Chrisler, W. B., Resat, H., Bollinger, N., Opresko, L. K. and Wiley, H. S.** (2009). Rapid and sustained nuclear–cytoplasmic ERK oscillations induced by epidermal growth factor. *Mol. Syst. Biol.* **5**, 332.
- Sharrocks, A. D.** (2001). The ETS-domain transcription factor family. *Nat. Rev. Mol. Cell Biol.* **2**, 827–837.
- Shi, W. and Levine, M.** (2008). Ephrin signaling establishes asymmetric cell fates in an endomesoderm lineage of the *Ciona* embryo. *Dev. Camb. Engl.* **135**, 931–940.
- Shi, X., Hapiak, V., Zheng, J., Muller-Greven, J., Bowman, D., Lingerak, R., Buck, M., Wang, B.-C. and Smith, A. W.** (2017). A role of the SAM domain in EphA2 receptor activation. *Sci. Rep.* **7**,.
- Shilo, B.-Z.** (2005). Regulating the dynamics of EGF receptor signaling in space and time. *Development* **132**, 4017–4027.
- Shimokawa, K., Kimura-Yoshida, C., Nagai, N., Mukai, K., Matsubara, K., Watanabe, H., Matsuda, Y., Mochida, K. and Matsuo, I.** (2011). Cell Surface Heparan Sulfate Chains Regulate Local Reception of FGF Signaling in the Mouse Embryo. *Dev. Cell* **21**, 257–272.
- Shindo, Y., Iwamoto, K., Mouri, K., Hibino, K., Tomita, M., Kosako, H., Sako, Y. and Takahashi, K.** (2016). Conversion of graded phosphorylation into switch-like nuclear translocation via autoregulatory mechanisms in ERK signalling. *Nat. Commun.* **7**, 10485.
- Sigismund, S., Woelk, T., Puri, C., Maspero, E., Tacchetti, C., Transidico, P., Di Fiore, P. P. and Polo, S.** (2005). Clathrin-independent endocytosis of ubiquitinated cargos. *Proc. Natl. Acad. Sci. U. S. A.* **102**, 2760–2765.
- Sigismund, S., Argenzio, E., Tosoni, D., Cavallaro, E., Polo, S. and Di Fiore, P. P.** (2008). Clathrin-mediated internalization is essential for sustained EGFR signaling but dispensable for degradation. *Dev. Cell* **15**, 209–219.
- Simske, J. S. and Kirn, S. K.** (1995). Sequential signalling during *Caenorhabditis elegans* vulval induction. *Nature* **375**, 142–146.
- Sternberg, P. W.** (2005). Vulval development. *WormBook*.

- Sternberg, P. W. and Horvitz, H. R.** (1986). Pattern formation during vulval development in *C. elegans*. *Cell* **44**, 761–772.
- Sternberg, P. W. and Horvitz, H. R.** (1989). The combined action of two intercellular signaling pathways specifies three cell fates during vulval induction in *C. elegans*. *Cell* **58**, 679–693.
- Stetak, A., Hoier, E. F., Croce, A., Cassata, G., Di Fiore, P. P. and Hajnal, A.** (2006a). Cell fate-specific regulation of EGF receptor trafficking during *Caenorhabditis elegans* vulval development. *EMBO J.* **25**, 2347–2357.
- Stetak, A., Hoier, E. F., Croce, A., Cassata, G., Di Fiore, P. P. and Hajnal, A.** (2006b). Cell fate-specific regulation of EGF receptor trafficking during *Caenorhabditis elegans* vulval development. *EMBO J.* **25**, 2347–2357.
- Stolfi, A., Wagner, E., Taliaferro, J. M., Chou, S. and Levine, M.** (2011a). Neural tube patterning by Ephrin, FGF and Notch signaling relays. *Dev. Camb. Engl.* **138**, 5429–5439.
- Stolfi, A., Wagner, E., Taliaferro, J. M., Chou, S. and Levine, M.** (2011b). Neural tube patterning by Ephrin, FGF and Notch signaling relays. *Dev. Camb. Engl.* **138**, 5429–5439.
- Struhl, G., Struhl, K. and Macdonald, P. M.** (1989). The gradient morphogen bicoid is a concentration-dependent transcriptional activator. *Cell* **57**, 1259–1273.
- Sturm, O. E., Orton, R., Grindlay, J., Birtwistle, M., Vyshemirsky, V., Gilbert, D., Calder, M., Pitt, A., Kholodenko, B. and Kolch, W.** (2010). The Mammalian MAPK/ERK Pathway Exhibits Properties of a Negative Feedback Amplifier. *Sci. Signal.* **3**, ra90–ra90.
- Sun, P., Watanabe, H., Takano, K., Yokoyama, T., Fujisawa, J. and Endo, T.** (2006). Sustained activation of M-Ras induced by nerve growth factor is essential for neuronal differentiation of PC12 cells. *Genes Cells Devoted Mol. Cell. Mech.* **11**, 1097–1113.
- Swanson, C. I., Schwimmer, D. B. and Barolo, S.** (2011). Rapid evolutionary rewiring of a structurally constrained eye enhancer. *Curr. Biol. CB* **21**, 1186–1196.
- Tan, P. B., Lackner, M. R. and Kim, S. K.** (1998). MAP Kinase Signaling Specificity Mediated by the LIN-1 Ets/LIN-31 WH Transcription Factor Complex during *C. elegans* Vulval Induction. *Cell* **93**, 569–580.
- Tassy, O., Daian, F., Hudson, C., Bertrand, V. and Lemaire, P.** (2006a). A Quantitative Approach to the Study of Cell Shapes and Interactions during Early Chordate Embryogenesis. *Curr. Biol.* **16**, 345–358.
- Tassy, O., Daian, F., Hudson, C., Bertrand, V. and Lemaire, P.** (2006b). A quantitative approach to the study of cell shapes and interactions during early chordate embryogenesis. *Curr. Biol. CB* **16**, 345–358.
- Tassy, O., Dauga, D., Daian, F., Sobral, D., Robin, F., Khoueiry, P., Salgado, D., Fox, V., Caillol, D., Schiappa, R., et al.** (2010). The ANISEED database: digital representation, formalization, and elucidation of a chordate developmental program. *Genome Res.* **20**, 1459–1468.
- Tautz, D.** (1988). Regulation of the *Drosophila* segmentation gene hunchback by two maternal morphogenetic centres. *Nature* **332**, 281–284.

- Tautz, D., Lehmann, R., Schnürch, H., Schuh, R., Seifert, E., Kienlin, A., Jones, K. and Jäckle, H.** (1987). Finger protein of novel structure encoded by hunchback, a second member of the gap class of *Drosophila* segmentation genes. *Nature* **327**, 383–389.
- Teis, D., Taub, N., Kurzbauer, R., Hilber, D., de Araujo, M. E., Erlacher, M., Offterdinger, M., Villunger, A., Geley, S., Bohn, G., et al.** (2006). p14-MP1-MEK1 signaling regulates endosomal traffic and cellular proliferation during tissue homeostasis. *J. Cell Biol.* **175**, 861–868.
- To, T.-L. and Maheshri, N.** (2010). Noise can induce bimodality in positive transcriptional feedback loops without bistability. *Science* **327**, 1142–1145.
- Toettcher, J. E., Weiner, O. D. and Lim, W. A.** (2013). Using Optogenetics to Interrogate the Dynamic Control of Signal Transmission by the Ras/Erk Module. *Cell* **155**, 1422–1434.
- Tokuhiro, S., Tokuoka, M., Kobayashi, K., Kubo, A., Oda-Ishii, I. and Satou, Y.** (2017). Differential gene expression along the animal-vegetal axis in the ascidian embryo is maintained by a dual functional protein Foxd. *PLoS Genet.* **13**, e1006741.
- Traverse, S., Seedorf, K., Paterson, H., Marshall, C. J., Cohen, P. and Ullrich, A.** (1994). EGF triggers neuronal differentiation of PC12 cells that overexpress the EGF receptor. *Curr. Biol.* **4**, 694–701.
- Turing, A. M.** (1952). The Chemical Basis of Morphogenesis. *Philos. Trans. R. Soc. Lond. B. Biol. Sci.* **237**, 37–72.
- Turner, N. and Grose, R.** (2010). Fibroblast growth factor signalling: from development to cancer. *Nat. Rev. Cancer* **10**, 116–129.
- Ullrich, A. and Schlessinger, J.** (1990). Signal transduction by receptors with tyrosine kinase activity. *Cell* **61**, 203–212.
- van Boxtel, A. L., Economou, A. D., Heliot, C. and Hill, C. S.** (2018). Long-Range Signaling Activation and Local Inhibition Separate the Mesoderm and Endoderm Lineages. *Dev. Cell* **44**, 179–191.e5.
- Venero Galanternik, M., Kramer, K. L. and Piotrowski, T.** (2015). Heparan Sulfate Proteoglycans Regulate Fgf Signaling and Cell Polarity during Collective Cell Migration. *Cell Rep.* **10**, 414–428.
- Venuti, J. M. and Jeffery, W. R.** (1989). Cell lineage and determination of cell fate in ascidian embryos. 16.
- Vercauteren, D., Vandenbroucke, R. E., Jones, A. T., Rejman, J., Demeester, J., De Smedt, S. C., Sanders, N. N. and Braeckmans, K.** (2010). The Use of Inhibitors to Study Endocytic Pathways of Gene Carriers: Optimization and Pitfalls. *Mol. Ther.* **18**, 561–569.
- Vihanto, M. M.** (2006a). Caveolin-1 is required for signaling and membrane targeting of EphB1 receptor tyrosine kinase. *J. Cell Sci.* **119**, 2299–2309.
- Vihanto, M. M.** (2006b). Caveolin-1 is required for signaling and membrane targeting of EphB1 receptor tyrosine kinase. *J. Cell Sci.* **119**, 2299–2309.

- Wada, H., Saiga, H., Satoh, N. and Holland, P. W. H.** (1998). Tripartite organization of the ancestral chordate brain and the antiquity of placodes: insights from ascidian Pax-2/5/8, Hox and Otx genes. *10*.
- Wagner, E. and Levine, M.** (2012). FGF signaling establishes the anterior border of the *Ciona* neural tube. *Development* **139**, 2351–2359.
- Wang, L.-H., Rothberg, K. G. and Anderson, R. G.** (1993). Mis-assembly of clathrin lattices on endosomes reveals a regulatory switch for coated pit formation. *J. Cell Biol.* **123**, 1107–1117.
- Whitehurst, A., Cobb, M. H. and White, M. A.** (2004). Stimulus-Coupled Spatial Restriction of Extracellular Signal-Regulated Kinase 1/2 Activity Contributes to the Specificity of Signal-Response Pathways. *Mol. Cell. Biol.* **24**, 10145–10150.
- Wilson, M. Z., Ravindran, P. T., Lim, W. A. and Toettcher, J. E.** (2017). Tracing Information Flow from Erk to Target Gene Induction Reveals Mechanisms of Dynamic and Combinatorial Control. *Mol. Cell* **67**, 757-769.e5.
- Wimmer-Kleikamp, S. H., Janes, P. W., Squire, A., Bastiaens, P. I. H. and Lackmann, M.** (2004). Recruitment of Eph receptors into signaling clusters does not require ephrin contact. *J. Cell Biol.* **164**, 661–666.
- WIREs Authors** (2017). Same Signal, Different Tissues: Morphogen Interpretation. *Adv. Sci. News*.
- Wolpert, L.** (1969). Positional information and the spatial pattern of cellular differentiation. *J. Theor. Biol.* **25**, 1–47.
- Wong, K.-L., Akiyama, R., Bessho, Y. and Matsui, T.** (2018). ERK Activity Dynamics during Zebrafish Embryonic Development. *Int. J. Mol. Sci.* **20**, 109.
- Xiong, F., Tentner, A. R., Huang, P., Gelas, A., Mosaliganti, K. R., Souhait, L., Rannou, N., Swinburne, I. A., Obholzer, N. D., Cowgill, P. D., et al.** (2013). Specified Neural Progenitors Sort to Form Sharp Domains after Noisy Shh Signaling. *Cell* **153**, 550–561.
- Yamamoto, T., Ebisuya, M., Ashida, F., Okamoto, K., Yonehara, S. and Nishida, E.** (2006). Continuous ERK activation downregulates antiproliferative genes throughout G1 phase to allow cell-cycle progression. *Curr. Biol. CB* **16**, 1171–1182.
- Yang, B. S., Hauser, C. A., Henkel, G., Colman, M. S., Van Beveren, C., Stacey, K. J., Hume, D. A., Maki, R. A. and Ostrowski, M. C.** (1996). Ras-mediated phosphorylation of a conserved threonine residue enhances the transactivation activities of c-Ets1 and c-Ets2. *Mol. Cell. Biol.* **16**, 538–547.
- Yasuo, H. and Hudson, C.** (2007). FGF8/17/18 functions together with FGF9/16/20 during formation of the notochord in *Ciona* embryos. *Dev. Biol.* **302**, 92–103.
- Yasuo, H. and McDougall, A.** (2018a). Practical Guide for Ascidian Microinjection: *Phallusia mammillata*. In *Transgenic Ascidians* (ed. Sasakura, Y.), pp. 15–24. Singapore: Springer Singapore.
- Yasuo, H. and McDougall, A.** (2018b). Practical Guide for Ascidian Microinjection: *Phallusia mammillata*. In *Transgenic Ascidians* (ed. Sasakura, Y.), pp. 15–24. Singapore: Springer.

- Yoo, A. S.** (2004a). Crosstalk Between the EGFR and LIN-12/Notch Pathways in *C. elegans* Vulval Development. *Science* **303**, 663–666.
- Yoo, A. S.** (2004b). Crosstalk Between the EGFR and LIN-12/Notch Pathways in *C. elegans* Vulval Development. *Science* **303**, 663–666.
- Yoo, A. S., Bais, C. and Greenwald, I.** (2004). Crosstalk Between the EGFR and LIN-12/Notch Pathways in *C. elegans* Vulval Development. *Science* **303**, 663–666.
- Yu, S. R., Burkhardt, M., Nowak, M., Ries, J., Petrášek, Z., Scholpp, S., Schwille, P. and Brand, M.** (2009). Fgf8 morphogen gradient forms by a source-sink mechanism with freely diffusing molecules. *Nature* **461**, 533–536.
- Zhang, Q., Huang, H., Zhang, L., Wu, R., Chung, C.-I., Zhang, S.-Q., Torra, J., Schepis, A., Coughlin, S. R., Kornberg, T. B., et al.** (2018). Visualizing Dynamics of Cell Signaling In Vivo with a Phase Separation-Based Kinase Reporter. *Mol. Cell* **69**, 334-346.e4.
- Zhu, A. J. and Scott, M. P.** (2004). Incredible journey: how do developmental signals travel through tissue? *Genes Dev.* **18**, 2985–2997.

Experimental condition	a6.5>a6.7	a6.7>a6.6	a6.6>a6.8	N= (half embryos)
Cell surface contacts (pool of 4 independent experiments). Fig. 1B	100%	90.5%	100%	42
Exp. 1 Control dpERK. Fig. 2B	99%	94%	83%	100
Exp. 2 Control dpERK. Fig.S1A	100%	78%	91%	100
Exp. 3 Control dpERK. Fig. S1C	99%	94%	81%	84
Exp. 1 NVP dpERK. Fig. 1C	99%	100%	82%	102
Exp. 2 NVP dpERK. Fig. S1B	99%	96%	93%	100
Exp. 3 NVP dpERK. Fig. S1D	90%	99%	91%	100
ERK-KTR 6 mins. Fig. 4B	100%	80%	50%	10

**Table 1.** Percentage of cases, per half embryo, where cell surface contacts with the A-line mesendoderm cells or ERK activation levels between the given two a-line ectoderm cells are as indicated (example a6.5>a6.7).

**Figure 1. Cell-specific areas of cell surface contacts between ectoderm and mesendoderm cells.** A) Left, a drawing of an animal pole view of a 32-cell stage *Ciona* embryo with the 16-animal cells highlighted with a red dotted line. The a-line cells are coloured in this and all subsequent figures with a6.5 in magenta, a6.6 in green, a6.7 in blue and a6.8 in grey. Second panel, confocal section of 32-cell stage *Ciona* embryo injected with *PH-GFP* mRNA and stained with anti-GFP immunofluorescence (IF). Embryo is in the same orientation as the drawing (left). a6.5 is indicated. Third panel, 32-cell stage embryo reconstructed with Amira software. Mesendoderm cells are coloured in aqua, b-line ectoderm cells are white and a-line ectoderm cells are coloured with the same colour code as above. Right, same embryo rendered transparent with Amira software, the left a6.5 cell is coloured with its cell surface contacts highlighted in aqua. B) Relative area of cell surface contact to A-line mesendoderm cells (surface contact A-line/total cell surface) for each a-line ectoderm cell in 21 reconstructed embryos. Each dot represents a single cell. Different shapes and shades represent independent experiments: experiment 1- four points (■) per cell-type; Experiment 2- four points (●) per cell-type; Experiment 3- ten points (▲) per cell-type, plus technical replicate in second tube (▼), fourteen points per cell-type; and Experiment 4- ten points (◆) per cell-type. Statistical tests are two tailed unpaired t-tests comparing each cell-type (pooled) based on the hierarchical order of their area of cell surface contact, i.e. comparing a6.5 to a6.7, a6.7 to a6.6, and a6.6 to a6.8. \*\*\*\*= $P < 0.0001$ . C) Relative area of cell surface contact to A-line cells mesendoderm (vegetal) cells versus relative area of cell surface contact with neighbouring ectoderm (animal) cells for all a-line cells. Pearson correlation results are shown.

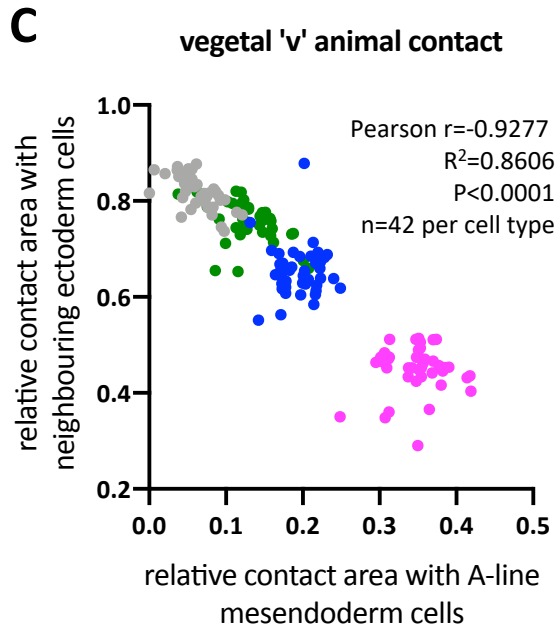
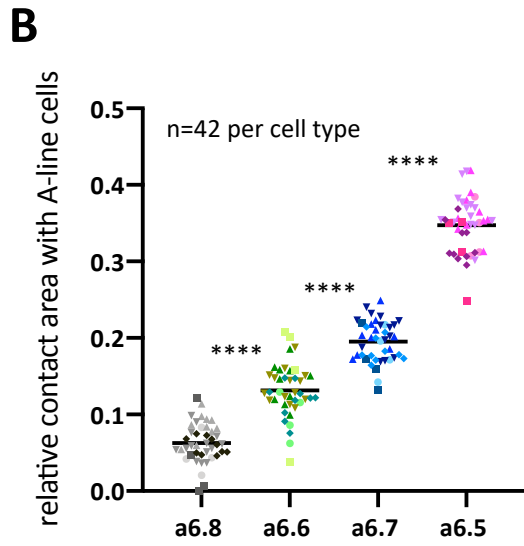
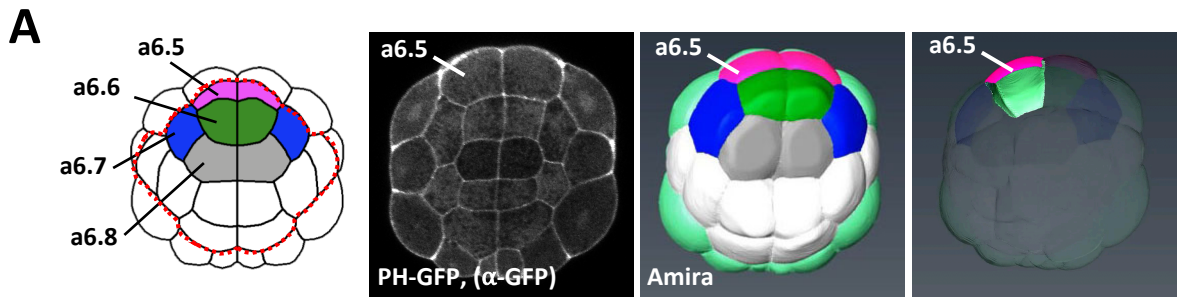


Figure 1

**Figure 2. Quantitative measurement of nuclear dpERK IF signals in ectoderm cells reveals a correlation with cell surface contact to A-line cells.** Data from different cell types are coloured as follows: a6.5 in magenta, a6.6 in green, a6.7 in blue and a6.8 in grey. A) First panel: Snapshot of Imaris 3D visualisation of confocal microscope stack of dpERK IF confocal scan of a 32-cell stage embryo. Second panel: Snapshot of Imaris 3D visualisation of confocal microscope stack of Histone H3 IF confocal scan of the same 32-cell stage embryo. Third panel: a-line nuclei are segmented based on H3 IF signal for determining nuclear dpERK average nuclear pixel intensity for each cell-type (coloured). B-E) Each dot on the graphs represent a single cell. B) Mean pixel intensity of nuclear dpERK IF signal for each cell for large data set of 50 embryos processed under identical conditions. C) Mean pixel intensity of nuclear dpERK IF signal for each cell for large data set of 51 NVP-treated embryos processed under identical conditions. The confocal laser was adjusted between control and NVP embryos to allow maximum range around the different sample intensities. B-C) Statistical tests are two tailed unpaired t-tests comparing each cell-type based on the hierarchal order of their nuclear dpERK signal, i.e. comparing a6.5 to a6.7, a6.7 to a6.6, and a6.6 to a6.8. \*\*\*\* $P < 0.0001$ , \*\*\* $P < 0.001$ , \*\* $P < 0.01$ , \* $P < 0.05$ , ns  $P \geq 0.05$ . Similar results from two additional independent experiments can be found in Figure S1A-D. D) Normalised (surface contact/total surface) area of cell surface contact with A-line (mesendoderm) cells and mean pixel intensity of nuclear dpERK IF signal was measured for each a-line cell in control embryos. Plot shows Spearman correlation of  $r = 0.7564$ . E) Normalised (surface contact/total surface) area of cell surface contact with A-line (mesendoderm) cells and mean pixel intensity of nuclear dpERK IF signal was measured for each a-line cell in NVP-treated embryos. Confocal laser was adjusted between control and NVP-treated samples. Plot shows Spearman correlation of  $r = 0.7881$ . Additional independent experiments can be found in Supplementary Figure 3.

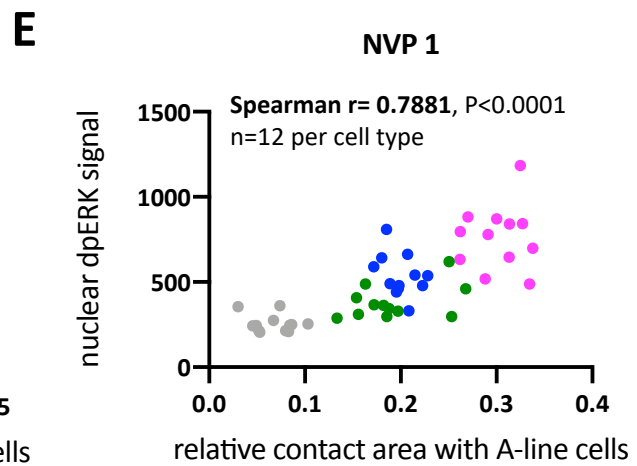
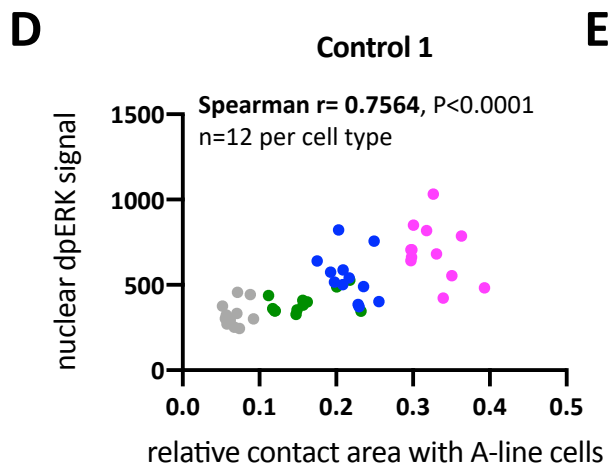
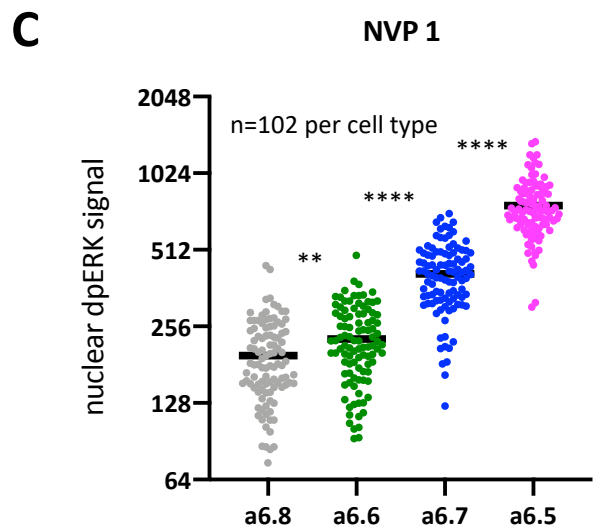
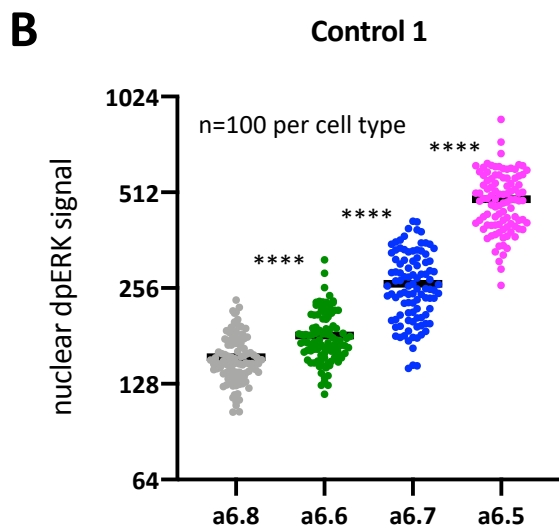
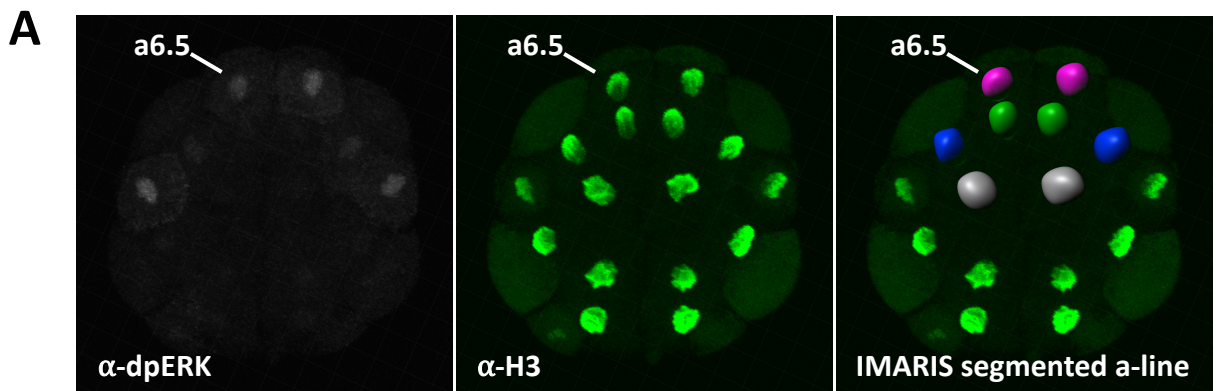


Figure 2

**Figure 3. ERK activation in FGF- or Eph-inhibited embryos.** Data from different cell types are coloured as follows: a6.5 in magenta, a6.6 in green, a6.7 in blue and a6.8 in grey. A) Left, schematic showing injection of *dnEph3* mRNA and FITC-dextran in one a4.2 cell of the 8-cell stage embryo. Relative cell surface contact with A-line cells was measured for each a-line cell on the control (C, ●) and injected (inj, ▲) half of the embryo. Ectopic activation of ERK in a6.7 on the injected side of all 9 embryos confirmed the efficiency of the injected *dnEph3* mRNA. Anti-dpERK IF was conducted using tyramide-based signal amplification in this experiment (Haupaix et al., 2013a) and embryos were reconstructed by manual segmentation following phalloidin staining. Image shows a maximum projection stack of selected z-slice images of phalloidin staining and anti-dpERK IF. The injected cells, identified by dextran (not shown) are circled with a green dashed line. Statistical tests are paired t-tests comparing each cell-type between control and injected sides. ns  $P \geq 0.05$ . B) Left, schematic showing injection of mRNA and FITC-dextran in one cell of the two-cell stage. Mean pixel intensity of nuclear dpERK IF signal was measured for each cell and a ratio was obtained as injected/control for each cell-type from the same embryo. The graph shows the ratios for embryos injected with mRNAs for *PH-GFP*, *dnFGFR*, *dnEph3* and *dnp120RasGAP*. Ratios larger than 1 indicate that the dpERK signal was stronger on the injected side, ratios smaller than 1 indicate that the dpERK signal was weaker on the injected side. The numbers in parentheses on the left indicate the number of ratios analysed for each cell-type. Statistical tests are one sample t-tests with a theoretical mean of 1. \*\*\*\* $P < 0.0001$ , \*\*\* $P < 0.001$ , \*\* $P < 0.01$ , \* $P < 0.05$ , ns  $P \geq 0.05$ .



**Figure 4. Quantitative measurement of ERK activity in ectoderm cells using ERK-KTR biosensor.** Data from different cell types are coloured as follows: a6.5 in magenta, a6.6 in green, a6.7 in blue and a6.8 in grey. *Phallusia mammillata* embryos were injected with *ERK-KTR-mClover* mRNA and *NLS-tdTomato* mRNA. Time-lapse movies were normalised to t=0 at the point of A6.4 nuclear envelope breakdown (NEBD). t= 4-8 corresponds to 'late 32-cell stage', when vegetal cells undergo de-compaction and embryos become flattened in shape. A) Stills from a time-lapse of a 32-cell stage *P. mammillata* embryo. In the last panel, the a-line cells are highlighted with a red dotted line and the position of each nucleus indicated on the drawing, right. In this particular time lapse imaging, the embryo was slightly squashed to the coverslip on the ectoderm side so that the nuclei of all a-line ectoderm cells were captured within same confocal z-sections. B) ERK-KTR cytoplasmic/nuclear (C/N) ratio for each cell type at t= 6'. Each dot on the graphs represents a single cell. Statistical tests are paired t-tests comparing each cell-type based on the hierarchal order of their ERK-KTR signal, i.e. comparing a6.5 to a6.7, a6.7 to a6.6, and a6.6 to a6.8. \* P=>0.01 to <0.05; \*\*\*\* P<0.0001; ns, P≥0.05 no significant difference. C) ERK-KTR cytoplasmic/nuclear (C/N) ratio for a-line ectoderm cells during the 32-cell stage in control and *dnFGFR* injected halves (n=3 embryos). On the *dnFGFR* graph, the a6.8 trace of the control side is included (black) to show that it groups with FGF-inhibited cells. D) Time course of ERK activity in a-line ectoderm cells during the 32-cell stage. C/N ratios of a6.5, a6.6 and a6.7 were normalised to the same side a6.8 C/N ratio. a6.8 measurements, which are normalised as 1 for each embryo half, are indicated on the graphs as a dotted grey line. Below is the same data-set expressed as a heatmap, showing stronger signal in a6.5 throughout the time of recording. Additional embryos were recorded from the early 32-cell stage and can be found in Supplementary Figure 2B.

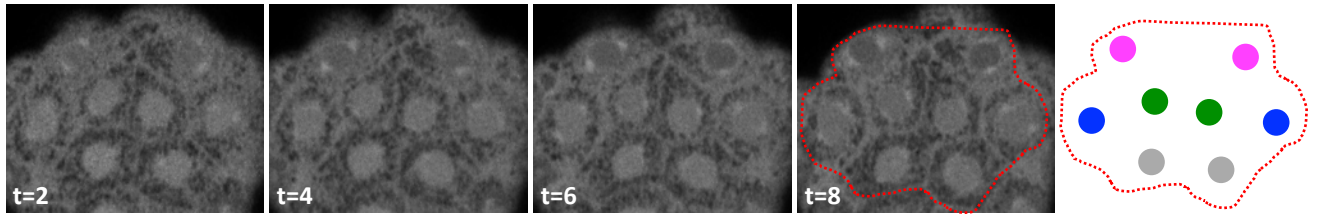
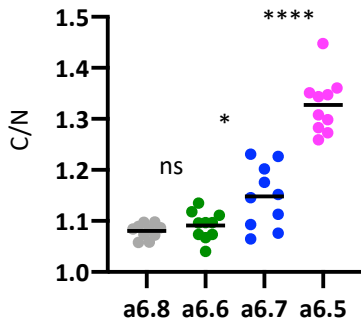
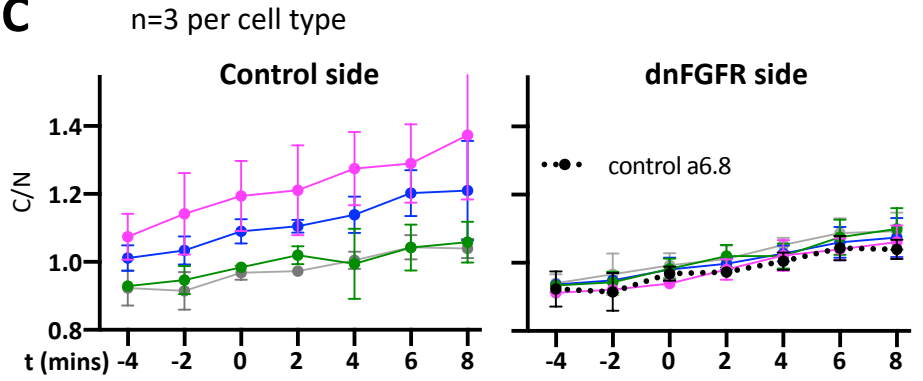
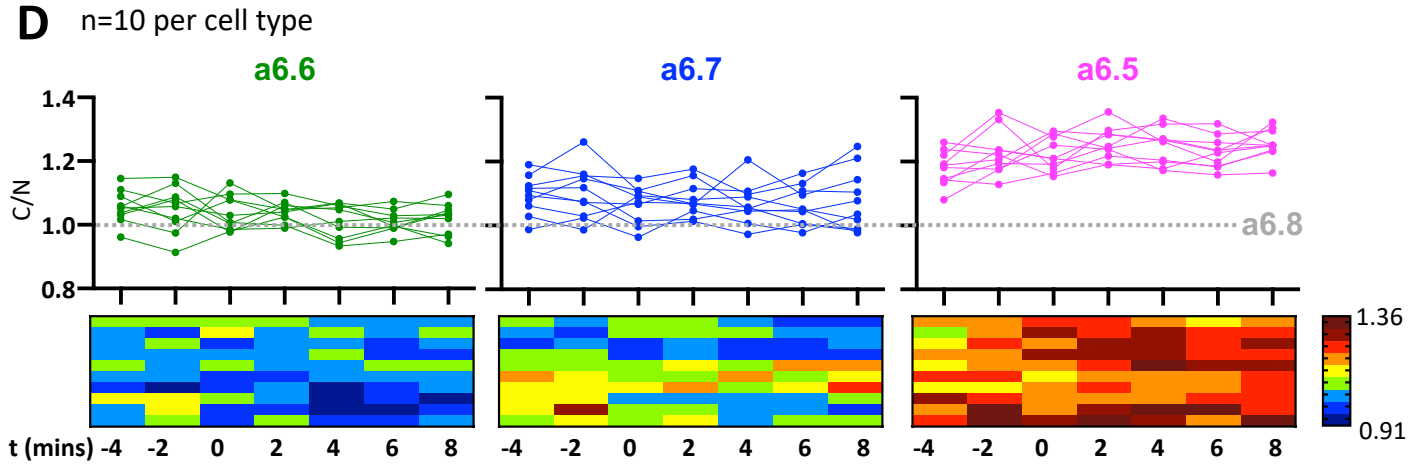
**A****B****C****D**

Figure 4

**Figure 5. Ex vivo analysis of ERK activation in response to exogenous FGF.** A) Schematic outline of experimental procedure. Embryos were bisected along the animal-vegetal axis at the 8-cell stage of development to isolate ectoderm explants. Explants were treated with or without NVP from the late 16-cell stage and from the early 32-cell stage with different doses of bFGF. Ectodermal explants were collected at the late 32-cell stage for western blot or IF analysis. B) Quantification of western blots showing the temporal response of ERK activation in ectodermal explants treated with two doses of bFGF. Additional examples can be found in Supplementary Figure 6A-C. C) Quantification (mean  $\pm$  SD) of 12 pairs of western blots showing the dose response of ERK activation in control and NVP-treated explants treated with exogenous FGF.  $n_H$  is the Hill coefficient from the best-fit non-linear regression of this data. Confidence intervals are indicated in the main text. Individual plots for each western blot can be found in Supplementary Figure 6D. B-C) For the western blot analysis, dpERK signals were normalised for aPKC levels as loading control and against a control “standard” whole embryo dpERK/aPKC ratio loaded onto every gel (see materials and methods for details). D) Single cell analysis of ERK activation in ectodermal explants treated with increasing doses of bFGF. Each dot represents the mean pixel intensity of the nuclear dpERK IF signal of a single cell. Untreated whole embryos dispersed between the tubes are shown on the right (a6.5 in magenta, a6.6 in green, a6.7 in blue and a6.8 in grey). n=number of cells analysed in explants per dose of FGF. Mean nuclear dpERK IF signals are indicated by orange bars. Results of two addition experiments can be found in Supplementary Figure 7A.

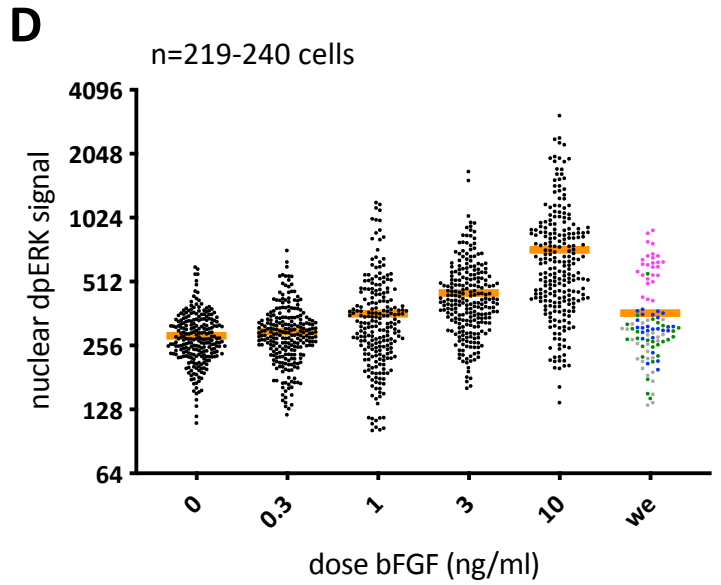
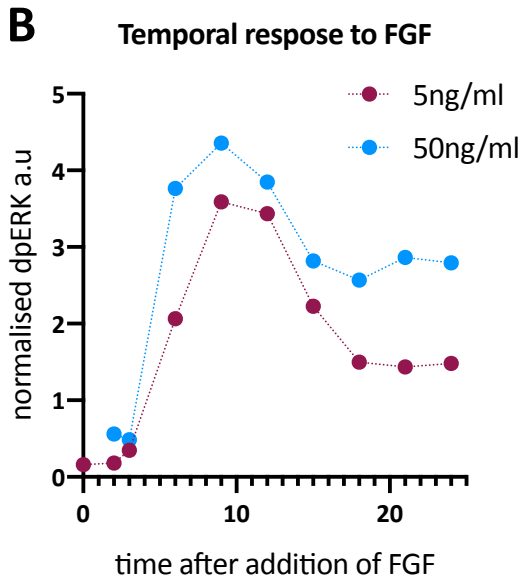
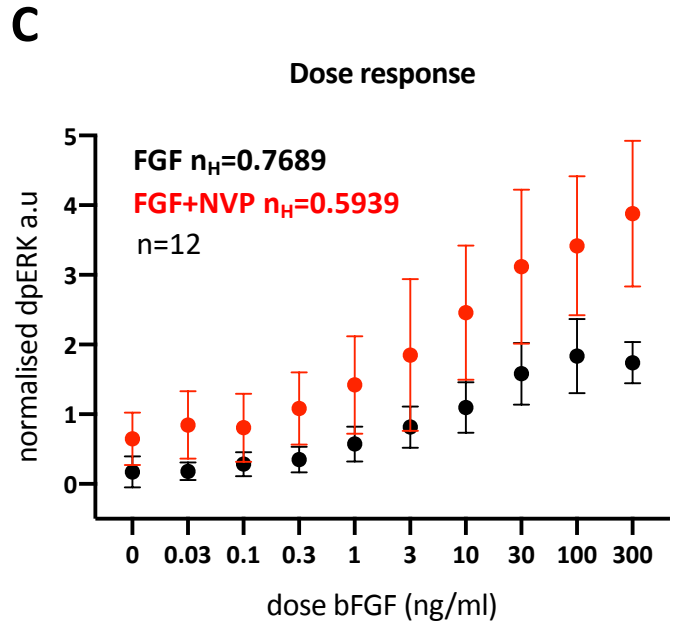
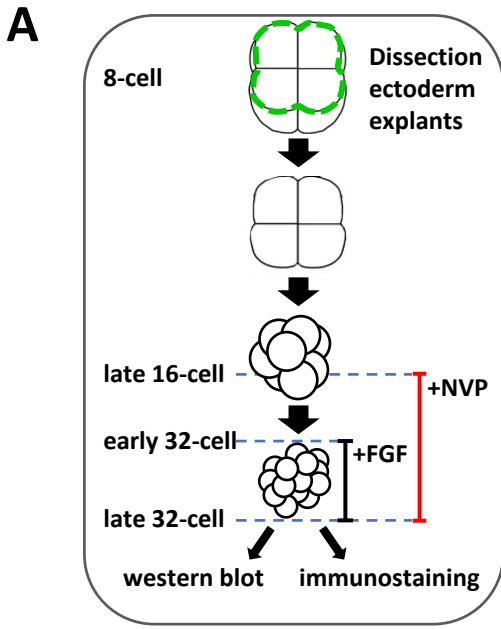


Figure 5

**Figure 6. Mathematical analysis showing higher sensitivity to changes in cell surface contact compared to changes in FGF concentration.** A, B) Schematic representations of signalling scenarios. Cells, grey boxes; nuclei in grey circles with shading depicting nuclear activation levels of signalling pathway; blue dots, ligand; red bars, receptors with shading depicting levels of receptor activation. A) Cell surface contact dependent signalling. Different cell shapes in the ascidian embryo result in differential areas of cell surface contact (or exposure of the FGFR, red lines) with FGF-expressing mesendoderm cells (blue bar). In the intercellular space between the inducing and responding cells, FGF (blue dots) does not diffuse and the concentration is constant. Cells have different levels of contact-dependent pathway activation due to different numbers of activated receptors. B) The schematic shows a more classic morphogen gradient scenario, a morphogen is expressed in a subset of cells within a tissue (blue and white bar) and releases a morphogen into the intracellular space, which diffuses and creates a gradient (blue dots). Receptors present at the same density in responding cells are differentially activated (red shaded bars) depending upon the concentration of the ligand. Thus, in this scenario, cells have different levels of activated receptor due to different concentrations of ligand, which results in different levels of pathway activation. C) Following the cell surface contact-dependent scenario in (A), the graph shows predicted ERK activity as a response to changes in cell surface contact, based on fitting the equation (bottom) to our data for cell surface contact versus ERK activity for NVP-treated embryos (experiment 1), presented in Figure 2E. Below the graph is the equation describing ERK as a function of R. D) The equation represented below graph (C), where  $n=2.6$ , is now resolved to show ERK as a function of changing FGF concentration at fixed R, similar to the scenario in (B). The exact Hill coefficient obtained from this conversion depends upon the value of R, but it is always lower than 2.6. Shown are plots resolving for different values of R, at 1000 (blue line; maximum ERK activity = 0.86; Hill coefficient = 1.57); 750 (orange line; maximum ERK activity 0.74; Hill coefficient 1.44); 500 (yellow line; maximum ERK activity 0.5; Hill coefficient 1.38) and 250 (purple line; maximum ERK activity 0.1416; Hill coefficient 1.21). E) Left, mathematical modelling of ERK activation levels by SOS ( $V_1$ ; FGF-signal input) and p120RasGAP ( $V_2$ ; ephrin-signal input) with basal RasGAPs ( $k_b$ ) depicting p120RasGAP-independent (and thus ephrin-independent) Ras GTPase-activating protein activity. Right, model output of ERK activity at  $k_b = 0.2$ . Below the graph are circles depicting six cells spread evenly across the gradients of FGF (SOS) and ephrin (p120RasGAP) at three different positions (arrows and empty circles on the graph), (a) differential SOS with no p120RasGAP (FGF only); (b) differential p120RasGAP with no SOS (ephrin only); and (c) both SOS and p120RasGAP (FGF + ephrin). Predicted ERK outputs at other  $k_b$  values can be found in Supplementary Figure S9.



**Figure 7. *Otx* single molecule FISH in control, and FGF- or Eph- signal inhibited embryos.** Data from different cell types are coloured as follows: a6.5 in magenta, a6.6 in green, a6.7 in blue and a6.8 in grey. A) Example of Imaris segmented nuclear *Otx* smFISH spots (red) in a control embryo. Embryos were counter-stained with DAPI (white) for the nuclear segmentation. The a-line cells are highlighted with a red dotted line. On the right is a drawing highlighting the nuclei of the a-line cells. B, D) Each dot represents the number of *Otx* smFISH spots per nucleus in a single cell. B) Results from *Otx* quantification from late 32-cell stage embryos from four independent experiments plotted on one graph. The four experiments are represented by different shades and shapes of the dots and show the consistency between experiments. Statistical tests are two tailed unpaired t-tests comparing each cell-type based on the hierarchal order of their ERK signal levels (as in Figure 2), i.e. a6.5 to a6.7, a6.7 to a6.6, and a6.6 to a6.8. \*\*\* P=0.0001 to 0.001; \*\*\*\* P<0.0001; ns, P≥0.05 no significant difference. C) Schematic drawing showing the experimental conditions for (D). Embryos were injected in one cell of the 2-cell stage embryo with mRNA and FITC-dextran for identification. D) Embryos injected in one cell of the two-cell stage embryo with *PH-GFP*, *dnFGFR*, *dnEph3*, or *dnp120RasGAP* mRNAs and processed for *Otx* smFISH. Below the graphs the number of independent experiments and number of pairs of cells. Statistical tests are paired t-tests comparing each cell-type between control and injected halves. \*\*\*\*P<0.0001, \*\*\*P<0.001, \*\*P<0.01, \*P<0.05, ns P≥0.05.

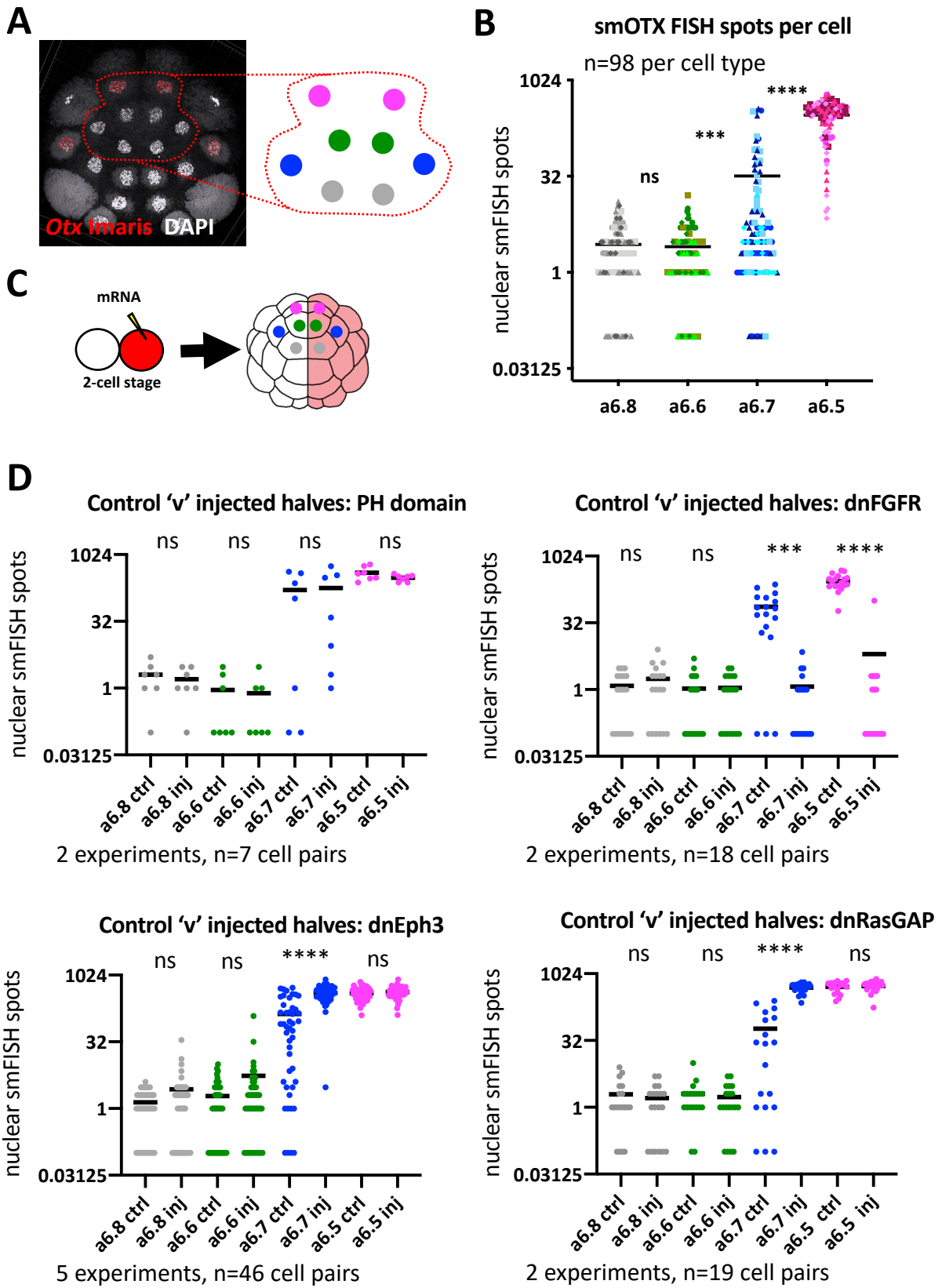


Figure 7

**Figure 8. A bimodal *Otx* transcriptional response and spatial restriction by Eph signals.** Data from different cell types are coloured as follows: a6.5 in magenta, a6.6 in green, a6.7 in blue and a6.8 in grey. A) Inhibition of Eph signals (NVP) results in ectopic activation of *Otx* in a6.7 (blue dots) and a6.6 (green dots). Addition of high doses of U0126 (2 $\mu$ M) to NVP-treated embryos suppresses all activation of *Otx*. An independent experiment can be found in Figure S11A. B) Ectodermal explants (procedure in Figure 5A) treated with increasing doses of FGF show a bimodal *Otx* activation response. Results of three additional independent experiments can be found in Figure S11B-D. C) Top: experimental design, embryos were injected with *dnEph3* mRNA and FITC-dextran for identification in one cell of the 2-cell stage. At the late 32-cell stage, embryos were fixed in two groups, one for anti-dpERK IF and the other for *Otx* smFISH. Bottom: mean dpERK signal normalised by subtracting mean control side a6.8 signal (a6.8 = 0) plotted against mean number of *Otx* smFISH spots for each cell type: a6.5, a6.6, a6.7 and a6.8 in control halves (●) and a6.5, a6.6, a6.7 and a6.8 in *dnEph3*-injected halves (◆). Non-linear regression gave a best-fit Hill coefficient of 6.65 (95% confidence interval 3.389 to ∞; upper limit could not be calculated). Results of two additional independent experiments can be found in Figure S11 E,F. D) Recovery of control *Otx* expression pattern in NVP-treated embryos with low doses of U0126. Top: Imaris segmented nuclear smFISH *Otx* spots (red) in examples of control, NVP-treated and NVP- plus low dose U0126- treated embryos. DAPI counter-stain in white. The graph shows the number of *Otx* smFISH spots per nucleus in the different cell-types following the treatments indicated. Statistical tests were conducted after *Otx* spot counts were re-tabulated based on treatment and cell-type. 2-way ANOVA analysis revealed a significant difference (\*\*\*\*  $P < 0.0001$ ) between control and NVP-treated embryos and no significant difference (ns,  $P \geq 0.05$ ) between control and NVP- plus low dose U0126-treatment, as indicated on the graph. Results of three additional independent experiments can be found in Supplementary Figure 12.

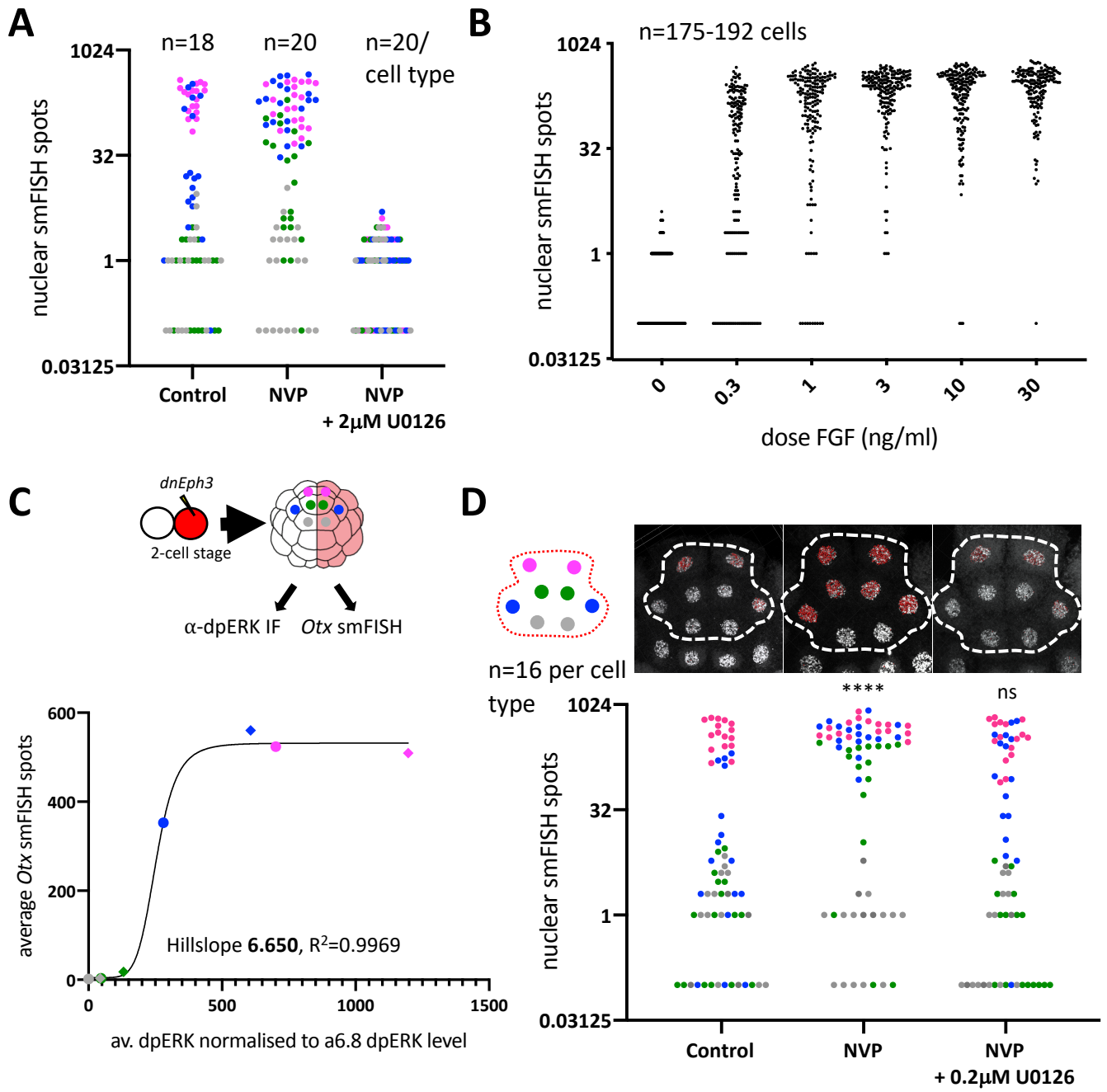


Figure 8



## **SUPPLEMENTARY INFORMATION**

**Supplementary Figures 1-12**

**Supplementary File**

**Supplementary Table 1**

**Figure S1. dpERK IF signal quantification in control, NVP- and U0126- treated embryos.**

Data from different cell types are coloured as follows: a6.5 in magenta, a6.6 in green, a6.7 in blue and a6.8 in grey. A-D) Mean pixel intensity of nuclear dpERK IF signal for each a-line cell for a large data set of approximately 50 embryos for control-untreated (A, C) or NVP-treated (B, D) embryos. Embryos within each sample (Control 2, NVP 2, Control 3 or NVP 3) were processed under identical conditions. Control 2 and NVP 2 were obtained from the same batch of eggs and sperm, as was Control 3 and NVP 3. Control and NVP samples were processed on different days under different confocal settings. Statistical tests are two tailed unpaired t-tests comparing each cell-type based on the hierarchal order of their dpERK signal levels, i.e. comparing a6.5 to a6.7, a6.7 to a6.6, and a6.6 to a6.8. \*\*  $P > 0.001$  to  $< 0.01$ ; \*\*\*\*  $P < 0.0001$ . E) Comparative analysis of ERK activation levels in a-line cells between control (C)-untreated (●) and U0126 (U)-treated (▼) embryos processed in the same tube for anti-dpERK IF. Control-untreated embryos in Exp. 1, Exp. 2 and Exp. 3 correspond to those in Figure 2B, Figure S1A and Figure S1C, respectively. Statistical tests are two tailed unpaired t-tests comparing each cell-type between control and U0126-treated embryos. \*\*\*\*  $P < 0.0001$ , \*\*\*  $P < 0.001$ , \*\*  $P < 0.01$ , \*  $P < 0.05$ , ns  $P \geq 0.05$ .

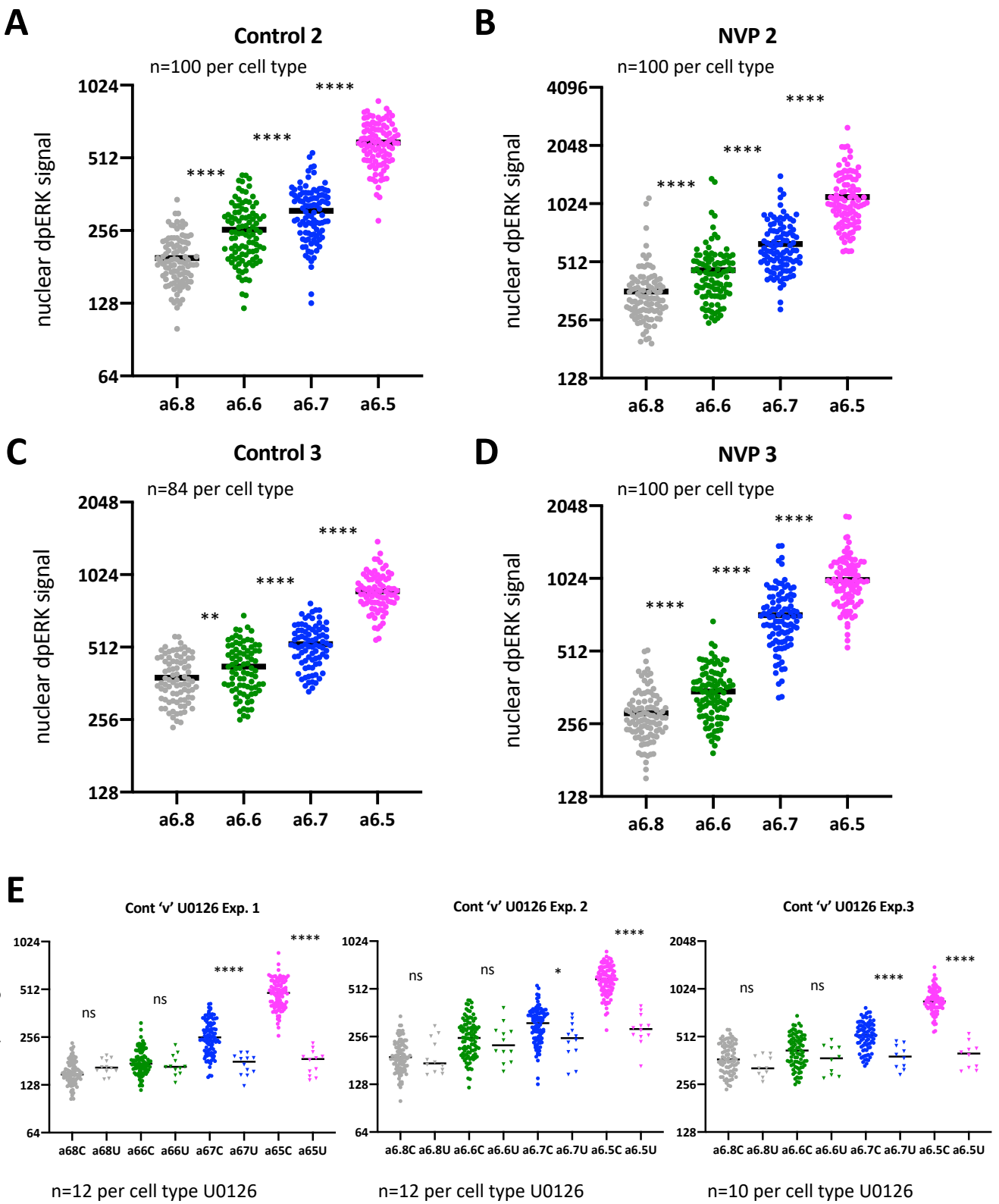


Figure S1

## IN PROGRESS

**Figure S2. ERK activity detected by ERK-KTR biosensor.** Data from different cell types are coloured as follows: a6.5 in magenta, a6.6 in green, a6.7 in blue and a6.8 in grey. *Phallusia mammillata* embryos were injected with *ERK-KTR-mClover* mRNA and *NLS-tdTomato* mRNA. Time-lapse movies were normalised to t=0 at the point of A6.4 nuclear envelope breakdown (NEBD). t= 4-8 corresponds to 'late 32-cell stage', when vegetal cells undergo de-compaction and embryos appear flattened in shape. A) ERK-KTR cytoplasmic/nuclear (C/N) ratio for a-line ectoderm cells during the 32-cell stage in U0126-treated embryos (n=2 embryos). B) IN PROGRESS. Time course of ERK activity in a-line ectoderm cells during the 32-cell stage. C/N ratios of a6.5, a6.6 and a6.7 were normalised to the same side a6.8 ratio. a6.8 measurements, which are normalised as 1 for each embryo half, are indicated on the graphs as a dotted grey line. Below is the same data-set expressed as a heatmap, showing stronger signal in a6.5 throughout the time of recording. Recording begun 8 minutes before A6.4 NEBD, when a-line cell nuclei form.

In progress

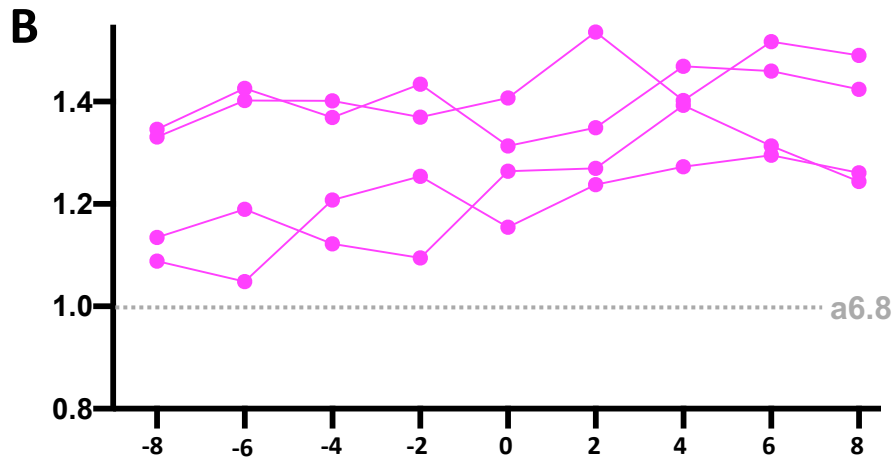
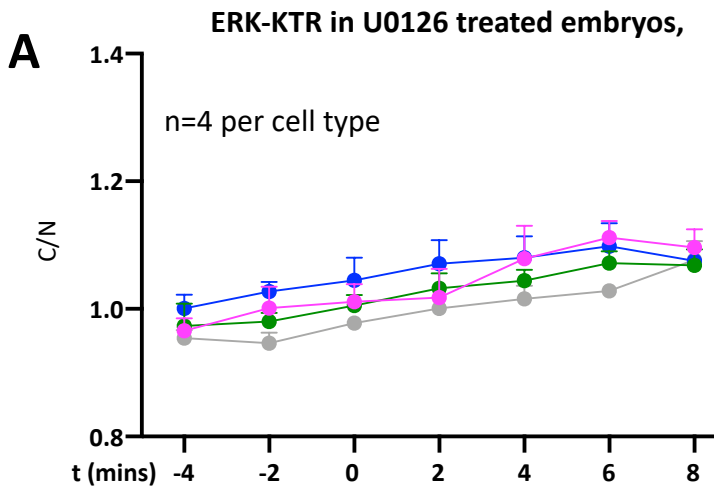


Figure S2

**Figure S3. Relationship between area of cell-surface contact with A-line mesendoderm cells and ERK activation level.** Data from different cell types are coloured as follows: a6.5 in magenta, a6.6 in green, a6.7 in blue and a6.8 in grey. Normalised cell surface contact (contact surface/total surface) with A-line (mesendoderm) cells and mean pixel intensity of nuclear dpERK IF signal were obtained for each a-line ectoderm cell in control or NVP-treated embryos. Confocal laser was adjusted between control and NVP- samples. Spearman correlations are shown on the graphs. 'Cont 3 bis' indicates a technical replicate of control 3 embryos, processed in a separate tube. Control 3 embryos are the same as those included as control 3 embryos in Figure 1B.

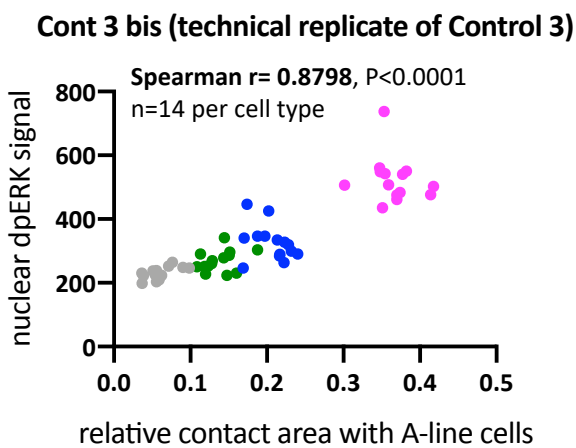
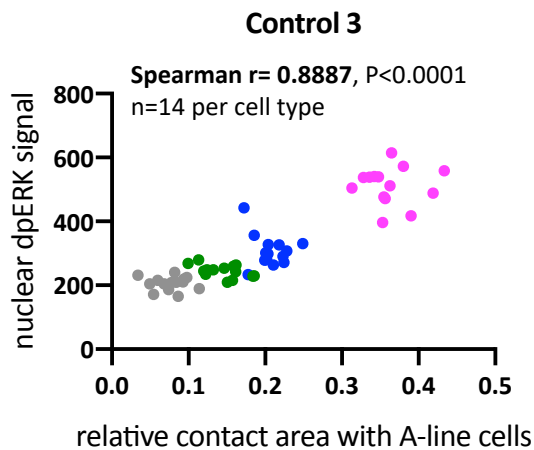
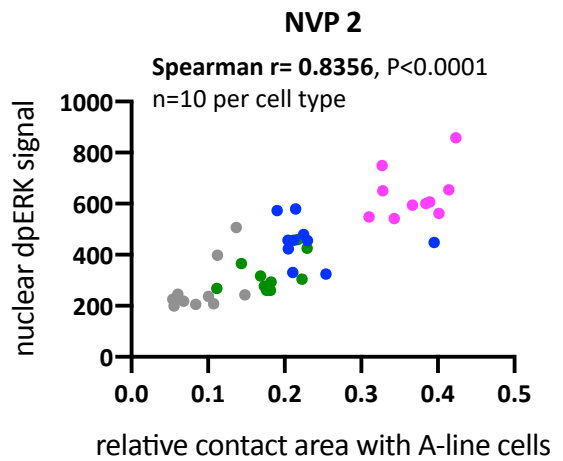
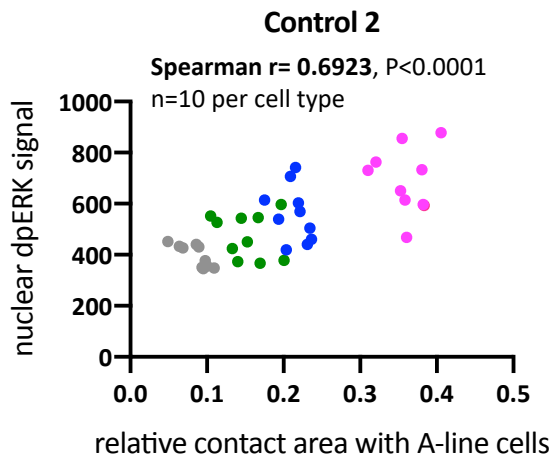


Figure S3

**Figure S4. NVP-treatment does not alter cell surface contacts.** Data from different cell types are coloured as follows: a6.5 in magenta, a6.6 in green, a6.7 in blue and a6.8 in grey. Normalised (contact surface/total surface) cell surface contact with A-line (mesendoderm) cells was obtained for each a-line ectoderm cell in control (C, ●) or NVP-treated (N, ▲) embryos. The data from experiment 1 is the same data as that in Figure 2D-E and experiment 2 is presented in Supplementary Figure 3 (top). Statistical tests are two tailed unpaired t-tests comparing each cell-type in control versus NVP-treated embryos. ns, no significant difference ( $P \geq 0.05$ ).

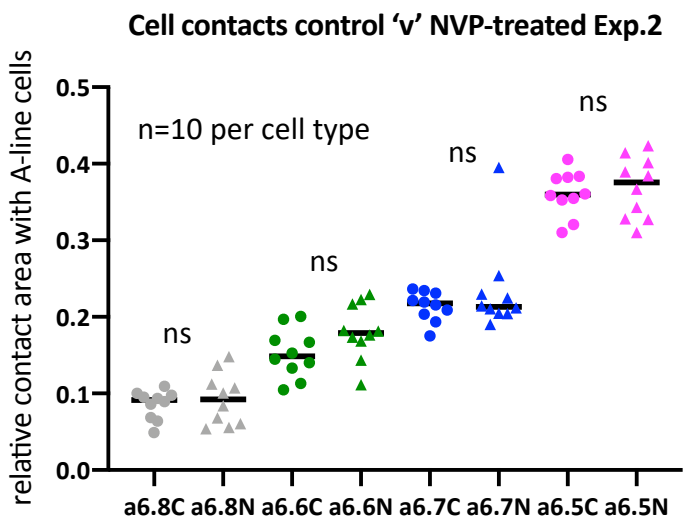
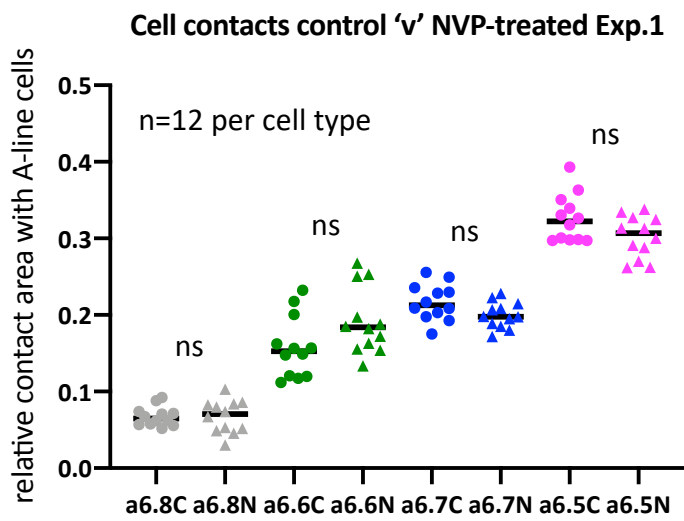
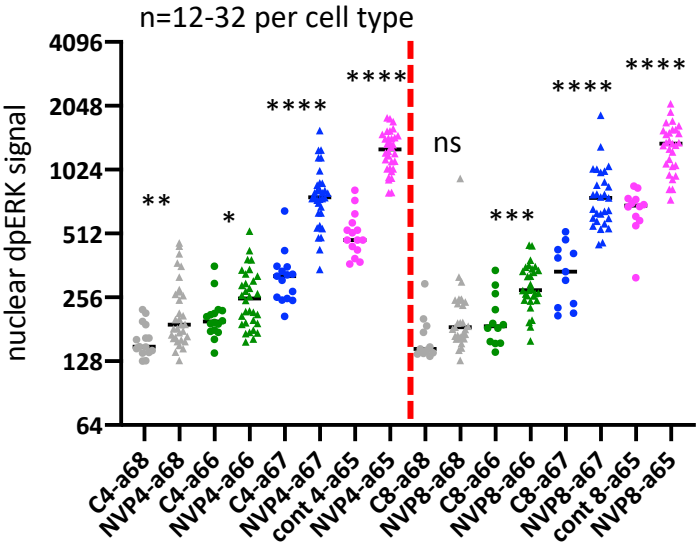


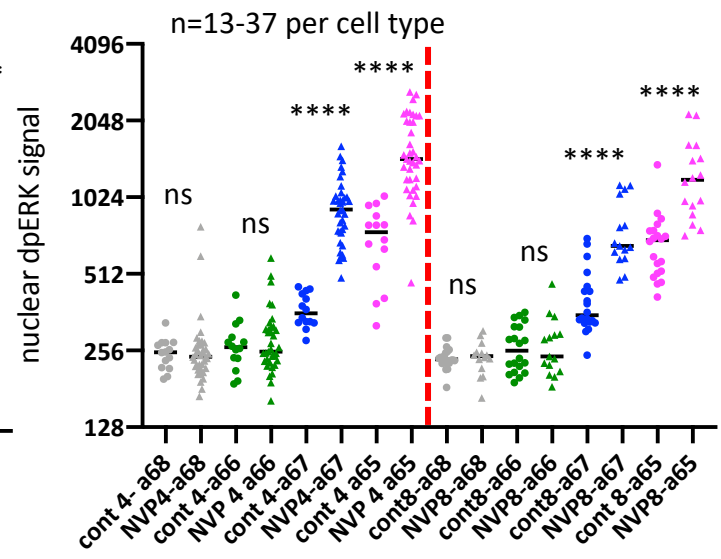
Figure S4

**Figure S5. ERK activation levels increase in embryos in which Eph signals are inhibited by NVP-treatment.** Data from different cell types are coloured as follows: a6.5 in magenta, a6.6 in green, a6.7 in blue and a6.8 in grey. Control embryos injected with fluorescent dextran were placed in the same tube as embryos treated with 4 $\mu$ M or 8 $\mu$ M NVP and processed under identical conditions. Two tubes (4 $\mu$ M or 8 $\mu$ M treatments, separated by a red dotted line) from three independent experiments are shown. Treatment with 2 $\mu$ M or 16 $\mu$ M NVP gave similar results, except 2 $\mu$ M appeared to have a slightly weaker effect (not shown). Statistical tests are two tailed unpaired t-tests comparing each cell-type under control versus NVP-treated conditions from the same tube. \*\*\*\*P<0.0001, \*\*\*P<0.001, \*\*P<0.01, \*P<0.05, ns P $\geq$ 0.05.

same tube Control 'v' NVP exp.1



same tube Control 'v' NVP exp.2



same tube Control 'v' NVP exp.3

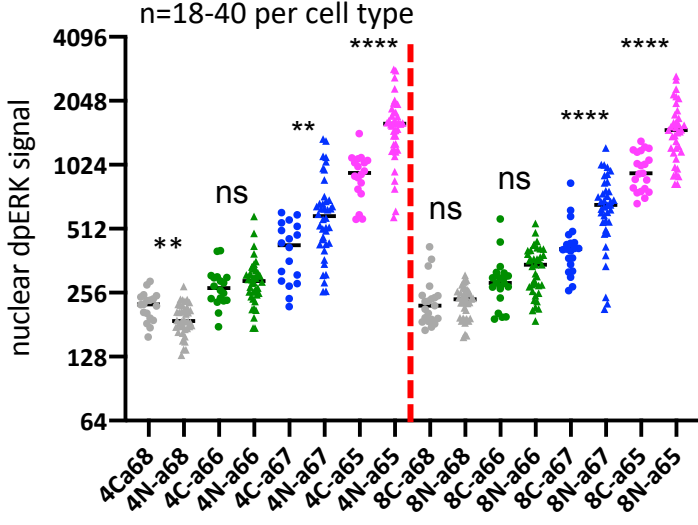
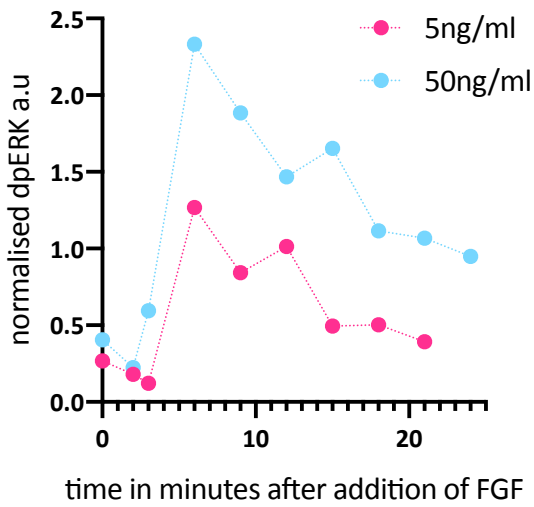
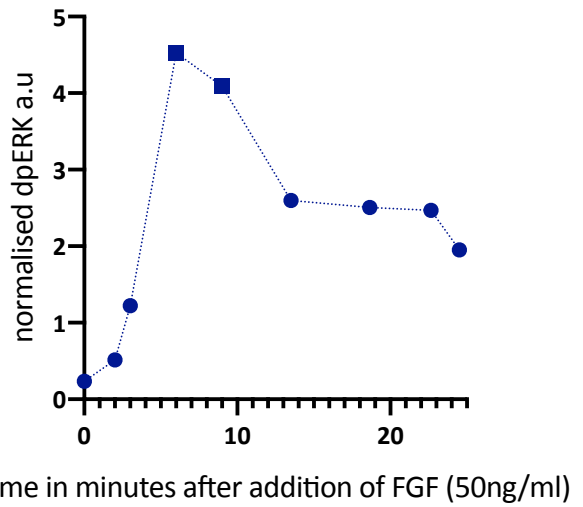
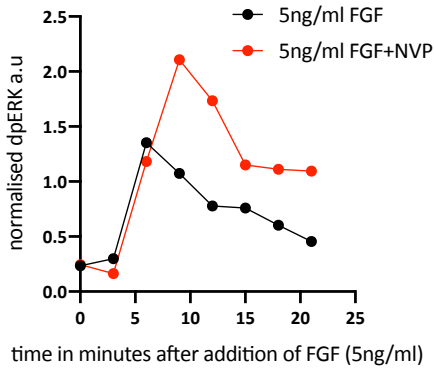


Figure S5

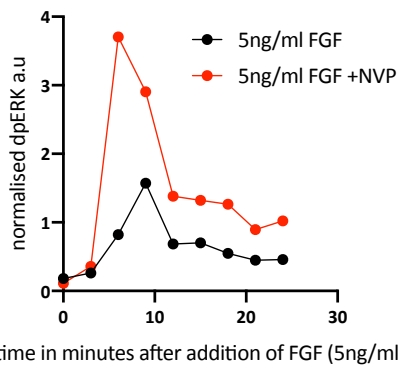
**Figure S6. Western blot analysis of ERK activation in response to exogenous FGF.** A-B) Quantification of western blots showing the temporal response of ERK activation in ectodermal explants treated with two doses of bFGF (A) or one dose (B). In B, the square points indicate that the corresponding signals on the western blot were out of the linear range. C) Temporal responses to 5ng/ml bFGF in the presence or absence of NVP. In two additional independent experiments, embryos were treated with 50ng/ml FGF with or without NVP and collected at 9 minutes for western blot analysis. In both cases, normalised dpERK levels were higher in the NVP-treated explants (not shown). D) Individual western blot data showing normalised dpERK signal in FGF- (left) or FGF- plus NVP- (right) treated explants (12 pairs of western blots).

**A** Temporal response to FGF- Exp.2**B** Temporal response to FGF- Exp.3**C**

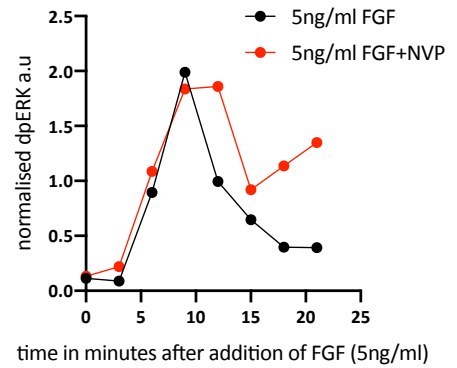
## Temporal response to FGF +/-NVP Exp.1



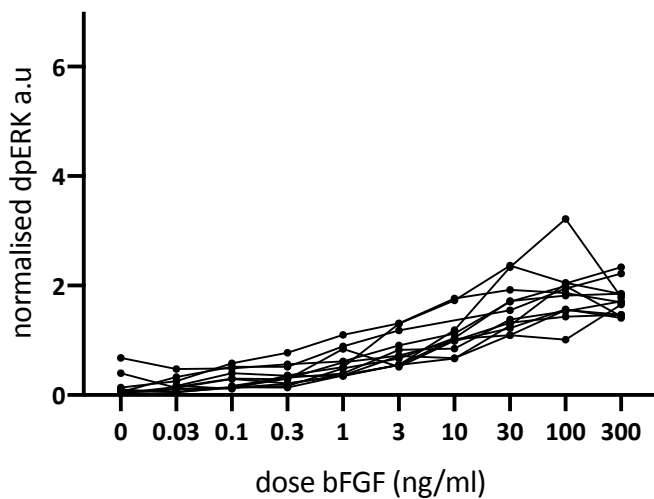
## Temporal response to FGF +/-NVP Exp.2



## Temporal response to FGF +/-NVP Exp.3

**D**

## FGF dose response of 12 individual w. blots



## FGF +NVP dose response of 12 individual w. blots

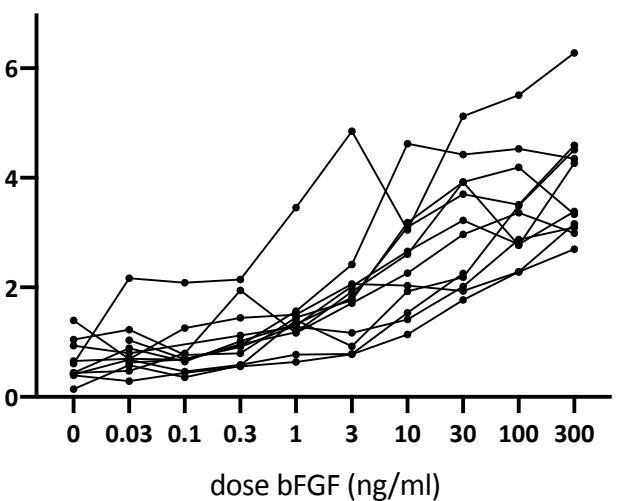


Figure S6 goes with Fig 5

**Figure S7. Single cell analysis of dose response of ERK activation in ectoderm explants treated with exogenous FGF.** Each dot represents the mean pixel intensity of nuclear dpERK IF signal in a single cell. Untreated whole embryos were placed in the same tubes with explants (shown on the right of each graph; a6.5 in magenta, a6.6 in green, a6.7 in blue and a6.8 in grey). n=number of cells analysed in explants per dose of FGF. Mean nuclear dpERK IF signals are indicated by orange bars. A) Samples were collected at 18 minutes following application of FGF. B) Samples were collected during the 'peak' at 6-9 minutes, one at 8 minutes, two at 7 minutes, following application of FGF.

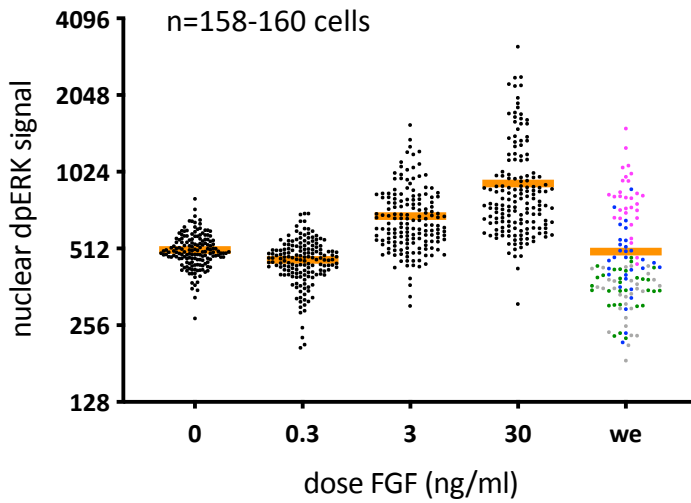
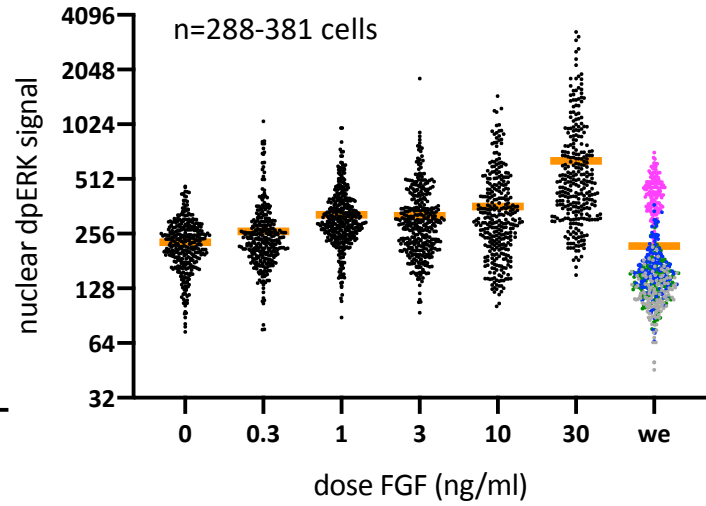
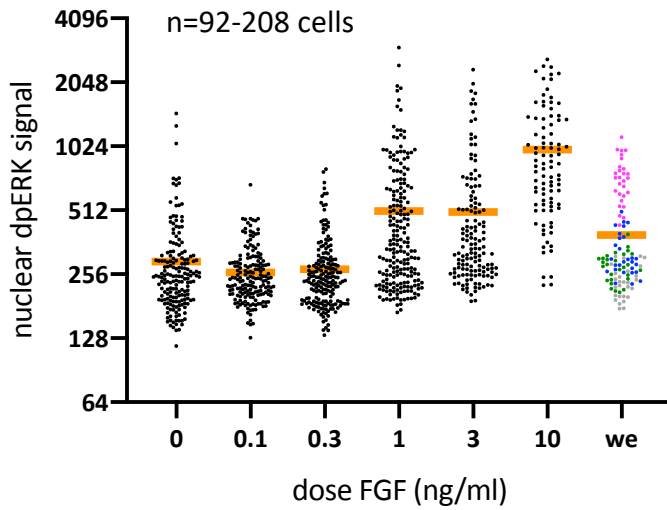
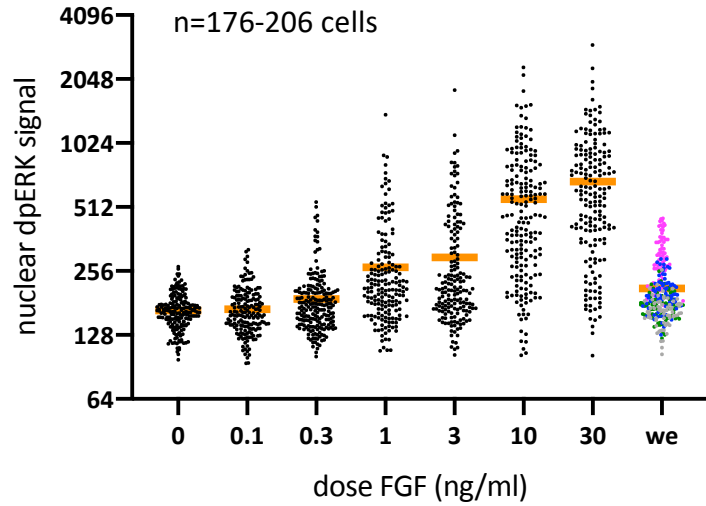
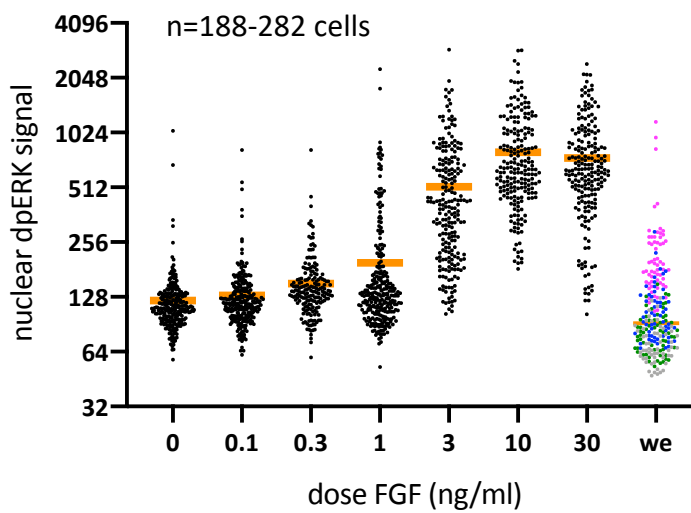
**A****dose response 18 mins Exp.2****dose response 18 mins Exp.3****B****dose response peak (8 mins) Exp. 1****dose response peak (7 mins) Exp. 2****dose response peak (7 mins) Exp. 3**

Figure S7

**Figure S8. Unimodal ERK activation and bimodal *Otx* activation: Hartigan's diptest for unimodality.** For whole embryo analyses (A, B, C, F, G), dots representing different cell types are coloured as indicated in the key, top right. For explant analyses (D, E), dots representing single cells in explants treated with different doses of FGF are coloured based on the dose of FGF, following the key on the middle right. Hartigan's diptest results are indicated ( $D=$ ) with the corresponding P-values in red. A) dpERK signal in control embryos from Figure 2B. The null hypothesis of a unimodal distribution is not rejected following Hartigan's diptest. Below the graph are the diptest results from additional independent experiments, Exp. 2 (Figure S1A) and Exp. 3 (Figure S1C). B) dpERK signal in NVP-treated embryos from Figure 2C. The null hypothesis of a unimodal distribution is not rejected following Hartigan's diptest. Below the graph are the diptest results from additional independent experiments, Exp. 2 (Figure S1B) and Exp. 3 (Figure S1D). C) *Otx* smFISH spot counts in control embryos, from Figure 7B. The null hypothesis of a unimodal distribution is rejected following Hartigan's diptest, suggesting at least a bimodal distribution. D) dpERK signal in explants treated with increasing doses of FGF, from Figure 5D. The null hypothesis of a unimodal distribution is not rejected following Hartigan's diptest. Below the graph are the diptest results from additional independent experiments, 18 minutes Exp. 2 and 3 (Figure S7A); peak (7 or 8 minutes) Exp. 1-3 (Figure S7B). E) *Otx* smFISH spot counts in explants treated with increasing doses of FGF, from Figure 8B. The null hypothesis of a unimodal distribution is rejected following Hartigan's diptest, suggesting at least a bimodal distribution. Below the graph are diptest results from additional independent experiments, Exp. 2-5 (Figure S11B-D; Exp. 5 not shown). F) *Otx* smFISH spot counts in control and NVP- treated embryos pooled from Figures 8A, 8D and Figures S11A, S12. The null hypothesis of a unimodal distribution is rejected following Hartigan's diptest, suggesting at least a bimodal distribution. G) *Otx* smFISH spot counts in control and *dnEph3* mRNA injected embryo halves from Figure 7D. The null hypothesis of a unimodal distribution is rejected following Hartigan's diptest, suggesting at least a bimodal distribution.

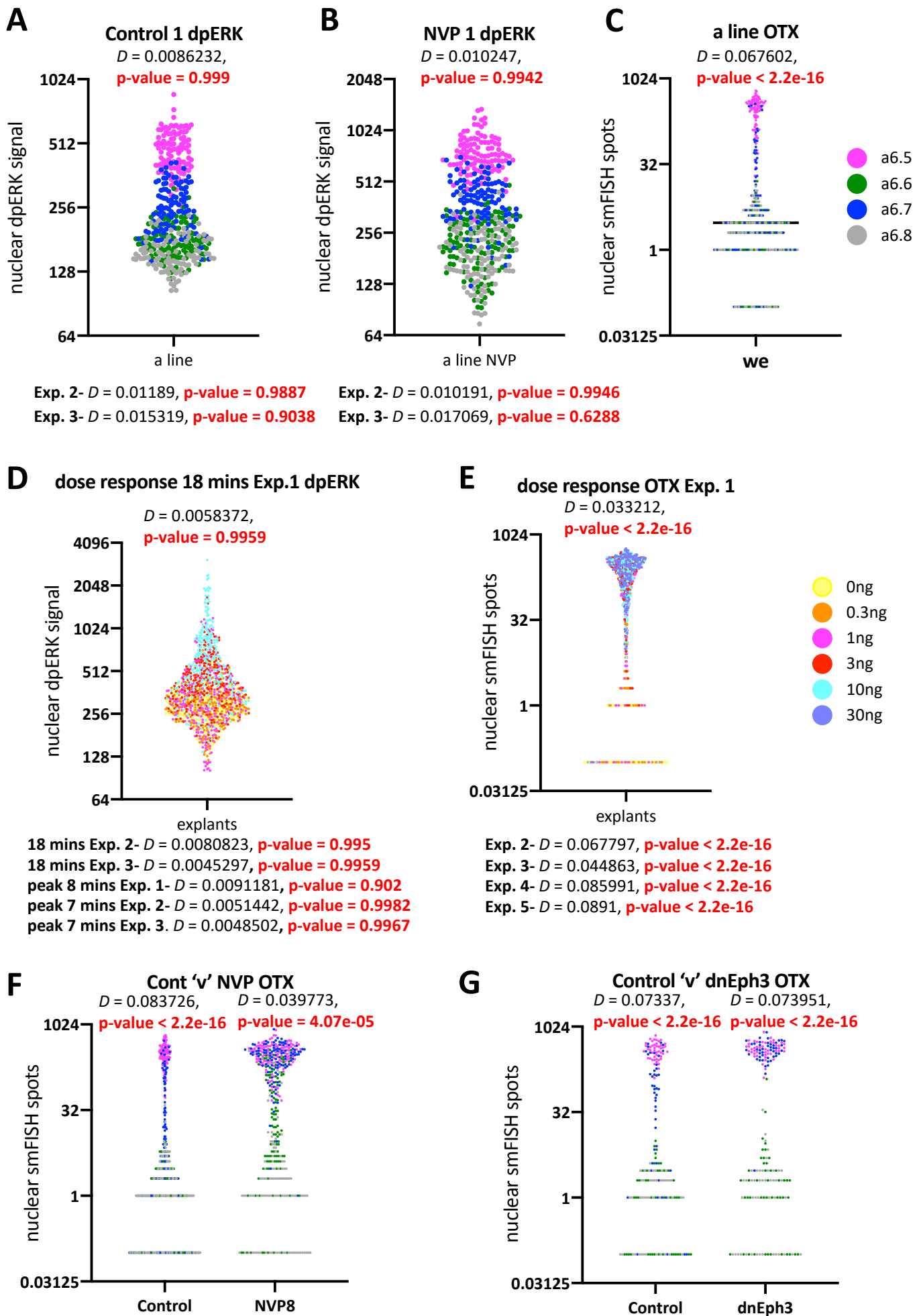


Figure S8

**Figure S9. Modelling ERK activation at different levels of SOS and RasGAP.** Top, modelling of ERK activation levels by SOS ( $V_1$ ; FGF- signal input) and p120RasGAP ( $V_2$ ; ephrin- signal input) with basal GAPs ( $k_b$ ), depicting p120RasGAP independent Ras GTPase-activating protein activity. Below are graphical model outputs of ERK activity at  $k_b = 0$ ,  $k_b = 0.2$  and  $k_b = 0.4$ . On the right of the graphs are circles depicting six cells spread evenly across the gradients of FGF (SOS) and ephrin (p120RasGAP) at three different positions (arrows and empty circles on the graph), **a**) differential SOS with no p120RasGAP (FGF only); **b**) differential p120RasGAP with no SOS (ephrin only); and **c**) both SOS and p120RasGAP (FGF + ephrin). The ERK heatmap with  $k_b = 0$  (top) is not consistent with our experimental data (Figure 2, 4, Figure S1, S2) as it predicts high ERK at all concentrations of SOS in the absence of p120RasGAP activity.

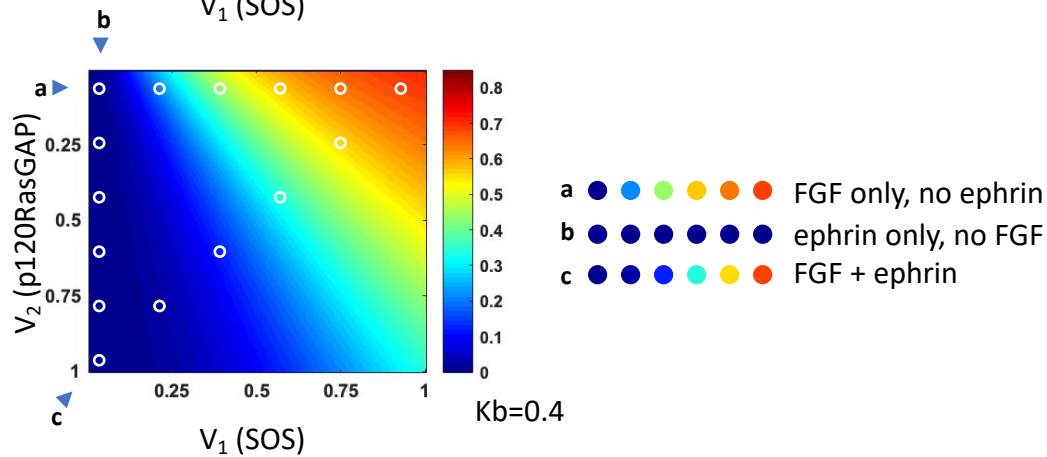
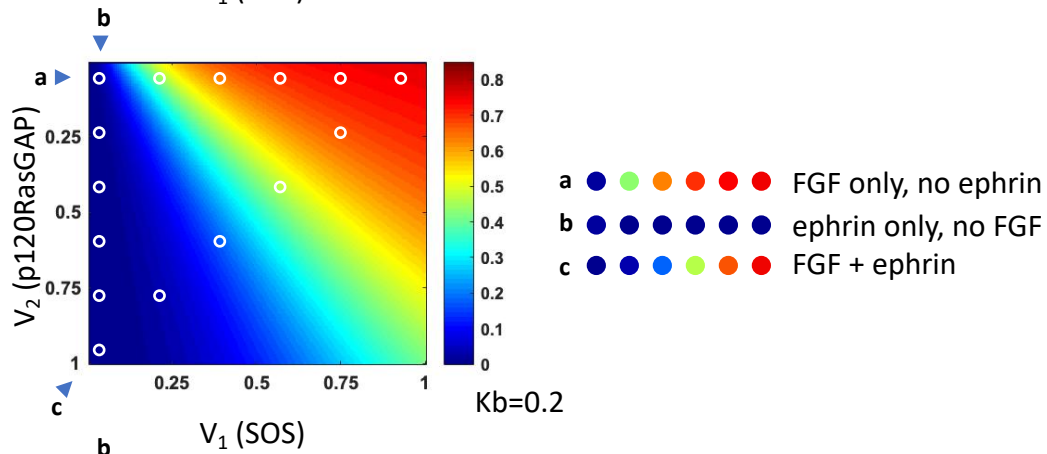
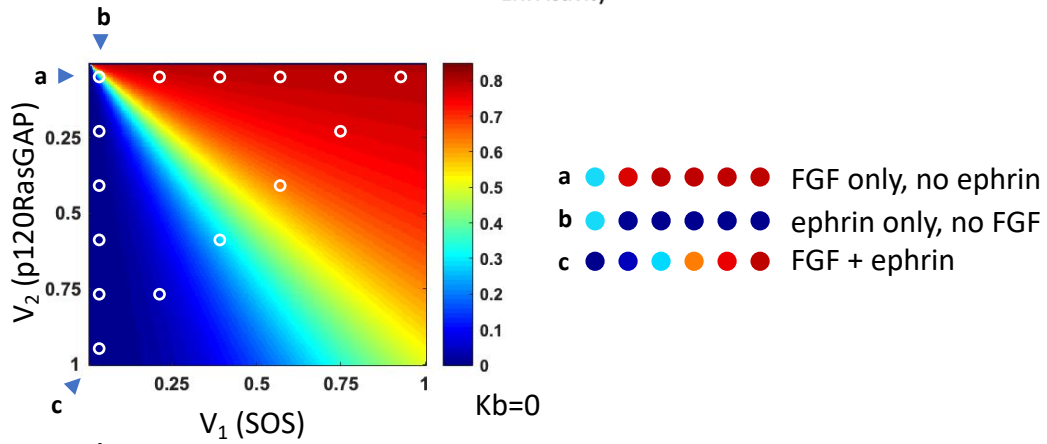
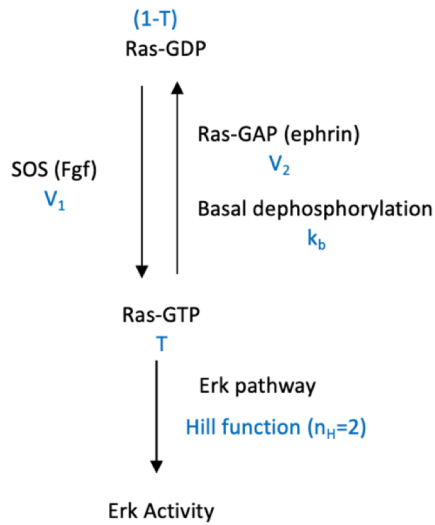


Figure S9

**Figure S10. Temporal profile of *Otx* activation in a6.5.** For this experiment, synchronised batches of embryos were chosen, collected every 3 minutes and processed for *Otx* smFISH. To ensure correct time categories, snapshots of endoderm cell nuclei were taken and matched to a time-lapse movie of endoderm cells so that each individual embryo was time adjusted to match this movie (see materials and methods for more details). A) Embryos were fixed every 3 minutes, marked with DAPI only and scanned by confocal imaging. Individual embryos were matched to the time-lapse movie. Images are Imaris segmented endoderm nuclei (A6.1 and B6.1 cell pairs, blue) and a6.5 (white) so show the relative positions and shape of the endoderm and a6.5 nuclei in different categories of time: 3-6 minutes (06'), 6-9 minutes (09') etc. B) In two independent experiments, embryos were fixed every 3 minutes and adjusted for developmental time based on the position and morphology of vegetal and a6.5 cell nuclei (as described above). Embryos were grouped into the developmental times shown on the graphs. The graphs show the number of *Otx* smFISH spots counted in a6.5 nuclei at each developmental time. Every dot represents a single a6.5 cell. C) Snapshots of Imaris 3D visualisations of confocal microscope stacks of a6.5 cell pairs, showing *Otx* smFISH spots (red) and DAPI (blue) at adjusted time points, from Time Series 2, prior to nuclear segmentation.

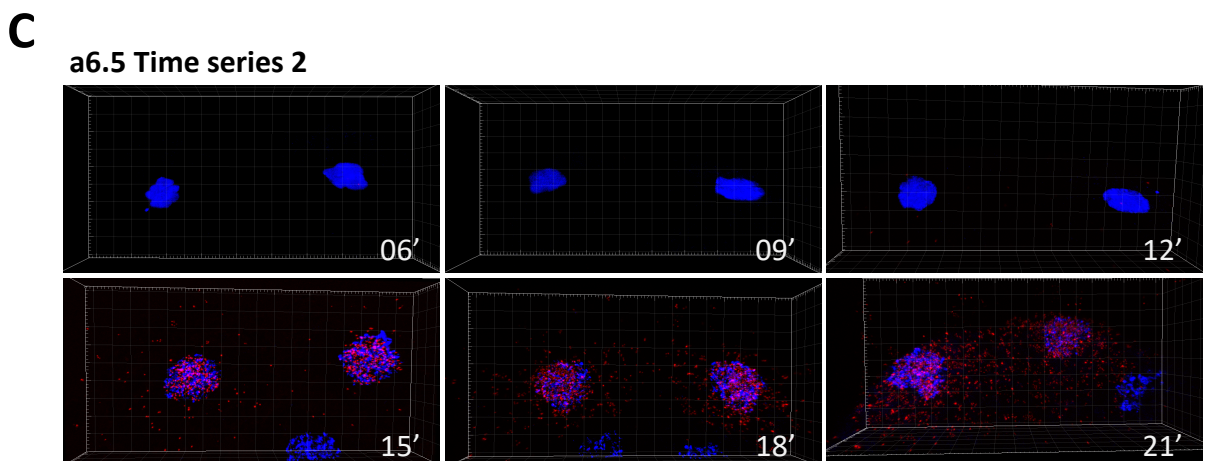
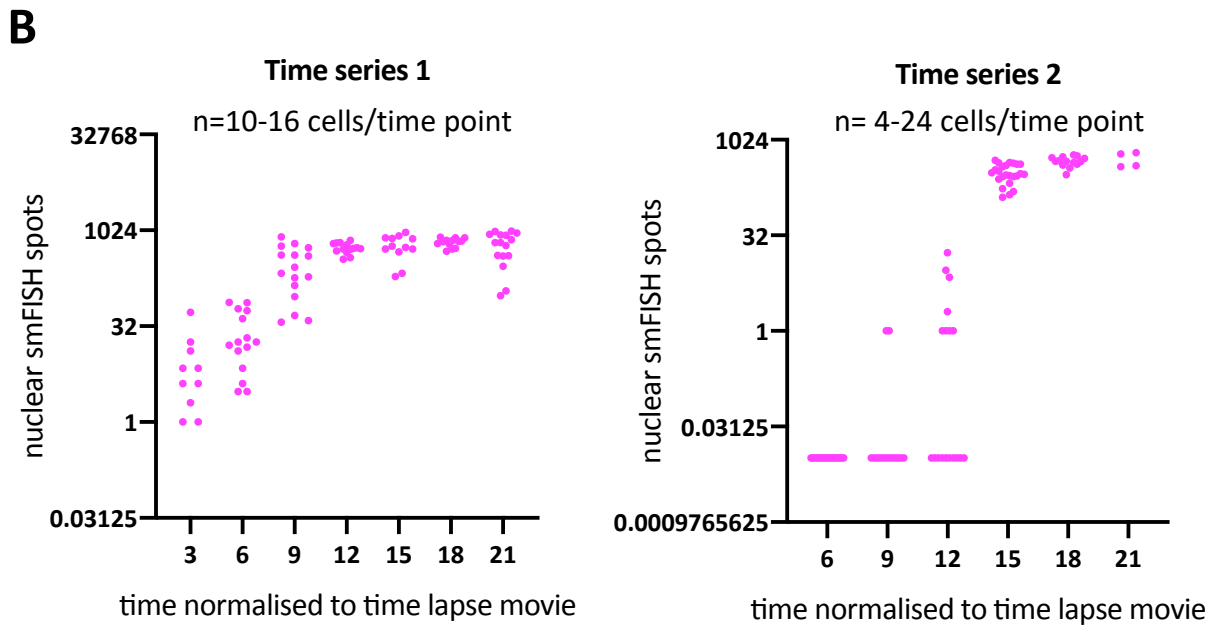
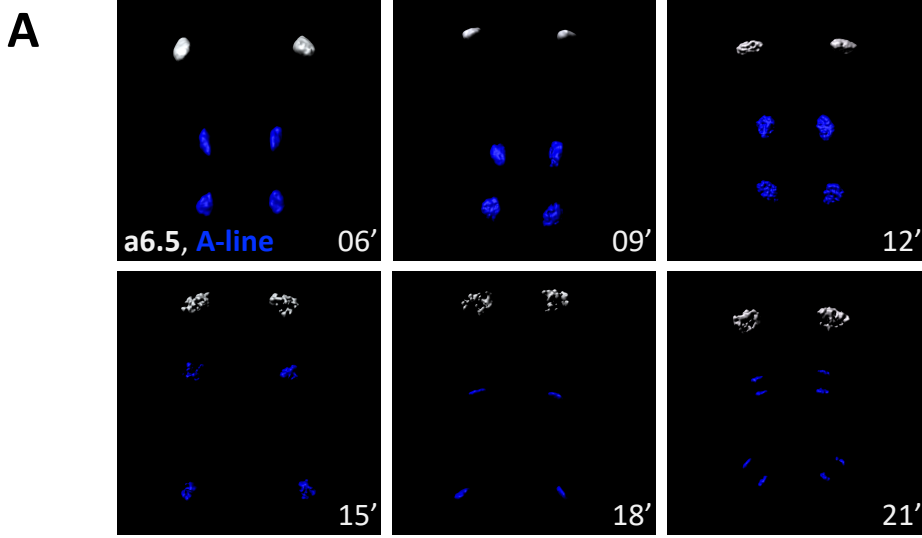


Figure S10

**Figure S11. Quantitative analyses of *Otx* expression.** A-D) Each dot represents *Otx* smFISH spot counts in a single nucleus. A, E-F) Data from different cell types are coloured as follows: a6.5 in magenta, a6.6 in green, a6.7 in blue and a6.8 in grey. A) Inhibition of ephrin signalling (NVP) results in ectopic activation of *Otx* in a6.7 (blue), a6.6 (green) and a6.8 (grey). Addition of high doses of U0126 (2 $\mu$ M) to NVP-treated embryos suppresses all activation of *Otx*. B-D) Ectodermal explants (as in Figure 5A) treated with increasing doses of FGF show a bimodal *Otx* activation response. E-F) Following the procedure in Figure 8C, mean dpERK signal normalised by subtracting mean control side a6.8 signal (a6.8 = 0) plotted against mean number of *Otx* smFISH spots for each cell type: a6.5, a6.6, a6.7 and a6.8 in control halves (●) and a6.5, a6.6, a6.7 and a6.8 in *dnEph3*-injected halves (◆). Non-linear regression gave a best-fit Hill coefficient of 10.68 and 3.374. 95% confidence intervals (CI) are 1.011 to ? (upper limit could not be calculated) for (E) and 2.230 to 6.548 for (F).  $R^2$  is shown on the graph.

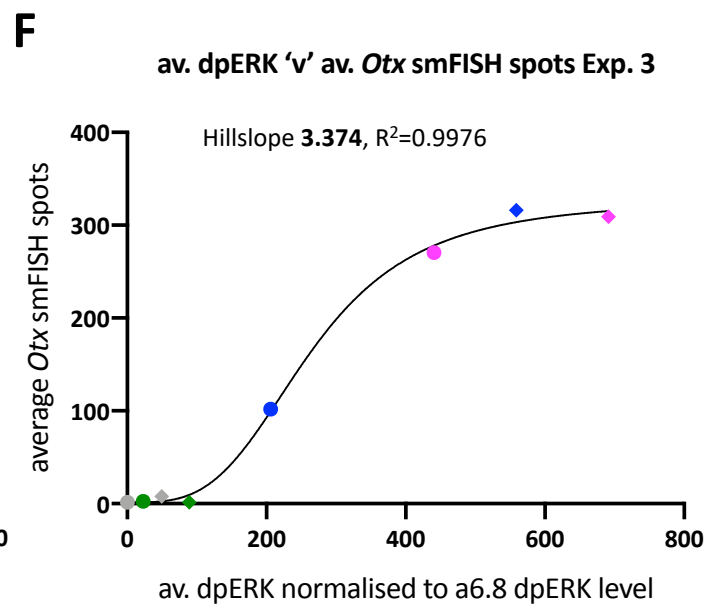
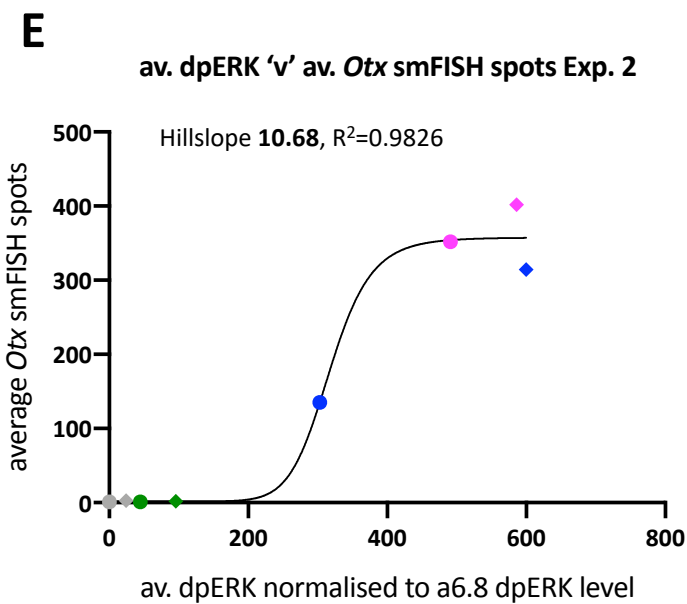
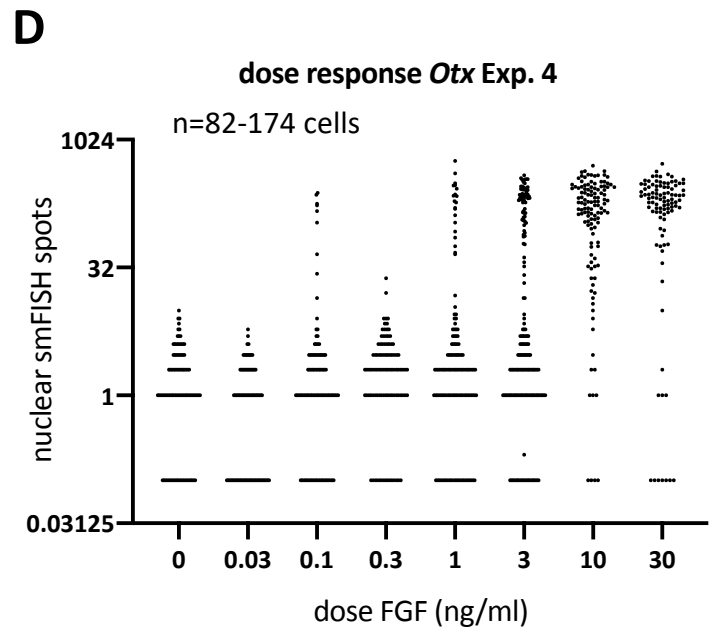
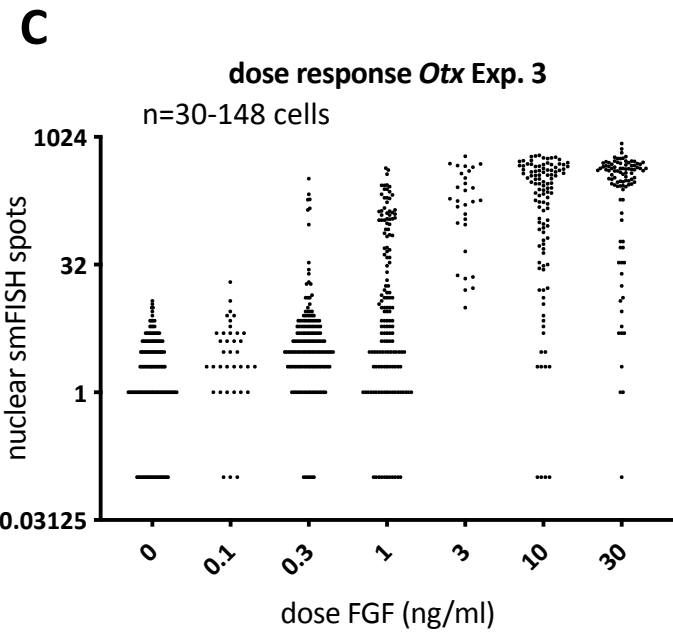
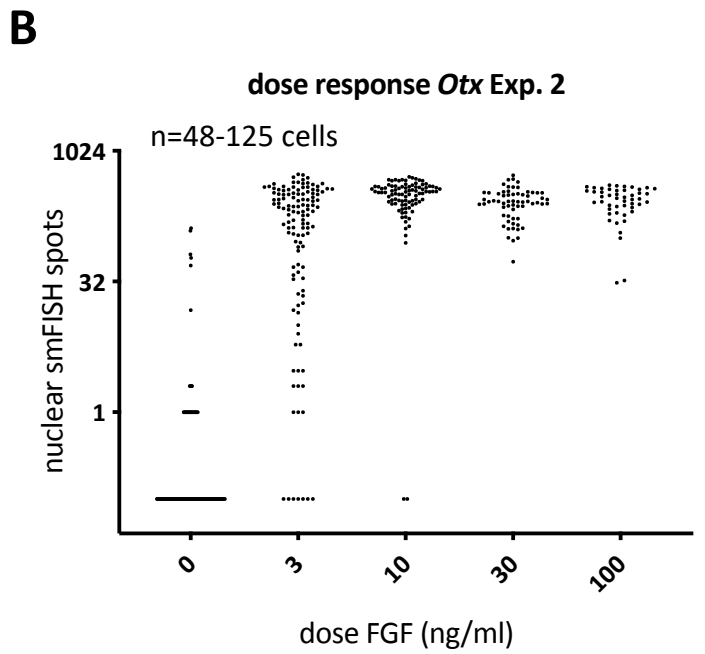
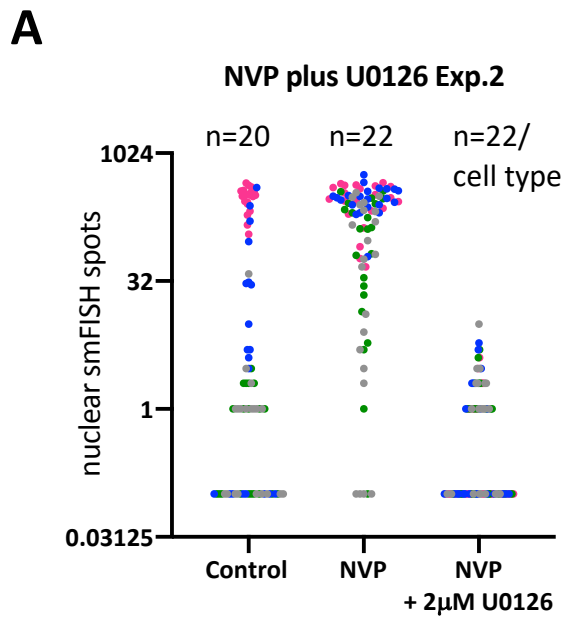
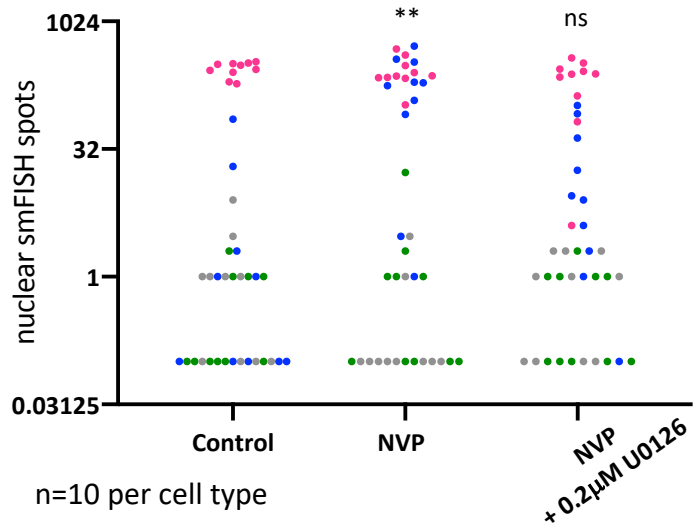


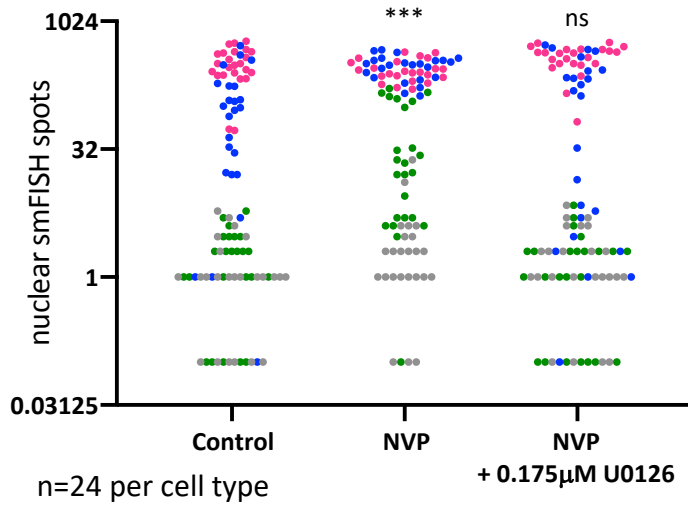
Figure S11

**Figure S12. Recovery of control *Otx* expression pattern in NVP-treated embryos by treatment with low doses of U0126.** Data from different cell types are coloured as follows: a6.5 in magenta, a6.6 in green, a6.7 in blue and a6.8 in grey. The graphs show the number of *Otx* smFISH spots per nucleus in each a-line cell following the treatments indicated. For statistical tests *Otx* smFISH spot counts were re-tabulated based on treatment and cell type and a 2-way ANOVA analysis was conducted comparing control to NVP-treated embryos or comparing control to NVP- plus low dose U0126- treated embryos. The results of the 2-way ANOVA analyses are placed above each experimental condition: \*\*  $P \geq 0.001$  to  $< 0.01$ ; \*\*\*  $P \geq 0.0001$  to  $< 0.001$ ; \*\*\*\*  $P < 0.0001$ ; ns, no significant difference ( $P \geq 0.05$ ).

'Recovery' of control *Otx* pattern Exp. 2



'Recovery' of control *Otx* pattern Exp. 3



'Recovery' of control *Otx* pattern Exp. 4

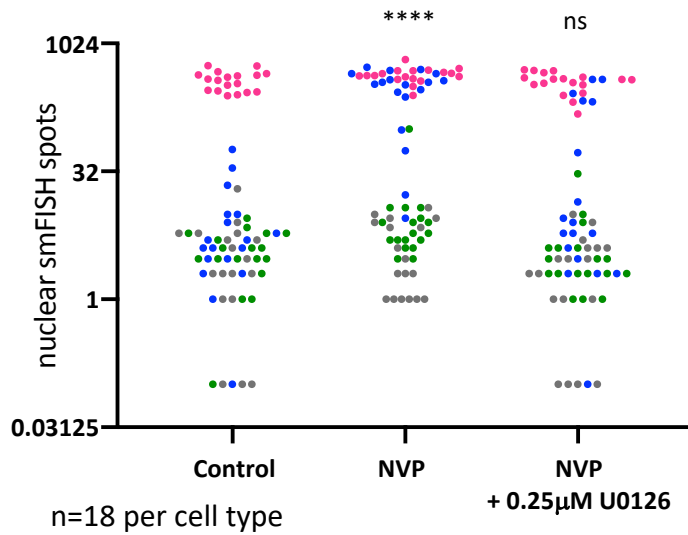


Figure S12

## Supplementary File 1

Here we express the Hill coefficient of the relationship between ERK and FGF ( $n_H$ ) in relation to the Hill coefficient of the relationship between ERK and R( $n$ ):

Equation (3) can be rewritten in the form:

$$Erk^* = \frac{1}{1 + \left( \frac{K_{DR}}{R} + \frac{K_{DR}K_D}{R[Fgf]} \right)^n} \quad (4)$$

To evaluate the Hill coefficient that characterises the relation between  $Erk^*$  and  $[Fgf]$ , we use the fact that it can be calculated in terms of potency as

$$n_H = \frac{\log(81)}{\log\left(\frac{[Fgf]_{90}}{[Fgf]_{10}}\right)} \quad (5)$$

where  $[Fgf]_{90}$  and  $[Fgf]_{10}$  are the concentrations of Fgf needed to produce 90% and 10% of the maximal Erk activity, respectively.

Inverting equation (4) leads to

$$[Fgf] = \frac{\frac{K_{DR}K_D}{R}}{\left( \frac{1}{Erk^*} - 1 \right)^{1/n} - \frac{K_{DR}}{R}} \quad (6)$$

The maximal value of  $Erk^*$  can be evaluated by letting  $[Fgf]$  tend to infinity in equation (4), and is thus equal to

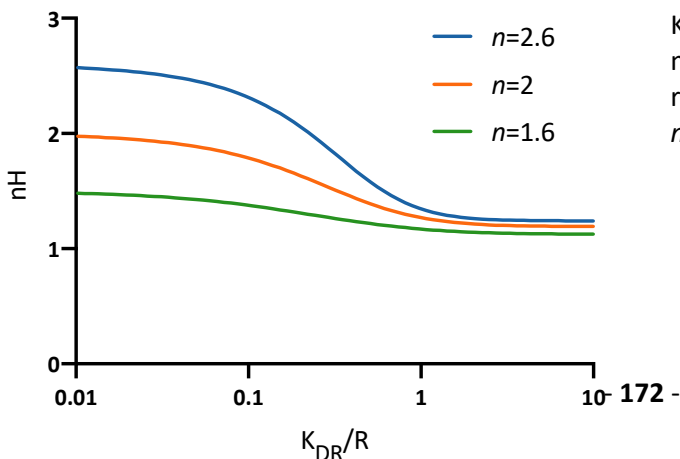
$$Erk^*_{max} = \frac{1}{\left( 1 + \left( \frac{K_{DR}}{R} \right)^n \right)} \quad (7)$$

Using equation (6) to calculate  $[Fgf]_{90}$ , which corresponds to  $0.9 Erk^*_{max}$  and  $[Fgf]_{10}$ , which corresponds to  $0.1 Erk^*_{max}$ , one obtains the relation between  $n_H$  (Hill coefficient with respect to  $[Fgf]$ ) and  $n$  (Hill coefficient with respect to the number of receptors):

$$n_H = \frac{\log(81)}{\log\left(\frac{\left(\frac{1+a^n}{0.1} - 1\right)^{1/n} - a}{\left(\frac{1+a^n}{0.9} - 1\right)^{1/n} - a}\right)} \quad (8)$$

where  $a$  stands for  $\frac{K_{DR}}{R}$ .

This shows that whatever the value of  $n$ ,  $n_H$  can only be smaller or equal to  $n$ , as shown on the graph,



left. The exact  $n$  depends on  $a$ , the ratio of the  $K_{DR}$  (the concentration of active R at half maximum ERK activity) to R (the number of receptors). The larger the  $K_{DR}/R$  the lower the  $n_H$ .

	Control		NVP	
	<i>nH</i>	CI	<i>nH</i>	CI
Control 1 v NVP 1	3,921	? to 11,39	2,619	0,7063 to 7,393
Control 2 v NVP 2	3,405	? to 14,96	1,607	0,1718 to ?
Control 3	5,226	2,497 to 10,71		
Control 3 bis	3,612	1,136 to 12,08		
Western blot	0,7689	0,5050 to 1,146	0,5939	0,2939 to 1,109

**Supplementary Table 1.** Hill coefficients (*nH*) and confidence intervals (CI) for Hill equation best fits. The first three lines show the response of ERK activity to changing area of cell surface contact. The last line shows the data obtained for the in vitro western blot analysis.



## II. Toward the mechanism underlying the switch-like transcriptional response of the *Otx* gene during neural induction

---

### 1) Introduction

During embryonic development, extracellular signals need to be interpreted transcriptionally by cells to give an appropriate response at the gene expression level. Appropriate interpretation of these signals is crucial for the developing embryo. Two modes of transcriptional responses to graded signals have been observed. The first mode includes that a transcriptional response takes place gradually in response to signal levels. In the second mode, a transcriptional response occurs above a threshold of the signal levels, leading to a bimodal response. Different synthetic promoter configurations have been tested in yeast or cell culture systems to address molecular underpinnings of these two modes of transcriptional response, indicating that a positive feedback loop and an activator and repressor competition for the same DNA element sites can convert otherwise gradually-responding promoters to adopt a bimodal response (Rossi et al., 2000; To and Maheshri, 2010). However, it remains largely unknown how bimodal transcriptional responses are controlled in endogenous genes.

During ascidian neural induction, *Otx* is directly activated by the FGF/MEK/ERK signalling cascade via Ets1/2, a member of the ETS family of transcription factors, well known for linking ERK activation to transcriptional responses. Consistently, a minimal FGF-responsive enhancer (55bp) of the *Otx* promoter contains two ETS binding sites. While neural inducing FGF signals activate ERK in a gradual manner among anterior

four ectoderm cells, only a6.5 ectoderm cell with the highest ERK activation level activates *Otx* transcription and adopts neural fates (Result part 1). We have found that the transcriptional activation of *Otx* operates in a bimodal manner exhibiting high Hill coefficients (ranging from 3.5 to 11) in response to different levels of ERK activation (Figures in Result part I). This switch-like response of *Otx* transcriptional activation is likely to play a critical role in generating the spatial precision of ascidian neural. In this study, we have addressed how the switch-like *Otx* transcriptional response is generated.

## 2) Results and discussion

### a. Suboptimization of the *Otx*-a enhancer

It has been shown previously that suboptimization of gene enhancer can underlie the precision and robustness of the gene expression. In cone cells of the developing *Drosophila* eye, the gene *dPax2* is activated via a Notch-regulated enhancer. The low binding affinity of binding sites for the Notch-regulated TF is required to prevent ectopic responses to Notch signal in non-cone cells (Swanson et al., 2011). Additionally, low affinity of binding sites in enhancer also give the specificity and the robustness in the *Hox* genes family. In *Drosophila* embryo, Ultrabithorax (Ubx), a Hox protein, in association with its cofactor Extradenticle (Exd), binds to clusters of low affinity binding sites in the *shavenbaby* gene enhancer. The low affinity of the binding sites gives the

specificity of Ubx binding while their clustering is also required for robust expression of genes (Crocker et al., 2015).

As described above, during neural induction of *Ciona* embryos, *Otx* is directly activated in response to ERK activation. A minimal enhancer of 55bp, called a-element, is able to mediate this transcriptional response (Bertrand et al., 2003). The a-element is composed of three binding sites for GATA4/5/6 and two binding sites for Ets1/2. The synergy between these two transcription factors is essential for the spatially precise transcriptional response of *Otx* to neural inducing FGF signals. A high-throughput analysis of the *Otx*-a enhancer has revealed that these GATA and ETS binding sites contain imperfect matches to consensus motifs and that they are not arranged at optimal intervals (Farley et al., 2015). Importantly, when the binding sites are "optimised", the resultant a-element drives robust but ectopic expression of the reporter gene when analysed at tailbud stages.

These studies prompted us to address whether the suboptimization of the *Otx* a-enhancer is involved in the spatial precision of the *Otx* gene activation during neural induction. In the non-neural ectodermal cells, the low level of ERK would result in a low level of activated Ets1/2 which might be insufficient to bind the suboptimized binding sites, leading to non-activation of the *Otx* gene. If this is the case, an optimised a-element enhancer might exhibit ectopic expression of the reporter gene in non-neural ectoderm in 32-cell stage embryos.

We injected *Otx-a-WT>mCherry* or *Otx-a-49Opt>mCherry* into eggs and fixed embryos at the late 32-cell stage for *in situ* hybridisation analyses. *Otx-a-*

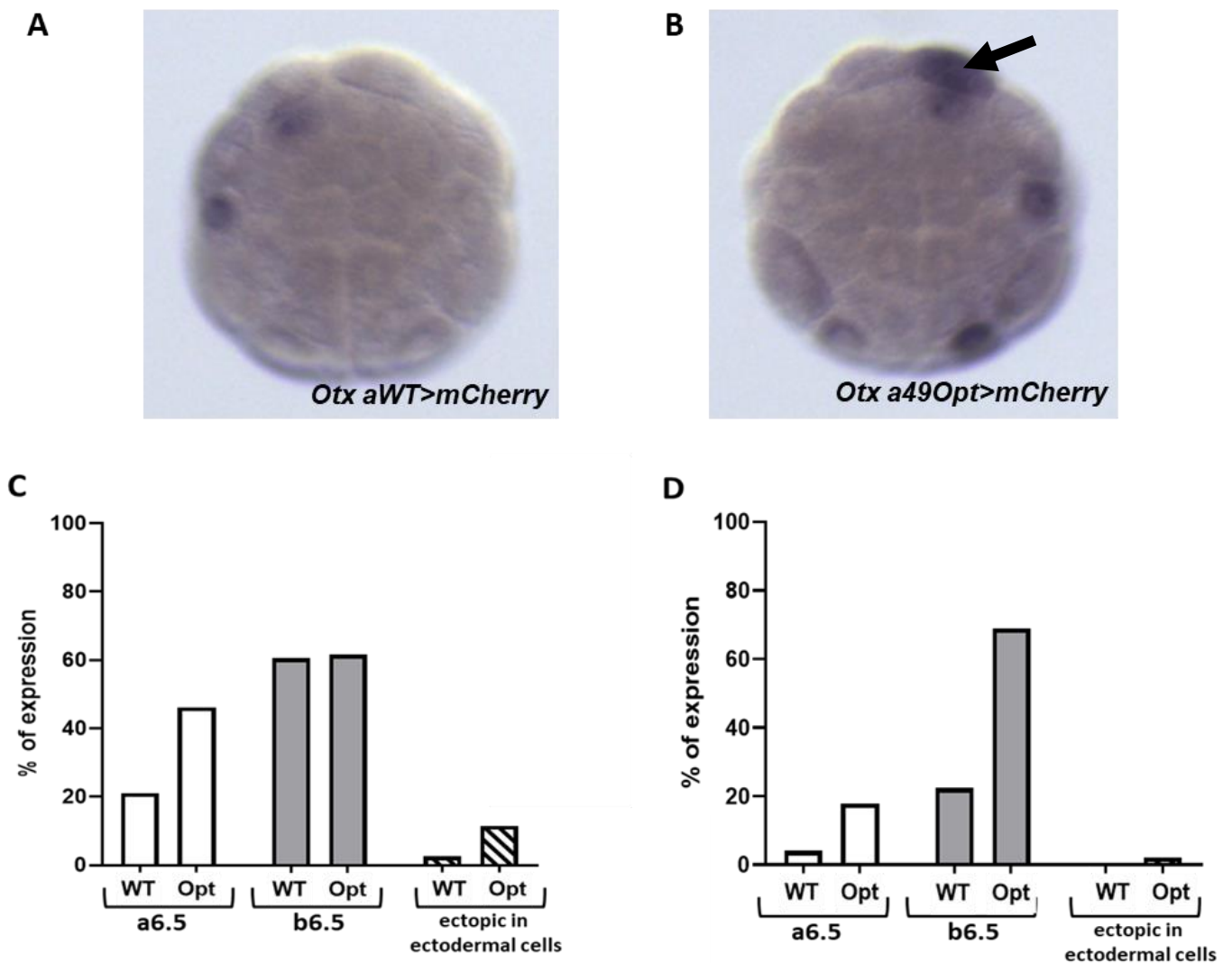


**Figure 29:** Comparison of embryos expressing WT *Otx aWT>mCherry* (A, C) and *Otx a49Opt>mCherry* (B, D). (A, B) In Situ Hybridization of *mCherry*. The arrow points one of notochord/neural precursors (NN cells), which express the reporter gene in a high frequency when it is driven by the optimised a-element. (C, D) Total number of embryonic halves in percentage expressing *mCherry*.

*49Opt>mCherry* consists of two optimised GATA site and two optimised ETS sites with optimal spacing (Farley et al., 2015). We counted numbers of embryonic halves expressing *mCherry* in the neural ectoderm cells, a6.5 or b6.5, and any of non-ectodermal cells (Figure 29A-B). The total number of embryonic halves was used to express the results in percentage. The two graphs (Figure 29C, D) represent the results of two independent experiments. Expression of the reporter gene is mostly restricted in the two neural precursor pairs, a6.5 and b6.5 both in *Otx-a-WT>mCherry* and *Otx-a-49Opt>mCherry* embryos, suggesting that the suboptimization of the *Otx a*-enhancer is unlikely to play a major role in generating the switch-like expression of *Otx* during the neural induction process.

**b. ERF1/2 acts as a transcriptional repressor of the *Otx* gene during neural induction of *Ciona* embryos**

In collaboration with Geneviève Dupont (Université Libre de Bruxelles) and Sophie de Buyl (Vrije Universiteit Brussel), we conducted mathematical modelling, based on the assumption that Ets1/2 binds to the two ETS binding sites cooperatively. As expected, this generated Hill coefficients of a maximum of 2 in response to increasing levels of ERK activity (data not shown). As well as positive regulators of transcription, it is known that the ETS gene family also includes transcription repressors whose activity is negatively controlled by ERK. When we incorporated a transcriptional repression via two ETS binding sites in the mathematical modelling, the Hill coefficient approached 3.6, which corresponds to the lowest end of the Hill coefficients that we obtained from

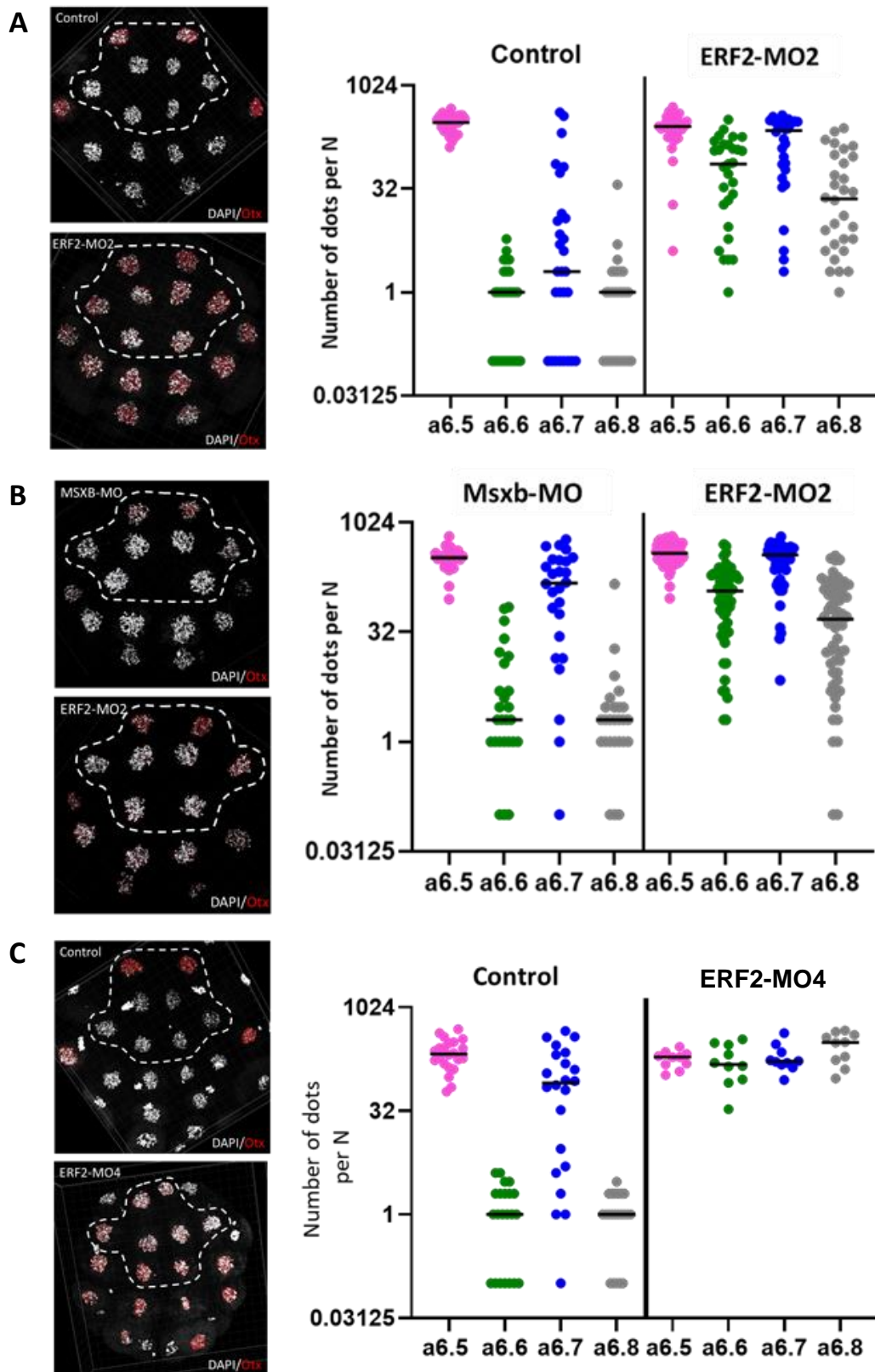


**Figure 30:** *Otx* single molecule FISH in control and ERF2-MO2 injected embryos (A) or Msxb-MO and ERF2-MO2 injected embryos (B) or control and ERF2-MO4 injected embryos (C). Embryos were pooled either from two different batches acquired on the same day (A) or from three independent experiments (B) or came from the same experiment (C). Data are coloured: a6.5 in magenta, a6.6 in green, a6.7 in blue and a6.8 in grey.

	Number of embryos	p-value	D	Divergence from unimodal distribution
Control embryos	14	2.276e-06	0.078571	YES
ERF2- MO2 embryos	15	0.8646	0.023537	NO
MSXB- MO embryos	13	0.01075	0.057692	YES
ERF2- MO2 embryos	29	0.5418	0.023276	NO
Control embryos	11	0.0007347	0.073864	YES
ERF2- MO4 embryos	5	0.9354	0.039747	NO

**Table 1:** Hartigan's diptest (Hartigan and Hartigan, 1985) results for Control/MO2-ERF2, MO-MSX/MO2-ERF2 and Control/MO4-ERF2 experiments. P-value range from 0 to 1. P-value <0.05 indicate significant divergence from unimodality,  $0.05 < p\text{-value} < 0.1$  suggests divergence with marginal significance. Dip test statistics D increases when distribution is deviant from an unimodal distribution. (Freeman and Dale, 2013)

experiments. Encouraged by this result, we looked for potential candidates for an ETS-domain transcription repressor. During an informal discussion with Dr. Kaoru Imai (Osaka University), it turned out that she had preliminary results showing that the *Ciona* homologue of ERF2 is the likely candidate. When she knocked down *ERF2* in *Ciona robusta*, she observed ectopic *Otx* expression in non-neural ectoderm cells at the 32-cell stage. We have decided to address the potential role of *ERF2* in generating the switch-like response of *Otx* as a collaborative project.

We were able to obtain two morpholino antisense oligos that appear to successfully knockdown *ERF2* in *Ciona intestinalis*. When either MO is injected in eggs of *Ciona intestinalis*, resultant embryos exhibit ectopic *Otx* expression in non-ectoderm cells at the 32-cell stage. Using *Otx* smFISH, we quantified expression levels of *Otx* in a-line ectoderm cells, a6.5, a6.6, a6.7 and a6.8, in embryos injected with ERF2-MO (Figure 30). When ERF2 is knocked down, the *Otx* gene is activated in all a-line ectoderm cells. Hartigans' diptest of these results shows that ERF-2 knockdown results in no divergence from an unimodal distribution (Table 1). This result strongly suggests that ERF2 acts a repressor of *Otx* transcription and that it is required for the spatial precision of neural induction. This result is consistent with the observation whereby point mutations of the two ETS-binding sites of the *Otx* a-element enhancer results in ectopic expression of the reporter gene in non-neural ectoderm cells (Rothbacher et al., 2007). We are planning to address whether the ectopic expression of *Otx* following ERF2-knockdown is dependent on FGF signals or derepression is sufficient to activate

the *Otx* gene. If the latter is the case, we will address whether the *Otx* expression in non-neural ectoderm cells depends on GATA4/5/6.

ERF is known to have a strong transcriptional repressor activity on promoters containing ETS binding sites and this repressor activity of ERF can antagonize the activity of ETS-transcriptional activators. ERF is inhibited by phosphorylation by ERK (Figure 31A) (Sgouras et al., 1995). The ERK-mediated phosphorylation of ERF lead to its export from the nucleus to the cytoplasm. The phosphorylated form of ERF is exported to the cytoplasm. This export is inhibited by ERK inhibitors and completely abolished when the phosphorylation site is mutated. When the growth factor stimulation ends, ERF is rapidly dephosphorylated and goes back to the nucleus (le Gallic et al., 1999).

In contrast to ERF, Ets1 and Ets2 are transcriptional activators whose activity is positively controlled by direct phosphorylation by ERK via a conserved threonine residue (Yang et al., 1996). Thus, ERK activation in a cell can lead to both activation of Ets transcriptional activators and inhibition of ERF transcriptional repressor. Interestingly, this relationship involving activator and repressor, which share same binding site and are controlled by same signal, has been shown to generate a bimodal transcriptional response in a synthetic promoter context (Rossi et al., 2000). This synthetic promoter system, based on combination of Tet-ON and Tet-OFF systems, consists of an activator, rtTA, and a repressor, tTR. The activator and repressor have opposite responses to tetracycline and its analogue doxycycline (dox). The repressor only binds the target site, tetO, in the absence of dox, whereas the activator only binds

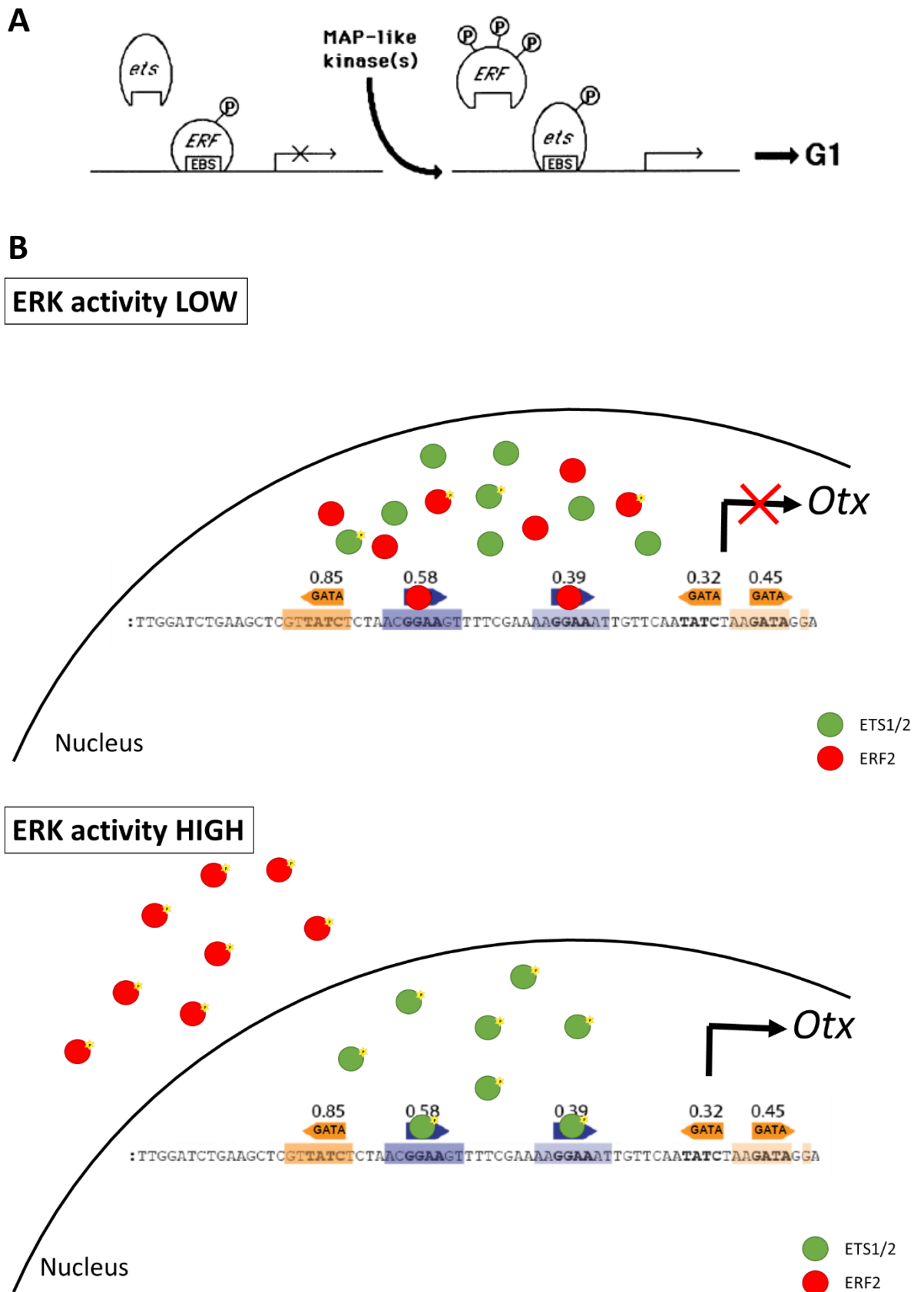


**Figure 31:** (A) Simplified model for ERF function (From Sgouras 1995) (B) schematic drawings of the hypothetical activator-repressor system involved in the ON/OFF response of the *Otx* gene during neural induction in *Ciona intestinalis* embryo.

the site in the presence of dox (Rossi et al., 1998). This system was implemented in mammalian culture cells (Rossi et al., 2000). When either activator or repressor alone was present, the system generated a graded transcriptional response to increasing doses of dox. In contrast, in the presence of both activator and repressor, the system exhibited an ON/OFF response with a Hill coefficient of 3.2, showing that a transcriptional regulatory network of competing transcription factors can establish a molecular ON/OFF switch (Rossi et al., 2000).

We are aiming to address whether the competing relationship of Ets1/2 and ERF2 in response to ERK activation underlies the switch-like *Otx* transcriptional response (Figure 31B). To this end, we would first like to reveal phosphorylation kinetics of Ets1/2 and ERF2 in response to increasing doses of FGF in ectoderm explants. Are they graded or switch-like? We also aim to develop an in vitro system based on recombinant proteins in order to assess DNA-binding kinetics of these transcription factors in response to increasing amounts of activated ERK. Since ERK-mediated regulation of Ets and ERF is involved in many biological and pathological contexts, outcomes of the project are likely to be broadly relevant and interest the wider scientific community.

### 3) Materials and Methods

#### a. Embryological experiments

Adult *Ciona intestinalis* were purchased from the Station Biologique de Roscoff (France). Cell nomenclature was previously described (Conklin, 1905). Ascidian embryo culture and microinjection have been described (Sardet et al., 2011; Yasuo and McDougall, 2018). Plasmids, *Otx-a-WT>mCherry* and *Otx-a-49Opt>mCherry*, were injected at 0.05 µg/µl.

#### b. Generation of *Otx a*-element reporter constructs

*pOtx-a-WT>mCherry* or *pOtx-a-49Opt>mCherry* were generated using Gibson Assembly Master Mix (New England Biolabs). For *pOtx-a-WT>mCherry*, three PCR-amplified fragments, aWT, bpFOG and mCherry, were assembled together with pBluescript II SK linearized with HindIII and BamHI. aWT fragments were amplified from pENTR-L3-a-element-L4 (Roure et al., 2007) using the following primers: aWT-F (GGTCGACGGTATCGATATTGGATCTGAAGCTCGTTATCTCTAACGGAAGTTT: underlined sequences overlap with pBluescript II SK) and aWT-R (TCCTATCTTAGATATTGAACAATTTCCTTTTCGAAAACCTCCGTTAGAGATA). bpFOG fragments were amplified from pENTR-L3-a-element-L4+pENTR-R4-bpFOG-L5 (Roure et al., 2007) using the following primers: bpFOG-F-aWT (TCAATATCTAAGATAGGAAAGCTTCGTGTATTGTACCG: underlined sequences overlap with aWT fragment) and bpFOG-R (TATGTGTGTTATTTTTGTATAGACCTG).

mCherry fragments were amplified using the following primer pair: mChe-F (ATACAAAATAACACACATAATGGTGAGCAAGGGCGAGGAG: underlined sequences overlap with bpFOG fragment) and mChe-R (we CCGCTCTAGAACTAGTGTTACTTGTACAGCTCGTCCATG: underlined sequences overlap with pBluescript II SK). For *pOtx-a-49Opt>mCherry*, aOpt49 fragments were amplified from *pOtx-a Opt49* ( a kind gift from Dr. Emma Farley, Farley et al., 2015) using the following primers: 49-Opt-F (GGTCGACGGTATCGATATTGGATCTGAAGCTCCTTATCTCTACTACCGGAAG: underlined sequences overlap with pBluescript II SK) and 49-Opt-R (TGCCTTATCTCGAACAACTTC). bpFOG fragments used for the construction of *pOtx-a-49Opt>mCherry* were amplified using 49-Opt-bpFOG-F (GTTGTTTCGAGATAAGGCAAAGCTTCGTGTATTGTACCG: underlined sequences overlap with aOpt49 fragment) and bpFOG-R (TATGTGTGTTATTTTTGTATAGACCTG). All PCR reactions were conducted using AccuPrime Pfx DNA Polymerase (Thermo Fisher Scientific) and resultant constructs were sequence-verified.

### c. Gene knockdown

Morpholinos (MOs) were purchased from GeneTools (Philomath, Oregon). The sequences of ERF2-MO2 and MO4 are as follows: ERF2-MO2, CATAATTAAGTCTTTGATAACAACG; ERF2-MO4, TAAGAAAATCTTGATAGGCAAGCTG. Morpholinos were injected at 0.5mM into

unfertilized eggs, which were kept overnight at 16°C before fertilized. As a control, we used *Msxb*-MO (a kind gift from Dr. Sebastian Darras) (Roure and Darras, 2016) since *Msxb* starts to be expressed at the 64-cell stage, one cell cycle after the effect of ERF2-MOs were analyzed in the current study.

#### d. *In situ* hybridization and RNAscope smFISH

The *in situ* hybridization protocol was previously described (Hudson et al., 2013). Digoxigenin-labelled *mCherry* probes were synthesized from PCR-amplified *mCherry* ORF fragments containing T7 promoter sequence. The RNAscope smFISH and quantification protocols were described in Result Part I.





# **DISCUSSION & PERSPECTIVES**

During neural induction of *C. intestinalis* embryos, happening at the 32-cell stage, ectodermal cells all received antagonistic signals. They received an FGF signal from the mesendodermal cells and ephrin signal from the other ectodermal cells (Bertrand et al., 2003; Ohta and Satou, 2013; Ohta et al., 2015; Picco et al., 2007). These two signals converge in the cell at the level of Ras (Haupaix et al., 2013). All the ectodermal cells are competent to adopt a neural fate. However, among the 16 ectodermal cells, only 4 cells will adopt a neural fate, the others will adopt epidermis fate. Neural fates are adopted by cells according to the activation of the MAPK and ERK pathways by the FGF signalling followed by the transcriptional activation of the *Otx* gene, which is an immediate target gene of ERK signalling in *Ciona* embryos. Previous studies suggest that ERK activation happens in a bimodal manner as the activation of the *Otx* gene. Nevertheless, these studies lack the quantitative approach. My PhD project aimed to uncover the mechanisms involved in the binary choice of ectodermal cells between neural and epidermis fate during neural induction in *Ciona* embryos. In order to unravel the mechanisms involved during neural induction, my project has one main objective: to understand how ectodermal cells interpret the gradual signals of FGF and ephrin to make a binary choice between neural fate and epidermis fate.

To this end, I looked at two different levels of the neural induction process. First I analysed the level of ERK activation in response to FGF signalling, using a semi-quantitative immunostaining protocol in 32-cell stage embryos. This analysis was semi-quantitative, as I developed a semi-quantifiable protocol for dpERK staining and

quantified the pixel intensity of the immunostaining signal using Imaris software (Oxford instruments). Second, I looked at the level of the activation of the *Otx* gene expression thanks to semi-quantitative technique called single molecule Fluorescent In Situ Hybridization (smFISH). This technique is based on RNAscope technology whereby the number of smFISH spots correlates linearly with the amount of *Otx* transcripts.

The project was based on our initial hypothesis that ERK activation operates in an ON/OFF manner in response to graded FGF inputs. Previous results obtained with anti-dpERK immunofluorescence coupled with a tyramide-amplification step supported this hypothesis. However, our newly developed semi-quantitative protocol for anti-dpERK immunofluorescence instead revealed that ERK activation in the ectodermal cells was gradual largely depending on the size of the cell surface contact with the FGF-expressing cells. This observation suggests that the binary response takes place downstream of ERK. I thus studied the activation of the *Otx* gene expression. To quantify this activation, I used the single molecule FISH (smFISH) technique based on RNAscope technology whereby the number of smFISH spots correlates linearly with the amount of *Otx* transcripts. We found that the activation of the *Otx* gene operates in an ON/OFF manner. We then tried to elucidate the role of the ephrin pathway in this cascade. Since ERK activation seemed to be proportional to FGF signals and *Otx* expression is bimodal, it was not clear in which way ephrin signals were involved in the binary fate decision. We found that ephrin signals are required to "dampen" the ERK signalling to permit that only the neural-destined ectoderm cells exhibit ERK activation levels above the threshold for the transcriptional activation of *Otx*.

Despite the significant step-forward in quantitative understanding the ascidian neural induction, much remains to be uncovered in further studies. Our data highlight that ERK activation levels correlate with the cell contact surfaces receiving FGF signals. Here, I will discuss a potential relationship between the level of signals received by ectoderm cells and their contact surface with ligand-expressing cells. During the neural induction, each ectoderm cell receives two antagonistic, an FGF signal from mesendoderm cells and an ephrin signal from neighbouring ectoderm cells. These signals converge at the level of Ras regulation. Then, I will discuss an endocytosis-mediated signal convergence as a potential mechanism underlying ascidian neural induction. Finally, I will discuss potential mechanisms underlying the switch-like transcriptional response of *Otx*.

## I. Correlation between the level of signals and the contact surface between inducing and responding cells

---

In this study (Result Part I), we assume that the cell contact surface between inducing and responding cells is correlated to the level of signals (FGF and ephrin) received by the responding cell. Numerical simulations based on this assumption are able to recapitulate ERK activation levels of a-line ectoderm cells observed in experimental settings (Figure 6 in Result Part I). Here, I will discuss how this assumption would be valid and will propose experiments to address it.

### 1) ephrin/Eph signalling

There are two classes of ephrin ligands; ephrin-A and ephrin-B. ephrin-As are attached to the membrane by a GPI (Glycosyl-Phosphatidyl-Inositol) anchor. ephrin-Bs are also attached to the membrane but by a single transmembrane domain that contains a short cytoplasmic PDZ-binding motif (Lisabeth et al., 2013). This attachment to the membrane is responsible for the cell contact-dependent nature of the ephrin/Eph signalling. Ciona *Efna.d*, involved in neural induction, encodes an ephrin-A ligand (Haupaix et al., 2013; Ohta and Satou, 2013; Ohta et al., 2015; Picco et al., 2007). One ephrin ligand binds to one Eph receptor. This high affinity interface is accompanied by distinct and lower affinity interface that mediates the assembly of a tetrameric complex consisting of two receptors and two ligands (reviewed in Poliakov et al., 2004). In contrast to others RTKs, Eph signalling requires a high density of Eph receptors to be

transduced efficiently. Crystallography studies revealed that the ligand binding triggers oligomerisation by incorporating ligand-unbound Eph receptors through receptor-receptor cis interfaces located in multiple sites in the extracellular domain, resulting in activation of ligand-unbound receptors (Himanen et al., 2010; Seiradake et al., 2010). Study on cell culture has shown that the level of activated receptors could be independent of the level of ligands but rather depends on the abundance of receptors in a given cell (Wimmer-Kleikamp et al., 2004). However, when retinal explants are treated with different amounts of ephrin ligands, induced axon growth induction exhibits a graded response, clearly showing that ephrin signals can mediate concentration-dependent graded cellular responses (Hansen et al., 2004). Apart from the identity of the ligand and the involvement of p120RasGAP as an intracellular effector (Haupaix et al., 2013), we know very little about the Eph signalling involved in ascidian neural induction. Interestingly, our experimental data and numerical simulations indicate that ephrin/Eph signals impact the ERK signalling in a gradual manner. These results support the concept that ephrin/Eph signalling can mediate concentration-dependant graded cellular responses exposed in Hansen et al. (Hansen et al., 2004).

## 2) FGF signalling

In the mouse and human genomes, 22 FGF genes have been described and can be phylogenetically classified into distinct subfamilies: intracellular FGF subfamily, hormone-like or endocrine FGF subfamily and canonical or paracrine FGF subfamily (reviewed in Ornitz and Itoh, 2015). Paracrine FGF ligands, which constitute the largest

subfamily, are secreted and rely primarily on diffusion in the extracellular space to influence target cells. The neural inducer in ascidian embryos, FGF9/16/20, belong to this subfamily (Bertrand et al., 2003). In the ascidian *Halocynthia roretzi*, using morpholino-mediated lineage-specific gene knockdown, it has been shown that FGF9/16/20 is a short-range ligand and only acts between juxtaposed cells (Miyazaki et al., 2007). How FGF diffusion is regulated in ascidians remains unknown, in mammalian embryogenesis Heparan Sulfate Proteoglycans (HSPGs) are known to play a role in FGF diffusion (reviewed in Ornitz and Itoh, 2015). HSPGs are glycoproteins consisting of a core protein, such as syndecans, glypicans and perlecan, to which heparan sulfate glycosaminoglycan polymer chains are covalently linked. HSPGs are known to regulate diffusion of paracrine FGF ligands via direct association (Matsuo and Kimura-Yoshida, 2014). HSPG binding increases the affinity of FGF to the FGFR and reduces FGF ligand diffusion in the extracellular space, effectively increasing the local concentration of ligand (reviewed in Ornitz and Itoh, 2015). For instance, during the collective cell migration in zebrafish lateral line, the loss of HS side chains of syndecans and glypicans results in increased diffusion of FGF ligands into the surrounding tissue (Venero Galanternik et al., 2015). Similarly, local retention of FGF4 and FGF8 ligands by HS side chains was shown to be important for the activation of FGF signalling in mouse extraembryonic ectoderm (Shimokawa et al., 2011). The distribution of HSPGs in ascidian embryos and how it might contribute to cell signalling remain to be addressed.

### 3) Distribution at the cell surface

So far, information about the distribution of FGF and ephrin ligands and receptors at the surface of the cell in ascidian are missing. Concerning Eph signalling, we know that it required pre-clustered ligands to induce efficient signal. Prior to EphR activation, receptors are widely distributed at the cell surface. After activation, ephrin ligands clusters appear and are necessary to induce a full kinase activity of the EphR. Thus, upon stimulation, dimerization of EphR is not sufficient for an optimal downstream signal but also required high density of ligands locally to induce full signalling (Nikolov et al., 2013).

It is known that some cells adapt the distribution of receptors and ligands on their surface depending on different factors of their environment through intracellular trafficking (Le Roy and Wrana, 2005). Generally, after synthesis, a new receptor will be addressed at the membrane. Here, upon ligand stimulation it can be internalized and then can follow two distinct paths: it can be either recycled and send back to the membrane or send to the lysosome for degradation. Then, the presence of a receptor at the cell surface depend on three different mechanisms: the delivery at the membrane of new receptors right after their synthesis, their internalization and their recycling.

Some factors as well as ligand concentration can affect the way cells will internalize their receptors and the way they treat them. It has been shown that EGFR are internalized either by clathrin mediated endocytosis at low ligand concentration or by both clathrin dependant and clathrin independent endocytosis when ligand concentration is high (Sigismund et al., 2005). Furthermore, it has been proposed that

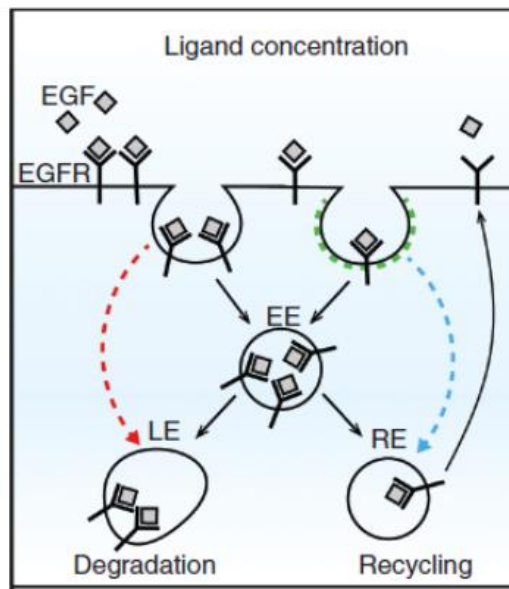


**Figure 32:** Ligand concentration can affect the clathrin-dependent or -independent internalization leading to different fate for the internalized receptors. Red arrow is in high EGF situation and blue arrow is in low EGF situation. Green dots correspond to clathrin. EE: Early Endosome, LE: Late Endosome, RE: Recycling Endosome. (Adapted from Miaczynska 2013)

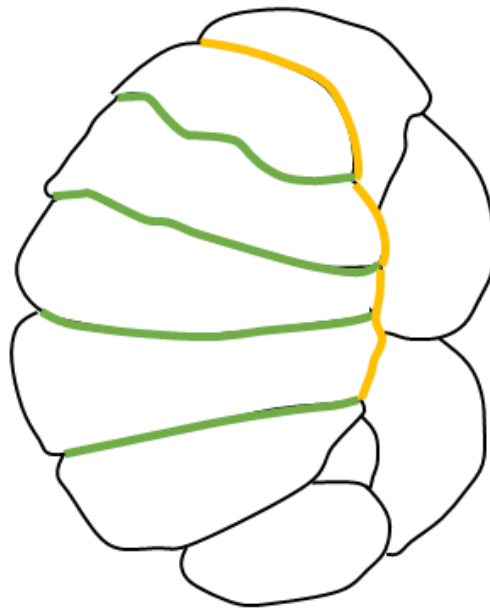
clathrin-mediated endocytosis leads preferentially to recycling of EGFR and that clathrin independent endocytosis leads to lysosomal degradation of EGFR (Figure 32) (Sigismund et al., 2008). This mechanism allows a sustained signalling thanks to the continuous recycling and redelivery of the receptors at the membrane when ligand concentration is low while high ligand concentration will lead to receptors degradation and then prevent cells to be overstimulated. This concept proposing that external factors can influence the recycling or degradation of receptors is very important to understand how cells adapt their signalling to the environmental clues and can be very interesting to go further in the comprehension of the link between cell surface and signal quantity. However, how FGF and Eph receptors are distributed on the cell surface of the 32-cell stage embryo is still unknown. We can hypothesize that this distribution is dynamic and that cells modulate the density of their receptors depending on the signal they receive.

#### **4) Perspectives**

In order to test our hypothesis that cell contact surfaces between inducing and responding cells is linked to the signalling level, it is necessary to quantify immediate early events downstream of ligand-mediated receptor activation. To this end, we have generated a series of constructs based on bimolecular fluorescence complementation (BiFC) assay. The BiFC assay is based on structural complementation between two non-fluorescent N-terminal and C-terminal fragments of a fluorescent protein. Our BiFC paired constructs include (1) Eph3-VN (VN: Venus N-terminal) and Eph3-VC

(VC: Venus C-terminal) to monitor ephrin-mediated receptor oligomerisation, (2) Eph3-VN and p120RasGAP-VC which associate with each other upon ephrin stimulation (Haupaix et al., 2013), (3) FGFR-VN and FGFR-VC to monitor ligand-mediated dimerisation, (4) PH-VN (PH: Pleckstrin homology domain) and Grb2-VC to monitor FGF-dependent membrane localization of Grb2 (Hanafusa et al., 2002). The BiFC assay allows quantitative imaging of protein-protein interactions. If these constructs turn out to be able to monitor interactions of these protein pairs in ascidian embryos, we expect to observe the ephrin-induced protein-protein interactions specifically in lateral membrane domains of ectoderm cells while the FGF-induced protein-protein interactions in their basal membrane domain. We also expect that mean pixel signal intensities in the corresponding membrane domains would be similar between different a-line ectoderm cells. We are hoping that this approach would allow us to validate the assumption that the cell contact surface areas between inducing and responding cells correlate with the signalling levels in responding cells.

**A**



- Surface contact with FGF-expressing cells
- Surface contact with ephrin-expressing cells

**B**

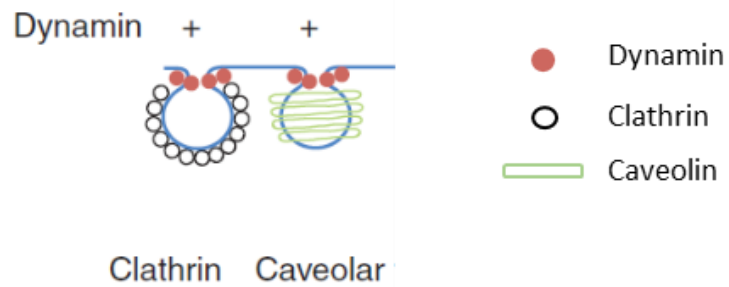


**Figure 33:** (A) Scheme of a sagittal cut of a 32-cell-stage embryo of *C. intestinalis*. Anterior is on the top and vegetal on right. (B) Clathrin and caveolin mediated endocytosis both need dynamin (Adapted from Mayor, Parton, and Donaldson 2014).

## II. Mechanisms involved in the convergence of FGF and ephrin signalling

---

During ascidian neural induction, each ectodermal cell receives two antagonistic signal inputs: FGF9/16/20 at the basal membrane and ephrin at the lateral membrane (Figure 33A). Previous study has shown that FGF and ephrin signals converge at the level of Ras regulation (Haupaix et al., 2013). Then, how do two signalling pathways activated in distinct membrane domains regulate the membrane-bound Ras?

After their activation, RTKs are internalized by endocytosis. RTKs continue to activate the downstream cascade from endocytic vesicles until their degradation or recycling (reviewed in Miaczynska 2013). Depending on the RTK type, different endocytosis pathways are involved. The most commonly used pathway is the clathrin-mediated endocytosis but other mechanisms exist such as the caveolin-mediated endocytosis (Figure 33B). Each of these endocytosis pathways uses different proteins. Clathrin is the major component of the clathrin coated pits. Clathrin proteins will associate via an adapter protein complex called AP-2 (Assembly Protein 2). AP-180, another member of the AP family, plays a crucial role in AP-2 recruitment. Caveolin-mediated endocytosis is another type of endocytosis. This endocytic pathway is not as well-known as the clathrin-mediated endocytosis and is completely independent of the clathrin molecule. However, it is clear that caveolin coated vesicle bud off from the plasma membrane as vesicle carriers. Dynamin is common to the Clathrin mediated endocytosis and the caveolin-mediated endocytosis. This GTPase is crucial for the fission of the vesicle from the plasma membrane.

Regarding the internalization of FGFR, a study demonstrated that clathrin inhibition in *Xenopus* embryos leads to an inhibition of FGF-dependant ERK activation preventing mesoderm formation (Jean et al., 2010). Later, using live cell imaging techniques, it has been shown that activated FGFRs are internalized in the cell by clathrin coated vesicle (Auciello et al., 2013; Haugsten et al., 2016).

Finally, internalization of EphR-ephrin complexes shows a specific feature: complexes can be internalized by both EphR and ephrin expressing cells. This process called trans-endocytosis can remove all the EphR-ephrin complexes from the cell surface and then is a key process in the cell repulsion role of the ephrin/EphR signalling. Depending on receptor types, Eph receptors are internalized by different endocytic pathways. While EphB1 are internalized through caveolin endocytosis (Vihanto, 2006), EphA4 in the adult mouse brain are localized in clathrin coated vesicle. A role of this EphA4 traffic in the synaptic plasticity has been suggested (Bouvier et al., 2010).

For a long time, endocytosis was thought to be a mechanism to switch off plasma membrane receptor signalling. However, it has been shown that the role of endocytosis is not only to terminate the signal from membrane receptors but it also permits internalization of signalling components. Indeed, it has been proven that receptors can still be in an active form once internalized in endosomes. Then it has been demonstrated that endosomes can be meeting points between different signalling pathways. It can regulate the localization of signalling complexes but also restrict spatially the signalling activity (reviewed in Di Fiore and De Camilli 2001). Another role of endosomes is to transport signalling components from the membrane to the nucleus

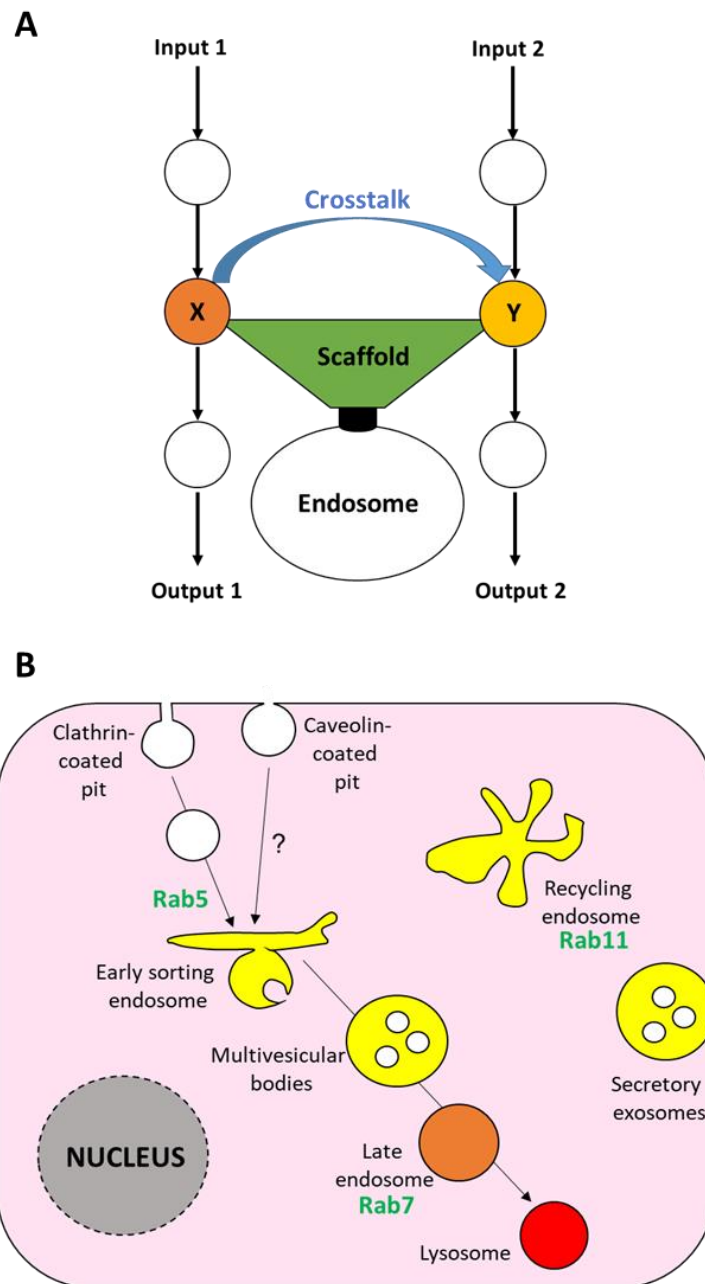


**Figure 34:** (A) Crosstalk between two signalling pathways can localize in endosomes. Endosomes can then serve as physical platform via scaffold protein for convergence of signalling pathway (Adapted from Pálffy et al., 2012). (B) Endocytic pathway (Adapted from Le Borgne, 2005).

(Casaletto and McClatchey, 2012). This role of endosomes as “meeting spot” for signalling components permits therefore crosstalks between signalling pathway (Murphy et al., 2009; Pálffy et al., 2012) (Figure 34A). For instance, in the EGF/MAPK pathway, MP1-p14 scaffold complex is anchored to late endosomal membrane by p18 protein. It localizes MEK1 to late endosomes and promotes the phosphorylation of ERK1/2 (Teis et al., 2006). Later study of the localization of a GFP-tagged Ras protein has shown that Ras/MAPK signalling pathway does not only localized at the plasma membrane but also exhibits activity in subcellular compartments including endosomes (Fehrenbacher et al., 2009).

### **Perspectives**

So far, the mechanisms responsible for EphR and FGFR internalization are unknown in *Ciona* embryos. However, we suspect that endocytosis mechanisms could be involved in the integration of FGF and ephrin signals during the neural induction process of *Ciona intestinalis* embryo. Indeed, during ascidian neural induction, each ectodermal cells receives two antagonistic signal inputs: FGF9/16/20 at the basal membrane and ephrin at the lateral membrane (Figure 33A). Previous study has revealed that FGF and eohrin signals converge at the level of Ras regulation (Haupaix et al., 2013). It remains however to demonstrate how two signalling pathways activated in distinct membrane domains can regulated the membrane-bound Ras. We suspect that endocytosis crosstalk between these two antagonistic signalling can be implied in the convergence of the signals.

To do so, we could use a drug inhibiting all the endocytic pathways. Dynasore is an inhibitor of the dynamin, a protein necessary for both clathrin and caveolin-mediated endocytosis (Macia et al., 2006). Preliminary trials of Dynasore treatment on *Ciona* embryos gave no clear results so far. Nevertheless, a more thorough characterization of the effect of this treatment is required. Additionally, it would be interesting to target more specifically either the clathrin or the caveolin endocytic pathway. To do so, we could use dominant negative form of the AP180 complex to inhibit the clathrin endocytosis or use a specific inhibitor of the clathrin-mediated endocytosis, such as the chlorpromazine (Vercauteren et al., 2010; Wang et al., 1993). To block specifically the caveolin-mediated endocytosis, we could use a dominant negative form of caveolin protein or use a specific inhibitor treatment like incadronate which blocks *CAV1* mRNA (Iguchi et al., 2006). Once clathrin or caveolin mediated endocytosis would be found to be implicated in the integration of FGF and ephrin signals, the use of tagged clathrin and tagged caveolin coupled to fluorescent tagged receptors could allow to see the colocalization of activated receptors and clathrin or caveolin coated vesicles. This kind of experiments could confirm the inhibitor treatment. Depending of their stages, different markers can be used to differentiate endosomes. Additionally, we should also study the potential colocalization of Ras in the endosomes. Tagged Ras coupled with tagged endosomes markers should allow us to confirm the endocytosis crosstalks between FGF and ephrin signalling.

Another interesting clue is the position of the nucleus in the cells. By simple observation, we can see that the nucleus of the neural precursor cells are localized in

the middle of the cell. In other cells, the nucleus is localized in an apical position far from the “bottom” and then from the FGF signal. Is there any possibility that, besides the fact that they do not receive as much FGF as the neural precursors, the distance between the bottom membrane and the nucleus can dilute the inducing signal? Mathematical approach revealed that in a system where GEFs are bound to the membrane and GAPs free in the cytoplasm, as the cell grows, the substrate becomes progressively inactivated. Then, distance in the cell is linked to signal propagation (Meyers et al., 2006). This line of research could be promising and should be considered in further studies.

### III. Potential mechanisms behind the ON/OFF response at the level of the *Otx* gene

---

During neural induction process, ectodermal cells have to integrate a gradual input (FGF) into a binary fate, neural or epidermal. In response to FGF stimulation, neural precursors will activate expression of the *Otx* gene. The *Otx* expression activation by FGF signalling takes place directly, without protein synthesis (Bertrand et al., 2003) and in about 20 minutes (Result Part I). This time is sufficient for cells to interpret the gradual inductive signal (FGF9/16/20) into an ON/OFF response at the level of *Otx*.

In *Drosophila* syncytium blastoderm embryos, a relative difference in Bcd concentration of 10% between two neighbouring nuclei can be converted into an ON or OFF state of the *hb* locus in the posterior border of *hb* expression domain (Porcher et al., 2010). Consistently, the *hb* gene responds to Bcd gradient in a ultrasensitive manner with a Hill coefficient of 7 (Lucas et al., 2018). As shown above (see Result Part I), when *Otx* expression levels were plotted as a function of ERK levels, non-linear regression gave best Hill coefficients of 3.374, 6.65, and 10.68 for three independent experiments. While they are highly variable, the lowest value, 3.4, still implies that the *Otx* transcriptional response to ERK activation is sigmoidal. Contrary to the *Drosophila* Bcd gradient system the difference of ERK activation levels between *Otx*-ON cells (a6.5) and *Otx*-ON/OFF cells (a6.7) is threefold in ascidian neural induction. This large difference in the input suggests that the transcriptional response of *Otx* to ERK inputs does not need to be as steep as that of the *hb* gene to Bcd gradient. Since the ERK

activation level in ectoderm cells correlate with the area of their cell contact surface with mesendoderm cells, the unique cellular configuration of the 32-cell embryo is a critical determinant underlying the spatial precision of *Otx* expression.

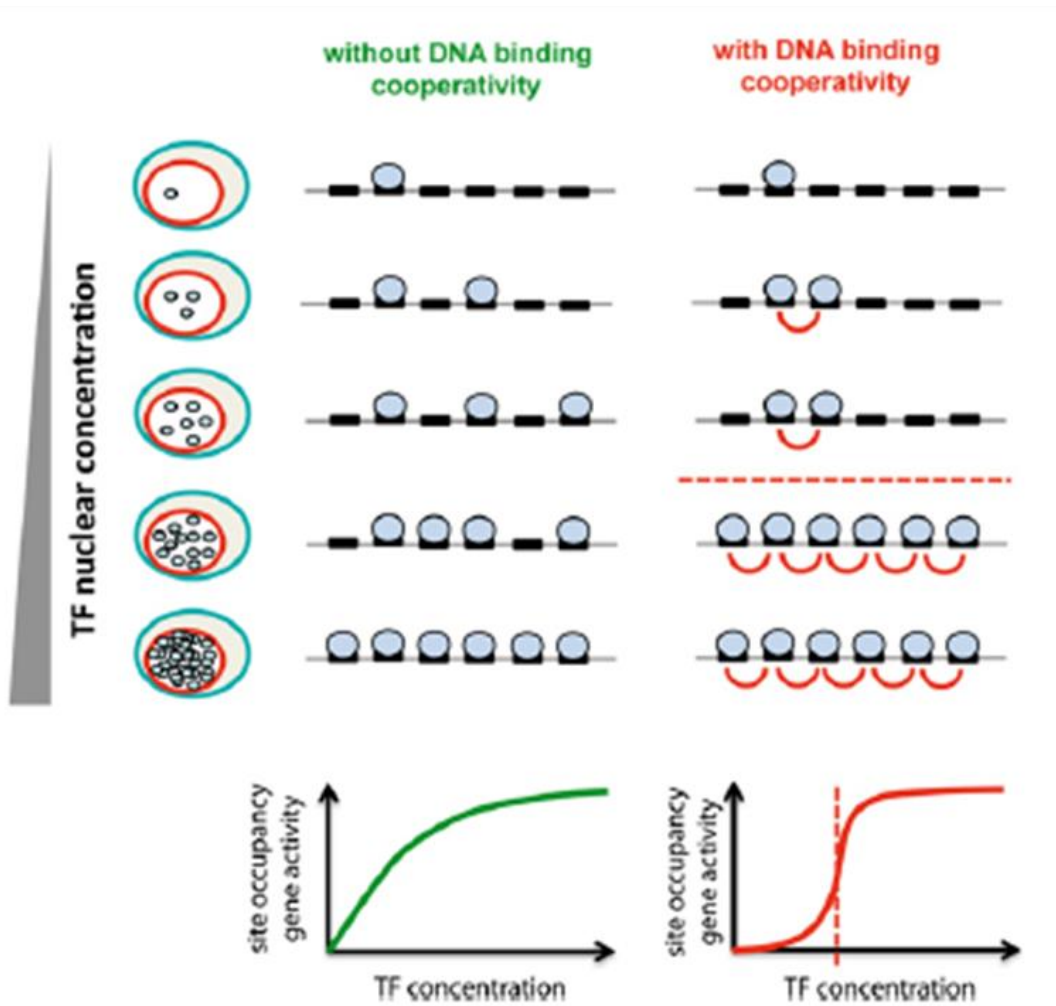
Several mechanisms can be involved in switch-like transcriptional responses. For instance, suboptimization of developmental enhancers has been shown to be involved in different processes in animal development (Crocker et al., 2015; Swanson et al., 2011). Some developmental enhancers show an under-optimized conformation in terms of the affinity of TF-binding sites and the spacing between sites, leading to a precise transcriptional response. In the case of *Otx*, the a-element enhancer has been shown to be suboptimized and that this suboptimization is required for tissue specificity in *Ciona* embryos (Farley et al., 2015). Nevertheless, our study of the optimized a-element at the 32-cell stage gives no evidence of an implication of this suboptimization in the spatial precision of the *Otx* expression during neural induction in *Ciona* embryos.

Another potential mechanism to explain the switch-like *Otx* transcriptional responses includes an activator/repressor system competing same binding sites (Rossi et al., 2000). Our study has shown that ERF2 is a transcriptional repressor of the *Otx* gene and a potential candidate for the competitor of Ets1/2 (See results part, section II). As described above, we are designing experiments to address whether the ERK-mediated competition between Ets1/2 and ERF2 for binding sites constitute the mechanism generating the switch-like *Otx* transcriptional response.

In addition to the mechanisms described above, we should also consider a cooperativity mechanism. Cooperative binding has first been studied in the oxygen

binding to the hemoglobin by Christian Bohr in 1904 (Bohr, 1904). When an oxygen molecule binds to one of hemoglobin's four binding sites, the affinity to oxygen of the three remaining available binding sites increases, allowing the second oxygen molecule to bind more easily, and the third and fourth even more easily. Cooperative binding can also be found in nucleic acid such as TF binding. In this context, cooperative binding happens through groups of adjacent binding sites for the same TF called homotypic clusters. Cooperative binding can be direct or indirect. Direct cooperativity happens through the direct TF-TF interactions whereas the indirect cooperativity happens without physical interaction between TFs, meaning that homotypic clusters allow TFs to stabilize each other's binding. If TF binding operates in a non-cooperative way, the proportion of TF-bound sites increases gradually when the concentration of TF increases. However, if the binding of TFs is cooperative, the interaction TF-TF can stabilize the binding and then the proportion of occupied sites shows a sigmoid shape as the function of TF concentration (Figure 35B).

Cooperative binding has been shown to be involved in different developmental context. Homotypic clusters are found in cis-regulatory modules of many developmental genes (Lifanov, 2003). Bcd cooperative binding seems to be one of the key mechanism by which the Bcd gradient along the A-P axis of the *Drosophila* embryo is converted into a sharp ON/OFF expression of Bcd target genes (Burz 1998). In the *Otx* a-element, there is two ETS binding sites showing different affinities (Farley et al., 2015). These two ETS binding sites are present next to each other forming a homotypic pair (Figure 35A). This proximity could allow interaction and stabilization between

**A****B**

**Figure 35:** (A) *Otx* a-enhancer is a 69bp sequence with 3 GATA binding sites and 2 ETS binding sites (Adapted from Farley 2015). (B) Cooperative binding of TFs generates sharp transcriptional response. If binding of TFs is not cooperative, the proportion of bound sites increases gradually when the concentration of TF increase. If binding of TFs is cooperative, the interaction TF-TF can stabilize the binding and then the proportion of occupied sites shows a sigmoid shape as a function of TF concentration (From Giorgetti et al., 2010).

Ets1/2 during their binding to the sites, potentially leading to cooperative binding. In order to test cooperative binding of Ets1/2 transcription factor on *Otx* a-enhancer, we could design construction of different *Otx* a-enhancer version. We should try for instance to separate spatially the two Ets binding sites and inject this construction in Ciona embryos and look the consequence at the level of *Otx* gene.

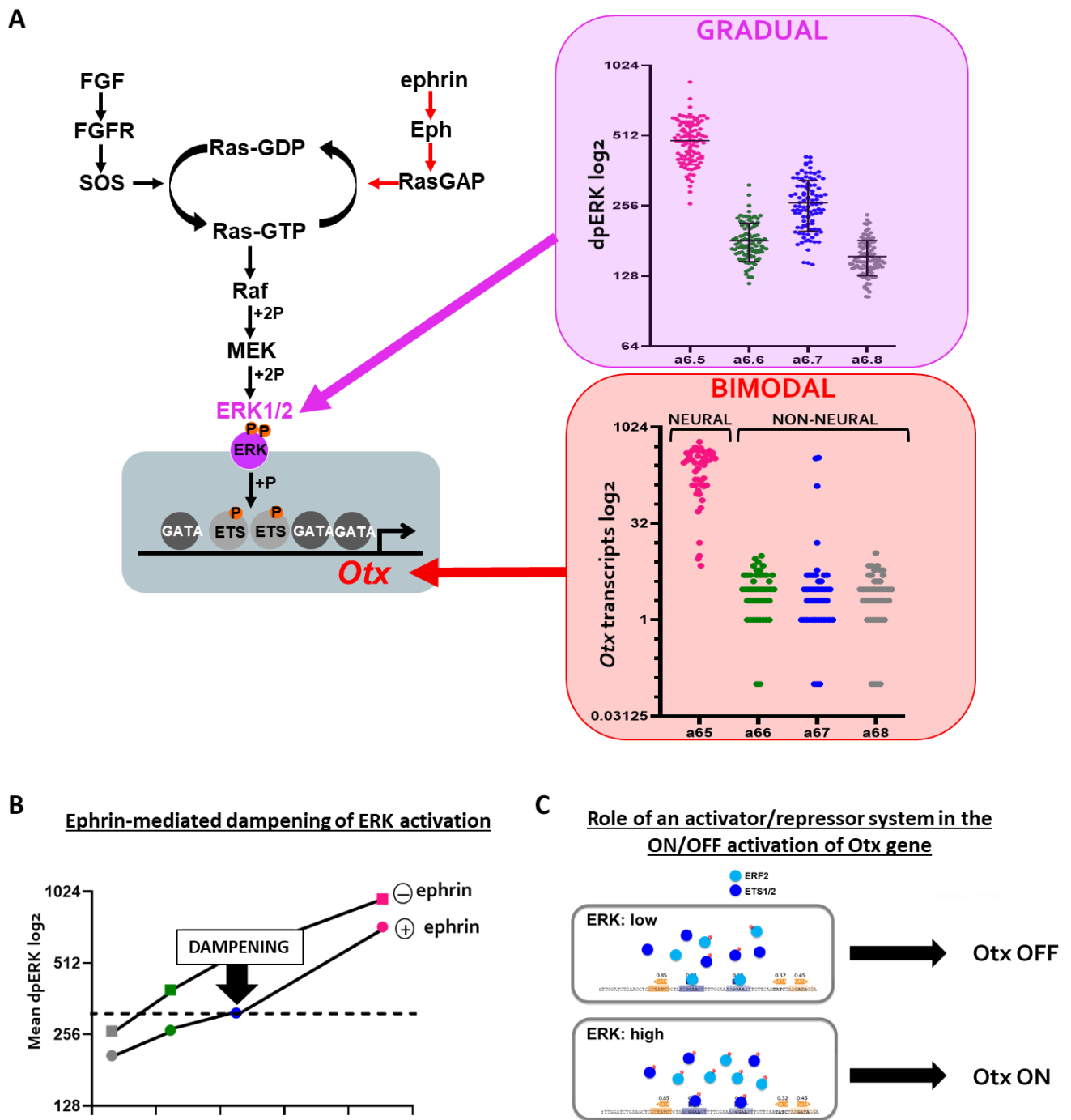


**Figure 36:** Overview of my PhD project. (A) Quantitative study of the ERK activation and the activation of the *Otx* gene expression (B) Dampening role of the ephrin pathway in the ERK activation is crucial for the spatial precision of *Otx* expression (C) Potential role of Ets1/2-ERF2 system in the transcriptional regulation of *Otx* expression.

# CONCLUSION

My project aim to study in a quantitative manner the neural induction process in *Ciona intestinalis* embryos to understand how cells interpret a gradual input into a binary response. All my results taken together give strong clues for a better understanding of the step-like response of *Otx* expression in neural precursors during the neural induction in *Ciona intestinalis* embryos. Results of my project suggest the following model for neural induction in *Ciona* embryos: at the 32-cell stage, all ectodermal cells receive an FGF signal, acting as a neural inducer, and an ephrin signals which antagonize FGF signal. FGF activate the MAPK/ERK pathway and the amount of activated ERK correlates with the surface contact with the FGF expressing cells. The role of the ephrin pathway is to attenuate the global activation of ERK. The activation of the *Otx* gene transcription is happening in a step-like manner i.e. bimodal. The attenuation of ERK by ephrin signal is crucial to permit the spatial precision of the *Otx* gene expression.

At the level of the activation of *Otx* expression, I began to study mechanisms involved in the ON/OFF activation of *Otx* transcription. An activator/repressor system involving Ets1/2 and ERF2 seems to play a role in the ON/OFF activation of the *Otx* gene expression. Nevertheless, further studies need to be realize to confirm the role of this activator/repressor system and to find other potential mechanisms involved in this ON/OFF response.

Thus, I propose the following overview to resume my PhD project (Figure 36).



# APPENDICES

## APPENDIX 1: FGF and ephrin signalling

At the multicellular level, cell signalling plays a crucial role in cell fate. Indeed, molecules like growth factors or hormones can lead a cell to adopt different fates. For instance, in the same cell type, EGFR activation will lead to cell proliferation contrary to NGFR activation which will promote neurite outgrowth (Marshall, 1995). These major factors enter in action by binding specific cell receptors which are activated and will transmit the signal inside the cell. Discovered in the 1960's, RTKs have been studied for a long time and are involved in important cellular processes like differentiation, cell migration and proliferation. Thus, mutations of RTKs generate cancer processes and other diseases (Ullrich and Schlessinger 1990; Lemmon and Schlessinger 2010; Du and Lovly 2018; Butti et al. 2018; Ornitz and Itoh 2015; Schlessinger 2014). All RTKs share a similar structure with an extracellular ligand binding region, one trans-membrane helix and a cytoplasmic region including juxta-membrane domain and tyrosine kinase domain (TKD). When ligands bind the receptors, two receptor monomers will dimerize through their extracellular domain and form an activated RTK dimer. TDKs will be released from auto-inhibition and RTK phosphorylate downstream signalling proteins. During the neural induction process in *C. intestinalis* embryos, the two signalling involved, FGF and ephrin/Eph, are activated via RTKs.

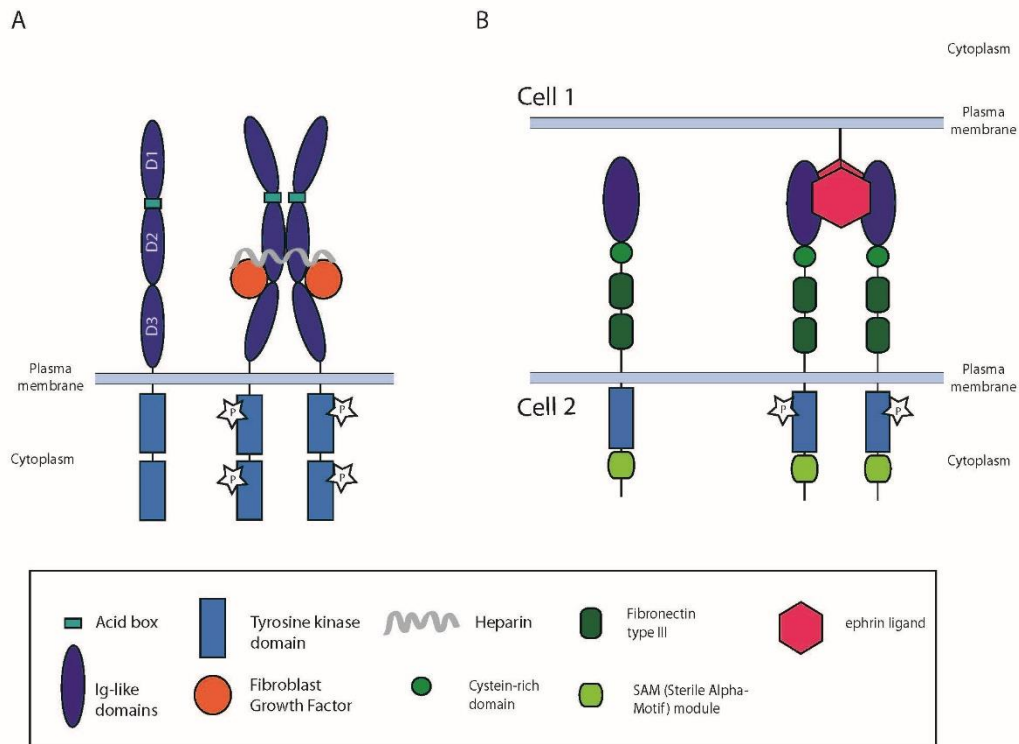


**Figure 37:** (A) FGFR are composed of three immunoglobulin-like (Ig-like) domains and an acid box in their extracellular part and two Tyrosine Kinase domains (TKDs) in their intracellular domains. FGF ligands bind FGFR on their D2-D3 Ig-like domains. (B) EphR and ephrin ligand structure. EphR-A and EphR-B have the same structure. They are composed of an Ig-like domain, a Cystein-rich domain (CRD), 2 Fibronectin type III domains (FN III) on their extracellular region. On their intracellular part, EphR are composed of a TKD and a Sterile Alpha Motif (SAM). Ephrin ligands bind EphR by its Ig-like domain. (reviewed in Lemmon and Schlessinger, 2010)

### a. FGF signalling

Since its discovery in 1974, Fibroblast Growth Factors (FGF) signalling pathway has been proved to be involved in a lot of biological processes such as organogenesis, homeostasis and differentiation in metazoan embryogenesis (Böttcher and Niehrs, 2005; Ornitz and Itoh, 2015). FGF receptors (FGFRs) are composed of three extracellular immunoglobulin-like domains (D1, D2 and D3) a transmembrane helix and two intracellular tyrosine kinase domain (figure 37A) (Lemmon and Schlessinger, 2010). FGF ligand, which diffuses from the emitting cell, binds to a monomere of FGFR by interacting with D2 and D3. FGF binding will trigger the dimerization of two complexes [FGFR-FGF]. Heparan Sulfate (HS), one the FGFR/FGF cofactors, interacts with FGF and FGFR and is suggested to increase affinity of FGF-FGFR dimers (Rapraeger et al., 1991). First target phosphorylated by RTKS are RTKS themselves. FGF ligand binding induces FGFR dimerization which brings the intracellular Tyrosine Kinase domains close enough and properly orientated to permit transphosphorylation. After auto-phosphorylation, target molecules are recruited either directly by phosphor-tyrosine of the receptors or by binding docking proteins. Four major intracellular signalling are regulated by activated FGFR: Ras-MAPK, PI3K-AKT, PLC $\gamma$  and STAT pathways. I will detail right under only the Ras-MAPK pathway. FGF Receptor Substrate 2  $\alpha$  (FRS2  $\alpha$ ) is the docking protein permitting target molecules to be phosphorylated by FGFRs (Ong et al., 2000). Phosphorylated FRS2  $\alpha$  recruits the adaptor protein Growth factor Receptor-Bound 2 (Grb2). Grb2

<i>C. intestinalis</i> FGF	Expression	Link with FGFs vertebrates
FGF L	No zygotic signal, maternal signal ++	
FGF 11/12/13/14	NONE	Confidently assigned
FGF 3/7/10/22	From neurula stage	Speculatively orthologous
FGF 4/5/6	No zygotic signal, maternal signal ++	Speculatively orthologous
FGF 8/17/18	From 64c stage	Confidently assigned
FGF 9/16/20	From 16c stage	Speculatively orthologous

**Table 2:** FGF ligands genes identified in *Ciona intestinalis* genome. (Imai, 2004; Satou et al., 2002)

then recruits the Guanine Exchange Factor (GEF) Son Of Sevenless (SOS). SOS will activate RAS GTPase which activate the downstream components of the MAPK pathway (Ornitz and Itoh, 2015). In the solitary ascidian *C. intestinalis* genome, six FGF ligands genes have been identified. Two of these genes were confidently assigned by phylogenetic analysis to vertebrate FGF8/17/18 and FGF 11/12/13/14. Three of the other Ciona FGF ligands genes might be orthologous to vertebrate FGF 3/7/10/22 FGF 4/5/6 and FGF 9/16/20. Finally, the last FGF ligand genes, Ci-FGFL, was not assigned to any types of vertebrates FGFs (Table 2). Ci-FGFR is the only FGFR gene in *C. intestinalis* genome. The best hit protein in the human proteome is FGFR-1 (Satou et al., 2002; Satou et al., 2003).

#### **b. Ephrin/EphR signalling**

After its discovery in 1987 (Hirai et al., 1987), ephrin/Eph (Erythropoietin-Producing Hepatocyte) signalling is known to be involved in many cellular processes (reviewed in Pasquale 2005). There are 2 classes of ephrin ligands: ephrin-a ligands which are attached to the membrane by a GPI (Glycosyl-Phosphatidyl-Inositol) anchor and ephrin-b ligands which are fixed to the membrane and possess a short cytoplasmic domain that can be phosphorylated to transmit the reverse signalling (Lisabeth et al., 2013). Ephrin receptors (EphRs) are composed of 1 Ig domain, 1 Cysteine-rich domain and 2 fibronectin III on their extracellular part. On the intracellular side, they possess 1 Tyrosine-kinase domain and a SAM (Sterile Alpha Motif) domain known to be involved

in the receptor activation (figure 37B) (Lemmon and Schlessinger, 2010; Shi et al., 2017). Activation of EphR happens through ephrin ligand binding. One ephrin ligand binds one EphR. After ephrin binding, EphR bind with each other via extracellular domain with low affinity forming heterotetramers. The ligand binding also triggers the oligomerization at the EphR-EphR level by recruiting other EphR in cis (Wimmer-Kleikamp et al., 2004). It is important to note that induction of efficient Eph signalling does not only rely on ligand binding and dimerization but also requires pre-clustered ligands (Davis et al., 1994). Thus, dimerization of EphR is not sufficient for an optimal signal downstream but high density of ligands locally is required to induce full signalling (Nikolov 2013). Another specific feature of the Eph-ephrin pathway is its ability to induce signalling in both ways: a forward signalling happening in the EphR-expressing cells and a reverse signalling in the ephrin-expressing cells.

In *C. intestinalis* genome, six different genes coding for EphR have been identified. Proteome comparison has shown that the best hit of *Ci-Eph1*, *Ci-Eph2* and *Ci-Eph3* in the human proteome is *EphRA4* receptor. For *Ci-Eph4* and *Ci-Eph-like*, best hit in human proteome is *EphRA7*. Finally, *EphRB3* is the best hit in the human proteome for *Ci-Eph5*. Additionally, *C. intestinalis* genome contains five genes for ephrin ligands: four of this gene are ortholog with ephrinA type and one with ephrinB type (Table 3) (Satou 2003).

Gene name	Best Hit with Human proteome	Other supporting evidence for the orthology
<i>Ci-EphrinA-a</i>	Ephrin-A4 precursor	Lacking a transmembrane domain, which is common feature of type-A ephrins
<i>Ci-EphrinA-b</i>	Ephrin-A5 precursor	Lacking a transmembrane domain, which is common feature of type-A ephrins
<i>Ci-EphrinA-c</i>	Ephrin-A3 precursor	Lacking a transmembrane domain, which is common feature of type-A ephrins
<i>Ci-EphrinA-d</i>	Ephrin-A4 precursor	Lacking a transmembrane domain, which is common feature of type-A ephrins
<i>Ci-EphrinB</i>	Ephrin-B3 precursor	Containing a transmembrane domain, which is common feature of type-B ephrins
<i>Ci-Eph1</i>	Ephrin type-A receptor 4 precursor	Tyrosine Kinase Domain, SAM domain
<i>Ci-Eph2</i>	Ephrin type-A receptor 4 precursor	Tyrosine Kinase Domain, SAM domain
<i>Ci-Eph3</i>	Ephrin type-A receptor 4 precursor	Tyrosine Kinase Domain, SAM domain
<i>Ci-Eph4</i>	Ephrin type-A receptor 7 precursor	Tyrosine Kinase Domain, SAM domain
<i>Ci-Eph5</i>	Ephrin type-B receptor 3	Tyrosine Kinase Domain, SAM domain
<i>Ci-Eph-like</i>	Ephrin type-A receptor 7 precursor	Tyrosine Kinase Domain

**Table 3:** Ephrin and EphR genes and their products in the *Ciona intestinalis* genome  
Adapted from Satou 2003



# REFERENCES

- Abu-Arish, A., Porcher, A., Czerwonka, A., Dostatni, N. and Fradin, C.** (2010). High Mobility of Bicoid Captured by Fluorescence Correlation Spectroscopy: Implication for the Rapid Establishment of Its Gradient. *Biophys. J.* **99**, L33–L35.
- Adachi, M., Fukuda, M. and Nishida, E.** (1999). Two co-existing mechanisms for nuclear import of MAP kinase: passive diffusion of a monomer and active transport of a dimer. *EMBO J.* **18**, 5347–5358.
- Albeck, J. G., Mills, G. B. and Brugge, J. S.** (2013). Frequency-Modulated Pulses of ERK Activity Transmit Quantitative Proliferation Signals. *Mol. Cell* **49**, 249–261.
- Alié, A., Hiebert, L. S., Scelzo, M. and Tiozzo, S.** (2020). The eventful history of nonembryonic development in tunicates. *J. Exp. Zool. B Mol. Dev. Evol.*
- Altan-Bonnet, G. and Germain, R. N.** (2005). Modeling T cell antigen discrimination based on feedback control of digital ERK responses. *PLoS Biol.* **3**, e356.
- Ando, R., Mizuno, H. and Miyawaki, A.** (2004). Regulated Fast Nucleocytoplasmic Shuttling Observed by Reversible Protein Highlighting. *Science* **306**, 1370–1373.
- Aoki, K., Yamada, M., Kunida, K., Yasuda, S. and Matsuda, M.** (2011). Processive phosphorylation of ERK MAP kinase in mammalian cells. *Proc. Natl. Acad. Sci.* **108**, 12675–12680.
- Aoki, K., Kumagai, Y., Sakurai, A., Komatsu, N., Fujita, Y., Shionyu, C. and Matsuda, M.** (2013). Stochastic ERK Activation Induced by Noise and Cell-to-Cell Propagation Regulates Cell Density-Dependent Proliferation. *Mol. Cell* **52**, 529–540.
- Attardi, A., Fulton, T., Florescu, M., Shah, G., Muresan, L., Lenz, M. O., Lancaster, C., Huisken, J., van Oudenaarden, A. van and Steventon, B.** (2018). Neuromesodermal progenitors are a conserved source of spinal cord with divergent growth dynamics. *Development* **145**,.
- Auciello, G., Cunningham, D. L., Tatar, T., Heath, J. K. and Rappoport, J. Z.** (2013). Regulation of fibroblast growth factor receptor signalling and trafficking by Src and Eps8. *J. Cell Sci.* **126**, 613–624.
- Balaskas, N., Ribeiro, A., Panovska, J., Dessaud, E., Sasai, N., Page, K. M., Briscoe, J. and Ribes, V.** (2012). Gene Regulatory Logic for Reading the Sonic Hedgehog Signaling Gradient in the Vertebrate Neural Tube. *Cell* **148**, 273–284.
- Bardwell, A. J., Abdollahi, M. and Bardwell, L.** (2003). Docking sites on mitogen-activated protein kinase (MAPK) kinases, MAPK phosphatases and the Elk-1 transcription factor compete for MAPK binding and are crucial for enzymic activity. *Biochem. J.* **370**, 1077–1085.
- Barkoulas, M., van Zon, J. S., Milloz, J., van Oudenaarden, A. and Félix, M.-A.** (2013). Robustness and Epistasis in the *C. elegans* Vulval Signaling Network Revealed by Pathway Dosage Modulation. *Dev. Cell* **24**, 64–75.

- Berset, T., Hoier, E. F., Battu, G., Canevascini, S. and Hajnal, A.** (2001). Notch Inhibition of RAS Signaling Through MAP Kinase Phosphatase LIP-1 During *C. elegans* Vulval Development. *Science*.
- Bertrand, V., Hudson, C., Caillol, D., Popovici, C. and Lemaire, P.** (2003). Neural tissue in ascidian embryos is induced by FGF9/16/20, acting via a combination of maternal GATA and Ets transcription factors. *Cell* **115**, 615–627.
- Bohr, C.** (1904). Die Saurestoffe des genuinen Blutfarbstoffes und des aus dem Blute darstellten Hämoglobins. *Cent. Für Physiol* **23**,.
- Böttcher, R. T. and Niehrs, C.** (2005). Fibroblast Growth Factor Signaling during Early Vertebrate Development. *Endocr. Rev.* **26**, 63–77.
- Bouvier, D., Tremblay, M.-È., Riad, M., Corera, A. T., Gingras, D., Horn, K. E., Fotouhi, M., Girard, M., Murai, K. K., Kennedy, T. E., et al.** (2010). EphA4 is localized in clathrin-coated and synaptic vesicles in adult mouse brain. *J. Neurochem.* **113**, 153–165.
- Boxtel, A. L. van, Economou, A. D., Heliot, C. and Hill, C. S.** (2018). Long-Range Signaling Activation and Local Inhibition Separate the Mesoderm and Endoderm Lineages. *Dev. Cell* **44**, 179-191.e5.
- Brewer, J. R., Mazot, P. and Soriano, P.** (2016). Genetic insights into the mechanisms of Fgf signaling. *Genes Dev.* **30**, 751–771.
- Briscoe, J. and Small, S.** (2015). Morphogen rules: design principles of gradient-mediated embryo patterning. *Development* **142**, 3996–4009.
- Briscoe, J. and Théron, P. P.** (2013). The mechanisms of Hedgehog signalling and its roles in development and disease. *Nat. Rev. Mol. Cell Biol.* **14**, 416–429.
- Briscoe, J., Sussel, L., Serup, P., Hartigan-O'Connor, D., Jessell, T. M., Rubenstein, J. L. R. and Ericson, J.** (1999). Homeobox gene Nkx2.2 and specification of neuronal identity by graded Sonic hedgehog signalling. *Nature* **398**, 622–627.
- Briscoe, J., Pierani, A., Jessell, T. M. and Ericson, J.** (2000). A Homeodomain Protein Code Specifies Progenitor Cell Identity and Neuronal Fate in the Ventral Neural Tube. *Cell* **101**, 435–445.
- Brunetti, R., Gissi, C., Pennati, R., Caicci, F., Gasparini, F. and Manni, L.** (2015). Morphological evidence that the molecularly determined *Ciona intestinalis* type A and type B are different species: *Ciona robusta* and *Ciona intestinalis*. *J. Zool. Syst. Evol. Res.* **53**, 186–193.
- Brunner, D., Dicker, K., Hafen, E. and Klimbitt, C.** (1994). The ETS domain protein Pointed-P2 Is a target of MAP kinase in the Sevenless signal transduction pathway. *4*.
- Burack, W. R. and Sturgill, T. W.** (1997). The activating dual phosphorylation of MAPK by MEK is nonprocessive. *Biochemistry* **36**, 5929–5933.
- Burz, D. S.** (1998). Cooperative DNA-binding by Bicoid provides a mechanism for threshold-dependent gene activation in the *Drosophila* embryo. *EMBO J.* **17**, 5998–6009.

- Butti, R., Das, S., Gunasekaran, V. P., Yadav, A. S., Kumar, D. and Kundu, G. C.** (2018). Receptor tyrosine kinases (RTKs) in breast cancer: signaling, therapeutic implications and challenges. *Mol. Cancer* **17**,.
- Casaletto, J. B. and McClatchey, A. I.** (2012). Spatial regulation of receptor tyrosine kinases in development and cancer. *Nat. Rev. Cancer* **12**, 387–400.
- Chabry, L.** (1887). *Embryologie normale et tératologique des Ascidie*. Paris: Felix Alcan Editeur.
- Chamberlain, C. E., Jeong, J., Guo, C., Allen, B. L. and McMahon, A. P.** (2008). Notochord-derived Shh concentrates in close association with the apically positioned basal body in neural target cells and forms a dynamic gradient during neural patterning. *Development* **135**, 1097–1106.
- Chen, N. and Greenwald, I.** (2004). The lateral signal for LIN-12/Notch in *C. elegans* vulval development comprises redundant secreted and transmembrane DSL proteins. *Dev. Cell* **6**, 183–192.
- Chen, H., Xu, Z., Mei, C., Yu, D. and Small, S.** (2012). A System of Repressor Gradients Spatially Organizes the Boundaries of Bicoid-Dependent Target Genes. *Cell* **149**, 618–629.
- Cohen, M., Kicheva, A., Ribeiro, A., Blassberg, R., Page, K. M., Barnes, C. P. and Briscoe, J.** (2015). Ptch1 and Gli regulate Shh signalling dynamics via multiple mechanisms. *Nat. Commun.* **6**, 6709.
- Cole, A. G. and Meinertzhagen, I. A.** (2004). The central nervous system of the ascidian larva: mitotic history of cells forming the neural tube in late embryonic *Ciona intestinalis*. *Dev. Biol.* **271**, 239–262.
- Conklin, E.** (1905). Mosaic development in ascidian eggs. *J. Exp. Zool.*
- Coppey, M., Boettiger, A. N., Berezhkovskii, A. M. and Shvartsman, S. Y.** (2008). Nuclear Trapping Shapes the Terminal Gradient in the *Drosophila* Embryo. *Curr. Biol.* **18**, 915–919.
- Crauk, O. and Dostatni, N.** (2005). Bicoid Determines Sharp and Precise Target Gene Expression in the *Drosophila* Embryo. *Curr. Biol.* **15**, 1888–1898.
- Crick, F.** (1970). Diffusion in Embryogenesis. 3.
- Crocker, J., Abe, N., Rinaldi, L., McGregor, A. P., Frankel, N., Wang, S., Alsaadi, A., Valenti, P., Plaza, S., Payre, F., et al.** (2015). Low affinity binding site clusters confer hox specificity and regulatory robustness. *Cell* **160**, 191–203.
- Das, A., Salloum, F. N., Xi, L., Rao, Y. J. and Kukreja, R. C.** (2009). ERK phosphorylation mediates sildenafil-induced myocardial protection against ischemia-reperfusion injury in mice. *Am. J. Physiol. Heart Circ. Physiol.* **296**, H1236-1243.
- Davis, S., Gale, N. W., Aldrich, T. H., Maisonpierre, P. C., Lhotak, V., Pawson, T., Goldfarb, M. and Yancopoulos, G. D.** (1994). Ligands for EPH-related receptor tyrosine kinases that require membrane attachment or clustering for activity. *Science* **266**, 816–819.
- de la Cova, C., Townley, R., Regot, S. and Greenwald, I.** (2017). A Real-Time Biosensor for ERK Activity Reveals Signaling Dynamics during *C. elegans* Cell Fate Specification. *Dev. Cell* **42**, 542-553.e4.

- Delsuc, F., Brinkmann, H., Chourrout, D. and Philippe, H.** (2006). Tunicates and not cephalochordates are the closest living relatives of vertebrates. *Nature* **439**, 965–968.
- Delsuc, F., Philippe, H., Tsagkogeorga, G., Simion, P., Tilak, M.-K., Turon, X., López-Legentil, S., Piette, J., Lemaire, P. and Douzery, E. J. P.** (2018). A phylogenomic framework and timescale for comparative studies of tunicates. *BMC Biol.* **16**,.
- Desponds, J., Tran, H., Ferraro, T., Lucas, T., Romero, C. P., Guillou, A., Fradin, C., Coppey, M., Dostatni, N. and Walczak, A. M.** (2016). Precision of Readout at the hunchback Gene: Analyzing Short Transcription Time Traces in Living Fly Embryos. *PLoS Comput. Biol.* **12**, e1005256.
- Dessaud, E., Yang, L. L., Hill, K., Cox, B., Ulloa, F., Ribeiro, A., Mynett, A., Novitch, B. G. and Briscoe, J.** (2007). Interpretation of the sonic hedgehog morphogen gradient by a temporal adaptation mechanism. *Nature* **450**, 717–720.
- Di Fiore, P. P. and De Camilli, P.** (2001). Endocytosis and Signaling: An Inseparable Partnership. *Cell* Vol. **106**, 1–4,.
- Driever, W. and Nüsslein-Volhard, C.** (1988a). A gradient of bicoid protein in *Drosophila* embryos. *Cell* **54**, 83–93.
- Driever, W. and Nüsslein-Volhard, C.** (1988b). The bicoid protein determines position in the *Drosophila* embryo in a concentration-dependent manner. *Cell* **54**, 95–104.
- Driever, W., Thoma, G. and Nüsslein-Volhard, C.** (1989). Determination of spatial domains of zygotic gene expression in the *Drosophila* embryo by the affinity of binding sites for the bicoid morphogen. *Nature* **340**, 363–367.
- Du, Z. and Lovly, C. M.** (2018). Mechanisms of receptor tyrosine kinase activation in cancer. *Mol. Cancer* **17**, 58.
- Dufour, H. D., Chettouh, Z., Deyts, C., de Rosa, R., Goridis, C., Joly, J.-S. and Brunet, J.-F.** (2006). Precranial origin of cranial motoneurons. *Proc. Natl. Acad. Sci.* **103**, 8727–8732.
- Ericson, J., Morton, S., Kawakami, A., Roelink, H. and Jessell, T. M.** (1996). Two Critical Periods of Sonic Hedgehog Signaling Required for the Specification of Motor Neuron Identity. *Cell* **87**, 661–673.
- Ericson, J., Rashbass, P., Schedl, A., Brenner-Morton, S., Kawakami, A., van Heyningen, V., Jessell, T. M. and Briscoe, J.** (1997). Pax6 Controls Progenitor Cell Identity and Neuronal Fate in Response to Graded Shh Signaling. *Cell* **90**, 169–180.
- Farley, E. K., Olson, K. M., Zhang, W., Brandt, A. J., Rokhsar, D. S. and Levine, M. S.** (2015). Suboptimization of developmental enhancers. *Science* **350**, 325–328.
- Fehrenbacher, N., Bar-Sagi, D. and Philips, M.** (2009). Ras/MAPK signaling from endomembranes. *Mol. Oncol.* **3**, 297–307.
- Ferrell, J. E. and Bhatt, R. R.** (1997). Mechanistic studies of the dual phosphorylation of mitogen-activated protein kinase. *J. Biol. Chem.* **272**, 19008–19016.

- Ferrell, J. E. and Ha, S. H.** (2014a). Ultrasensitivity part I: Michaelian responses and zero-order ultrasensitivity. *Trends Biochem. Sci.* **39**, 496–503.
- Ferrell, J. E. and Ha, S. H.** (2014b). Ultrasensitivity part II: multisite phosphorylation, stoichiometric inhibitors, and positive feedback. *Trends Biochem. Sci.* **39**, 556–569.
- Ferrell, J. E. and Ha, S. H.** (2014c). Ultrasensitivity part III: cascades, bistable switches, and oscillators. *Trends Biochem. Sci.* **39**, 612–618.
- Ferrell, J. E. and Machleder** (1998). The Biochemical Basis of an All-or-None Cell Fate Switch in *Xenopus Oocytes*. *Science* **280**, 895–898.
- Freeman, J. B. and Dale, R.** (2013). Assessing bimodality to detect the presence of a dual cognitive process. *Behav. Res. Methods* **45**, 83–97.
- Frohnhöfer, H. G. and Nüsslein-Volhard, C.** (1986). Organization of anterior pattern in the *Drosophila* embryo by the maternal gene bicoid. *Nature* **324**, 120–125.
- Fukuda, M., Gotoh, Y. and Nishida, E.** (1997). Interaction of MAP kinase with MAP kinase kinase: its possible role in the control of nucleocytoplasmic transport of MAP kinase. *EMBO J.* **16**, 1901–1908.
- Gabay, L., Scholz, H., Golembo, M., Klaes, A., Shilo, B. Z. and Klämbt, C.** (1996). EGF receptor signaling induces pointed P1 transcription and inactivates Yan protein in the *Drosophila* embryonic ventral ectoderm. *Dev. Camb. Engl.* **122**, 3355–3362.
- Gauthier, K. and Rocheleau, C.** (2017). *C. elegans* Vulva Induction: An In Vivo Model to Study Epidermal Growth Factor Receptor Signaling and Trafficking. *Methods Mol. Biol. Clifton NJ* **1652**, 43–61.
- Giorgetti, L., Siggers, T., Tiana, G., Caprara, G., Notarbartolo, S., Corona, T., Pasparakis, M., Milani, P., Bulyk, M. L. and Natoli, G.** (2010). Noncooperative Interactions between Transcription Factors and Clustered DNA Binding Sites Enable Graded Transcriptional Responses to Environmental Inputs. *Mol. Cell* **37**, 418–428.
- Goldbeter, A.** (2005). Zero-order switches and developmental thresholds. *Mol. Syst. Biol.* **1**, 2005.0031.
- Goldbeter, A. and Koshland, D. E.** (1981). An amplified sensitivity arising from covalent modification in biological systems. *Proc. Natl. Acad. Sci.* **78**, 6840–6844.
- Golembo, M., Raz, E. and Shilo, B. Z.** (1996). The *Drosophila* embryonic midline is the site of Spitz processing, and induces activation of the EGF receptor in the ventral ectoderm. *Dev. Camb. Engl.* **122**, 3363–3370.
- Greenwald, I. S., Sternberg, P. W. and Horvitz, H. R.** (1983). The *lin-12* locus specifies cell fates in *Caenorhabditis elegans*. *Cell* **34**, 435–444.
- Gregor, T., Wieschaus, E. F., McGregor, A. P., Bialek, W. and Tank, D. W.** (2007a). Stability and Nuclear Dynamics of the Bicoid Morphogen Gradient. *Cell* **130**, 141–152.
- Gregor, T., Tank, D. W., Wieschaus, E. F. and Bialek, W.** (2007b). Probing the Limits to Positional Information. *Cell* **130**, 153–164.

- Grimm, O., Zini, V. S., Kim, Y., Casanova, J., Shvartsman, S. Y. and Wieschaus, E.** (2012). Torso RTK controls Capicua degradation by changing its subcellular localization. *Development* **139**, 3962–3968.
- Guillemot, F.** (2007). Spatial and temporal specification of neural fates by transcription factor codes. *Development* **134**, 3771–3780.
- Guntas, G., Hallett, R. A., Zimmerman, S. P., Williams, T., Yumerefendi, H., Bear, J. E. and Kuhlman, B.** (2015). Engineering an improved light-induced dimer (iLID) for controlling the localization and activity of signaling proteins. *Proc. Natl. Acad. Sci.* **112**, 112–117.
- Hajnal, A., Whitfield, C. W. and Kim, S. K.** (1997). Inhibition of *Caenorhabditis elegans* vulval induction by gap-1 and by let-23 receptor tyrosine kinase. *Genes Dev.* **11**, 2715–2728.
- Hanafusa, H., Torii, S., Yasunaga, T. and Nishida, E.** (2002). Sprouty1 and Sprouty2 provide a control mechanism for the Ras/MAPK signalling pathway. *Nat. Cell Biol.* **4**, 850–858.
- Hanahan, D. and Weinberg, R. A.** (2011). Hallmarks of Cancer: The Next Generation. *Cell* **144**, 646–674.
- Hansen, M. J., Dallal, G. E. and Flanagan, J. G.** (2004). Retinal Axon Response to Ephrin-As Shows a Graded, Concentration-Dependent Transition from Growth Promotion to Inhibition. *Neuron* **42**, 717–730.
- Hartigan, J. A. and Hartigan, P. M.** (1985). The Dip Test of Unimodality. *Ann. Stat.* **13**,.
- Hashimoto, H., Robin, F. B., Sherrard, K. M. and Munro, E. M.** (2015). Sequential Contraction and Exchange of Apical Junctions Drives Zippering and Neural Tube Closure in a Simple Chordate. *Dev. Cell* **32**, 241–255.
- Haugsten, E. M., Sørensen, V., Kunova Bosakova, M., de Souza, G. A., Krejci, P., Wiedlocha, A. and Wesche, J.** (2016). Proximity Labeling Reveals Molecular Determinants of FGFR4 Endosomal Transport. *J. Proteome Res.* **15**, 3841–3855.
- Haupaix, N., Stolfi, A., Sirour, C., Picco, V., Levine, M., Christiaen, L. and Yasuo, H.** (2013). p120RasGAP mediates ephrin/Eph-dependent attenuation of FGF/ERK signals during cell fate specification in ascidian embryos. *Development* **140**, 4347–4352.
- Haupaix, N., Abitua, P. B., Sirour, C., Yasuo, H., Levine, M. and Hudson, C.** (2014). Ephrin-mediated restriction of ERK1/2 activity delimits the number of pigment cells in the *Ciona* CNS. *Dev. Biol.* **394**, 170–180.
- Hill, R. J. and Sternberg, P. W.** (1992). The gene *lin-3* encodes an inductive signal for vulval development in *C. elegans*. *Nature* **358**, 470–476.
- Himanen, J. P., Yermekbayeva, L., Janes, P. W., Walker, J. R., Xu, K., Atapattu, L., Rajashankar, K. R., Mensinga, A., Lackmann, M., Nikolov, D. B., et al.** (2010). Architecture of Eph receptor clusters. *Proc. Natl. Acad. Sci.* **107**, 10860–10865.
- Hirai, H., Maru, Y., Hagiwara, K., Nishida, J. and Takaku, F.** (1987). A novel putative tyrosine kinase receptor encoded by the *ephrin* gene. *Science* **238**, 1717–1720.

- Hiratsuka, T., Fujita, Y., Naoki, H., Aoki, K., Kamioka, Y. and Matsuda, M.** (2015). Intercellular propagation of extracellular signal-regulated kinase activation revealed by in vivo imaging of mouse skin. *Elife* **4**, e05178.
- Horikawa, Y., Matsumoto, H., Yamaguchi, F., Ishida, S. and Fujiwara, S.** (2013). Transcriptional regulation in the early ectodermal lineage of ascidian embryos. *Dev. Growth Differ.* **55**, 776–785.
- Houchmandzadeh, B., Wieschaus, E. and Leibler, S.** (2002). Establishment of developmental precision and proportions in the early *Drosophila* embryo. *Nature* **415**, 798–802.
- Huang, C. Y. and Ferrell, J. E.** (1996). Ultrasensitivity in the mitogen-activated protein kinase cascade. *Proc. Natl. Acad. Sci.* **93**, 10078–10083.
- Hudson, C.** (2016). The central nervous system of ascidian larvae: Nervous system development in ascidians. *Wiley Interdiscip. Rev. Dev. Biol.* **5**, 538–561.
- Hudson, C. and Lemaire, P.** (2001). Induction of anterior neural fates in the ascidian *Ciona intestinalis*. *Mech. Dev.* **100**, 189–203.
- Hudson, C., Darras, S., Caillol, D., Yasuo, H. and Lemaire, P.** (2003). A conserved role for the MEK signalling pathway in neural tissue specification and posteriorisation in the invertebrate chordate, the ascidian *Ciona intestinalis*. *Development* **130**, 147–159.
- Hudson, C., Kawai, N., Negishi, T. and Yasuo, H.** (2013).  $\beta$ -Catenin-Driven Binary Fate Specification Segregates Germ Layers in Ascidian Embryos. *Curr. Biol.* **23**, 491–495.
- Hudson, C., Sirour, C. and Yasuo, H.** (2016). Co-expression of *Foxa.a*, *Foxd* and *Fgf9/16/20* defines a transient mesendoderm regulatory state in ascidian embryos. *eLife* **5**,.
- Iguchi, K., Matsunaga, S., Nakano, T., Usui, S. and Hirano, K.** (2006). Inhibition of caveolin-1 expression by incadronate in PC-3 prostate cells. *Anticancer Res.* **26**, 2977–2981.
- Ikuta, T. and Saiga, H.** (2007). Dynamic change in the expression of developmental genes in the ascidian central nervous system: Revisit to the tripartite model and the origin of the midbrain–hindbrain boundary region. *Dev. Biol.* **312**, 631–643.
- Imai, K. S.** (2004). Gene expression profiles of transcription factors and signaling molecules in the ascidian embryo: towards a comprehensive understanding of gene networks. *Development* **131**, 4047–4058.
- Imai, K. S.** (2006). Regulatory Blueprint for a Chordate Embryo. *Science* **312**, 1183–1187.
- Imai, K., Takada, N., Satoh, N. and Satou, Y.** (2000).  $\beta$ -catenin mediates the specification of endoderm cells in ascidian embryos. *12*.
- Imai, K. S., Satoh, N. and Satou, Y.** (2002). Region specific gene expressions in the central nervous system of the ascidian embryo. *Mech. Dev.* **119**, S275–S277.
- Imai, K. S., Hudson, C., Oda-Ishii, I., Yasuo, H. and Satou, Y.** (2016). Antagonism between  $\beta$ -catenin and *Gata.a* sequentially segregates the germ layers of ascidian embryos. *Development* **143**, 4167–4172.

- Inazawa, T., Okamura, Y. and Takahashi, K.** (1998). Basic fibroblast growth factor induction of neuronal ion channel expression in ascidian ectodermal blastomeres. *J. Physiol.* **511**, 347–359.
- Jean, S., Mikryukov, A., Tremblay, M. G., Baril, J., Guillou, F., Bellenfant, S. and Moss, T.** (2010). Extended-Synaptotagmin-2 Mediates FGF Receptor Endocytosis and ERK Activation In Vivo. *Dev. Cell* **19**, 426–439.
- Jessell, T. M.** (2000). Neuronal specification in the spinal cord: inductive signals and transcriptional codes. *Nat. Rev. Genet.* **1**, 20–29.
- Johnson, H. E. and Toettcher, J. E.** (2019). Signaling Dynamics Control Cell Fate in the Early Drosophila Embryo. *Dev. Cell* **48**, 361-370.e3.
- Johnson, H. E., Goyal, Y., Pannucci, N. L., Schüpbach, T., Shvartsman, S. Y. and Toettcher, J. E.** (2017). The Spatiotemporal Limits of Developmental Erk Signaling. *Dev. Cell* **40**, 185–192.
- Johnson, H. E., Shvartsman, S. Y. and Toettcher, J. E.** (2019). Optogenetic rescue of a developmental patterning mutant. *bioRxiv* 776120.
- Juven-Gershon, T., Hsu, J.-Y. and Kadonaga, J. T.** (2008). Caudal, a key developmental regulator, is a DPE-specific transcriptional factor. *Genes Dev.* **22**, 2823–2830.
- Kaech, S. M., Whitfield, C. W. and Kim, S. K.** (1998). The LIN-2/LIN-7/LIN-10 complex mediates basolateral membrane localization of the C. elegans EGF receptor LET-23 in vulval epithelial cells. *Cell* **94**, 761–771.
- Katz, W. S., Hill, R. J., Clandinin, T. R. and Sternberg, P. W.** (1995). Different Levels of the C, elegans Growth Factor LIN-3 Promote Distinct Vulval Precursor Fates. **11**.
- Katz, W. S., Lesa, G. M., Yannoukakos, D., Clandinin, T. R., Schlessinger, J. and Sternberg, P. W.** (1996). A point mutation in the extracellular domain activates LET-23, the Caenorhabditis elegans epidermal growth factor receptor homolog. *Mol. Cell. Biol.* **16**, 529–537.
- Kay, R. R. and Thompson, C. R. L.** (2009). Forming Patterns in Development without Morphogen Gradients: Scattered Differentiation and Sorting Out. *Cold Spring Harb. Perspect. Biol.* **1**, a001503–a001503.
- Keduka, E., Kaiho, A., Hamada, M., Watanabe-Takano, H., Takano, K., Ogasawara, M., Satou, Y., Satoh, N. and Endo, T.** (2009). M-Ras evolved independently of R-Ras and its neural function is conserved between mammalian and ascidian, which lacks classical Ras. *Gene* **429**, 49–58.
- Khokhlatchev, A. V., Canagarajah, B., Wilsbacher, J., Robinson, M., Atkinson, M., Goldsmith, E. and Cobb, M. H.** (1998). Phosphorylation of the MAP Kinase ERK2 Promotes Its Homodimerization and Nuclear Translocation. *Cell* **93**, 605–615.
- Kholodenko, B. N.** (2007). Untangling the signalling wires. *Nat. Cell Biol.* **9**, 247–249.
- Kim, Y., Coppey, M., Grossman, R., Ajuria, L., Jiménez, G., Paroush, Z. and Shvartsman, S. Y.** (2010). MAPK substrate competition integrates patterning signals in the Drosophila embryo. *Curr. Biol. CB* **20**, 446–451.

- Kimmelman, A. C., Nuñez Rodriguez, N. and Chan, A. M.-L.** (2002). R-Ras3/M-Ras induces neuronal differentiation of PC12 cells through cell-type-specific activation of the mitogen-activated protein kinase cascade. *Mol. Cell. Biol.* **22**, 5946–5961.
- Koga, M. and Ohshima, Y.** (1995). Mosaic analysis of the let-23 gene function in vulval induction of *Caenorhabditis elegans*. *Development* **121**, 2655–2666.
- Kolch, W.** (2000). Meaningful relationships: the regulation of the Ras/Raf/MEK/ERK pathway by protein interactions. *Biochem. J.* **351**, 289–305.
- Komatsu, N., Aoki, K., Yamada, M., Yukinaga, H., Fujita, Y., Kamioka, Y. and Matsuda, M.** (2011). Development of an optimized backbone of FRET biosensors for kinases and GTPases. *Mol. Biol. Cell* **22**, 4647–4656.
- Kovalevsky, A.** (1859). *Mémoires de l'Académie impériale des sciences de St.-Pétersbourg*. St.-Petersburg : L'Académie.
- Lambert, C., Goudeau, H., Franchet, C., Lambert, G. and Goudeau, M.** (1997). Ascidian eggs block polyspermy by two independent mechanisms: One at the egg plasma membrane, the other involving the follicle cells. *Mol. Reprod. Dev.* **48**, 137–143.
- Lamy, C.** (2006). Ci-FoxA-a is the earliest zygotic determinant of the ascidian anterior ectoderm and directly activates Ci-sFRP1/5. *Development* **133**, 2835–2844.
- Le Borgne, R.** (2005). The roles of receptor and ligand endocytosis in regulating Notch signaling. *Development* **132**, 1751–1762.
- le Gallic, L., Sgouras, D., Beal, G. and Mavrothalassitis, G.** (1999). Transcriptional Repressor ERF Is a Ras/Mitogen-Activated Protein Kinase Target That Regulates Cellular Proliferation. *Mol. Cell. Biol.* **19**, 4121–4133.
- Le Roy, C. and Wrana, J. L.** (2005). Clathrin- and non-clathrin-mediated endocytic regulation of cell signalling. *Nat. Rev. Mol. Cell Biol.* **6**, 112–126.
- Lebrecht, D., Foehr, M., Smith, E., Lopes, F. J. P., Vanario-Alonso, C. E., Reinitz, J., Burz, D. S. and Hanes, S. D.** (2005). Bicoid cooperative DNA binding is critical for embryonic patterning in *Drosophila*. *Proc. Natl. Acad. Sci.* **102**, 13176–13181.
- Lee, J., Platt, K. A., Censullo, P. and Ruiz i Altaba, A.** (1997). Gli1 is a target of Sonic hedgehog that induces ventral neural tube development. *Dev. Camb. Engl.* **124**, 2537–2552.
- Lemmon, M. A. and Schlessinger, J.** (2010). Cell Signaling by Receptor Tyrosine Kinases. *Cell* **141**, 1117–1134.
- Lifanov, A. P.** (2003). Homotypic Regulatory Clusters in *Drosophila*. *Genome Res.* **13**, 579–588.
- Lim, B., Dsilva, C. J., Levario, T. J., Lu, H., Schüpbach, T., Kevrekidis, I. G. and Shvartsman, S. Y.** (2015). Dynamics of Inductive ERK Signaling in the *Drosophila* Embryo. *Curr. Biol.* **25**, 1784–1790.
- Lisabeth, E. M., Falivelli, G. and Pasquale, E. B.** (2013). Eph Receptor Signaling and Ephrins. *Cold Spring Harb. Perspect. Biol.* **5**, a009159–a009159.

- Litingtung, Y. and Chiang, C.** (2000). Specification of ventral neuron types is mediated by an antagonistic interaction between Shh and Gli3. *Nat. Neurosci.* **3**, 979–985.
- Löhr, U., Chung, H.-R., Beller, M. and Jäckle, H.** (2009). Antagonistic action of Bicoid and the repressor Capicua determines the spatial limits of *Drosophila* head gene expression domains. *Proc. Natl. Acad. Sci.* **106**, 21695–21700.
- Lucas, T., Tran, H., Perez Romero, C. A., Guillou, A., Fradin, C., Coppey, M., Walczak, A. M. and Dostatni, N.** (2018). 3 minutes to precisely measure morphogen concentration. *PLOS Genet.* **14**, e1007676.
- Ma, X., Yuan, D., Diepold, K., Scarborough, T. and Ma, J.** (1996). The *Drosophila* morphogenetic protein Bicoid binds DNA cooperatively. *Development* 1195–1206.
- Macia, E., Ehrlich, M., Massol, R., Boucrot, E., Brunner, C. and Kirchhausen, T.** (2006). Dynasore, a Cell-Permeable Inhibitor of Dynamin. *Dev. Cell* **10**, 839–850.
- MacKeigan, J. P., Murphy, L. O., Dimitri, C. A. and Blenis, J.** (2005). Graded Mitogen-Activated Protein Kinase Activity Precedes Switch-Like c-Fos Induction in Mammalian Cells. *Mol. Cell Biol.* **25**, 4676–4682.
- Markevich, N. I., Hoek, J. B. and Kholodenko, B. N.** (2004). Signaling switches and bistability arising from multisite phosphorylation in protein kinase cascades. *J. Cell Biol.* **164**, 353–359.
- Marshall, C. J.** (1995). Signaling: Transient versus Sustained Extracellular Signal-Regulated Kinase Activation. *Cell* **80**, 178–185.
- Matise, M. P. and Joyner, A. L.** (1999). Gli genes in development and cancer. *Oncogene* **18**, 7852–7859.
- Matise, M. P., Epstein, D. J., Park, H. L., Platt, K. A. and Joyner, A. L.** (1998). Gli2 is required for induction of floor plate and adjacent cells, but not most ventral neurons in the mouse central nervous system. *Dev. Camb. Engl.* **125**, 2759–2770.
- Matsuo, I. and Kimura-Yoshida, C.** (2014). Extracellular distribution of diffusible growth factors controlled by heparan sulfate proteoglycans during mammalian embryogenesis. *Philos. Trans. R. Soc. B Biol. Sci.* **369**, 20130545.
- Mayor, S., Parton, R. G. and Donaldson, J. G.** (2014). Clathrin-Independent Pathways of Endocytosis. *Cold Spring Harb. Perspect. Biol.* **6**, a016758–a016758.
- McCarthy, S. A., Chen, D., Yang, B. S., Garcia Ramirez, J. J., Cherwinski, H., Chen, X. R., Klagsbrun, M., Hauser, C. A., Ostrowski, M. C. and McMahon, M.** (1997). Rapid phosphorylation of Ets-2 accompanies mitogen-activated protein kinase activation and the induction of heparin-binding epidermal growth factor gene expression by oncogenic Raf-1. *Mol. Cell Biol.* **17**, 2401–2412.
- Melen, G. J., Levy, S., Barkai, N. and Shilo, B.** (2005). Threshold responses to morphogen gradients by zero-order ultrasensitivity. *Mol. Syst. Biol.* **1**,.
- Meyers, J., Craig, J. and Odde, D. J.** (2006). Potential for Control of Signaling Pathways via Cell Size and Shape. *Curr. Biol.* **16**, 1685–1693.

- Miaczynska, M.** (2013). Effects of Membrane Trafficking on Signaling by Receptor Tyrosine Kinases. *Cold Spring Harb. Perspect. Biol.* **5**, a009035–a009035.
- Mineo, A., Furriols, M. and Casanova, J.** (2018). The trigger (and the restriction) of Torso RTK activation. *Open Biol.* **8**, 180180.
- Miyazaki, Y., Nishida, H. and Kumano, G.** (2007). Brain induction in ascidian embryos is dependent on juxtaposition of FGF9/16/20-producing and -receiving cells. *Dev. Genes Evol.* **217**, 177–188.
- Moreno, E., Valon, L., Levillayer, F. and Levayer, R.** (2019). Competition for Space Induces Cell Elimination through Compaction-Driven ERK Downregulation. *Curr. Biol.* **29**, 23–34.e8.
- Morgan, T. H.** (1901). *Regeneration*. Macmillan.
- Murphy, J. E., Padilla, B. E., Hasdemir, B., Cottrell, G. S. and Bunnett, N. W.** (2009). Endosomes: a legitimate platform for the signaling train. *Proc. Natl. Acad. Sci.* **106**, 17615–17622.
- Nikolov, D. B., Xu, K. and Himanen, J. P.** (2013). Eph/ephrin recognition and the role of Eph/ephrin clusters in signaling initiation. *Biochim. Biophys. Acta BBA - Proteins Proteomics* **1834**, 2160–2165.
- Nishida, H.** (1987). Cell Lineage Analysis in Ascidian Embryos by Intracellular Injection of a Tracer Enzyme. 16.
- Nishida, H. and Satoh, N.** (1983). Cell Lineage Analysis in Ascidian Embryos by Intracellular Injection of a Tracer Enzyme. 13.
- Novitsch, B. G., Chen, A. I. and Jessell, T. M.** (2001). Coordinate Regulation of Motor Neuron Subtype Identity and Pan-Neuronal Properties by the bHLH Repressor Olig2. *Neuron* **31**, 773–789.
- Nunns, H. and Goentoro, L.** (2018). Signaling pathways as linear transmitters. *eLife* **7**,
- Ochoa-Espinosa, A., Yucel, G., Kaplan, L., Pare, A., Pura, N., Oberstein, A., Papatsenko, D. and Small, S.** (2005). The role of binding site cluster strength in Bicoid-dependent patterning in *Drosophila*. *Proc. Natl. Acad. Sci.* **102**, 4960–4965.
- Ochoa-Espinosa, A., Yu, D., Tsigos, A., Struffi, P. and Small, S.** (2009). Anterior-posterior positional information in the absence of a strong Bicoid gradient. *Proc. Natl. Acad. Sci.* **106**, 3823–3828.
- Oda-Ishii, I., Kubo, A., Kari, W., Suzuki, N., Rothbacher, U. and Satou, Y.** (2016). A Maternal System Initiating the Zygotic Developmental Program through Combinatorial Repression in the Ascidian Embryo. *PLoS Genet.* **12**, e1006045.
- Ogura, Y., Wen, F.-L., Sami, M. M., Shibata, T. and Hayashi, S.** (2018). A Switch-like Activation Relay of EGFR-ERK Signaling Regulates a Wave of Cellular Contractility for Epithelial Invagination. *Dev. Cell* **46**, 162–172.e5.
- Ohta, N. and Satou, Y.** (2013). Multiple Signaling Pathways Coordinate to Induce a Threshold Response in a Chordate Embryo. *PLoS Genet.* **9**, e1003818.

- Ohta, N., Waki, K., Mochizuki, A. and Satou, Y.** (2015). A Boolean Function for Neural Induction Reveals a Critical Role of Direct Intercellular Interactions in Patterning the Ectoderm of the Ascidian Embryo. *PLoS Comput. Biol.* **11**, e1004687.
- O'Neill, M. and Rubin, G. M.** (1994). The Activities of Two Ets-Related Transcription Factors Required for Drosophila Eye Development Are Modulated by the Ras/MAPK Pathway. **11**.
- Ong, S. H., Guy, G. R., Hadari, Y. R., Laks, S., Gotoh, N., Schlessinger, J. and Lax, I.** (2000). FRS2 Proteins Recruit Intracellular Signaling Pathways by Binding to Diverse Targets on Fibroblast Growth Factor and Nerve Growth Factor Receptors. *Mol. Cell. Biol.* **20**, 979–989.
- Ornitz, D. M. and Itoh, N.** (2015). The Fibroblast Growth Factor signaling pathway. *Wiley Interdiscip. Rev. Dev. Biol.* **4**, 215–266.
- Pálffy, M., Reményi, A. and Korcsmáros, T.** (2012). Endosomal crosstalk: meeting points for signaling pathways. *Trends Cell Biol.* **22**, 447–456.
- Park, H. L., Bai, C., Platt, K. A., Matise, M. P., Beeghly, A., Hui, C. C., Nakashima, M. and Joyner, A. L.** (2000). Mouse Gli1 mutants are viable but have defects in SHH signaling in combination with a Gli2 mutation. *Dev. Camb. Engl.* **127**, 1593–1605.
- Pasquale, E. B.** (2005). Eph receptor signalling casts a wide net on cell behaviour. *Nat. Rev. Mol. Cell Biol.* **6**, 462–475.
- Perrett, R. M., Fowkes, R. C., Caunt, C. J., Tsaneva-Atanasova, K., Bowsher, C. G. and McArdle, C. A.** (2013). Signaling to Extracellular Signal-regulated Kinase from ErbB1 Kinase and Protein Kinase C: FEEDBACK, HETEROGENEITY, AND GATING. *J. Biol. Chem.* **288**, 21001–21014.
- Picco, V., Hudson, C. and Yasuo, H.** (2007). Ephrin-Eph signalling drives the asymmetric division of notochord/neural precursors in Ciona embryos. *Dev. Camb. Engl.* **134**, 1491–1497.
- Poliakov, A., Cotrina, M. and Wilkinson, D. G.** (2004). Diverse Roles of Eph Receptors and Ephrins in the Regulation of Cell Migration and Tissue Assembly. *Dev. Cell* **7**, 465–480.
- Porcher, A. and Dostatni, N.** (2010). The Bicoid Morphogen System. *Curr. Biol.* **20**, R249–R254.
- Porcher, A., Abu-Arish, A., Huart, S., Roelens, B., Fradin, C. and Dostatni, N.** (2010). The time to measure positional information: maternal Hunchback is required for the synchrony of the Bicoid transcriptional response at the onset of zygotic transcription. *Development* **137**, 2795–2804.
- Prodon, F., Sardet, C. and Nishida, H.** (2008). Cortical and cytoplasmic flows driven by actin microfilaments polarize the cortical ER-mRNA domain along the a–v axis in ascidian oocytes. *Dev. Biol.* **313**, 682–699.
- Purvis, J. E. and Lahav, G.** (2013). Encoding and Decoding Cellular Information through Signaling Dynamics. *Cell* **152**, 945–956.
- Qiao, L., Nachbar, R. B., Kevrekidis, I. G. and Shvartsman, S. Y.** (2007). Bistability and Oscillations in the Huang-Ferrell Model of MAPK Signaling. *PLoS Comput. Biol.* **3**, 8.
- Rapraeger, A. C., Krufka, A. and Olwin, B. B.** (1991). Requirement of Heparan Sulfate for bFGF-Mediated Fibroblast Growth and Myoblast Differentiation. *Sci. New Ser.* **252**, 1705–1708.

- Rauen, K. A.** (2013). The RASopathies. *Annu. Rev. Genomics Hum. Genet.* **14**, 355–369.
- Rebay, I. and Rubin, G. M.** (1995). Yan functions as a general inhibitor of differentiation and is negatively regulated by activation of the Ras1/MAPK pathway. *Cell* **81**, 857–866.
- Regot, S., Hughey, J. J., Bajar, B. T., Carrasco, S. and Covert, M. W.** (2014). High-Sensitivity Measurements of Multiple Kinase Activities in Live Single Cells. *Cell* **157**, 1724–1734.
- Roelink, H., Porter, J. A., Chiang, C., Tanabe, Y., Chang, D. T., Beachy, P. A. and Jessell, T. M.** (1995). Floor plate and motor neuron induction by different concentrations of the amino-terminal cleavage product of sonic hedgehog autoproteolysis. *Cell* **81**, 445–455.
- Rossi, F. M. V., Guicherit, O. M., Spicher, A., Kringstein, A. M., Fatyol, K., Blakely, B. T. and Blau, H. M.** (1998). Tetracycline-regulatable factors with distinct dimerization domains allow reversible growth inhibition by p16. *Nat. Genet.* **20**, 389–393.
- Rossi, F. M. V., Kringstein, A. M., Spicher, A., Guicherit, O. M. and Blau, H. M.** (2000). Transcriptional Control: Rheostat Converted to On/Off Switch. *Mol. Cell* **6**.
- Rothbacher, U., Bertrand, V., Lamy, C. and Lemaire, P.** (2007). A combinatorial code of maternal GATA, Ets and -catenin-TCF transcription factors specifies and patterns the early ascidian ectoderm. *Development* **134**, 4023–4032.
- Roure, A. and Darras, S.** (2016). Msxb is a core component of the genetic circuitry specifying the dorsal and ventral neurogenic midlines in the ascidian embryo. *Dev. Biol.* **409**, 277–287.
- Roure, A., Rothbacher, U., Robin, F., Kalmar, E., Ferone, G., Lamy, C., Missero, C., Mueller, F. and Lemaire, P.** (2007). A Multicassette Gateway Vector Set for High Throughput and Comparative Analyses in *Ciona* and Vertebrate Embryos. *PLOS ONE* **2**, e916.
- Roure, A., Lemaire, P. and Darras, S.** (2014). An Otx/Nodal Regulatory Signature for Posterior Neural Development in Ascidians. *PLoS Genet.* **10**, e1004548.
- Ruiz i Altaba, A.** (1999). Gli proteins encode context-dependent positive and negative functions: implications for development and disease. *Dev. Camb. Engl.* **126**, 3205–3216.
- Ryan, K., Lu, Z. and Meinertzhagen, I. A.** (2016). The CNS connectome of a tadpole larva of *Ciona intestinalis* (L.) highlights sidedness in the brain of a chordate sibling. *eLife* **5**.
- Santos, S. D. M., Verveer, P. J. and Bastiaens, P. I. H.** (2007). Growth factor-induced MAPK network topology shapes Erk response determining PC-12 cell fate. *Nat. Cell Biol.* **9**, 324–330.
- Sardet, C., McDougall, A., Yasuo, H., Chenevert, J., Pruliere, G., Dumollard, R., Hudson, C., Hebras, C., Le Nguyen, N. and Paix, A.** (2011). Embryological methods in ascidians: the Villefranche-sur-Mer protocols. *Methods Mol. Biol. Clifton NJ* **770**, 365–400.
- Sasaki, H., Hui, C., Nakafuku, M. and Kondoh, H.** (1997). A binding site for Gli proteins is essential for HNF-3beta floor plate enhancer activity in transgenics and can respond to Shh in vitro. *Dev. Camb. Engl.* **124**, 1313–1322.
- Sasaki, H., Nishizaki, Y., Hui, C., Nakafuku, M. and Kondoh, H.** (1999). Regulation of Gli2 and Gli3 activities by an amino-terminal repression domain: implication of Gli2 and Gli3 as primary mediators of Shh signaling. *Development* **126**, 3915–3924.

- Satoh, N.** (2014). *Developmental Genomics of Ascidians*.
- Satou, Y., Imai, K. and Satoh, N.** (2002). Fgf genes in the basal chordate *Ciona intestinalis*. *Dev. Genes Evol.* **212**, 432–438.
- Satou, Y., Sasakura, Y., Yamada, L., Imai, K. S., Satoh, N. and Degnan, B.** (2003). A genomewide survey of developmentally relevant genes in *Ciona intestinalis*: V. Genes for receptor tyrosine kinase pathway and Notch signaling pathway. *Dev. Genes Evol.* **213**, 254–263.
- Schlessinger, J.** (2014). Receptor Tyrosine Kinases: Legacy of the First Two Decades. *Cold Spring Harb. Perspect. Biol.* **6**, a008912–a008912.
- Schröder, C., Tautz, D., Seifert, E. and Jäckle, H.** (1988). Differential regulation of the two transcripts from the *Drosophila* gap segmentation gene *hunchback*. *EMBO J.* **7**, 2881–2887.
- Seiradake, E., Harlos, K., Sutton, G., Aricescu, A. R. and Jones, E. Y.** (2010). An extracellular steric seeding mechanism for Eph-ephrin signaling platform assembly. *Nat. Struct. Mol. Biol.* **17**, 398–402.
- Sgouras, D. N., Athanasiou, M. A., Beal, G. J., Fisher, R. J., Blair, D. G. and Mavrothalassitis, G. J.** (1995). ERF: an ETS domain protein with strong transcriptional repressor activity, can suppress ets-associated tumorigenesis and is regulated by phosphorylation during cell cycle and mitogenic stimulation. *EMBO J.* **14**, 4781–4793.
- Shah, N. A. and Sarkar, C. A.** (2011). Robust Network Topologies for Generating Switch-Like Cellular Responses. *PLoS Comput. Biol.* **7**, e1002085.
- Sharrocks, A. D.** (2001). The ETS-domain transcription factor family. *Nat. Rev. Mol. Cell Biol.* **2**, 827–837.
- Shi, X., Hapiak, V., Zheng, J., Muller-Greven, J., Bowman, D., Lingerak, R., Buck, M., Wang, B.-C. and Smith, A. W.** (2017). A role of the SAM domain in EphA2 receptor activation. *Sci. Rep.* **7**, .
- Shilo, B.-Z.** (2005). Regulating the dynamics of EGF receptor signaling in space and time. *Development* **132**, 4017–4027.
- Shimokawa, K., Kimura-Yoshida, C., Nagai, N., Mukai, K., Matsubara, K., Watanabe, H., Matsuda, Y., Mochida, K. and Matsuo, I.** (2011). Cell Surface Heparan Sulfate Chains Regulate Local Reception of FGF Signaling in the Mouse Embryo. *Dev. Cell* **21**, 257–272.
- Shindo, Y., Iwamoto, K., Mouri, K., Hibino, K., Tomita, M., Kosako, H., Sako, Y. and Takahashi, K.** (2016). Conversion of graded phosphorylation into switch-like nuclear translocation via autoregulatory mechanisms in ERK signalling. *Nat. Commun.* **7**, 10485.
- Sigismund, S., Woelk, T., Puri, C., Maspero, E., Tacchetti, C., Transidico, P., Di Fiore, P. P. and Polo, S.** (2005). Clathrin-independent endocytosis of ubiquitinated cargos. *Proc. Natl. Acad. Sci. U. S. A.* **102**, 2760–2765.
- Sigismund, S., Argenzio, E., Tosoni, D., Cavallaro, E., Polo, S. and Di Fiore, P. P.** (2008). Clathrin-mediated internalization is essential for sustained EGFR signaling but dispensable for degradation. *Dev. Cell* **15**, 209–219.

- Simske, J. S. and Kirn, S. K.** (1995). Sequential signalling during *Caenorhabditis elegans* vulval induction. *Nature* **375**, 142–146.
- Sternberg, P. W.** (2005). Vulval development. *WormBook*.
- Sternberg, P. W. and Horvitz, H. R.** (1986). Pattern formation during vulval development in *C. elegans*. *Cell* **44**, 761–772.
- Sternberg, P. W. and Horvitz, H. R.** (1989). The combined action of two intercellular signaling pathways specifies three cell fates during vulval induction in *C. elegans*. *Cell* **58**, 679–693.
- Stetak, A., Hoier, E. F., Croce, A., Cassata, G., Di Fiore, P. P. and Hajnal, A.** (2006). Cell fate-specific regulation of EGF receptor trafficking during *Caenorhabditis elegans* vulval development. *EMBO J.* **25**, 2347–2357.
- Stolfi, A., Wagner, E., Taliaferro, J. M., Chou, S. and Levine, M.** (2011). Neural tube patterning by Ephrin, FGF and Notch signaling relays. *Dev. Camb. Engl.* **138**, 5429–5439.
- Struhl, G., Struhl, K. and Macdonald, P. M.** (1989). The gradient morphogen bicoid is a concentration-dependent transcriptional activator. *Cell* **57**, 1259–1273.
- Sturm, O. E., Orton, R., Grindlay, J., Birtwistle, M., Vyshemirsky, V., Gilbert, D., Calder, M., Pitt, A., Kholodenko, B. and Kolch, W.** (2010). The Mammalian MAPK/ERK Pathway Exhibits Properties of a Negative Feedback Amplifier. *Sci. Signal.* **3**, ra90–ra90.
- Sun, P., Watanabe, H., Takano, K., Yokoyama, T., Fujisawa, J. and Endo, T.** (2006). Sustained activation of M-Ras induced by nerve growth factor is essential for neuronal differentiation of PC12 cells. *Genes Cells Devoted Mol. Cell. Mech.* **11**, 1097–1113.
- Swanson, C. I., Schwimmer, D. B. and Barolo, S.** (2011). Rapid evolutionary rewiring of a structurally constrained eye enhancer. *Curr. Biol. CB* **21**, 1186–1196.
- Tan, P. B., Lackner, M. R. and Kim, S. K.** (1998). MAP Kinase Signaling Specificity Mediated by the LIN-1 Ets/LIN-31 WH Transcription Factor Complex during *C. elegans* Vulval Induction. *Cell* **93**, 569–580.
- Tassy, O., Daian, F., Hudson, C., Bertrand, V. and Lemaire, P.** (2006). A Quantitative Approach to the Study of Cell Shapes and Interactions during Early Chordate Embryogenesis. *Curr. Biol.* **16**, 345–358.
- Tautz, D.** (1988). Regulation of the *Drosophila* segmentation gene hunchback by two maternal morphogenetic centres. *Nature* **332**, 281–284.
- Tautz, D., Lehmann, R., Schnürch, H., Schuh, R., Seifert, E., Kienlin, A., Jones, K. and Jäckle, H.** (1987). Finger protein of novel structure encoded by hunchback, a second member of the gap class of *Drosophila* segmentation genes. *Nature* **327**, 383–389.
- Teis, D., Taub, N., Kurzbauer, R., Hilber, D., de Araujo, M. E., Erlacher, M., Offterdinger, M., Villunger, A., Geley, S., Bohn, G., et al.** (2006). p14-MP1-MEK1 signaling regulates endosomal traffic and cellular proliferation during tissue homeostasis. *J. Cell Biol.* **175**, 861–868.

- To, T.-L. and Maheshri, N.** (2010). Noise can induce bimodality in positive transcriptional feedback loops without bistability. *Science* **327**, 1142–1145.
- Toettcher, J. E., Weiner, O. D. and Lim, W. A.** (2013). Using Optogenetics to Interrogate the Dynamic Control of Signal Transmission by the Ras/Erk Module. *Cell* **155**, 1422–1434.
- Tokuhiro, S., Tokuoka, M., Kobayashi, K., Kubo, A., Oda-Ishii, I. and Satou, Y.** (2017). Differential gene expression along the animal-vegetal axis in the ascidian embryo is maintained by a dual functional protein Foxd. *PLOS Genet.* **13**, e1006741.
- Traverse, S., Seedorf, K., Paterson, H., Marshall, C. J., Cohen, P. and Ullrich, A.** (1994). EGF triggers neuronal differentiation of PC12 cells that overexpress the EGF receptor. *Curr. Biol.* **4**, 694–701.
- Turing, A. M.** (1952). The Chemical Basis of Morphogenesis. *Philos. Trans. R. Soc. Lond. B. Biol. Sci.* **237**, 37–72.
- Ullrich, A. and Schlessinger, J.** (1990). Signal transduction by receptors with tyrosine kinase activity. *Cell* **61**, 203–212.
- Venero Galanternik, M., Kramer, K. L. and Piotrowski, T.** (2015). Heparan Sulfate Proteoglycans Regulate Fgf Signaling and Cell Polarity during Collective Cell Migration. *Cell Rep.* **10**, 414–428.
- Venuti, J. M. and Jeffery, W. R.** (1989). Cell lineage and determination of cell fate in ascidian embryos. 16.
- Vercauteren, D., Vandenbroucke, R. E., Jones, A. T., Rejman, J., Demeester, J., De Smedt, S. C., Sanders, N. N. and Braeckmans, K.** (2010). The Use of Inhibitors to Study Endocytic Pathways of Gene Carriers: Optimization and Pitfalls. *Mol. Ther.* **18**, 561–569.
- Vihanto, M. M.** (2006). Caveolin-1 is required for signaling and membrane targeting of EphB1 receptor tyrosine kinase. *J. Cell Sci.* **119**, 2299–2309.
- Wada, H., Saiga, H., Satoh, N. and Holland, P. W. H.** (1998). Tripartite organization of the ancestral chordate brain and the antiquity of placodes: insights from ascidian Pax-2/5/8, Hox and Otx genes. 10.
- Wagner, E. and Levine, M.** (2012). FGF signaling establishes the anterior border of the *Ciona* neural tube. *Development* **139**, 2351–2359.
- Wang, L.-H., Rothberg, K. G. and Anderson, R. G.** (1993). Mis-assembly of clathrin lattices on endosomes reveals a regulatory switch for coated pit formation. *J. Cell Biol.* **123**, 1107–1117.
- Whitehurst, A., Cobb, M. H. and White, M. A.** (2004). Stimulus-Coupled Spatial Restriction of Extracellular Signal-Regulated Kinase 1/2 Activity Contributes to the Specificity of Signal-Response Pathways. *Mol. Cell. Biol.* **24**, 10145–10150.
- Wilson, M. Z., Ravindran, P. T., Lim, W. A. and Toettcher, J. E.** (2017). Tracing Information Flow from Erk to Target Gene Induction Reveals Mechanisms of Dynamic and Combinatorial Control. *Mol. Cell* **67**, 757-769.e5.

- Wimmer-Kleikamp, S. H., Janes, P. W., Squire, A., Bastiaens, P. I. H. and Lackmann, M.** (2004). Recruitment of Eph receptors into signaling clusters does not require ephrin contact. *J. Cell Biol.* **164**, 661–666.
- WIREs Authors** (2017). Same Signal, Different Tissues: Morphogen Interpretation. *Adv. Sci. News*.
- Wolpert, L.** (1969). Positional information and the spatial pattern of cellular differentiation. *J. Theor. Biol.* **25**, 1–47.
- Xiong, F., Tentner, A. R., Huang, P., Gelas, A., Mosaliganti, K. R., Souhait, L., Rannou, N., Swinburne, I. A., Obholzer, N. D., Cowgill, P. D., et al.** (2013). Specified Neural Progenitors Sort to Form Sharp Domains after Noisy Shh Signaling. *Cell* **153**, 550–561.
- Yamamoto, T., Ebisuya, M., Ashida, F., Okamoto, K., Yonehara, S. and Nishida, E.** (2006). Continuous ERK activation downregulates antiproliferative genes throughout G1 phase to allow cell-cycle progression. *Curr. Biol. CB* **16**, 1171–1182.
- Yang, B. S., Hauser, C. A., Henkel, G., Colman, M. S., Van Beveren, C., Stacey, K. J., Hume, D. A., Maki, R. A. and Ostrowski, M. C.** (1996). Ras-mediated phosphorylation of a conserved threonine residue enhances the transactivation activities of c-Ets1 and c-Ets2. *Mol. Cell. Biol.* **16**, 538–547.
- Yasuo, H. and Hudson, C.** (2007). FGF8/17/18 functions together with FGF9/16/20 during formation of the notochord in *Ciona* embryos. *Dev. Biol.* **302**, 92–103.
- Yasuo, H. and McDougall, A.** (2018). Practical Guide for Ascidian Microinjection: *Phallusia mammillata*. In *Transgenic Ascidians* (ed. Sasakura, Y.), pp. 15–24. Singapore: Springer.
- Yoo, A. S.** (2004). Crosstalk Between the EGFR and LIN-12/Notch Pathways in *C. elegans* Vulval Development. *Science* **303**, 663–666.
- Yoo, A. S., Bais, C. and Greenwald, I.** (2004). Crosstalk Between the EGFR and LIN-12/Notch Pathways in *C. elegans* Vulval Development. *Science* **303**, 663–666.
- Zhang, Q., Huang, H., Zhang, L., Wu, R., Chung, C.-I., Zhang, S.-Q., Torra, J., Schepis, A., Coughlin, S. R., Kornberg, T. B., et al.** (2018). Visualizing Dynamics of Cell Signaling In Vivo with a Phase Separation-Based Kinase Reporter. *Mol. Cell* **69**, 334-346.e4.
- Zhu, A. J. and Scott, M. P.** (2004). Incredible journey: how do developmental signals travel through tissue? *Genes Dev.* **18**, 2985–2997.





## SUMMARY

During my PhD project, I studied the initial step of ascidian neural induction to address how a cell interprets a graded signal to generate a threshold response. During this process, four ectoderm cells among a total of sixteen are selected as neural precursors. FGF9/16/20, derived from mesendoderm cells, acts as a neural inducer and directly activates *Otx* expression through the canonical RTK-Ets pathway. Quantitative measurement of cell surface contacts between ectoderm cells and FGF-expressing mesendoderm cells has revealed that each ectoderm cell is in direct contact with mesendoderm cells and is thus exposed to FGF, with neural precursors having the largest area of cell surface contact and thus, presumably, the highest FGF exposure. Using quantitative measurements of endogenous ERK activation, we have revealed that each ectoderm cell exhibits a level of ERK activation largely corresponding to its area of cell surface contact with FGF-expressing mesendoderm cells. In contrast, smFISH analysis of *Otx* expression showed that this transcriptional response is restricted to only the four neural precursors. Consistently, when explanted ectoderm cells are treated with increasing doses of exogenous FGF, while ERK activation levels increase gradually, the *Otx* gene is activated in a bimodal manner (ON or OFF). These results suggest that a threshold response is in operation and acts at the level of *Otx* transcriptional regulation. In addition to FGF, ephrin signals also play a critical role during ascidian neural induction. An ephrin ligand, EfnA.d, is expressed in the ectoderm cells and forward ephrin/Eph signals, mediated intracellularly via p120RasGAP, act antagonistically to FGF signals at the level of Ras regulation. In embryos inhibited for ephrin/Eph signals, ERK activation levels are increased in all ectoderm cells, in a manner proportional to their cell surface contact with the FGF-expressing mesendoderm cells. Under these conditions, the spatial precision of *Otx* expression is lost with additional ectoderm cells exhibiting the 'ON' status of *Otx* expression. This suggests that ephrin/Eph signals act to reduce the overall levels of ERK activation, such that the non-neural ectoderm cells remain below the threshold required for *Otx* gene activation. In other words, ephrin/Eph signals are required simply to "damp-down" FGF signalling. To test whether a damping-down mechanism was sufficient to explain the spatial precision of the *Otx* response, we treated embryos, in which ephrin signals were blocked, with low doses of the MEK inhibitor U0126. This treatment was sufficient to re-establish the normal *Otx* expression profile specifically in the four neural precursors. Our study has thus uncovered a mechanism whereby signal damping underlies the spatial precision of threshold response to graded signal inputs. Mechanisms underlying the interpretation of a gradual signal (ERK) into a bimodal response at the transcriptional level (*Otx*) still need to be studied. However, preliminary results suggest a role of the Ets repressor ERF in the interpretation of the gradual ERK signal into the ON/OFF response of *Otx*.